PHOTOPHYSICAL AND PHOTOCHEMICAL STUDIES OF NON-TRANSITION METAL PHTHALOCYANINE DERIVATIVES

A thesis submitted in fulfillment of the requirements for the degree of

DOCTOR OF PHILOSOPHY

Of

RHODES UNIVERSITY

By

ABIMBOLA OLUKAYODE OGUNSIPE

December 2004

To

Bisola,

for the love she gives,

and

Debola,

for the joy he brings.

ACKNOWLEDGEMENTS

"I can do all things through Christ which strengtheneth me" **Philippians 4:13.**

I give Glory to God for giving me life, strength, wisdom and understanding. It is He who made it possible for me to have gone this far in life.

I thank my supervisor, Prof Tebello Nyokong for allowing me to do research under her tutelage; her untiring zeal to offer suggestions and objective criticism is unequalled. *"If you have knowledge, let others light their candles at it"* – **Margaret Fuller**. I have lit the candle of my academic career at your knowledge. Thank you 'Mama Prof', May God continue to bless you.

"...how sharper than a serpent's tooth it is to have a thankless child" – **William Shakespeare**. Dad, Mum, I thank you for bringing me to life and for making it worth living for me. I appreciate your moral and financial support; and prayers. Remembering that I have you gives me the courage to say "all is well". No amount of words can adequately express my gratitude to you.

Many thanks to my wife, Bisola, for her love, concern and perseverance; Darling, you are a rare gem in my life and I will for ever be grateful to you.

To all my siblings, friends and well-wishers in South Africa and Nigeria (too numerous to mention names), I acknowledge your thoughtfulness prayers and moral support. To you all I shall forever be appreciative.

I thank all co-students in the Chemistry department of Rhodes University, for the superb experience we shared together. I hope I could continue to work with you guys for ever; I will keep the contact.

Financial support from Rhodes University and the National Research Foundation (NRF) of South Africa; as well as scholarships from Andrew Mellon Foundation and ICSC World laboratory, are gratefully acknowledged.

Finally, I thank University of Lagos for granting me a study leave to undertake this programme.

ABSTRACT

A detailed photophysicochemical study of some non-transition metal (Al, Zn, Si, Ge, and Sn) metallophthalocyanine (MPc) derivatives is presented. The effects of substituents, central metal ions and solvents on the photophysical and photochemical properties are investigated and rationalized accordingly. The presence of peripheral substituents on the macrocycle enhances the yield of the triplet state. Near infra-red absorptions of the solvents reveal that solvents which absorb around 1100 nm and around 1270 nm, quench the triplet state of the MPc derivative and singlet oxygen, respectively. Although water has a high singlet oxygen quenching effect, the singlet oxygen quantum yield (Φ_Δ) value for sulphonated zinc phthalocyanine in water is still reasonably high at 0.48, which may provide an explanation for the efficient photosensitization by this molecule in photodynamic studies.

The lowering of Φ_Δ following protonation of the MPc macrocycle is attributed to the lowering of triplet energy to the level where energy transfer to ground state oxygen is no longer favourable. MPc inclusion complexes with cyclodextrins showed larger Φ_Δ values when compared to the complexes before inclusion. Job's plots show that 2:1 and 4:1 (CD:MPc) complexes may be formed.

Fluorescence quenching by electron donors and acceptors were analysed by Stern-Volmer relationship and the results used in determining fluorescence lifetimes of the complexes.

Qualitative and quantitative interpretations of the interaction of sulphonated MPcs with bovine serum albumin (BSA) are provided in this thesis. 1:1 adducts were formed with BSA, but the binding feasibilities varied markedly. Spectral, photophysical and photochemical properties of the complexes are altered in the presence of BSA.

TABLE OF CONTENTS

LIST OF SYMBOLS

α	Fraction of incident light absorbed
D	Diffusion coefficient
ε	Molar extinction coefficient
F	Fluorescence intensity
Φ	Quantum yield
Φ_{CT}	Charge transfer quantum yield
Φ_{-DPBF}	quantum yield of disappearance of DPBF
Φ_{ExT}	Excitation transfer quantum yield
Φ_F	Fluorescence quantum yield
Φ_{IC}	Internal conversion quantum yield
Φ_{ISC}	Intersystem crossing quantum yield
Φ_{Ph}	Phosphorescence quantum yield
Φ_{Pd}	Photodegradation quantum yield
Φ_T	Triplet quantum yield
Φ_{VR}	Vibrational relaxation quantum yield
I_{abs}	Intensity of light absorbed
K_b	Binding constant
k_{CT}	Charge transfer rate constant
K_D	Dynamic quenching constant (employed when both dynamic and static quenching mechanisms are at play.
k_d	First order decay constant
k_{ET}	Energy transfer rate constant
k_{ExT}	Excitation transfer rate constant
k_F	Fluorescence rate constant
k_{IC}	Internal conversion rate constant
k_{ISC}	Intersystem crossing rate constant
k'_{ISC}	Triplet to singlet intersystem crossing rate constant
k_{Ph}	Phosphorescence rate constant
k_{Pd}	Photodegradation rate constant

k_Q	Diffusion-controlled bimolecular quenching rate constant.
k_R	Diffusion-controlled bimolecular rate constant
K_S	Static quenching constant
K'_S	Sphere of action static quenching constant
K_{SV}	Stern-Volmer quenching constant
k_{VR}	Vibrational relaxation rate constant
n	Frequency of light
N_A	Avogadro's constant
$O_2(^1\Delta_g)$	Singlet molecular oxygen
$O_2(^1\Sigma_g^+)$	Unstable form of singlet molecular oxygen
$O_2(^3\Sigma_g^-)$	Ground state molecular oxygen (triplet)
R	Radius of molecule
S_0	Ground singlet state
S_1	Excited singlet state
S_2	Second excited singlet state
τ	Fluorescence lifetime
T	Transmittance
τ_0	Natural radiative lifetime
τ_F^0	Fluorescence lifetime in the absence of quencher
T_1	First excited triplet state
T_2	Second excited triplet state
u	Ungerade (non-even parity)
v_0	Non-vibrational state
v_n	nth vibrational state

LIST OF ABBREVIATIONS

A	Absorbance
Abs	Absorption
ADMA	Tetrasodium anthracene-9.10-bis-ethylmalonate
AQDS	Anthraquinone-2,6-disodium sulphonate
BQ	Benzoquinone
BSA	Bovine serum albumin
BV	Benzyl viologen
CD	Cyclodextrin
CD-RW	Rewritable optical media (compact disc)
CT	Charge transfer
CTS	Charge transfer state
DABCO	Diazabicyclooctane
DBN	1,5-Diazabicyclo [4.3.0] non-5-ene
DBU	1,8-Diazabicyclo [5.4.0] undec-7-ene
DMF	N,N′-dimethylformamide
DMSO	Dimethylsulphoxide
DPBF	1,3-Diphenyl*iso*benzofuran
ET	Energy transfer
ExT	Excitation transfer
F	Fluorescence
HOMO	Highest Occupied Molecular Orbital
HPLC	High Performance Liquid Chromatography
HQ	Hydroquinone
IC	Internal conversion
ICT	Internal charge transfer
ISC	Intersystem crossing
LB	Langmuir-Blodgett
LES	Locally excited state
LUMO	Lowest Unoccupied Molecular Orbital
MPc	Metallophthalocyanine
$MPcS_{mix}$	Mixture of differently sulphonated MPc
MTSPc	Tetrasulphonated MPc

MV	Methyl viologen
PBS	Phosphate buffer solution
Pc	Phthalocyanine
PDT	Photodynamic therapy
Ph	Phosphorescence
pip	Piperidine
PMT	Photomultiplier tube
py	Pyridine
SAQM	Sphere of action quenching model
S-V	Stern-Volmer
TABP	Tetraazatetrabenzoporphyrin
TAP	Tetraazaporphyrin
TBP	Tetrabenzoporphyrin
TEA	Triethylamine
TFA	Trifluoroacetic acid
THF	Tetrahydrofuran
Ti(IV)Pc	Titanium(IV) phthalocyanine
TLC	Thin Layer Chromatography
TPP	Tetraphenylporphyrin
TX	Triton X-100
UV	Ultraviolet
UV-Vis	Ultraviolet-Visible
VR	Vibrational relaxation
ZnTSPc	Tetrasulphonatezinc phthalocyanine

LIST OF SCHEMES

LIST OF TABLES

LIST OF FIGURES

The results presented in this thesis culminated in the publishing of the following articles in high-impact peer-reviewed journals. These articles are not referenced in this thesis:

1. "Influence of cyclodextrins on the fluorescence, photostability and singlet oxygen quantum yield of zinc phthalocyanine and naphthalocyanine complexes".

   Prudence Tau, **Abimbola Ogunsipe**, Suzzanne Maree, David Maree and Tebello Nyokong, *J. Porphyrins Phthalocyanines*, 2003, **7**, 438-445.

2. "Solvent effects on the photochemical and fluorescence properties of zinc phthalocyanine derivatives".

   Abimbola Ogunsipe, David Maree and Tebello Nyokong, *J. Mol. Struc.*, 2003, **650**, 131-140.

3. "Effects of substituents and solvents on the photochemical properties of protonated zinc phthalocyanine derivatives".

   Abimbola Ogunsipe and Tebello Nyokong, *J. Mol. Struc.*, 2004, **689**, 89-97.

4. "Photophysical and photochemical studies of zinc(II) phthalocyanine derivatives – Effects of substituents and solvents".

   Abimbola Ogunsipe, Ji-Yao Chen and Tebello Nyokong, *New J. Chem.*, 2004, **7**, 822-827.

5. "Effects of central metal on the photophysical and photochemical properties of non-transition metal sulfophthalocyanines".

   Abimbola Ogunsipe and Tebello Nyokong, *J. Porphyrins Phthalocyanines,* **in press.**

6. "Synthesis and photophysical properties of a covalently linked porphyrin-phthalocyanine conjugate".

   Zhixin Zhao, **Abimbola Ogunsipe**, David Maree and Tebello Nyokong, *J. Porphyrins Phthalocyanines,* **in press.**

7. "Photophysical and photochemical studies of non-transition metal phthalocyanine sulphonates in aqueous and non-aqueous media".

   Abimbola Ogunsipe and Tebello Nyokong, *J. Photochem. Photobiol. A: Chem.*, **accepted for publication.**

8. "Photophysicochemical consequences of bovine serum albumin binding to non-transition metal phthalocyanine sulphonates".

   Abimbola Ogunsipe and Tebello Nyokong, *Photochem. Photobiol. Sci.,* **submitted.**

1. INTRODUCTION

The purpose of this chapter is to provide an introductory account of the basic concepts of photophysics and photochemistry, since these techniques form the integral part of the thesis. Also, a general review of the photophysical, photochemical and binding properties of metallophthalocyanines is presented in this chapter

1.1 PHOTOPHYSICS AND PHOTOCHEMISTRY

Photophysics is the study of the interaction of light with molecules which results in net physical (not chemical) change, and **photochemistry** is defined as the study of the interaction of light with molecules which results in net chemical change.

1.1.1 Laws of photochemistry

1.1.1.1 Grotthus and Draper law

The first law of photochemistry, attributed to Grotthus and Draper in the 1800s **(Grotthus and Draper law)** states: Only the light absorbed by a molecule can be effective in producing a photochemical change. In other words, molecules that do not absorb light of a particular frequency will not undergo a photochemical reaction when irradiated at that frequency.

1.1.1.2 Stark-Einstein law

The second law of photochemistry, states that for each photon of light absorbed by a chemical system, only one molecule is activated for photochemical reaction. The law means that each photon of light can cause a photochemical reaction of only one light-absorbing molecule. A related law states that the amount of photoreaction that takes place is directly proportional to the product of the light intensity and the time of illumination. In other words, more light produces more photoproduct.

1.1.1.3 The Energy gap law ("Proximity effects" in radiationless transitions)

This law is exemplified by *N*-heterocycles and aromatic carbonyls which posses nπ* and ππ* states in close proximity. Molecular vibrations associated with these states can be modified by manipulating features like substitution, solvent and temperature. Such manipulation changes the energy separation between nπ* and ππ* states. For example, methyl substitution reduces the nπ*- ππ* energy difference in pyrazine [1,2], resulting in lower values of luminescence quantum yield and lifetime, and which is tantamous to an increase in the rate of non-radiative deactivation. The enhancement in fluorescence of iso-quinoline in protic solvents [3] is attributed to an increase in nπ*- ππ* energy gap, due to hydrogen bonding. The consequence is a reduction in the rate of non-radiative deactivation. Again, the observed decrease in fluorescence quantum yield and lifetime of iso-quinoline in alcoholic solutions as the temperature is raised, could be explained in terms of reduction of the nπ*- ππ* energy gap [1]. The concentration of hydrogen-bonded species is less at high temperatures and so the nπ*- ππ* energy gap becomes smaller, and radiationless deactivation is enhanced. The energy gap law states that radiationless decay from the lower lying state of a vibrationally coupled pair is enhanced by decreasing the energy separation between the coupled states [4,5].

1.1.2 The Jablonski diagram

The S_0 state: Most polyatomic organic molecules do not have unpaired electrons in their electronic structures hence they adopt the singlet spin state. Prior to excitation, the

molecules are in the ground state represented as S_0. When photons are absorbed, electrons move into higher valence orbitals called excited singlet states.

The processes which occur during the absorption and emission of light are usually illustrated by a Jablonski diagram [6] (Fig. 1.1). According to the Franck-Condon principle, molecular excitation is not to the lowest vibrational level of the excited state (corresponding to a non-vibrational state), but somewhere higher (Franck-Condon state). This means that the molecule finds itself, after the absorption act, in a non-equilibrium state, and equilibrium can be established through a non-radiative relaxation to the non-vibrational v_0 state.

The T_1 state: This state is formed as a result of intersystem crossing and it is an excited triplet state. The spin multiplicity is changed due to a change in the spin state of an electron.

The fate of the excited molecule

A molecule, photochemically promoted to an excited state, does not stay there for long. Excitations to S_2 and higher singlet states take place, but in liquids and solids these higher states usually drop very rapidly to the S_1 state (about 10^{-13} to 10^{-11} sec) by giving up the energy to the environment. This process is called an *energy cascade* (vibrational relaxation). In a similar manner, molecules at different vibrational levels of S_1 cascade down to the lowest vibrational level of $S_1(v_0)$ as discussed above. Therefore, in most cases, the lowest vibrational level of the S_1 state is the only important level. This state can undergo various physical processes:

Internal conversion – The process by which molecules in the lowest vibrational level of an electronic state are converted to upper vibrational levels of a lower-energy electronic state of the same spin multiplicity, via radiationless transition.

Intersystem crossing – Molecules in the S_1 state can cross to a T_1 state without loss of energy (radiationless transition) and cascade down to its lowest vibrational level.

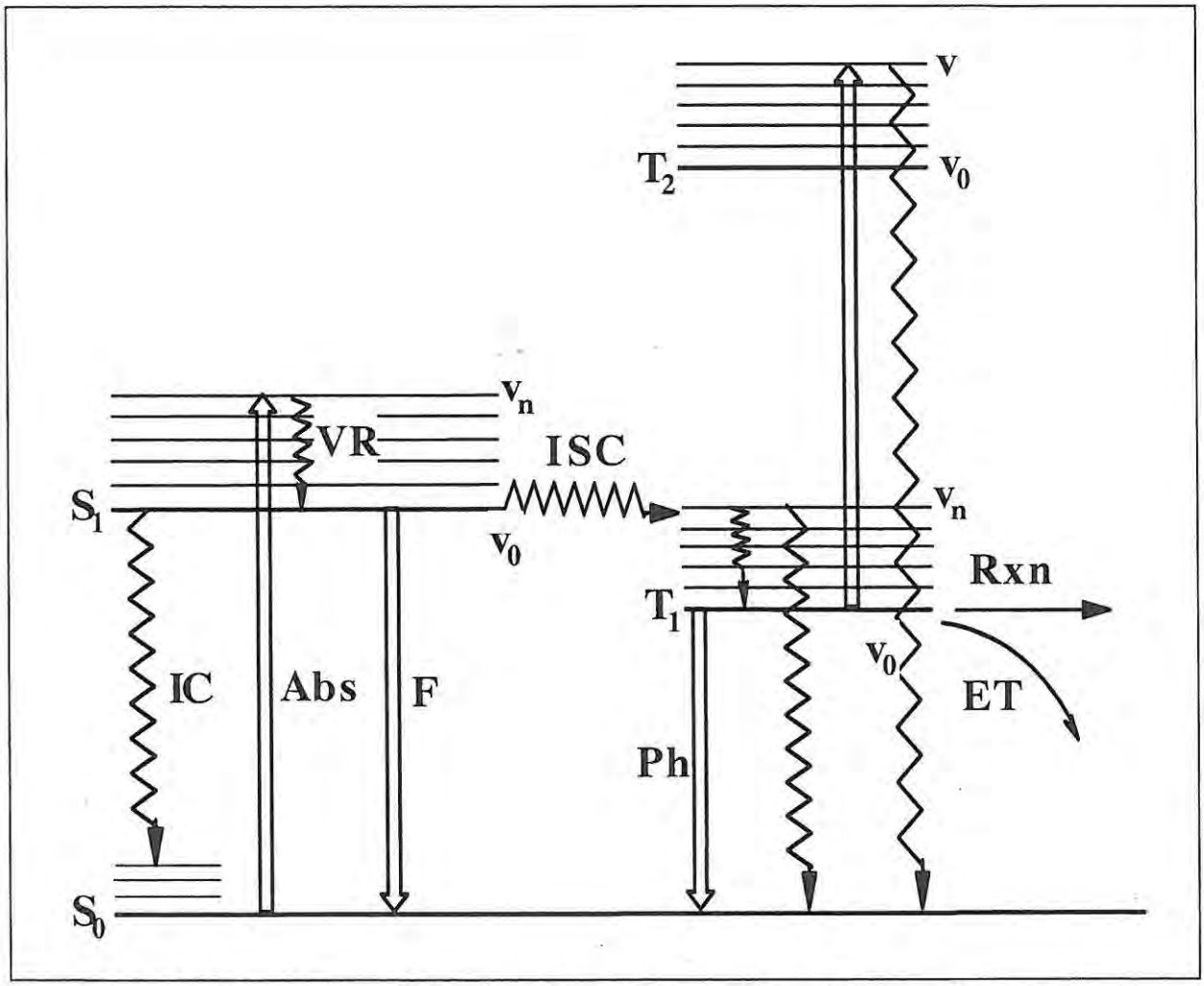

Figure 1.1: Modified Jablonski diagram showing transitions between the excited electronic states and the ground state.

Abs = Absorption; VR = Vibrational deactivation; IC = Internal conversion; ISC = Intersystem crossing; F = Fluorescence; Ph = Phosphorescence; Rxn = Chemical reaction; ET = Energy transfer. Radiative transitions are indicated with straight arrows, while radiationless transitions are indicated with wavy arrows.

Fluorescence – A molecule in the S_1 state drops to some low vibrational level of the S_0 state at once by giving off the energy in the form of light. This process generally happens within 10^{-9} sec, and is common for small and/or rigid molecules. As an aftermath of the post-absorption vibrational relaxation, the energy of fluorescence is usually less than that of absorption. Therefore, fluorescence naturally occurs at lower energies (longer wavelengths) than absorption. The difference between the spectral positions of the band maxima of absorbance and fluorescence arising from the electronic transition is called the **Stokes'shift** (Fig. 1.2). For many of the common fluorophores, the vibrational energy level spacing is similar for the ground and excited states, which results in a fluorescence spectrum that strongly resembles the mirror image of the absorption spectrum. This is due to the fact that the same transitions are most favorable for both absorption and emission. Although the Franck-Condon principle provided its interpretation, the phenomenon of Stokes' shift has been well established before the advent of the Franck-Condon principle.

Phosphorescence – A molecule in the T_1 state may return to the S_0 state by giving off light.

In most typical cases, the fluorescent state is the lowest excited singlet state and the phosphorescent state, the lowest triplet state (Kasha's rule); the ground state being a singlet.

Electronic excitation transfer – A molecule in an excited state (S_1 or T_1) may pass on its excitation to another molecule in the environment, in a process called photosensitization. The excited molecule thus drops to S_0 while the other molecule becomes excited.

The excited state could also undergo a chemical reaction **(photochemistry)**.

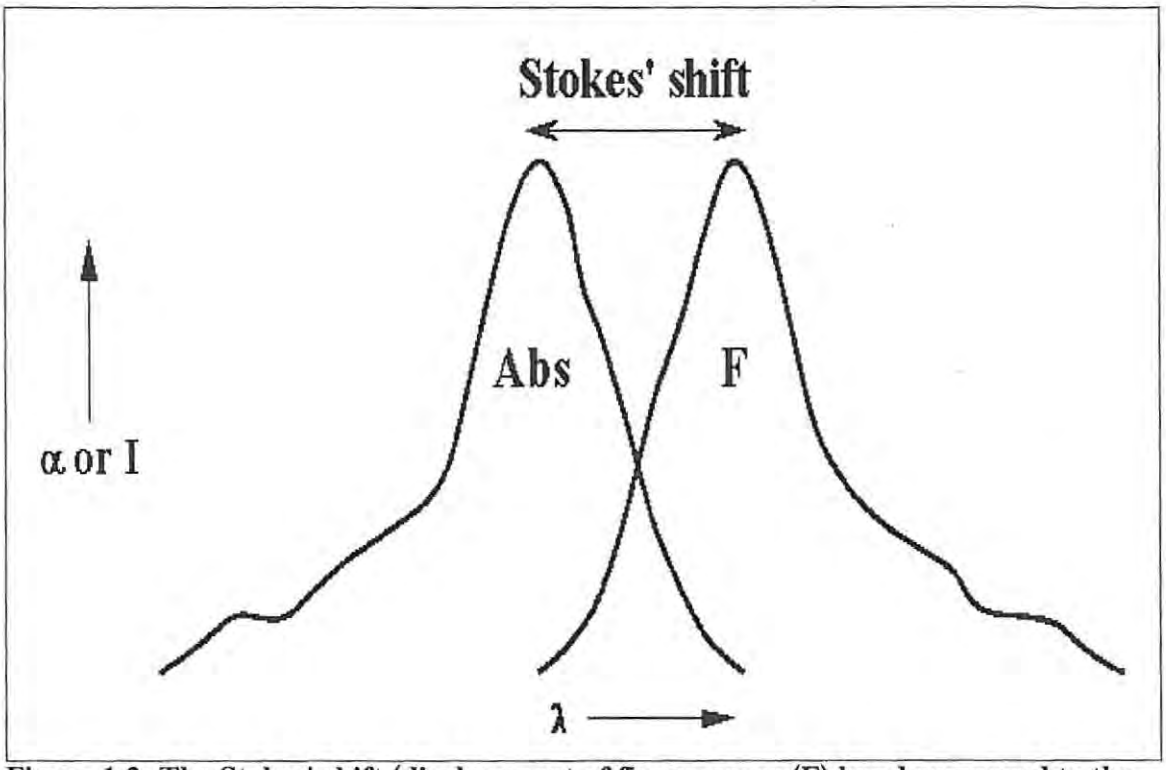

Figure 1.2: The Stokes' shift (displacement of fluorescence (F) band compared to the absorption (Abs) band of a molecule).

1.1.3 The Stokes' shift

As discussed above, the fluorescence spectrum is a mirror image of the absorption spectrum. Several factors influence the magnitude of the Stokes' shift. If the environment is rigid so that little rearrangement is possible then the Stokes shift is expected to be small. The magnitude of the shift depends on factors such as solvent polarity, viscosity and polarizability. It also depends on whether the excited state can undergo any specific interactions such as proton transfer or charge transfer to other molecules or (sometimes) within the same molecule.

Sometimes, there could be non-conformity to the mirror image rule for absorption and fluorescence. Such deviations are indicative of a change in geometry of the absorbing species soon after excitation and prior to emission. This implies that the ground state and the excited states now have different geometrical arrangements of their nuclei. Apart from change in geometry, excited state reactions could also result in a breakdown of the mirror image rule. For example the absorption and emission spectra of anthracene (in the presence of diethylaniline) [7] are not mirror images, due to the formation of a charge-transfer complex between the excited state of anthracene and diethyaniline.

1.1.4 Selection rules

A selection rule is a quantum mechanical rule that describes the types of quantum mechanical transitions that are permitted. Transitions not permitted by selection rules are said to be "forbidden," although in practice, such transitions are generally forbidden "to first order" only, which means they may occur in practice but with low probability. Light absorption is a resonant process; hence the most fundamental condition for absorption is that the energy of the incoming photon must match the difference in energy between the two energy states involved in the transition ($\Delta E = h\nu$). In addition to this energy matching, the probability of an electronic transition is predicted using a set of selection rules, which may be summarized as follows:

1.1.4.1 Spin selection rule ($\Delta S = 0$)

Transitions involving spin changes (T←S or S←T; where S = singlet and T = triplet) are strongly forbidden. This rule can be relaxed in the presence of heavy atoms and paramagnetic species. The fact that spin-forbidden transitions can be observed at all is as a result of the phenomenon of *spin-orbit coupling*, which is the interaction of the electron's spin magnetic moment with its orbital magnetic moment. This interaction introduces a new term into the Hamiltonian operator which operates on both spin and space variables. In the presence of this new term, the zero-order wave functions of the system, which were pure singlets and triplets, are combined to form new wave functions of mixed multiplicity. T←S and S←T transitions therefore become somewhat probable because the singlet state is no longer pure singlet but has some triplet character mixed with it. The triplet state also has some singlet character.

1.1.4.2 LaPorte selection rule (g↔u; $\Delta l = \pm 1$)

Whether spin-allowed or spin-forbidden, some transitions (e.g. d-d) are generally very weak. This could be due to the LaPorte selection rule which forbids transitions involving no change of parity (p↔p, d↔d, f↔f). If the sign of the wave function changes on reflection through a centre of smmetry, then the symmetry is referred to as *ungerade* denoted *u*; if it is unchanged, it is termed *gerade* denoted *g*. Then according to this rule, u←g and g←u transitions are allowed, while u←u and g←g transitions are forbidden. The corollary of the LaPorte rule is that d↔p and s↔p transitions are allowed, while d↔d, and s↔d transitions are forbidden. The selection rule which states that transitions that cause a large change in linear or angular momentum of the molecule are forbidden, is

also consistent with the LaPorte rule. However, the LaPorte rule does not strictly apply in the presence of minor static distortions or asymmetric vibrational motions which remove the exact centrosymmetry. This could be responsible for the observed intensities of the d←d transitions in octahedral complexes.

1.1.4.3 Franck-Condon selection rule

The classical Franck-Condon principle requires that, because an electronic transition is "instantaneous", the nuclear coordinates and momenta do not change. As a result of this transition, electron density is rapidly built up in new regions of the molecule and removed from others. The change in electron density causes a new force field on the stationary nuclei, which causes the molecules to vibrate. The most probable transition is from the ground state to the vibrational state lying vertically above it. In quantum mechanical terms, transitions are most probable when the wave function of the upper vibrational state most closely resembles the ground state vibrational wave function.

1.1.4.4 Orbital overlap selection rule

Orbitals involved in an electronic transition need to overlap. For example, the $\pi^* \leftarrow \pi$ transition in carbonyls is highly probable because the orbitals involved do overlap. This is not the case for the $\pi^* \leftarrow$ n transition, which is forbidden.

1.1.5 The Quantum yield

By definition, quantum yield is the number of defined events which occur per photon absorbed by the system. The quantum yield (Φ) represents and quantifies the efficiency of a photophysical or photochemical process, Eq. 1.1:

$$\Phi = \frac{\text{number of events}}{\text{number of photons absorbed}} \qquad \text{(Eq. 1.1)}$$

This definition emanates from the first and second laws of photochemistry, which proposed that for any photochemical process to take place, there must be absorption of photons, and that one photon activates only one molecule. Many factors, intrinsic and extrinsic to the system, can influence the efficiency of a photochemical process. Φ is a measure of the efficiency of such processes after light absorption. The efficiencies of all photochemical and photophysical processes are quantified by the quantum yield. The quantum yields for some photophysical and photochemical processes (which are of interest in this work) are defined by Eqs. 1.2 to 1.7:

Fluorescence quantum yield:

$$\Phi_F = \frac{\text{no of fluorescing molecules}}{\text{no of photons absorbed}} \qquad \text{(Eq. 1.2)}$$

Internal conversion:

$$\Phi_{IC} = \frac{\text{no of molecules undergoing internal conversion}}{\text{no of photons absorbed}} \qquad \text{(Eq. 1.3)}$$

Intersystem crossing:

$$\Phi_{ISC} = \frac{\text{no of molecule undergoing intersystem crossing}}{\text{no of photons absorbed}} \qquad \text{(Eq. 1.4)}$$

Phosphorescence:

$$\Phi_{Ph} = \frac{\text{no of phosphorescing molecules}}{\text{no of photons absorbed}} \qquad \text{(Eq. 1.5)}$$

Photodegradation:

$$\Phi_{Pd} = \frac{\text{no of photodegraded molecules}}{\text{no of photons absorbed}} \qquad \text{(Eq. 1.6)}$$

Singlet oxygen:

$$\Phi_{\Delta} = \frac{\text{no of singlet oxygen molecules formed}}{\text{no of photons absorbed}} \qquad \text{(Eq. 1.7)}$$

Table 1.1 gives the representation of some of the processes which result, following excitation of a molecule.

Table 1.1: Description of the regular photophysical properties

Process	Notation	Quantum yield designation	Timescale (s)	Rate constant designation
Vibrational Relaxation	VR	Φ_{VR}	10^{-13}	k_{VR}
Internal Conversion	IC	Φ_{IC}	10^{-12}	k_{IC}
Fluorescence	F	Φ_{F}	10^{-9}	k_{F}
Intersystem Crossing	ISC	Φ_{ISC}	10^{-12}	k_{ISC}
Phosphorescence	Ph	Φ_{Ph}	10^{-6}	k_{Ph}

1.1.6 Fluorescence quenching

The fluorescence of a substance is said to be quenched if the addition of another substance to it reduces the intensity of fluorescence, provided that no chemical reaction occurs between the fluorescing substance (fluorescer or fluorophore) and the quenching material (quencher). According to Stern and Volmer [8], the quenching process is a reaction of the second order, which competes with all other molecular and radiative processes, and is defined by Eq. 1.8:

$$\frac{I_0}{I} = 1 + K_{SV}[Q] \qquad \text{(Eq. 1.8)}$$

Where I_0 and I are the intensities of fluorescence in the absence and presence of the quencher, respectively; [Q] is the concentration of the quencher, and K_{SV}, the Stern-Volmer constant defined by Eq. 1.9

$$K_{SV} = \tau_F^0 k_Q \qquad \text{(Eq. 1.9)}$$

where k_Q is the bimolecular quenching constant, and τ_F^0, the fluorescence lifetime of the fluorophore in the absence of quencher. Deviations from the Stern-Volmer relationship could be due to: presence of several excited states, the ionic strength of the solution and reactions between the fluorophore and the quencher. In such cases, the Stern-Volmer equation is modified to suit the situation.

1.1.7 Flash photolysis

The idea of flash photolysis is to 'very quickly' introduce an intense pulse of light into an absorbing system to produce a sufficient concentration of a transient species; and then 'very quickly' analyze the time evolution of the system by absorption or emission spectroscopy. When the excitation pulse is from laser source, the technique is called **Laser flash photolysis**. Flash photolysis uses two light beams: the excitation pulse and the analyzing light. The excitation pulse is directed to the sample to populate the excited states, while the analyzing light, usually very intense, passes through the sample into a detector.

Flash photolysis has found a lot of use in the study of highly reactive and short-lived species like the excited singlet and triplet states as well as radicals. This technique enables the recording of kinetics in time ranges varying from a few picoseconds to seconds. For example, if the $T_n \leftarrow T_1$ transition (Fig. 1.1) is moderately allowed, or if the rate constant of intersystem crossing is moderately high, it is generally possible to detect T_1 by the measurement of its absorption spectrum. Once the absorption spectrum is established, the decay kinetics of T_1 may be measured. Apart from triplet absorption detection, flash photolysis also gives information about the lifetime of an excited state or of any transient species formed after absorption, e.g., charge transfer states, exciplexes, excimers, etc.

1.2 METALLOPHTHALOCYANINE CHEMISTRY

The chemistry of phthalocyanines (Pcs, **2**, Fig. 1.3) has continued to gain popularity in the last few decades because of the extensive application of these compounds in man's everyday life. The robust chemistry of Pcs is exploited in their use as electrocatalysts and photocatalysts. However, not many Pc derivatives can play both roles efficiently. While electrocatalysis requires the central metal in the metallophthalocyanine (MPc) to be electroactive, the existence of a transient but relatively long-lived excited state is vital in photocatalysis. Such a metastable state could be rapidly "quenched" in the presence of features which promote charge (electron) transfer. This excludes Pcs containing electroactive transition metal centres from photocatalytic activity. A diamagnetic metal centre is neither electroactive nor does it rapidly quench the metastable excited state. The choice of zinc (II) as the centre in this work is due to the potential use of zinc phthalocyanine derivatives in photocatalysis and photosensitization. Aluminium phthalocyanine derivatives have been successfully used in the photodynamic therapy (PDT) of cancer [9-11], and there is an on-going aggressive effort to use the zinc analogue for the same purpose. It is believed that zinc would have some advantages over aluminium, as it is not alien to the animal body system. Zinc is an essential nutrient for the functioning of a large number of enzymes involved in the growth of animals.

The chemistry of phthalocyanines is not only of academic interest. The application of Pcs in man's everyday life and the industry cannot be overemphasized. Again, because of the similarity of the Pc structure to that of porphyrin, **1** (Fig.1.3), which is the core framework in hemoglobin and chlorophyll, Pcs have attracted much attention as replicates of such vital biological systems.

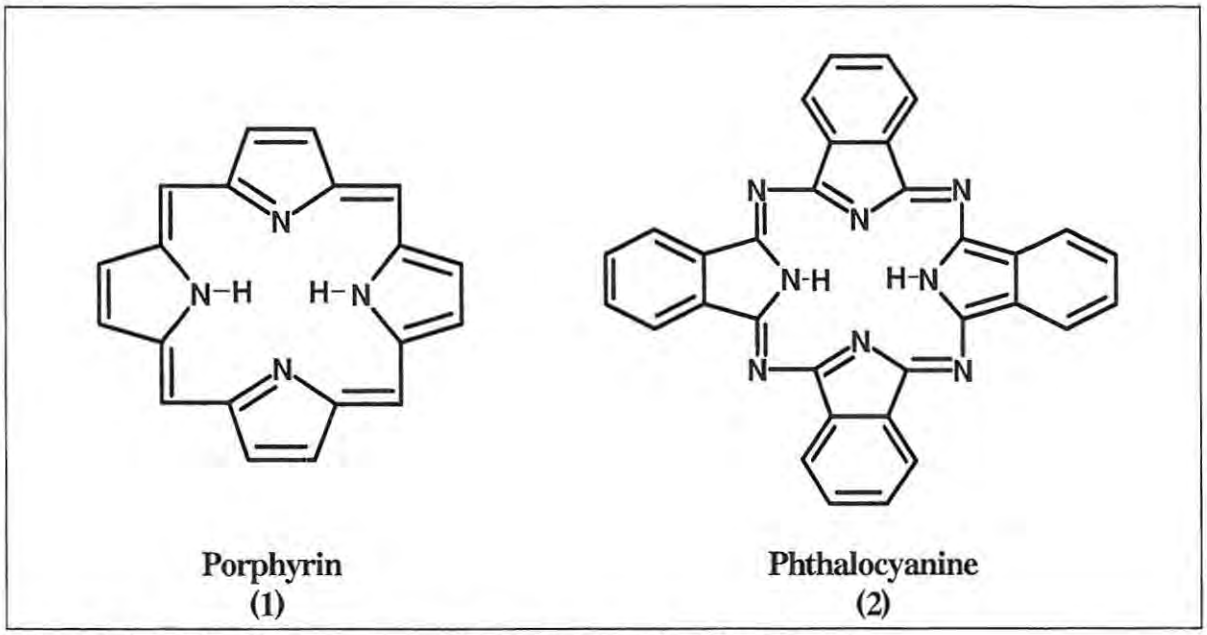

Porphyrin (1) **Phthalocyanine** (2)

Figure 1.3: Molecular structures of porphyrin and phthalocyanine.

1.2.1 General applications of phthalocyanines

The substituted Pc derivatives function as active components in various processes driven by visible light [12,13]. In this respect, they find applications in photoredox reactions, photooxidations in solution [14,15], photochemical cells and photovoltaic cells [16]. Pcs also possess electronic and morphological characteristics that are especially favourable for semiconductive or conductive properties [12]. Pcs also find use as light absorbing layers in rewritable optical media (CD-RW) [17-19], photoconducting materials in laser printers [20], non-linear optics (optical communication) [13,21,22], chemical sensors [23,24], Langmuir-Blodgett (LB) films, [25-27] and as conventional dyestuffs. In fact, the Royal Mint uses the popular copper substituted variety as a blue dye in 5 pound notes. Worth stressing is the use of phthalocyanines in oncology, particularly PDT [28-33]. For this purpose, transition metal Pcs are not applicable, and so attention is focused on

phthalocyanines containing non-transition metal centres. For PDT action, it is necessary that the drug be easy to administer via injection into the blood stream. As the blood itself is a water-based system, water solubility then becomes an essential requirement for a PDT drug. Additionally, the drug will have to traverse lipid membranes – consequently, it should also be lipophilic. One should then speak of a water-soluble lipophilic drug. The Pc macrocycle itself is lipophilic, and water solubility could be achieved by introducing sulphonate ions as ring substituents. Mixed-sulphonated aluminium phthalocyanine ($AlPcS_{mix}$) commercially known as Photosens® has been developed as a PDT drug in Russia, and has been used in hospitals with a fair measure of success [30].

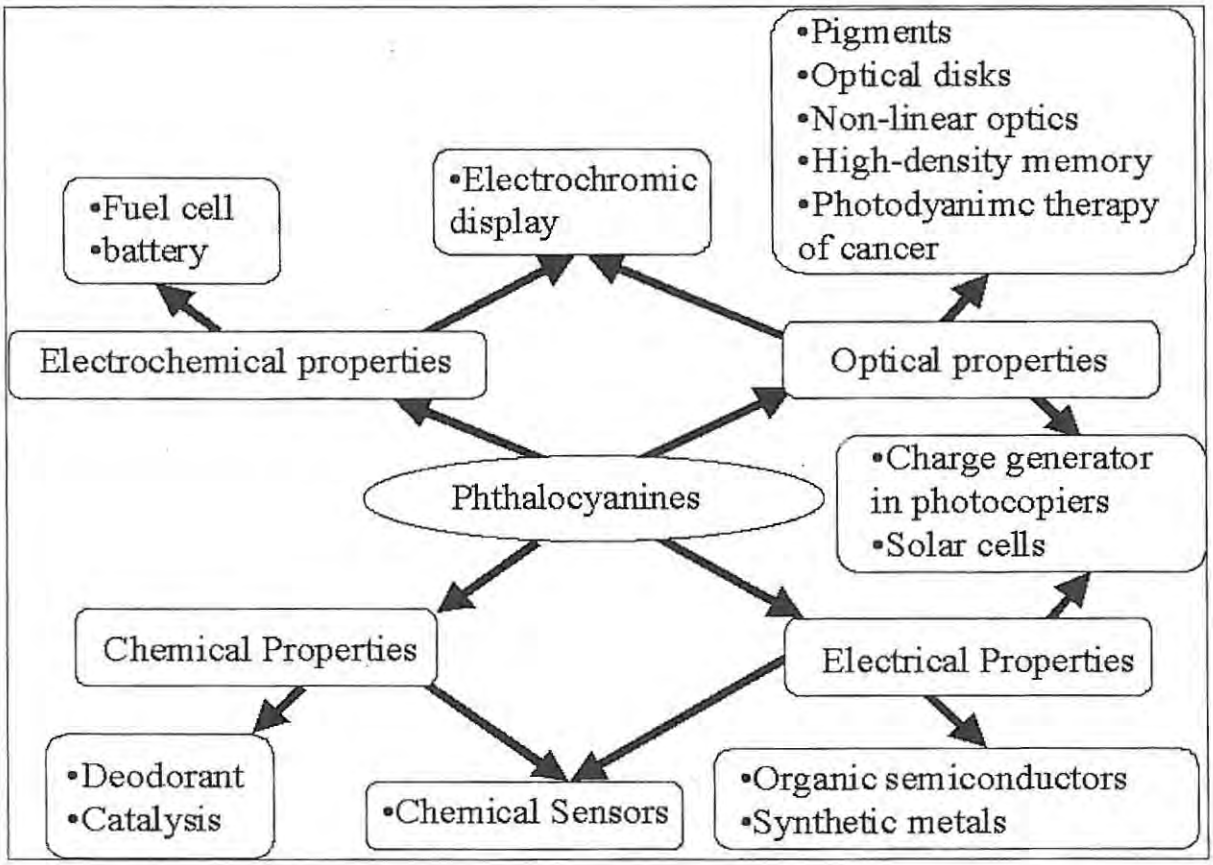

Figure 1.4: Actual and potential applications of phthalocyanines in the industry [34].

In summary, the potential industrial applications of Pcs can be represented by Fig. 1.4, with some overlaps among the various categories.

1.2.2 Electronic structure and spectroscopy of Phthalocyanines

The phthalocyanine molecule contains four isoindole groups, linked by four nitrogen atoms to form a symmetrical 18π electron conjugated aromatic macrocycle which is related to the naturally occurring porphyrins and possessing very high thermal and chemical stability. Pc (**2**) is known systematically as tetraazatetrabenzoporphyrin (TABP) (Fig. 1.3). Other related synthetic porphyrins include tetraphenylporphyrin (**3**, TPP), tetrabenzoporphyrin (**4**, TBP) and tetraazaporphyrin (**5**, TAP) (Fig. 1.5). Pc was discovered accidentally in 1907 by Braun and Tcherniac, as a by-product during the synthesis of o-cyanobenzamide [35].

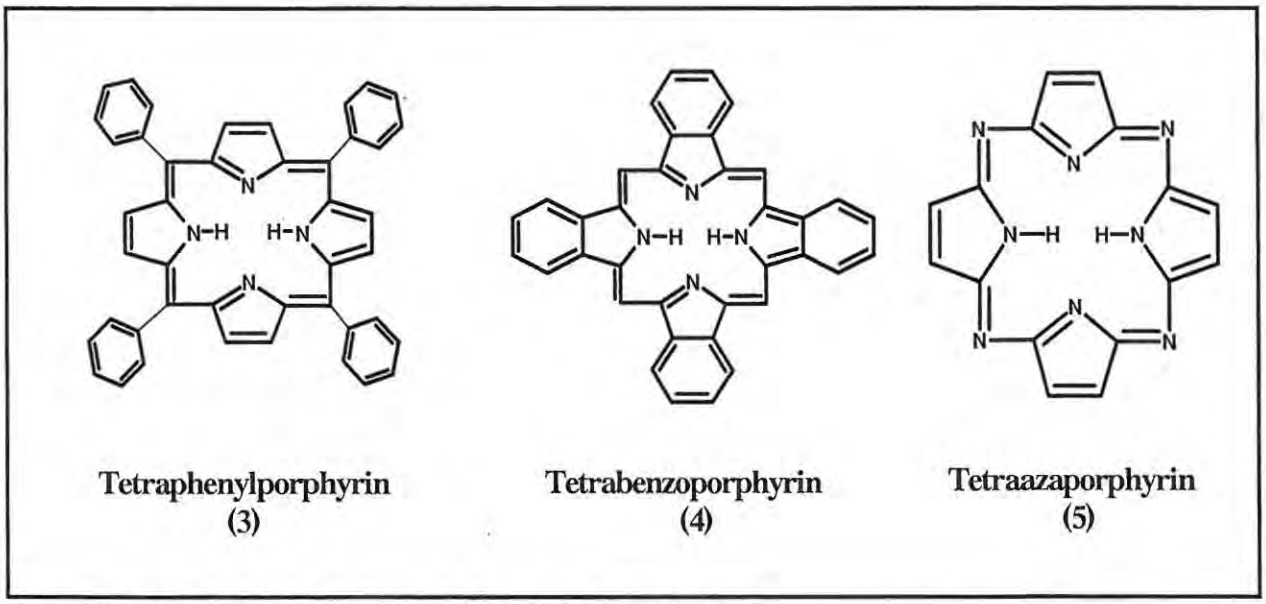

Figure 1.5: Molecular structures of synthetic porphyrins.

The phthalocyanine structure was only determined about two decades later by independent efforts of Linstead [36-39] and Robertson [40-42]. The X-ray diffraction analyses of Robertson also suggested the structure of metallophthalocyanine (MPc, **6**) (Fig. 1.6).

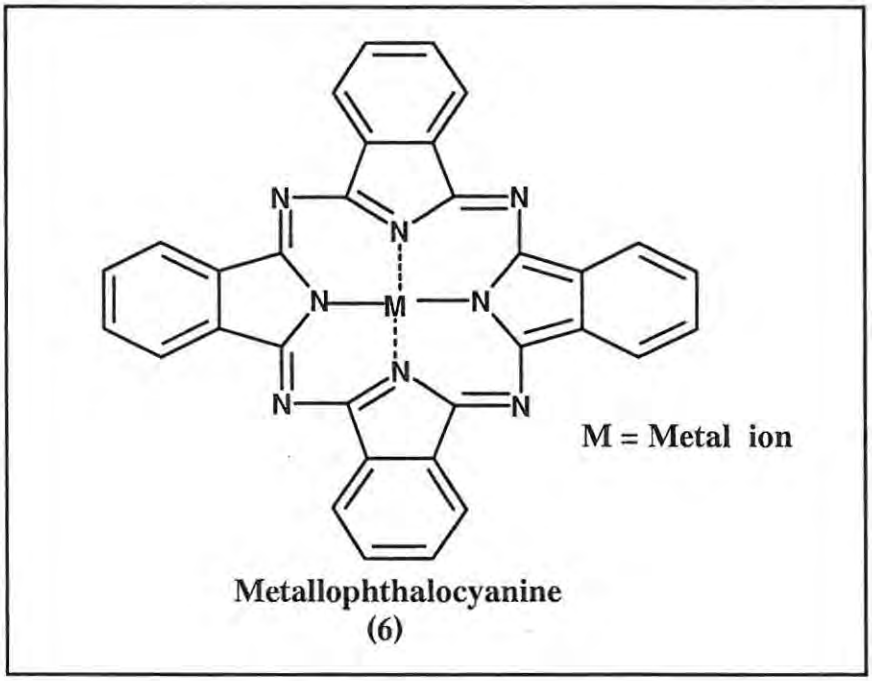

Figure 1.6: Molecular structure of metallophthalocyanines.

The four pyrrole nitrogens in the phthalocyanine structure form a cavity into which metal ions can bind by coordinate-covalent bonds between the metal and the nitrogens. Like the porphyrins, the Pc macrocycle can play host to over seventy different metal ions in its central cavity. In the absence of a metal ion, protons may bind to the negatively charged nitrogens, forming the so-called free base phthalocyanine (H_2Pc, **2**), Fig. 1.3. Other phthalocyanine analogues include subphthalocyanine (**7**) and naphthalocyanine (**8**) (Fig. 1.7).

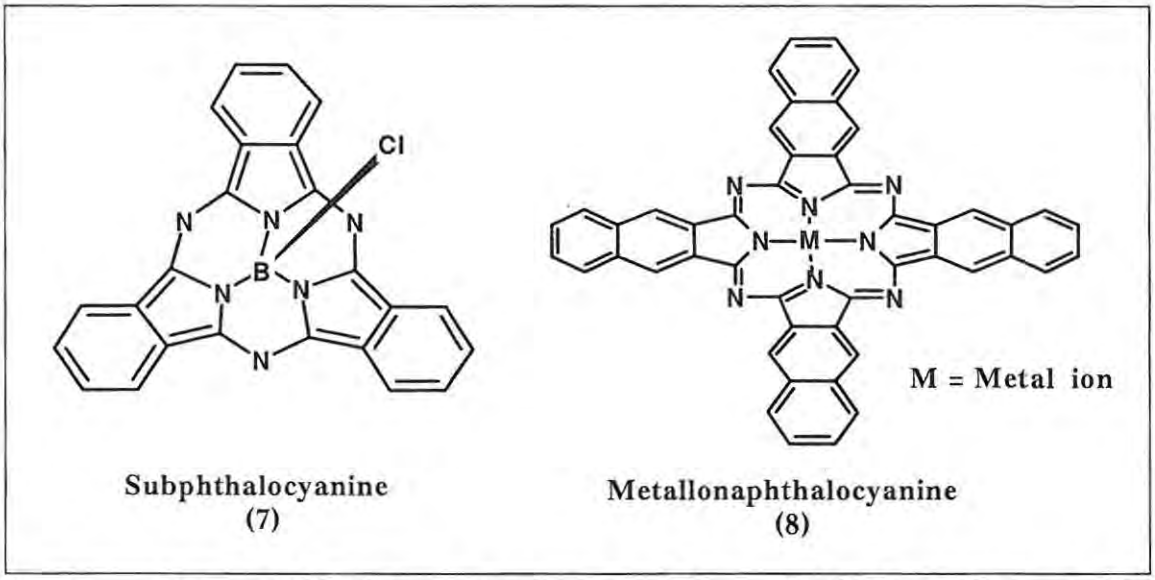

Subphthalocyanine (7)

Metallonaphthalocyanine (8)

Figure 1.7: Molecular structures of subphthalocyanine and metallonaphthalocyanine.

The geometry of the nuclear skeleton is almost perfectly square planar with a π-electron system of D_{2h} symmetry and C_2 axes in the x, y and z directions. The insertion of a metal into the cavity of the free-base phthalocyanine, while still maintaining the planarity of the molecules increases the symmetry from D_{2h} of H_2Pc to D_{4h} of MPc. The increase in symmetry is also reflected in the reduction in number of allowed electronic transitions within the molecule, resulting in spectra shown in Fig. 1.8.

However, some metals do not perfectly fit into the Pc cavity, in which case the symmetry drops to C_{4v}. For example in zinc phthalocyanines [43,44], zinc is displaced 45 pm from the plane of the aromatic ring, with Zn-N bond lengths of 206.1 pm, to form a domed shape. Also in tin phthalocyanine [45,46], tin is protruded out of the Pc cavity due to its ionic size. It is known [47,48] that the diagonal N-N distance is smaller in phthalocyanines (396 pm) than in most porphyrins (402 pm), which implies that in some

cases, metals that form planar porphyrin complexes will form square pyramids in phthalocyanine complexes.

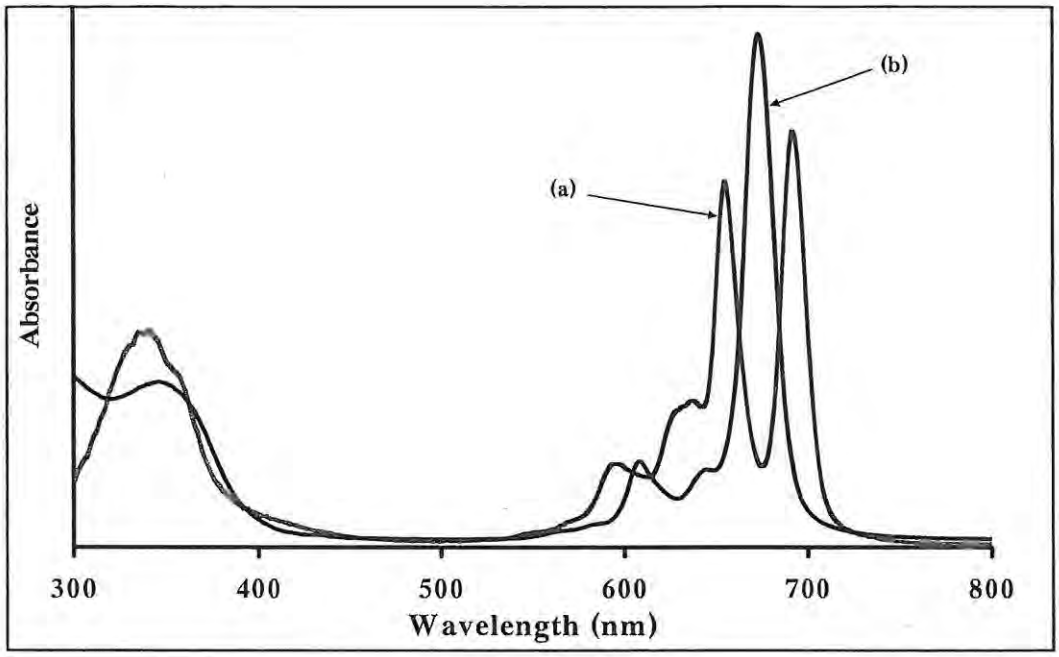

Figure 1.8: Ground state electronic absorption spectra of free-base phthalocyanine (a) and metallated phthalocyanine (b).

There have been several meticulous theoretical calculations and experimental data for the molecular orbitals of phthalocyanines; however, it is convenient to use the four-orbital model proposed by Gouterman's group [49-51]. Gouterman proposed that the spectral properties of porphyrin analogues may be understood qualitatively by considering four frontier orbitals: the HOMO-1, HOMO, LUMO and LUMO+1 orbitals. The first two are occupied (and nearly degenerate in porphyrins) while the last two are unoccupied and degenerate when the macrocycle is perfectly square planar. The introduction of an aza or benzo group into the porphyrin skeleton (resulting in an MPc) destroys the accidental degeneracy of the HOMO-1 and HOMO in the porphyrin [49,50,52] (Fig. 1.9).

The assignment of the ground state electronic absorption bands in MPcs may be done qualitatively on the basis of the Gouterman's model. The Q and B (Soret) bands both arise from π-π^* transitions and can be explained in terms of linear combination of transitions from a_{1u} and a_{2u} HOMO orbitals to the doubly degenerate e_g (LUMO) orbitals.

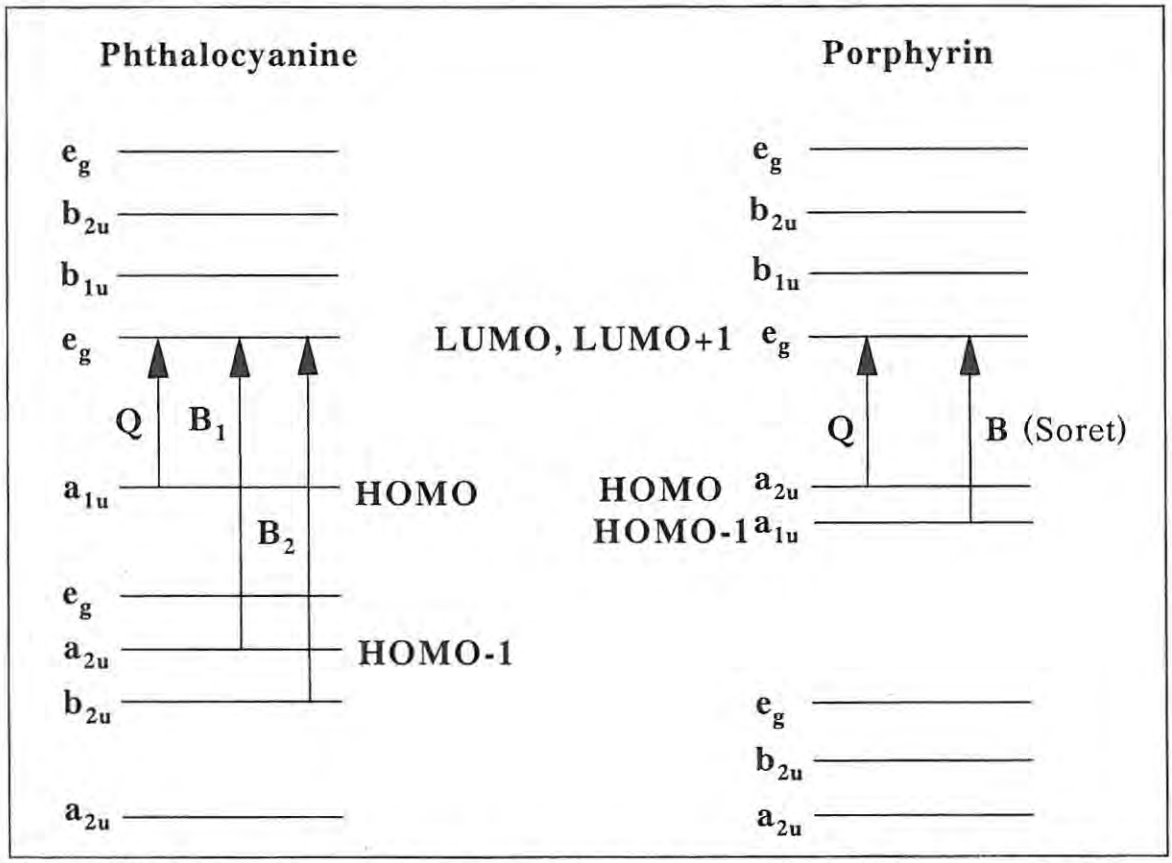

Figure 1.9: Electronic transitions in phthalocyanines and porphyrins – Origin of Q and B absorption bands.

The accidental degeneracy of the a_{1u} and a_{2u} orbitals of porphyrins is expected to lead to almost coincident absorption bands due to $e_g \leftarrow a_{1u}$ and $e_g \leftarrow a_{2u}$ transitions, but in fact these two transitions mix together by a process known as "configurational interaction", resulting in two bands with very different intensities and wavelengths (Fig. 1.10).

Constructive interference leads to the intense high-energy B band, while the weak low-energy Q band is a result of destructive interference.

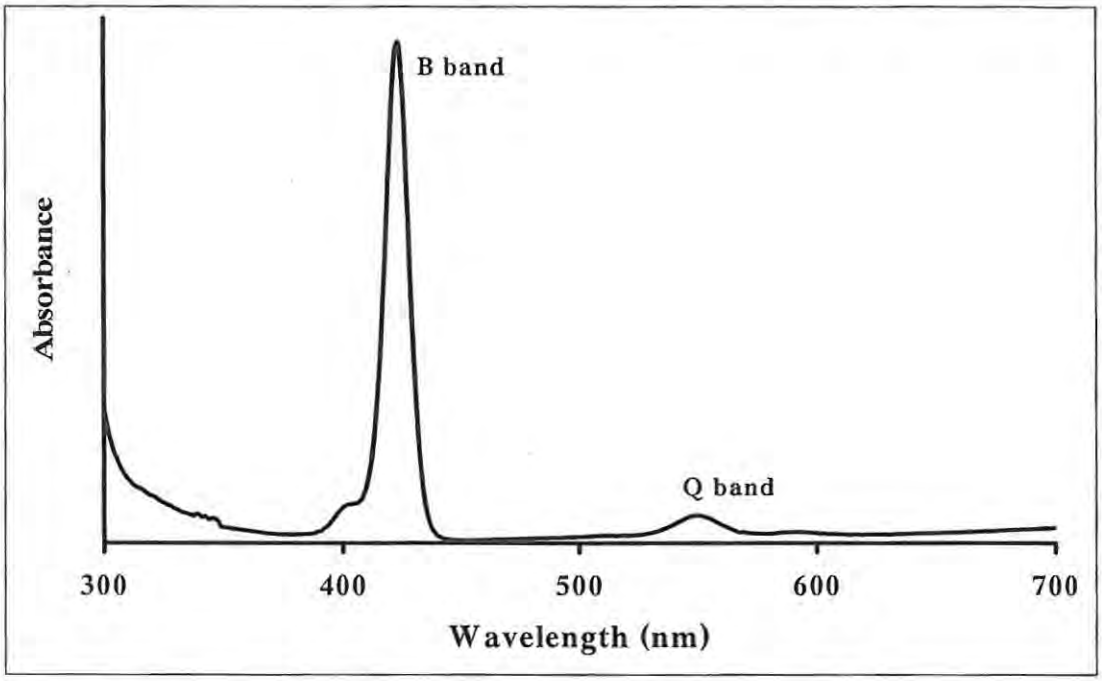

Figure 1.10: Ground state electronic absorption spectrum of *tetra*phenylzinc porphyrin (ZnTPP) in DMSO.

On the contrary in phthalocyanines, the a_{1u} and a_{2u} orbitals are widely separated, giving no room for configurational interaction. The Q and B bands are ~ 320 nm apart (Fig. 1.11).

The UV/vis spectrum of an MPc typically has a Q band near 670 nm with extinction coefficient greater than 10^5 L mol^{-1} cm^{-1}, and accompanied by a series of vibrational bands. It has been evidenced [53-57] that the Soret of MPcs is a superimposition of two bands B_1 and B_2 in the 350 nm expanse, especially in the absence of strong axial ligands. Additionally, three other transitions could be observed below 300 nm in the ground state

electronic absorption spectra of diamagnetic MPcs such as ZnPc and MgPc [43]. These give rise to the N, L and C bands in order of increasing energy respectively.

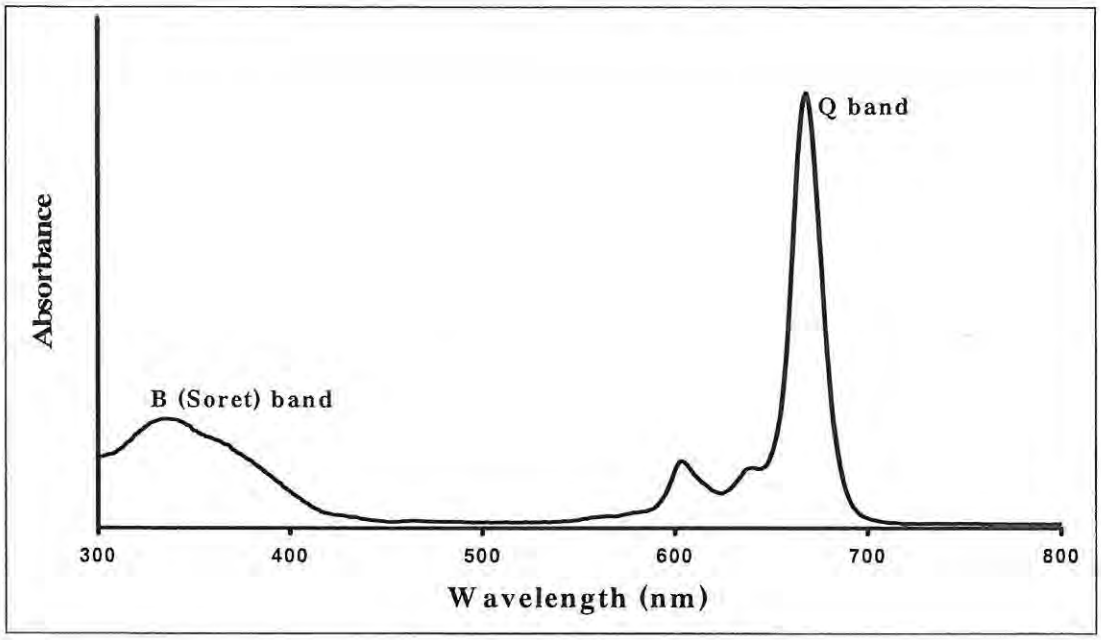

Figure 1.11: Ground state electronic absorption spectrum of zinc phthalocyanine (ZnPc) in DMF.

A tricky situation is also observed in the optical spectra of MPcs, which is due to the presence of non-bonding electrons on the azomethine nitrogens of the macrocycle. The n orbitals are proximal in energy to the π orbitals (HOMO) and consequently, the $\pi^* \leftarrow n$ transition is expected to be coupled with $\pi^* \leftarrow \pi$ transition. Huang *et al.* [58,59] proposed that the band around 605 in the optical spectra of MPcs could have a partial contribution from the $\pi^* \leftarrow n$ transition. This idea was supported by the clear observance of the 605 nm band in the spectra of oxidized and reduced MPc ions, in which case the normal $\pi^* \leftarrow \pi$ (Q and Q_{vib}) transition probabilities are drastically weakened around the 605 nm and 670 nm regions [60], but the 605 nm band does not change.

1.2.3 Methods of Phthalocyanine synthesis

1.2.3.1 Metal-free phthalocyanines

The earliest synthesis of phthalocyanine (**2**) was achieved by heating *o*-cyanobenzamide (**9**) in ethanol under reflux [35], to yield the blue product in low yield (Scheme 1.1a). Linstead and co-workers [36] later showed that better yields could be obtained if Mg^{2+} ions are mixed with **9**, the reaction mixture heated above 230 ^{0}C and the resultant metallophthalocyanine demetalated with conc. H_2SO_4 (Scheme 1.1b). However, an attempt to synthesize substituted phthalocyanine using this method was unsuccessful.

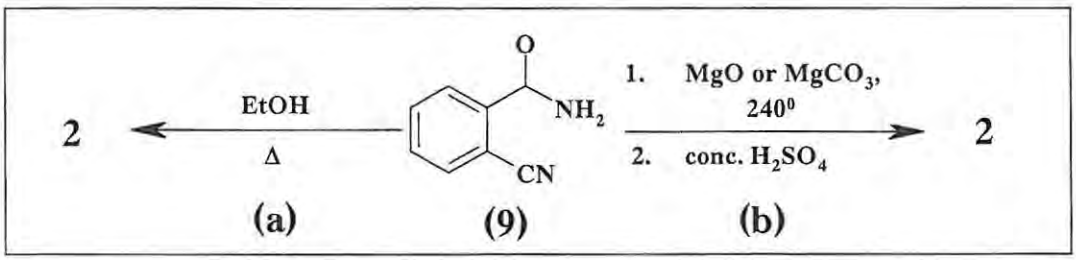

Scheme 1.1: Synthesis of metal-free phthalocyanines from *o*-cyanobenzamide.

Later studies showed that **2** can be synthesized by treating phthalonitrile (**10**) with an alkali metal *n*-pentoxide in alcoholic solutions at 140 ^{0}C (Scheme 1.2a). This reaction gave the alkali metal phthalocyanine, which was then demetalated to **2** with conc. H_2SO_4 [37,61]. A simpler method involved the treatment of **10** with ammonia gas in 2-*N*,*N*-dimethylaminoethanol to give **2** in very good yield [62] (Scheme 1.2b) . Phthalonitrile (**10**) can be fused with magnesium or sodium metal above 200 ^{0}C to give metallophthalocyanines [37,63], from which **2** can be obtained by acid treatment (Scheme 1.2c). In the presence of a reducing agent like hydroquinone, substituted phthalonitriles

(**10**) can be fused at 180 ^{0}C to give the corresponding substituted phthalocyanine in good yield, Scheme 1.2d.

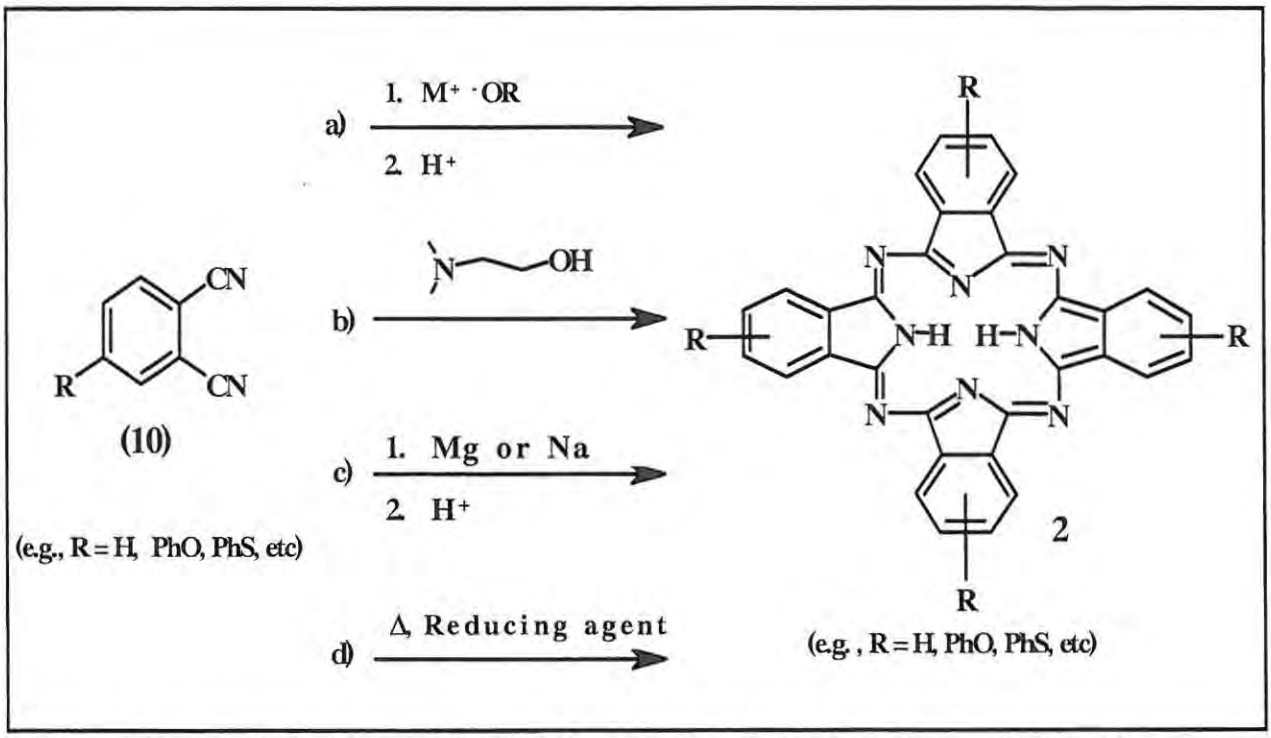

Scheme 1.2: Synthesis of metal-free phthalocyanine derivatives from substituted phthalonitrile.

1.2.3.2 Unsubstituted Metallophthalocyanines (Scheme 1.3; R = H)

Linstead and co-workers [37,63,64] first described the synthesis of metallophthalocyanines by heating a metallic salt with phthalodinitrile (**10**) in a high boiling solvent (Scheme 1.3a). This reaction was used for the synthesis of phthalocyanine pigments like copper phthalocyanine in industry. Phthalic anhydride (**11**) (or related compounds like phthalic acid, phthalimide and phthalamide) has been used extensively in the preparation of metallophthalocyanines (**6**) [65-68] (Scheme 1.3b). Alternatively, **6** could be prepared by refluxing **2** in the presence of a metal ion in organic solvents such as quinoline [69] (Scheme 1.3c). Tomoda *et al.* [69] reported that a variety of MPcs could

be prepared under mild conditions with strong organic bases such as 1,8-diazabicyclo [5.4.0] undec-7-ene (DBU) or 1,5-diazabicyclo [4.3.0] non-5-ene (DBN). The reaction involves heating to reflux a mixture of phthalonitrile (**10**) and a metal salt in the presence of DBU or DBN as catalyst, in a primary alcohol such as 1-pentanol (Scheme 1.3d). However, the products of these reactions usually lack purity, which calls for a vigorous purification procedure.

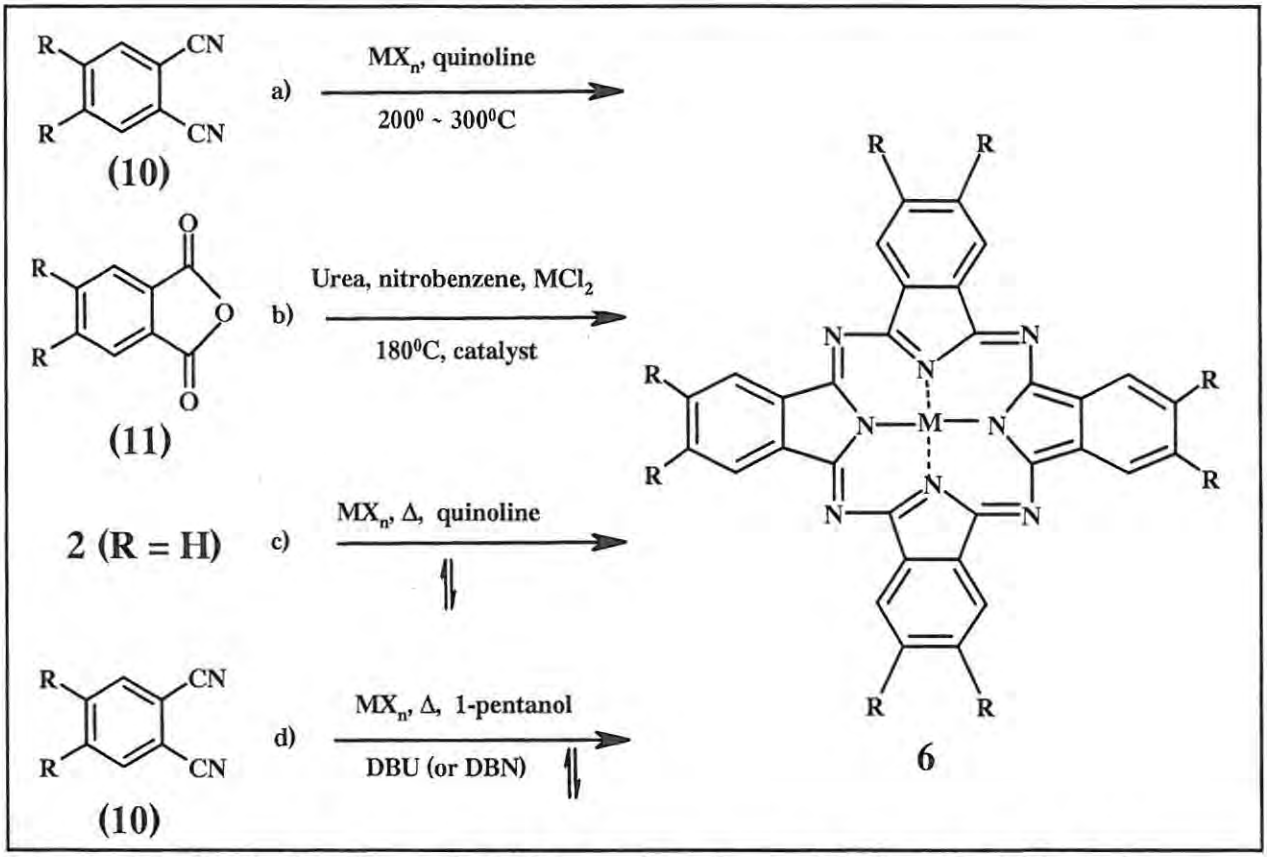

Scheme 1.3: Synthesis of metallophthalocyanines from phthalic anhydride and related compounds.

MPcs have also been prepared quickly and efficiently by the reaction of **10** with hydrated metal salts without solvents and under microwave irradiation [70,71] (Scheme 1.4).

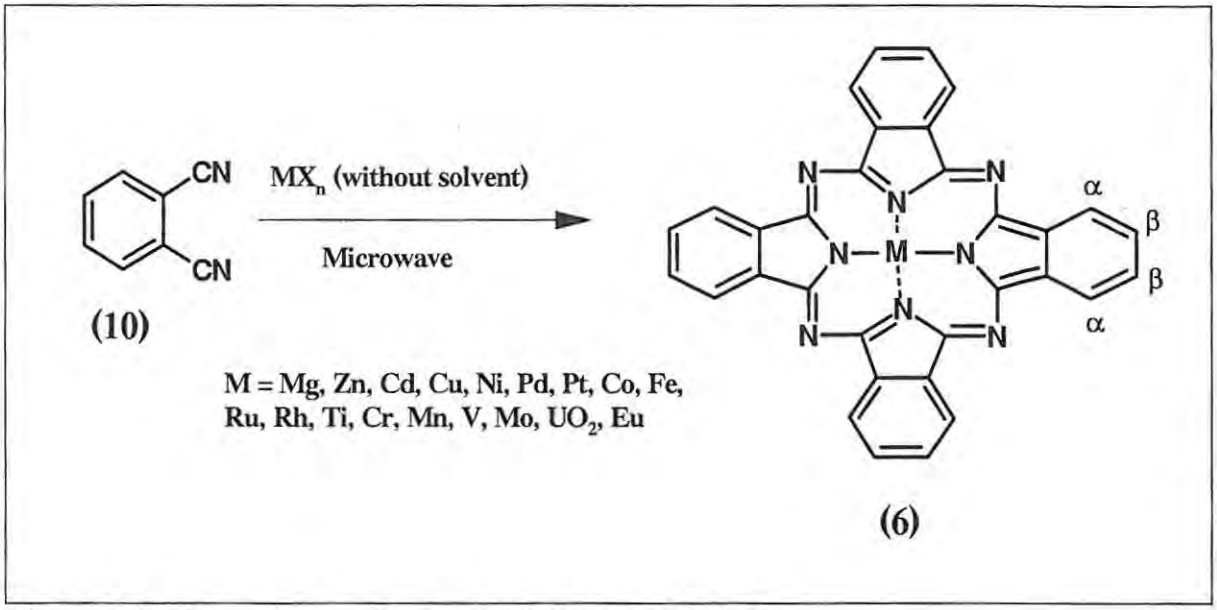

Scheme 1.4: Microwave synthesis of metallophthalocyanines

1.2.3.3 Ring-substituted MPcs (Scheme 1.3; R variable)

The most usual method of synthesizing ring-substituted Pcs is by cyclotetramerization of substituted phthalonitriles [72,73] (Scheme 1.3 a,d). If monosubstituted phthalonitriles are employed, tetrasubstituted Pcs are obtained, with the drawback of a mixture of positional isomers [72,74]. 4,5-Disubstituted phthalonitriles are used as starting materials for octasubstituted Pcs, with no problem of isomerism if the phthalonitrile substituents are similar [72,74-77]. The tetra- or octa-substituted Pc can now be metalated as described above (Scheme 1.3c). Weber and Busch [78] synthesized tetrasulphonated metallophthalocyanine complexes by reacting 4-sulphophthalic acid (**12**) and a metal salt in the presence of ammonium chloride, urea and ammonium molybdate, in nitrobenzene (Scheme 1.5).

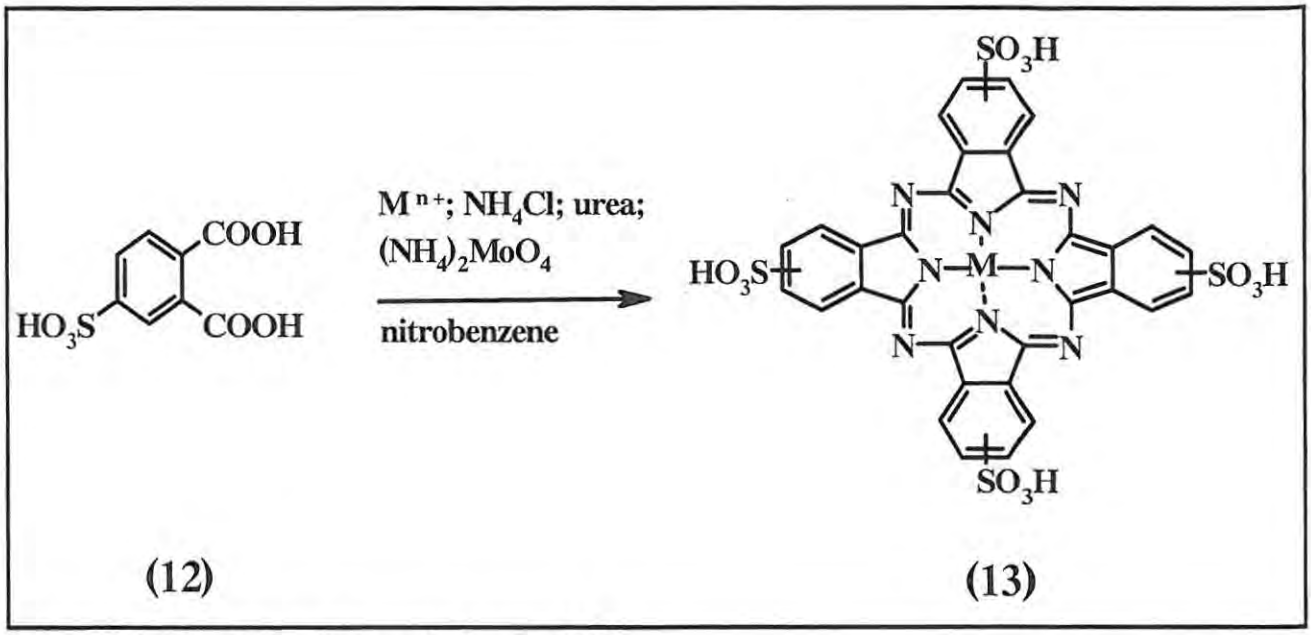

Scheme 1.5: Synthesis of tetrasulphonated MPc

The reaction of an unsubstituted MPc with fuming sulphuric acid or oleum at 100 ^{0}C gave a mixture of differently sulphonated MPcs [79]. The mixture was shown to contain mono-, di-, tri- and tetra-sulphonated MPc [79] (Scheme 1.6).

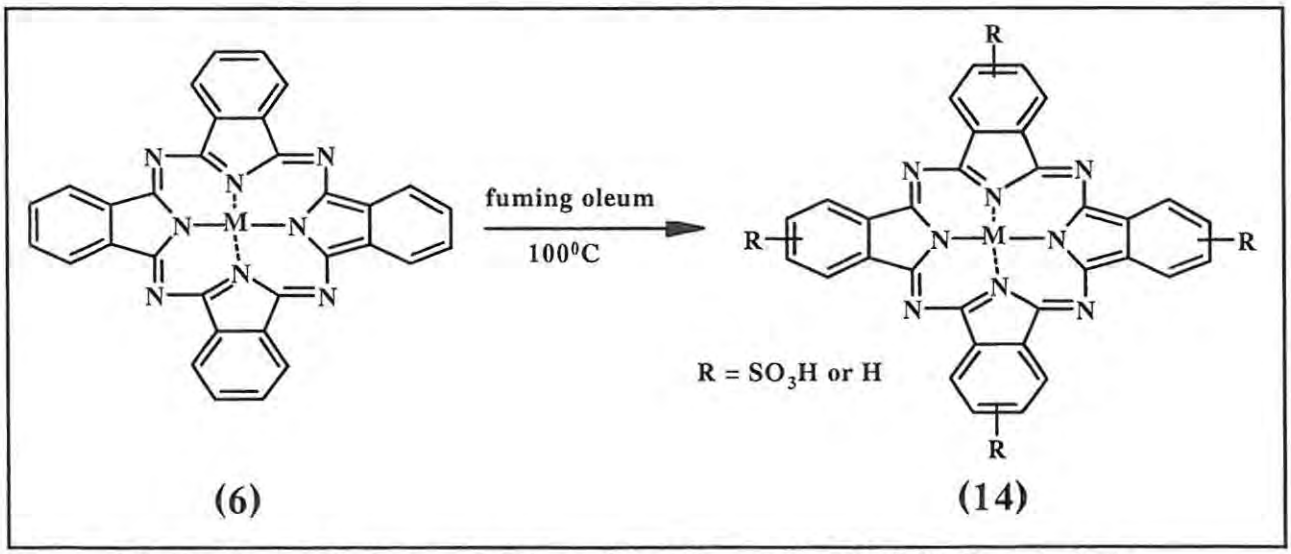

Scheme 1.6: Synthesis of mixture of differently sulphonated MPc (MPcSn; n = 1, 2, 3, or 4)

In this thesis, the photophysics, photochemistry and potential applications of sulpho-substituted Pc and other substituted Pcs will be explored.

1.2.4 Metallophthalocyanine aggregation

MPc aggregation is recognized by broadening and/or splitting of Q band, indicating the presence of additional electronic levels of the aggregates. The overlapping of energy levels leads to radiationless excited state deactivation, thus making aggregates photo-inactive. The aggregation behaviour of MPcs is well documented [80-84]. MPc aggregates could be formed in a number of ways, which include the following:

(a) Direct linkage or bridge between two or more Pc rings, where the rings are close enough in space to allow intramolecular association [85]

(b) Covalent bonding involving the metal as μ oxo links, especially for iron, manganese and silicon-containing Pcs [86].

(c) Sandwitch-type complex formation, whereby two Pc rings share one central metal [67, 87,88].

(d) Weak association in which peripheral substituents hold two Pc rings that are adjacent in space [89,90].

The degree of aggregation strongly depends on the metal inside the ring and the peripheral substitution at the benzo group [90,91]. For example, Pcs containing Si or Ge are not expected to form aggregates due to the presence of axial ligands on the metal, which tend to prevent π-π stacking between adjacent rings. It has been suggested [92] that π-π interactions between adjacent molecular rings stabilize columnar aggregates.

Aggregation tendency has been observed to be large in aqueous solutions for MPcs that contain substituents that impart water solubility, e.g., sulphonated derivatives [9,10,83,93]. However, aggregation in aqueous solution is very similar to that observed in the solid phase of tetrasulphonated copper(II)phthalocyanine [90]. In contrast, non-substituted copper(II)phthalocyanine molecules do not form dimers even in the solid phase [90]. In view of these results, it is obvious that the hydrophylic groups at the benzo group must play a crucial role in the aggregation.

MPc aggregation has a great influence on the intermolecular photoinduced processes, and it is easily characterised by a broadening and diminishing of the red absorption band, coupled with a blue shift of the band by 30 to 50 nm [94]. Aggregation can be overcome by either, synthesizing metallophthalocyanines in which the metal has an axial ligand such as chlorine, or by adding bulky peripheral substitution to prevent the phthalocyanine macrocycle aggregating by simple steric hindrance. Bulky peripheral groups prevent an effective π-π interaction between the phthalocyanine subunits [95]. Alpha substitution (see Scheme 1.4 for notation) has also been shown to hinder phthalocyanine aggregation [96]. Bulky α-substituents impose a steric constraint on the molecule, thereby restricting conformational freedom and consequently, obstructing the approach of a second molecule to form a coplanar dimer.

In this work, β-substituted MPcs are studied and their properties compared with those of unsubstituted MPcs. The effects of aggregation on the photosensitizing capabilities of the β-substituted MPcs are also examined.

1.2.5 Reactions of Metallophthalocyanines

Unsubstituted MPcs are generally impervious to chemical treatment. For example, heating to very high temperatures (> 500 ^{0}C) would not lead to the macrocycle's decomposition, with only a change of state (sublimation) being observed. Metal chelation with the four pyrrole nitrogen atoms of the macrocycle stabilizes the complex. Hence, metallophthalocyanines are more stable than their metal-free counterparts. However, a few reactions of MPcs have been observed and documented:

1.2.5.1 Redox reactions

These are the most notable of all MPc reactions. Oxidation and reduction can be achieved in three principal ways viz: electrochemical, photochemical and chemical. The Pc ring has a great propensity to undergo redox reactions and its redox behaviour dominates the redox chemistry of the complex, especially if the central metal is not electroactive, e.g. zinc. With electroactive metals like the transition metals, the redox chemistry of the complex becomes complicated, as there is need to distinguish the redox attributes of the metal centre from those of the ring. The redox activity of the Pc ring is directly associated with the frontier orbitals (HOMO and LUMO) in the molecule. Oxidation implies the removal of electron(s) from the HOMO while reduction means the addition of electron(s) to the LUMO. In the light of this, it is logical to think that there is a correlation between HOMO energy and the ease of oxidation; and the LUMO energy and the ease of reduction. The Pc skeleton exists as a dianion Pc(-2), and the removal of one and two electrons from the HOMO (a_{1u}) results in the formation of Pc(-1) and Pc(0) respectively.

For Pc reduction, up to four electrons can be added to the LUMO, terminating in Pc(-6) species (Table 1.2), since the e_g orbital is degenerate.

Table 1.2: Electronic description of phthalocyanine oxidation states

Species	Pc(0)	Pc(-1)	Pc(-2)	Pc(-3)	Pc(-4)	Pc(-5)	Pc(-6)
G.E.C	$(a1_u)^0(e_g)^0$	$(a1_u)^1(e_g)^0$	$(a1_u)^2(e_g)^0$	$(a1_u)^2(e_g)^1$	$(a1_u)^2(e_g)^2$	$(a1_u)^2(e_g)^3$	$(a1_u)^2(e_g)^4$

G.E.C – Ground state electronic configuration.

Electrochemical oxidation/reduction of the Pcs involves the deliberate application of potential to the electrode. Electrodes used in electrochemistry are composed of metals, or metal-like materials. In these materials there are no distinct orbitals, but continuous bands of energy that the electrons can occupy. Like the HOMO in a molecule, there is a Fermi level in a metal. All the energy levels below the Fermi level are occupied at O K. When one applies a negative potential to the electrode, the Fermi level moves to higher energy (higher tendency to reduce the analyte). On the other hand, application of a positive potential moves the Fermi level to lower energy (higher tendency to oxidize the analyte) (Fig. 1.12). If the HOMO energy of the Pc molecule is increased, oxidation is favoured, while a lowering of the LUMO energy favours reduction. The literature on electrochemical redox processes of Pc is robust [97,98] and the rich electrochemistry of Pcs is exploited in many applications.

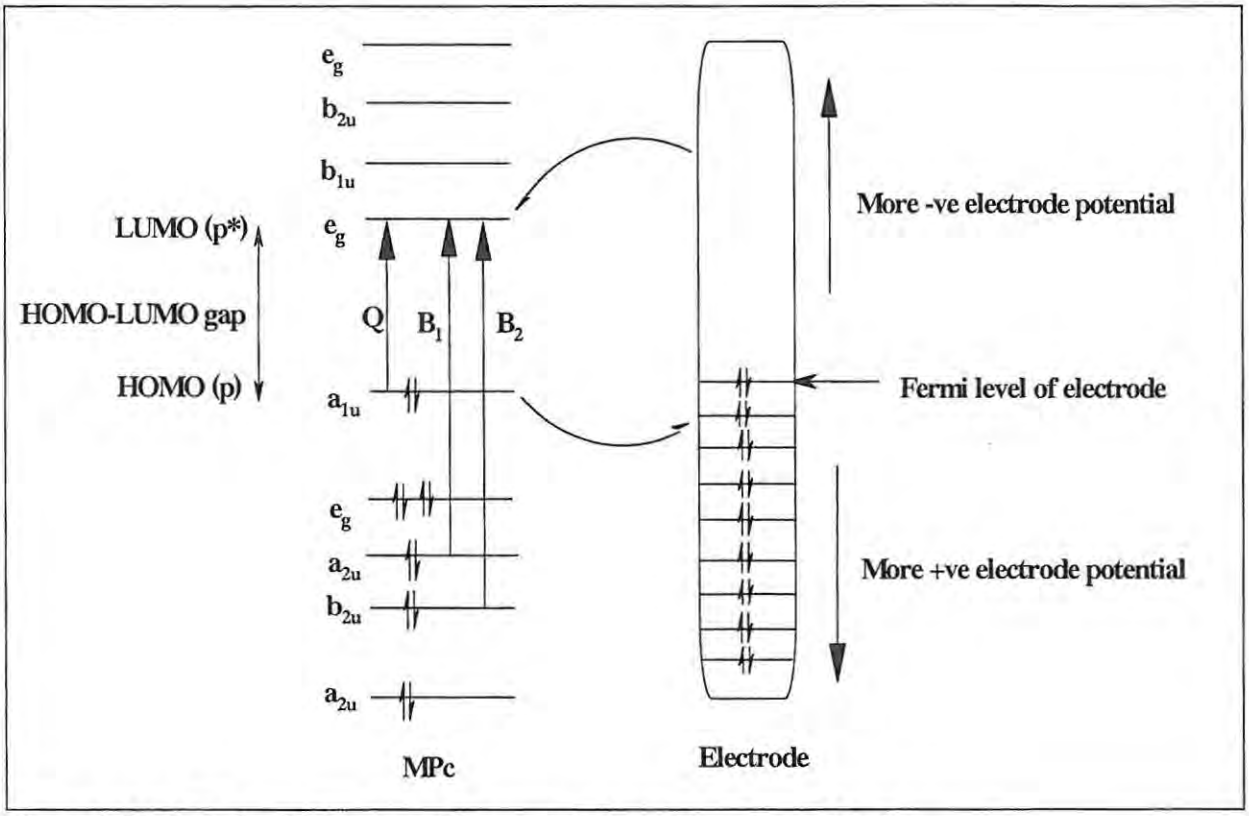

Figure 1.12: Relation between redox potentials and frontier orbitals.

Photochemical redox reactions of Pcs are carried out at room temperature using visible-wavelength light and an electron donor or acceptor. In the photo-assisted reduction, Stillman's group used hydrazine as the electron donor and CBr_4 as electron acceptor in organic solvents [43, 99-103]. However, it was very difficult to obtain stable solutions of the oxidized and reduced species despite degassing the solutions before the experiments. Chemical reduction of MPcs has been achieved by direct reaction with a strong reducing agent (alkali metal film in an air-free vial) to give the reduced species [104-106].

1.2.5.2 Decolouration and destruction in aqueous solutions

The destruction of MPcs (M = Co, Fe) in aqueous solutions has been reported [107]. These reactions take place in the presence of an alkali and a stream of oxygen, and are oxidative in nature.

1.2.5.3 Reaction with ligating agents

Most MPc complexes interact with a variety of molecules such as pyridine [108], cyanide [109], carbon monoxide [110] and imidazole [111], to form axially coordinated species. Axial ligand displacements have also been reported, and are known to be dissociative and occur in stepwise manner [108,110,111].

1.2.5.4 Reaction with acids

The reaction of MPcs with acids leads to a successive protonation of the azomethine nitrogens. These reactions have been studied using dilute or concentrated sulphuric acid, HCOOH, HSO_3Cl [112-115], CF_3COOH [116] and a mixture of H_2SO_4 and CF_3COOH [117,118]. MPc protonation has also been observed from reaction with Lewis acids [119,120] in organic solvents. A harsh acid treatment on MPcs leads to substitution reactions at the benzo rings. For example, sulphonated MPcs are usually synthesized by heating the MPc in oleum or fuming sulphuric acid at 100 ^{0}C [79] (Scheme 1.6). The stepwise protonation of the MPc ring gives rise to characteristic successive bathochromic shifts of the Q band [121,122], with the tetra-protonated species absorbing about 170 nm to the red of the unprotonated Pc [123]. These protonated species have been found to be fluorescent and their emission spectra are also red shifted, compared with those of the

unprotonated Pcs [123]. However, the fluorescence quantum yield and lifetime are reduced on protonation [123]. An interesting feature in the spectra of the protonated species is the change in symmetry accompanying consecutive protonation. Theoretical investigations of the Pc [116,124] using a four orbital model, describe the spectral changes upon protonation. It has been shown that monoprotonation leads to a reduction in symmetry from D_{4h} to C_{2v}, resulting in a splitting of the Q band. Di (*trans*)- and tri-protonation results in a splitting of the Q band due to C_{2v} or D_{2h} symmetry while the Q band of the diprotonated *cis* form is not expected to split [119]. Tetraprotonation reverts back to the D_{4h} symmetry and only one Q band is predicted.

Apart from input by Beeby's group and a few others [121,123,125,126], literature is very sparse on the effects of protonation on the photophysicochemical properties of MPcs. Beeby *et al.* [123] demonstrated that protonation reduces the energy of the excited states and their lifetimes. In particular, the triplet energy is lowered to a value where energy transfer to ground state oxygen is no longer favourable. This work investigates the effects of substituents, solvents and acid strength on the ease of protonation of MPcs with various ring substituents and axial ligands; as well as the effects of protonation on the photophysicochemical properties (e.g. fluorescence quantum yield, Φ_F; singlet oxygen quantum yield, Φ_Δ; and photodegradation quantum yield, Φ_{Pd}) of the complexes.

1.2.6 Solvent effects on MPc spectra

The wavelength and intensity of absorption bands are both affected when a molecule is in a solvent environment compared with its spectrum in the gas phase. This is due to the

unequal perturbation of the ground and excited electronic states of the molecule, which depends on the nature of the solvent-solute interactions in the two states. Solvent effects on spectra of organic molecules have been linked with a range of solute and solvent properties. For example, solvents effects were used to distinguish between $\pi^* \leftarrow \pi$ and $\pi^* \leftarrow$ n transitions [127,128]; changing from a non-polar solvent (e.g., hexane) to a polar solvent (ethanol) results is a shift of the ($\pi^* \leftarrow$ n) band to shorter wavelengths (blue shift), and the ($\pi^* \leftarrow \pi$) band to longer wavelengths (red shift) [127]. The observed solvent shifts in the aromatics were also attributed to hydrogen bonding, which tends to cause electron migration in the solute molecule [129]. Solvent effects have also been ascribed to the stabilization of preferred resonance structures in the solute by certain solvents due to their dielectric constants and their acid-base properties [130,131].

The shifts in the absorption wavelength are often interpreted in terms of the dielectric constant (relative permittivity) and refractive index of the solvent. A qualitative account of these effects in terms of dipole, polarization and hydrogen-bonding forces has been given [132].

The interpretation of solvent effects is difficult because they are often small and not easy to measure precisely and also because they are often the result of several individual effects which sometimes reinforce one another and sometimes cancel out. All organic solution spectra are subject to a general polarization red shift. The electromagnetic field of the absorbed light induces in the solute molecules an electric dipole moment, which oscillates at the same frequency of the incident field; the 'transition dipole' thereby formed induces a momentary polarization in the solvent molecules. The solute's excited

state, now polar, experiences a greater stabilization from the solvent than the ground state, the result being a red shift in the spectrum.

Superimposed on the polarization red shift are other shifts due to the fact that the solute molecule, in accordance with the Franck-Condon principle, at the instant of excitation is not in equilibrium and is therefore in a state of strain with respect to its environment. This Franck-Condon strain can be related partly to the polarity of the solute and solvent molecules and the changes in dipole moment of the solute during the transition (orientation strain); and partly due to parking strain arising from changes in the dimensions of the solute due to the excitation.

It has been suggested [133,134] that the interaction between coordinating solvents with Pc molecules stabilizes the LUMO of the complexes. The band positions in titanium(IV) phthalocyanine (Ti(IV)Pc) complexes were red shifted as the polarity of the solvent increased for non-coordinating solvents, with the magnitude of the red shift following the order hexane < toluene < chloroform < 1-chloronaphthalene. The electronic absorption spectra of MPc complexes in various organic solvents have been analysed using the method originally described by Bayliss [135] (Eq. 1.10),

$$F = \frac{n^2 - 1}{2n^2 + 1} \qquad \text{(Eq. 1.10)}$$

F is the polarizability function and n, the solvent's refractive index.

The positions of the Q band absorption of Ti(IV)Pc complexes showed a linear dependence on the function F in Eq. 1.10, suggesting that the shifts were caused mainly by solvation [133].

The effect of solvents and the environment on MPc fluorescence spectra are complex, and there is no simple theory which can account for all these effects. Spectral shifts result from the general effects of solvent polarity whereby the energy of the excited MPc decreases with increasing solvent polarity. This effect is usually accounted for by the Lippert equation (Eq. 1.11) [136].

$$\bar{\nu}_A - \bar{\nu}_F = \frac{2}{hc}\left(\frac{\varepsilon - 1}{2\varepsilon + 1} - \frac{n^2 - 1}{2n^2 + 1}\right)\frac{(\mu_E - \mu_G)^2}{a^3} + \text{constant} \quad \text{(Eq. 1.11)}$$

Where $\bar{\nu}_A$ and $\bar{\nu}_F$ are the wavenumbers (cm^{-1}) of the absorption and emission, respectively; h, the Planck's constant; c, the speed of light; and a, the radius of the cavity in which the absorbing molecule resides. ε, n and μ are solvent parameters – dielectric constant, refractive index and dipole moment, respectively while the subscripts 'E' and 'G' denote the excited state and ground states respectively.

Spectral shift can also occur due to specific fluorophore-solvent interactions and due to charge separations in the excited state, as polar solvents are expected to support charge separation while non-polar solvents are not. Absorption spectra are generally less sensitive to solvent polarity than emission spectra. This is because absorption of light occurs in about 10^{-15} s, a time which is too short for motion of the absorbing molecule or solvent. Absorption spectra are not affected by the post-absorption decrease in the excited-state energy.

The effects of solvents on the photophysical and photochemical properties of MPcs have not been fully explored. Thus this thesis studies the effects of a wide range of solvents on the photophysical and photochemical properties of selected MPc complexes.

1.2.7 Photophysics and photochemistry of MPcs

The literature on photophysics and photochemistry of MPcs is very extensive. As earlier stated, MPc species show a strong absorption in the red region (Q band) of the solar spectrum ($\varepsilon \sim 10^5$ M^{-1} cm^{-1}) and a moderately intense (broader) one in the near-UV region (Soret or B band). When an MPc molecule is irradiated at its Q band maximum, the excited triplet state is populated (as a result of intersystem crossing from the excited singlet state). The efficiency of this intersystem crossing is quantified by the triplet quantum yield (Φ_T), which in turn is determined by flash photolysis. The T_1(MPc) state absorbs in the region 450-500 nm, with ε values of $\sim 10^4$ M^{-1} cm^{-1}. Both the S_1(MPc) and T_1(MPc) states undergo radiative and non-radiative deactivation processes and fall back to the ground state (S_0), as described in the Jablonski diagram (Fig. 1.1).

1.2.7.1 Fluorescence and triplet lifetimes (and quantum yields) of MPcs

The lifetime of an excited state is defined as the time taken for the concentration of the molecules in that state to decrease to 1/e of its original value. The usual lifetime of the first singlet excited (S_1) state of MPcs is of the order a few nanoseconds (ns), and is strongly dependent of factors which include: (i) the nature of the central metal ion, (ii) nature of peripheral and/or non peripheral substituents, (iii) nature of the solvent and (iv) the presence of other species interacting with the molecule in the S_1 state. The typical lifetime a T_1(MPc) state ranges between the microsecond (μs) and millisecond (ms). The $T_1 \rightarrow S_0$ transition is forbidden; and this is responsible for the longer lifetime if the T_1(MPc) state. The metastable nature of the T_1 state makes it a good candidate for sensitization and photochemistry. The S_1(MPc) state is deemed too short-lived for any

substantial sensitization or chemical reaction. During the lifetime of the T_1 state, the molecule is more susceptible to non-radiative deactivation or quenching than luminescence. As a result, MPc phosphorescence is not readily observed in solution at room temperature. MPc phosphorescence can mainly be observed by trapping the T_1 state in a rigid glass (matrix) [43].

Fluorescence and intersystem crossing are two complementary photophysical processes. Hence in Table 1.3, high Φ_F values are accompanied by low Φ_T values for the MPc complexes. The nature of the central metal ion has a great effect on Φ_F and Φ_T values; heavy metal ions and paramagnetic metal ions enhance the yield of the triplet state. The paramagnetic effect, as anticipated, shortens the lifetime of the triplet excited state (τ_T), due to the presence of low-lying d-orbitals, which promote the quenching of the T_1 state by charge transfer processes; the same features that promote $T_1 \leftarrow S_1$ transition, would also promote the $S_0 \leftarrow T_1$ transition. In particular, MPcs in which M is a paramagnetic transition metal ion (e.g. Cu^{2+}, Cr^{2+}) posses very short τ_T values (Table 1.3).

MPcs show higher Φ_T values than the metal-free Pc. Apart from the heavy atom effect, other factors like molecular rigidity and solvent type have also been reported to influence MPc fluorescence and intersystem crossing. For instance, solvents like chloroform and carbon tetrachloride, which contain heavy Cl atoms, tend to promote intersystem crossing; hence fluorescence would be weak in such solvents.

Again, features that impart greater rigidity on the macrocycle, are expected to make it more fluorescent, as there exists a less likelihood of electronic energy 'leaking out' non-radiatively. This explains why the Φ_F value of silicon naphthalocyanine (SiNPc, 0.38) is

higher than that of silicon phthalocyanine (SiPc, 0.18) [137]. The fusion of an extra benzo group in SiNPc makes the molecule more rigid.

Table 1.3: Photophysical properties of some metallophthalocyanines [138].

Compound	τ_S (ns)	Φ_F	τ_T (μs)	Φ_T
H_2Pc	6.0	0.70	140	0.14
H_2TSPc	9.8	0.62	170	0.22
ZnPc	3.8	0.30	-	-
ZnTSPc	2.9	0.32	245	0.56
AlClPc	6.8	0.58	500	0.40
AlTSPc	5.3	-	500	-
CuPc	-	-	0.035	> 0.70
CuTSPc	-	$< 10^{-4}$	0.065	0.92
CrPc	-		0.02	-

Much has been reported on the photophysics and photochemistry of MPc derivatives [76,77,139-143], however there is still ample room for literature expansion in this area. For example, the photophysics and photochemistry of MPc complexes of silicon, germanium and tin, though, present in the literature [76,139,140], are yet to be fully explored; there is no account of the photophysicochemical studies of water-soluble derivatives of these complexes. Again, the zinc analogues, although, well documented [77,143-145], have not been studied in a systematic manner. This work gives an in-depth

account of the effects of substituents, solvents and different metals on the photophysical and photochemical properties of various MPc derivatives. The prospects of their relevance in PDT and other applications are also examined.

1.2.7.2 UV (versus visible) irradiation of MPcs - Photophysical and photochemical consequences

The photophysicochemical consequences of UV irradiation of MPc complexes were well reviewed by Tokumaru [146]. Red visible light irradiation of MPc complexes leads to the population of the S_1(MPc) state, while UV irradiation populates higher excited states (S_2 and higher). UV light irradiation is known to result in more efficient reactions than red light irradiation [147,148]. For example, it was found that red light irradiation of copper(II) tetrakis(*N*-octyldecylsulfamoyl)phthalocyanine in chloroform did not give any product but UV irradiation led to substitution of the $CHCl_2$ group (from the solvent) on to the Pc ring [149]. Also, rhodium(III) acidophthalocyanine ($Rh^{III}Pc(CH_3OH)X$; X = halide) in acetonitrile, in the presence of 2-propanol under UV irradiation and xenon flash light (~ 600 nm) oxidized 2-propanol to acetone more efficiently than when red light was used [150,151]. It was also found that zinc(II) tetrasulphophthalocyanine (ZnTSPc) was stable towards visible light but degraded under strong UV irradiation [152]. A lot more has been reported on the photochemical behaviour of ZnTSPc; for example, Nishimura *et al.* [153] observed no result when an acetonitrile solution of ZnTSPc was irradiated with red light in the presence of triethanolamine; but ZnTSPc was reduced when UV irradiation was used. Transient absorption showed that the T_1(ZnTSPc) state was not quenched by the amine, and so the reactive species was presumed to be a higher excited singlet state.

Kaneko *et al.* [154] also observed similar results for ZnTSPc and CuTSPc in aqueous acetonitrile and in the presence of amines (triethanolamine, triethylamine and ethylenediaminetetraacetic acid). Irradiation of ZnTSPc and CuTSPc at 365 nm resulted in the macrocycles' reduction. 656 nm irradiation did not induce such a reaction, and the mechanism of the reaction was discussed in terms of the participation of a higher excited singlet state of the macrocycles. In a similar manner, α-octabutoxyphthalocyanine (α-$H_2(OBu)_8Pc$) was reduced by triethanolamine under UV irradiation, but not with red light [154].

With UV excitation, ZnTSPc (in aqueous acetonitrile) and α-$H_2(OBu)_8Pc$ (in ethanol) fluoresce at 450 nm and 440 nm, respectively and with quantum yields of 0.038 and 0.013 respectively. Whereas with red excitation, their fluorescence occurred at 680 nm ($\Phi_F = 0.31$) and 788 nm ($\Phi_F = 0.19$) respectively [155]. There is also a report [156] that α-octaalkoxyphthalocyanines (α-$H_2(OR)_8Pc$, where R = OC_2H_5, OC_3H_7, OC_4H_9, OC_5H_{11} and $OC_{10}H_{21}$), on UV excitation in ethanol, fluoresce at ~ 420 nm, but with considerably lower quantum yields than those of red fluorescence. The triplet quantum yields with UV- and red-excitations were found to be 0.53 and 0.44, respectively, for the (α-$H_2(OR)_8Pc$ molecules. The higher Φ_T value with UV excitation was ascribed to the presence of an additional pathway for intersystem crossing from the higher excited singlet state. Accordingly, this state rapidly undergoes intersystem crossing to a higher triplet state at a higher rate than the competing internal conversion to the S_1 state. This also explains the observed lower Φ_F values with UV excitation than those with red excitation.

Generally, an increase of energy gap between the lowest and a higher excited state tends to reduce the rate constant of deactivation from the higher to the lower state; this lengthens the lifetime of the higher state, therefore making the state more susceptible to reactions with other species [146]. Photochemical irradiation of MPcs with UV light populates their higher excited states, which rapidly dissipate in a unique manner different from the lowest excited states (populated under visible light irradiation of the Q band). The higher excited states often exhibit characteristic emission and enhanced reactivity via electron transfer, energy transfer, etc, competing with rapid fluorescence. This is an exception to the Kasha-Vavilov rule, which states that the quantum yield of luminescence is independent of the excitation wavelength. In almost every case in which an MPc has been used to sensitize a photo-reaction, it is the excited triplet state that is active [145]. The longer lifetime of the T_1(MPc) state compared with that of the S_1(MPc) or S_n(MPc) state is a significant advantage since at a given concentration of quencher the number of diffusional encounters between a molecule in an excited state and a quencher molecule increases as the lifetime of the excited state increases.

This work will concentrate on visible irradiation for the study of photophysical properties of sulpho- and other substituted MPc complexes. As earlier stated, the effects of substituents and solvents will be investigated.

1.2.8 MPc fluorescence quenching

The study of fluorescence quenching using phthalocyanine compounds (which are related to biologically important chlorophyll) is of interest. In plants, chlorophyll is responsible

for trapping the solar energy that will be used to make sugars. Once extracted from plants, chlorophyll no longer has the ability to trap energy to make sugars, and the energy is emitted and observed as fluorescence. It is possible to block this fluorescence by adding a compound that interacts with the excited chlorophyll molecules, thus reducing the intensity of light emitted as fluorescence. As in chlorophyll, the process of MPc fluorescence quenching permits the capture of solar energy and storage for subsequent use for other purposes. There are two main modes of fluorescence quenching namely energy transfer (ET) and charge transfer (CT). Energy transfer is only possible if the energy of the fluorophore's excited state is greater than that of the quencher, while the possibility of charge transfer could be determined by considering the electrode potentials of the couples involved in the charge transfer process. It is known from the literature that the following compounds efficiently quench MPc fluorescence: azaferrocence [157], methyl viologen [158,159], benzoquinone [160], and hydroquinone [159] to mention but a few.

MPc fluorescence quenching by CT is well documented [157,159,161]. The suitability of a particular substance as an MPc fluorescence quencher by CT could be predicted from a comparison of the redox potentials of the excited MPc and the supposed quencher. For example, the triplet state of sulphonated aluminium phthalocyanine, T_1(AlPcS), did not react with methyl viologen (MV), benzyl viologen (BV) and anthraquinone-2,6-disodium sulphonate (AQDS) [159], because the redox potential of the *AlPcS/AlPcS$^{\cdot+}$ (triplet) couple is ~ -0.02 V, while the redox potentials of MV, BV and AQDS are -0.44 V, -0.36 V and -0.33 V respectively. Whereas the *AlPcS/AlPcS$^{\cdot+}$ (singlet) couple has a redox potential of ~ -0.63, and so its reaction with the quenchers is feasible.

Fluorescence quenching of differently substituted MPcs using benzoquinone (BQ) and hydroquinone (HQ) in different solvents will be explored in this thesis. The use of fluorescence quenching techniques for the determination of MPc fluorescence lifetimes is not known in literature, and is reported in this thesis.

The chemistry of light harvesting and energy transducing molecular arrays has attracted a lot of attraction over the years because of their ability to mimic the function of chlorophyll in artificial photosynthesis [162,163]. These molecular arrays have also found use as light harvesters in molecular phototonics [163-165]. Ideally, a light harvesting system should be able to capture solar energy over a broad spectral range and channel the energy swiftly for use in chemical reactions. An important prerequisite for a good molecular photonic device is the ability to undergo excited state charge transfer. Multiporphyrin-phthalocyanine arrays have proved to be successful candidates for application in light harvesting and molecular photonics due to reasons which include: (1) a spread of ground state absorptions covering the entire visible region of the solar spectrum, (2) the absorption spectra of porphyrins and phthalocyanines do not overlap, (3) there is a considerable overlap between the emission spectra of porphyrins and the absorption spectra of phthalocyanines, which makes energy transfer to be possible, and (4) phthalocyanines are easier to reduce than porphyrins, implying that charge transfer is possible between the two. There has been a lot of input into the study of phthalocyanine-porphyrin heterodimers [166,167], but apart from the efforts by Lindsey's group and a few others [164,165], literature is scanty on the synthesis and photophysics of higher phthalocyanine-porphyrin oligomers.

In order to elucidate the mechanism of intramolecular fluorescence quenching, the effect of solvent viscosity, polarity and temperature on the fluorophore's fluorescence must be studied. The mechanism for the intramolecular quenching, of a tetraporphyrin-phthalocyanine heteropentamer is investigated in this thesis.

1.3 MPcs AND PHOTODYNAMIC THERAPY

1.3.1 Photodynamic therapy

Chemotherapy and radiotherapy are the two principal techniques used for cancer treatment, apart from radical surgery. While combating cancerous escalation with some success, both methods can also bring on grave consequences largely because they destroy indiscriminately both normal and cancerous cells. As a result of this inadequacy, discriminative tumour destruction has become a major goal in oncology research over the last few decades [168]. Photodynamic therapy (PDT) has developed as a preferred alternative for treatment of certain types of cancer.

PDT is a non-invasive, oxygen-dependent treatment modality involving the dynamic use of specific-wavelength visible light. The light is used to excite light-sensitive (photosensitizer) dyes within target cells and generate cytotoxic radical and non-radical derivatives of oxygen (e.g. $O_2(^1\Delta_g)$, O_2^-, $O_2^{\cdot}$ and $OH^{\cdot}$). The highly reactive nature of these derivatives limits the effects of PDT to the immediate vicinity of the photosensitizer. Consequently, the intracellular location of the photosensitizer plays an important role in determining the ultimate fate of the target cell(s) since certain subcellular structures

within a cell are more prone to PDT-induced damage than others; mitochondria and nuclei are known to be particularly PDT-sensitive. It is therefore of interest to design photosensitizers which display precise intracellular targeting in order to maximize PDT-induced cell death. For most applications of PDT, the cytotoxic species is produced by one of two different processes: Type I and Type II, Scheme 1.7. These processes are mediated by excited triplet state of the photosensitizer which is sufficiently long lived, hence has enough time to intercept other species [168].

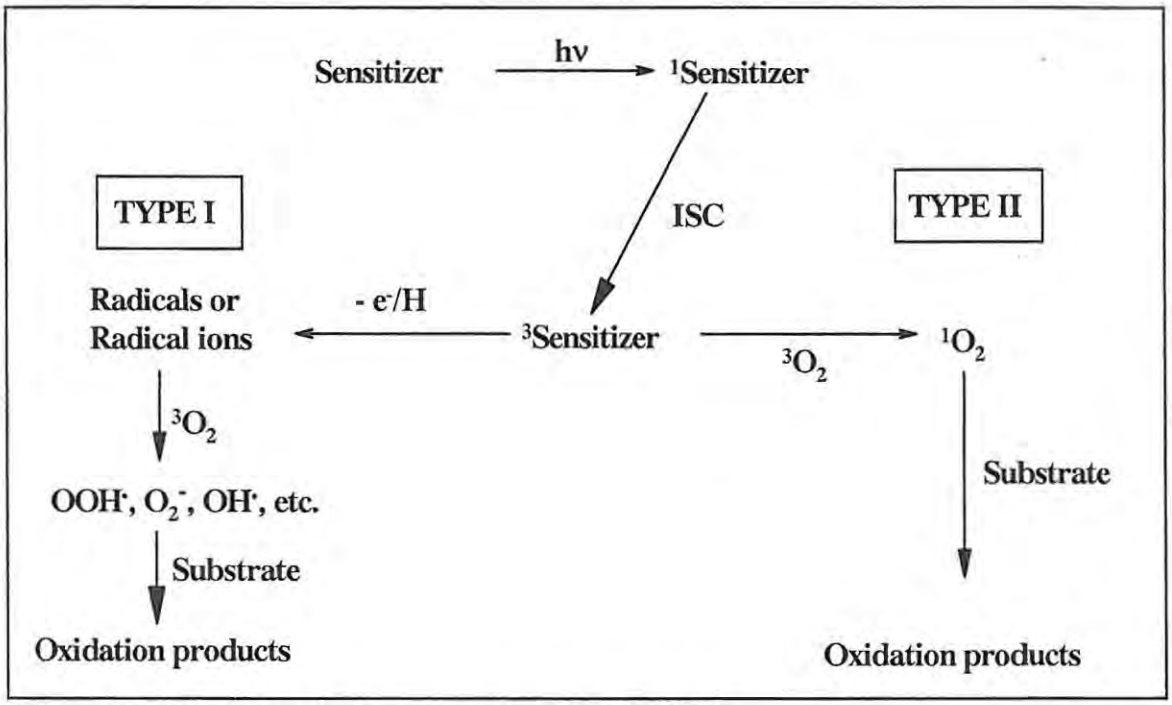

Scheme 1.7: Photochemical processes involved in PDT.

Type I mechanism involves electron/hydrogen transfer directly from the photosensitiser, producing ions or radicals. These then react rapidly, usually with oxygen, resulting in the production of highly reactive oxygen species (e.g. the superoxide and the peroxide anions or radicals), which then attack cellular targets.

Type II reactions produce the electronically excited and highly reactive state of oxygen known as singlet oxygen. Direct interaction of the excited triplet state photosensitiser with ground state molecular oxygen results in the photosensitiser returning to its singlet ground state and the formation of singlet oxygen.

In PDT, it is difficult to distinguish between the two reaction mechanisms. There is probably a contribution from both Types I and II processes indicating that the mechanism of damage is dependent on oxygen and photosensitiser concentrations. However, the generation of singlet oxygen via the Type II pathway in solution is fairly easily identified and analyzed either by chemical traps (scavengers) or by its weak phosphorescence at ~ 1268 nm using a near infra-red photodetector. The observation of singlet oxygen phosphorescence *in vivo*, although very rare (with only a few reported claims of direct observation), led to the widespread belief that singlet oxygen (Type II mechanism) is invariably the mediator in PDT [168]. MPcs are becoming more acceptable for use in PDT [28-33]. Their superior attributes, such as (i) red or near infra-red light absorption, (ii) non-toxicity, with low skin photosensitizing potency, (iii) selective localization in tumours, (iv) efficient generation of singlet oxygen and (v) appreciable fluorescence for visualization; makes them to be first-rate candidates for this purpose. The attributes mentioned here are obligatory for any PDT sensitizer.

1.3.2 Photosensitized singlet oxygen production by MPcs

Photosensitization is the process by which a photochemical or photophysical alteration occurs in one molecular entity as a result of initial absorption of radiation by another

molecular entity called a photosensitizer. MPcs have proved to be efficient photosensitizers, essentially due to their strong light absorption and also due to the relatively long lifetime of their excited triplet state. Oxygen is a potent quencher of the excited states of molecules. When the quenching of an excited state takes place, the excitation energy may be transferred to the oxygen molecule, generating the first excited state of the oxygen molecule known as singlet oxygen. **Oxygen is unusual in that it has a triplet ground state**, and hence relaxation of the singlet state to the ground state is spin forbidden, resulting in a long lifetime for singlet oxygen. Singlet oxygen is a highly reactive species and is responsible for oxidative damage in a number of systems [28,29,169-176].

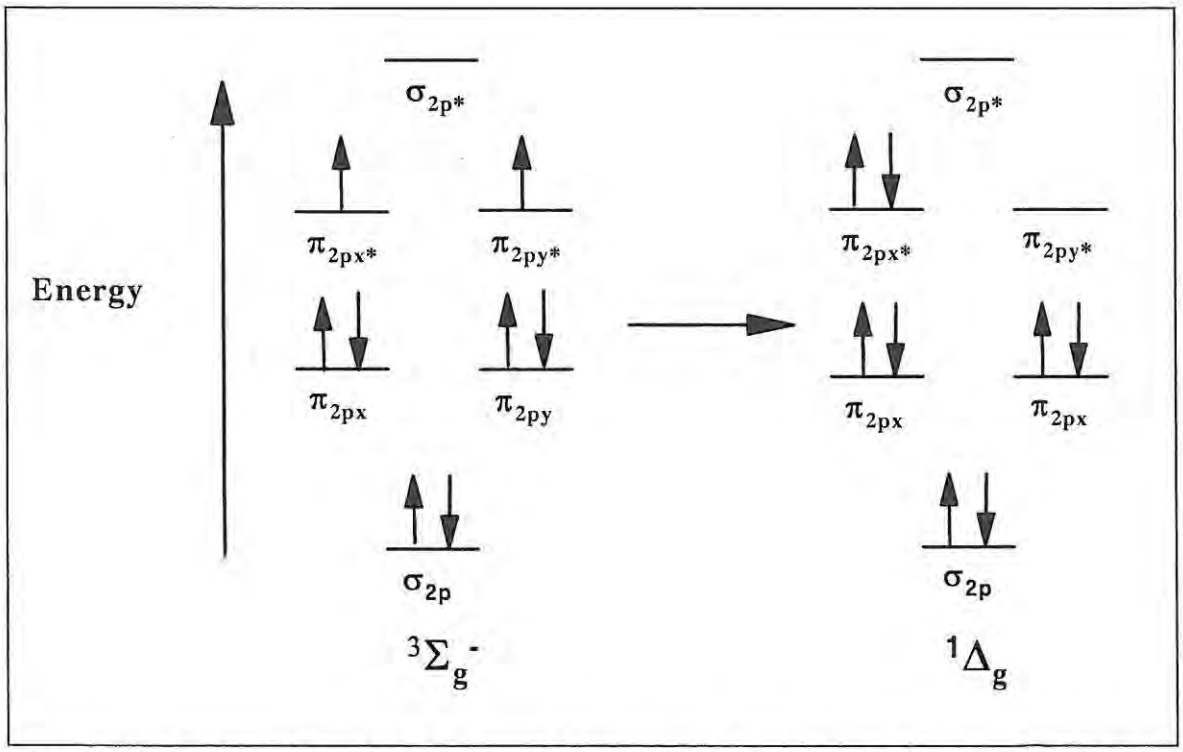

Scheme 1.8: Molecular orbital diagrams showing the electron distribution in triplet triplet and singlet oxygen.

In the ground state, the outermost electrons are distributed according to Hund's of maximum multiplicity, in the π_{2px*} and π_{2py*} antibonding orbitals [177,178]. The extreme reactivity of $(O_2)^1\Delta_g$ arises from the pairing of two electrons into one of the π_{2p*} antibonding orbitals (Scheme 1.8).

Singlet oxygen

The two electronically excited states immediately above the ground state are both singlet states: $^1\Sigma_g^+$ and $^1\Delta_g$.

$^1\Sigma_g^+$ is very short-lived, and rapidly decays to the lower singlet state $^1\Delta_g$. For practical purposes we can regard the $^1\Sigma_g^+$ state, if formed in solution, as being deactivated immediately to the $^1\Delta_g$ state, which has a lifetime of a few microseconds in the condensed phase. Consequently, singlet oxygen is conventionally referred to as $^1\Delta_g$. The properties of the three states of oxygen are summarized in Table 1.4 [30].

Table 1.4: The three lowest electronic states of dioxygen.

State Designation	Common Name	Energy		Lifetime in Condensed Phase	Electronic Configuration of HOMO
		KJ mol^{-1}	ν cm^{-1}		
$^1\Sigma_g^+$	—	155	13120	$< 10^{-9}$ s	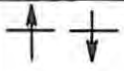
$^1\Delta_g$	Singlet oxygen $^1O_2$	94	7882	~ 10 μs	
$^3\Sigma_g^-$	Oxygen, $^3O_2$	0	0	∞	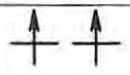

However, the description given here does not properly reveal the zwitterionic character of $O_2(^1\Delta_g)$. Perturbation by an attacking reagent will polarize the electronic structure. Scheme 1.9 shows Lewis structures depicting the zwitterionic character of singlet oxygen.

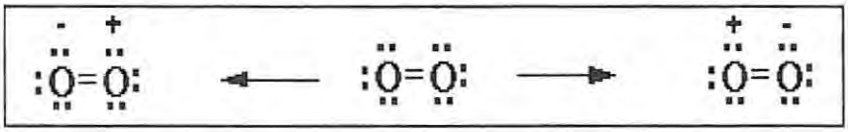

Scheme 1.9: Lewis structures depicting the zwitterionic character of singlet oxygen.

The lifetime of singlet oxygen in solution is solvent-dependent (Table 1.5).

Table 1.5: Lifetimes of singlet oxygen in various solvents

Solvent	H_2O	MeOH	C_6H_6	CS_2	CCl_4	C_6F_6	D_2O	[Air, 1 atm.]
τ_Δ (μs)	2	7	24	200	700	3900	20	~ 76000

1.3.2.1 Singlet oxygen generation

Photosensitization (Scheme 1.10) is by far the most common method of producing $O_2(^1\Delta_g)$ in the laboratory.

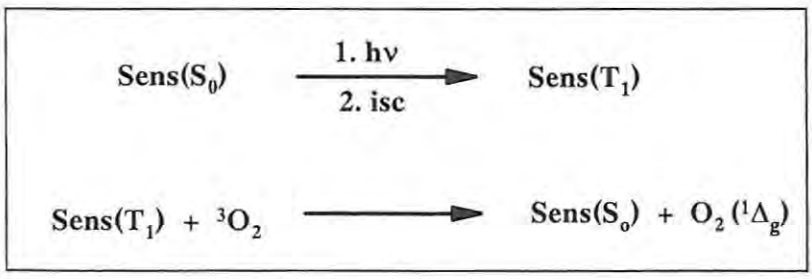

Scheme 1.10: Generation of singlet oxygen by photosensitization.

Other methods of $O_2(^1\Delta_g)$ generation can be classified into chemical and physical methods as itemized below (Scheme 1.11).

Chemical methods:

(a) Reaction of hydrogen peroxide with sodium hypohalite

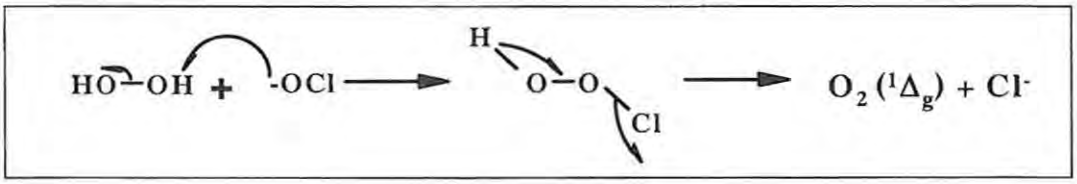

(b) Reaction of *N*-chlorosuccinimide with alkaline hydrogen peroxide

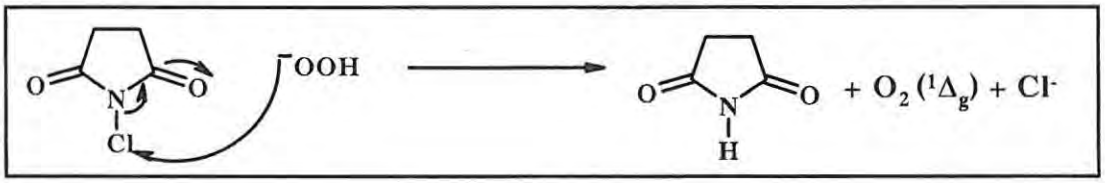

(c) Thermolysis of endoperoxides

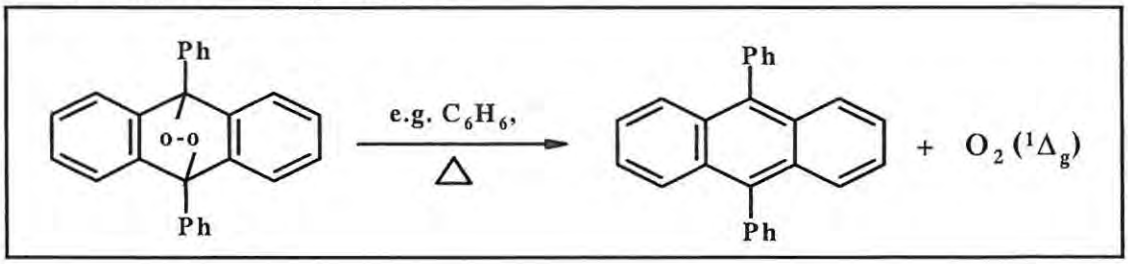

(d) Thermolysis of phosphate-ozone complexes.

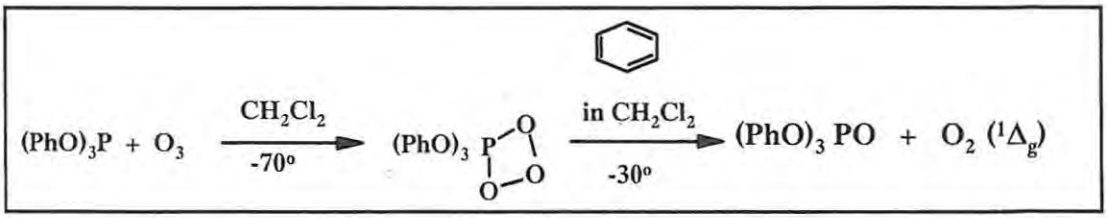

Scheme 1.11: Chemical methods for singlet oxygen generation.

Physical methods:

- By direct excitation
- By microwave discharge, Scheme 1.12.

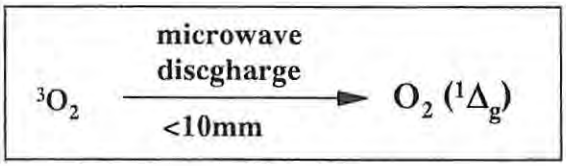

Scheme 1.12: Singlet oxygen generation by microwave discharge.

Singlet oxygen has been implicated in photosensitized oxidation reactions. Such reactions have been exploited in, for example, photodamage of viruses [169,170], photodynamic therapy (PDT) [28,29], photocarcinogenesis [171,172] and photodegradation of pollutants [173,174]. The enormous reactivity of singlet oxygen also finds applications in bleaching and disinfection reactions as well as in many chemical syntheses, such as the reaction of singlet oxygen with aromatic compounds, which leads to the formation of endoperoxides [175,176].

1.3.2.2 Detection of singlet oxygen

Luminescence

As $O_2(^1\Delta_g)$ decays (in first order kinetics) back to the ground state, some of its energy is emitted as light. The light from O_2 ($^1\Delta_g$) appears in the near infra-red as ~ 1268 nm [179] as shown in Eq. 1.12.

$$O_2(^1\Delta_g) \longrightarrow O_2(^3\Sigma_g) + h\nu_{(1268\ nm)} \qquad \text{(Eq. 1.12)}$$

Singlet oxygen scavengers

$O_2(^1\Delta_g)$, once generated, can be trapped using an appropriate singlet oxygen scavenger (quencher). The disappearance of the quencher can then be determined spectroscopically, and thus serves as a monitor for singlet oxygen. Examples of singlet oxygen quenchers include DPBF (1,3-diphenyl*iso*benzofuran), ADMA (tetrasodium anthracene-9,10-bis-methylmalonate), carotene, ascorbate, thiols and histidine. The reaction of $O_2(^1\Delta_g)$ with DPBF gives an endoperoxide (Scheme 1.13).

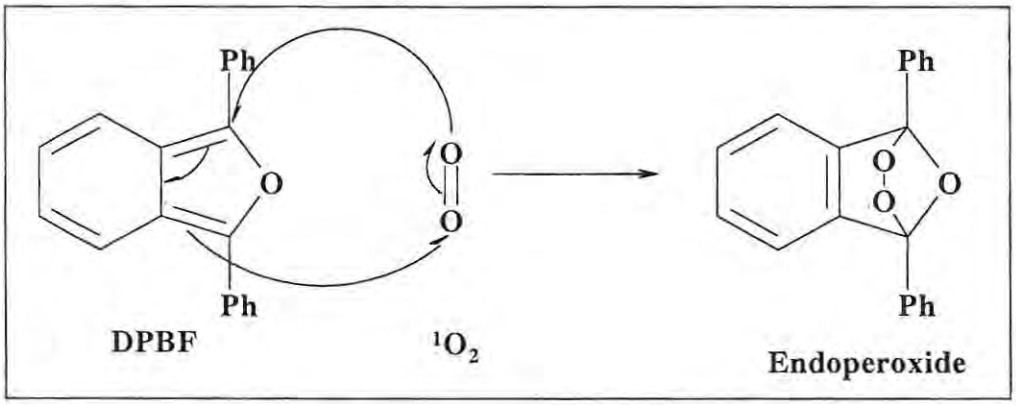

Scheme 1.13: [4+2] cycloaddition reaction of DPBF with singlet oxygen.

1.3.2.3 Photodegradation of MPcs by singlet oxygen

Photodegradation is the photochemical transformation of a molecule into lower molecular weight fragments, usually in an oxidation process. The ability of singlet oxygen to react with macrocyclic metal complexes has been documented [180,181]. Singlet oxygen reacts with tetra-azaporphyrin derivatives in a Diels-Alder [4+2]-cycloaddition, with the MPc ring acting as a diene and singlet oxygen as the dienophile. For MPcs, phthalimide was found to be the photo-oxidation product [181] (Scheme 1.14).

Photodegradation (photobleaching) studies are undertaken in order to determine the stability of the MPcs towards photo-irradiation. As stated above, it is widely believed that photodegradation is a singlet oxygen-mediated process and so its efficiency should depend on the concentration of singlet oxygen. The presence of electron-donating substituents on the MPc ring was reported [77] to bring about rapid photodegradation, which is attributed to the ease of oxidation of the ring due to the presence of these substituents.

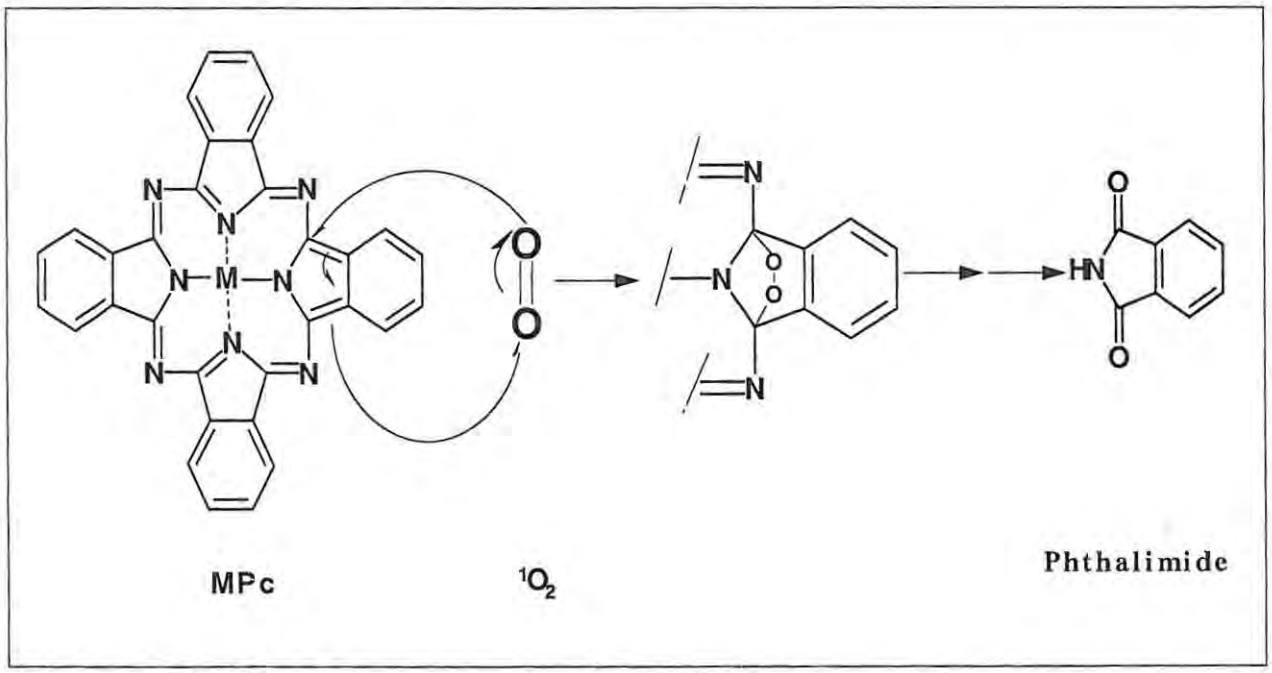

Scheme 1.14: [4+2] cycloaddition reaction of MPc with singlet oxygen.

On the other hand, electron-withdrawing substituents tend to stabilize the ring in the presence of light; therefore, complexes containing electron-withdrawing groups are more difficult to oxidize and hence more resistant to oxidative degradation. Experiments performed in deuterated solvents gave enhanced photodegradation [77, 140]. It is known that singlet oxygen has a longer lifetime in deuterated solvents; therefore, the probability of its reaction with the MPc ring is increased, giving rise to enhanced degradation. In the

presence of diazabicyclooctane (DABCO), a singlet oxygen scavenger, photodegradation rate was found to decrease [77,140]. This observation further supports the suggestion that singlet oxygen is actually involved in the photodegradation process. In aqueous solutions, photobleaching rate is low, presumably due to aggregation. Singlet oxygen generation is low for the aggregated species; hence photodegradation rate is expected to be low. In spite of all the above, literature on photodegradation of MPcs is still very slim. For instance, there exists no report relating MPc photodegradation to organic solvent parameters; also, the effect of protonation on MPc photodegradation is not known in literature. This thesis aims at exploring the effects of solvents and protonation on the photodegradation properties of MPc complexes.

1.3.3 Cyclodextrins

For PDT action, it is necessary that the drug be easy to administer via injection into the blood stream. As the blood itself is a water-based system, water solubility then becomes an essential requirement for a PDT drug. Additionally, the drug will have to traverse lipid membranes – consequently, it should also be lipophilic. The question now is how to produce a water-soluble lipophilic drug. The Pc macrocycle itself is lipophilic, but as already stated; water solubility could be achieved by introducing sulphonate ions as ring substituents. The study of the photophysical and photochemical behaviour of water-soluble MPc complexes is of importance for their potential application in PDT. Apart from the use of solubility-imparting substituents, an appropriate drug delivery system (such as cyclodextrins) could also be used in administering hydrophobic sensitizers.

Cyclodextrins (CDs) are a class of non-reducing, cavity-containing, cyclic compounds able to form molecular inclusion complexes. CDs (the host) provide a method for anchoring or entrapping other chemical compounds (the guest), without the formation of covalent bonds. The guest molecule may be wholly or partially contained in the cavity. CDs with six, seven or eight glucopyranose rings (known as α, β and γ cyclodextrin respectively) are known and can be synthesized. The basic structure of CDs (Fig. 1.13) consists of glucopyranose units joined together by α-1,4-linkages. The units are arranged in such a way that the molecule forms a cone shape with the hydroxyl groups on the open ends of the cone, the primary hydroxyl groups on the narrow end and the secondary hydroxyl groups on the wide end, oriented towards the outer surface. This arrangement results in the molecule having a hydrophobic cavity, suitable for inclusion of hydrophobic molecules, and a hydrophilic outer surface which renders CDs soluble in aqueous medium. Thus for photosensitizer administration in PDT, a hitherto insoluble molecule can be made soluble by encapsulating it within the CD cavity, without necessarily compromising the photosensitizing capability of the molecule. The natural CDs, α, β and γ CDs have internal diameters of about 0.5, 0.6, and 0.8 nm respectively. Inclusion in CDs can exert a profound effect on the physicochemical properties of the guest molecules as they are temporarily caged within the CD cavity, giving rise to beneficial modifications of guest molecules not otherwise achievable. Inclusion complexes between porphyrin derivatives and CDs have been reported [182-189].

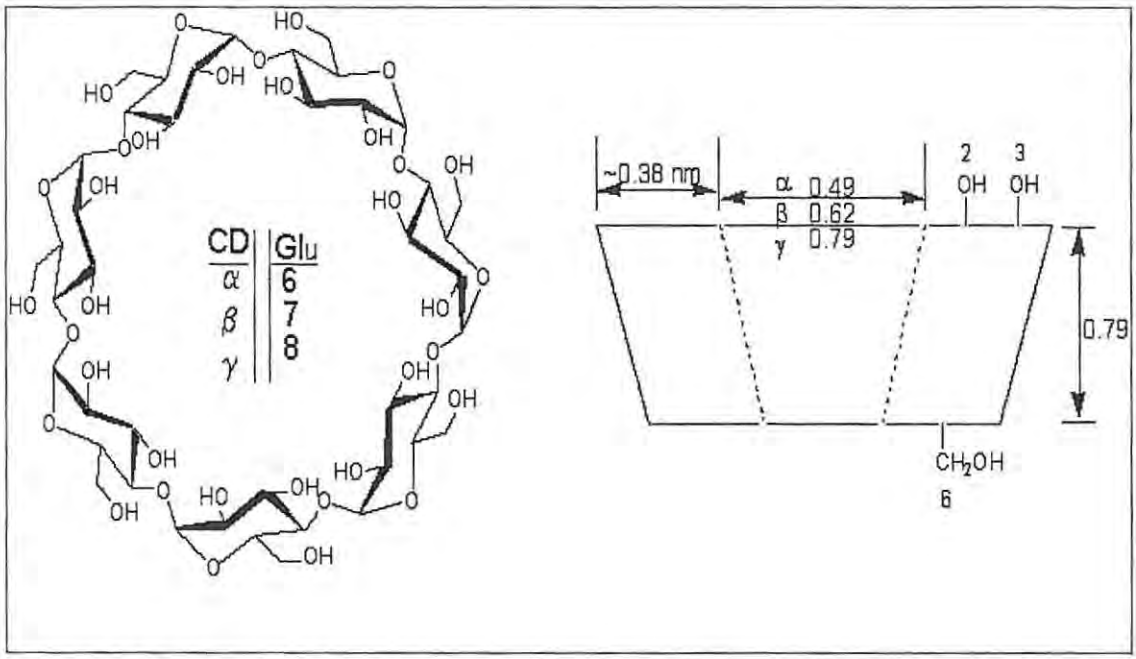

Figure 1.13: Basic cyclodextrin structure.

MPc-CD inclusion complexes and their photochemical properties have received little attention hence literature in this field could be expanded considerably. This thesis presents the influence of cyclodextrin encapsulation on the fluorescence and photochemical properties of non-water-soluble zinc phthalocyanine derivatives.

1.3.4 Serum albumin

The efficiency of PDT depends on the development of new drugs and the ability of these drugs to accumulate selectively in tumour tissues in comparison to normal tissue. Most MPcs are insoluble in water and biologically compatible solvents. Thus, they must be administered *in vivo* by means of delivery systems [190,191] as described above. The transport of porphyrins in the blood stream via liposomes has been shown to provide a larger and more selective accumulation of the drugs in neoplastic tissues [192,193], a fact

that is a basic requirement for PDT. The association of porphyrin-like sensitizers with serum proteins can also enhance the preferential uptake of hydrophobic photosensitizers by tumour tissues, since serum albumin is one of the key components in blood that influence drug distribution. It is therefore pertinent to carry out studies on the interaction of MPcs with serum albumin and the photophysicochemical consequences of such binding, as will be reported in this thesis.

Serum albumin is one of the most widely studied proteins and is the most abundant protein in plasma with a typical concentration of 5g/100ml. Albumin is generally regarded to mean serum albumin or plasma albumin.

Plasma: This is the yellow or grey-yellow, protein containing fluid portion of the blood in which the blood cells and platelets are normally suspended. It contains water and its dissolved constituents including proteins (as albumin, fibrinogen and globulin), electrolytes (as Na^+ and Cl^-), sugars (as glucose), lipids (as cholesterol and triglycerides) metabolic waste products (as urea), amino acids, hormones and vitamins. **Serum** is obtained by defibrinating plasma. It is the watery portion of plasma remaining after coagulation (after fibrinogen, prothrombin and other clotting factors have been removed by clot formation). The word **'albumin'** is used to describe a crystallizable protein or a group of proteins defined by water solubility. Albumin is the most abundant protein in the circulatory system and constitutes about 80% to colloid osmotic blood pressure [194]. It has now been determined that serum albumin is chiefly responsible for the maintenance of blood pH [195].

The investigation of binding of porphyrin-like drugs with albumin is of interest and much energy has been invested into it [196-199]. Bovine serum albumin (BSA) is well-suited

for this investigation because it has been extensively characterized [200-202]. BSA is the serum albumin of a ruminant mammal of the genus ***Bos***, such as an ox, cow or buffalo. Studying binding phenomena will help to explain the relationship between the structures and functions of proteins [203,204]. Since the intrinsic fluorescence of proteins is usually quenched upon binding to tetrapyrrolic compounds [205], this spectroscopic behaviour provides a means of studying the interaction between these compounds and BSA, permitting the determination of the binding constant and the binding stoichiometry of the complex formed [206]. In this thesis, the photophysical and photochemical behaviour of MPcs in the presence of BSA is studied.

1.4 AIMS OF THE THESIS

Metallophthalocyanines have once been described as "superman molecules" [34] due to their numerous applications to man; and such applications are not unconnected to their intrinsic photophysical and photochemical properties. Photophysical and photochemical studies on these compounds would further explicate their potential as photocatalysts in the industry and in oncology. As a result, a detailed photophysicochemical study of MPcs is inevitably desirable to the chemistry world at large.

The major aims of this thesis are to:

1. Synthesize non-transition metal metallophthalocyanines derivatives (including water-soluble ones) to be used for photophysical and photochemical studies,

2. Carry out detailed photophysical and photochemical experiments and calculations, leading to the determination of the following parameters:

   Lifetimes - fluorescence (τ_F) and triplet lifetime (τ_T); Quantum yields – fluorescence quantum yield (Φ_F), triplet quantum yield (Φ_T), photodegradation quantum yield (Φ_{Pd}) and singlet oxygen quantum yield (Φ_Δ).

3. Investigate the effects of different solvents and acid protonation on the spectral, photophysical and photochemical properties of the MPcs,
4. Study the fluorescence quenching of the MPc complexes in the presence of different quenchers and compare the calculated quenching constants,
5. Study the interaction of MPcs with proteins and cyclodextrins, and investigate the spectral, photophysical and photochemical consequences of the interaction.

The MPc complexes to be studied (Fig. 1.14a,b) are:

Unsubstituted zinc phthalocyanine (ZnPc, **15**);

Tetrasubstituted ZnPc derivatives: tetraaminozinc phthalocyanine (ZnTAPc, **16**), tetranitrozinc phthalocyanine (ZnTNPc, **17**), tetrasulphonatezinc phthalocyanine (ZnTSPc, **18**) and tetra(*tert*-butylphenoxy)zinc phthalocyanine (ZnTBPPc, **19**);

Octasubstituted ZnPc derivatives: Octaestronezinc phthalocyanine (ZnOEPc, **21**), octaphenoxyzinc phthalocyanine (ZnOPPc, **22**) and octamethylphenoyzinc phthalocyanine (ZnOMPPc, **23**);

ZnPc with axial ligands: cyanozinc phthalocyanine {(CN)ZnPc, **24**}, piperidinozinc phthalocyanine {(pip)ZnPc, **25**} and pyridinozinc phthalocyanine {(py)ZnPc, **26**};

Mixtures of differently sulphonated metallophthalocyanines: $AlPcS_{mix}$ (**27**), $ZnPcS_{mix}$ (**28**), $SiPcS_{mix}$ (**29**), $GePcS_{mix}$ (**30**) and $SnPcS_{mix}$ (**31**);

Zinc naphthalocyanine (ZnNPc, **32**); and

Phthalocyanine-*tetra*porphyrin heteropentamer : {zinc(II) *tetrakis*(5-phenoxy-10,15,20-*tri*phenylporphyrin)) zinc(II) phthalocyanine, (ZnPc-(O-ZnTPP)$_4$, (**20**)}.

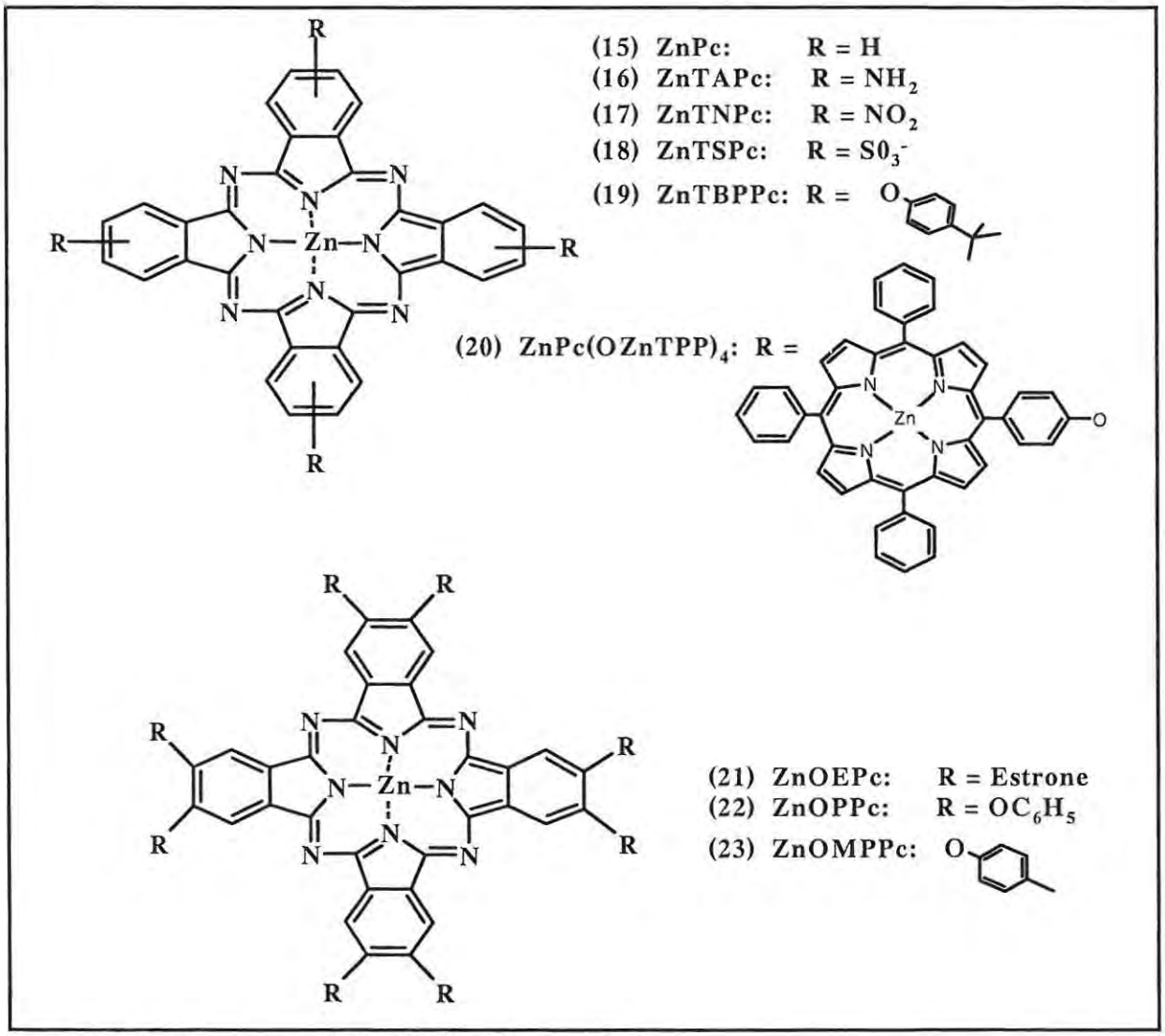

Figure 1.14a: Structures of MPc derivatives studied

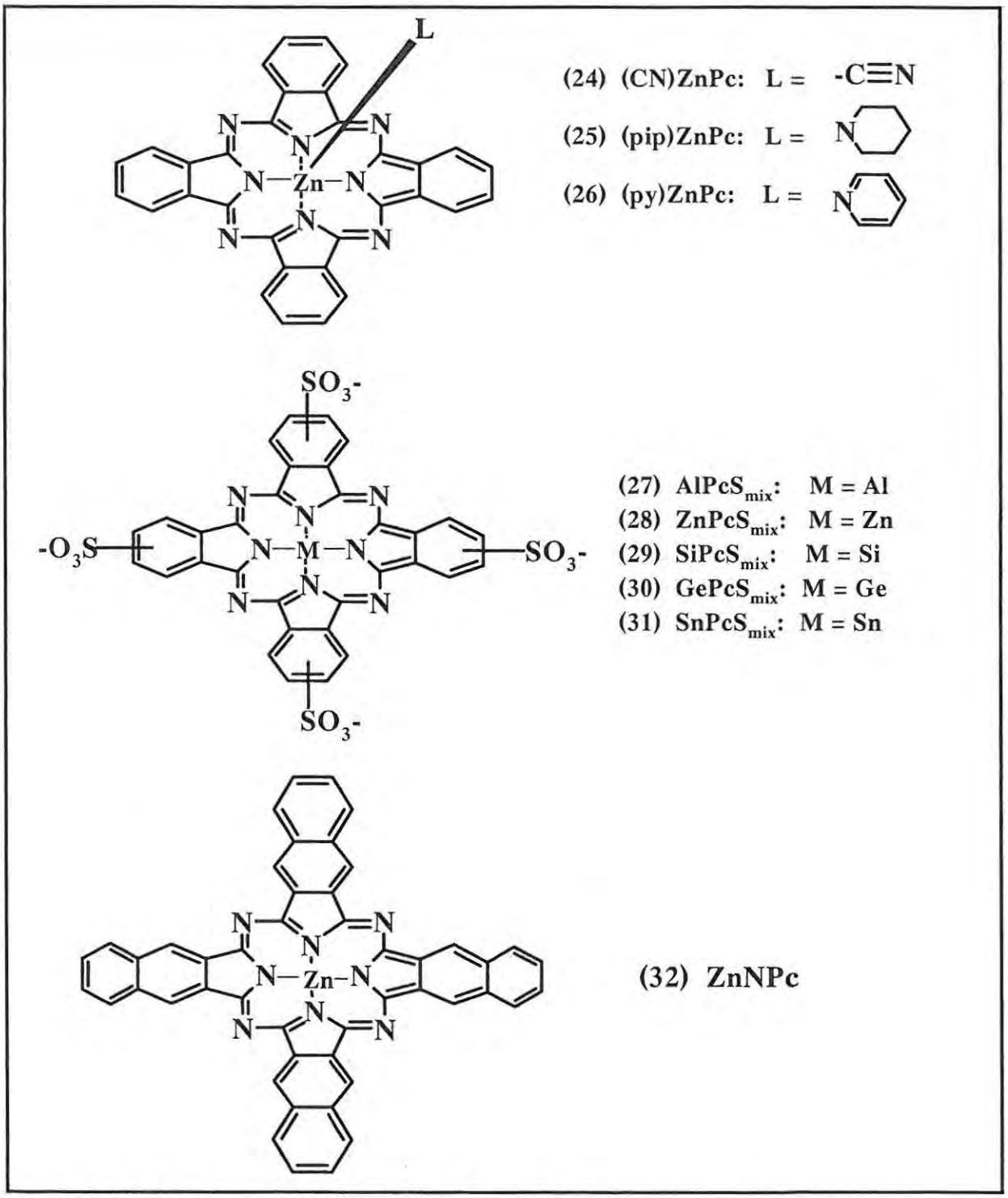

Figure 1.14b: Structures of MPc derivatives studied

CHAPTER 2

EQUATIONS AND DERIVATIONS

This chapter introduces and elucidates the various equations and derivations associated with the photophysical and photochemical studies on the metallophthalocyanines derivatives. The chapter serves as a bridge between the concepts discussed in Chapter 1 and the experimental details of these concepts that will be discussed in Chapter 3.

2.1 Absorption

When light is directed at a sample solution, some of it is transmitted or reflected, while the rest is absorbed. According to the first law of photochemistry, only the light absorbed by a molecule can be effective in producing a photochemical change, hence it is imperative to determine the exact amount of light absorbed by the solution.

The Beer-Lambert law for light absorption is given by Eq. 2.1:

$$A = \varepsilon c l \qquad \text{(Eq. 2.1)}$$

A is the absorbance, ε, the molar extinction coefficient (M^{-1} cm^{-1}) and l, the path length.

The fraction of incident light intensity absorbed (α) is given by Eq. 2.2:

$$\alpha = \frac{I_0 - I}{I} = 1 - T \qquad \text{(Eq. 2.2)}$$

Where T is the transmittance, I_0, the intensity of incident light and I, the intensity of transmitted light.

$$T = 10^{-\varepsilon c l} \qquad \text{(Eq. 2.3)}$$

Combining Eqs. 2.2 and 2.3 gives Eq. 2.4:

$$\alpha = 1 - 10^{-\varepsilon c l} \qquad \text{(Eq. 2.4)}$$

Eq. 2.4 is only valid for a monochromatic light. If however a polychromatic light is used, the integrated fraction of light absorbed is the sum of the αs over the entire band of incident light, and is given mathematically by equation 2.5:

$$\alpha = \int_{\lambda_1}^{\lambda_2} (1 - 10^{-A(\lambda)}) d\lambda \qquad \text{(Eq. 2.5)}$$

λ_1 and λ_2 are the lower and upper wavelength limits of the incident light.

2.2 Fluorescence

Fluorescence intensity I_F varies linearly with the absorbed intensity I_{abs}

$$I_F = kI_{abs} \qquad \text{(Eq. 2.6)}$$

$$I_F = kI_0(1-10^{-\varepsilon cl}) \qquad \text{(Eq. 2.7)}$$

Eq. 2.7 implies that fluorescence intensity varies non-linearly with the concentration of the analyte. However, a linear dependence may be assumed between the two parameters as long as the absorbance is < 0.05 [207].

By definition, fluorescence quantum yield Φ_F is the fraction of the excited molecules that get deactivated by emitting a fluorescence photon. It is the ratio of the number of emitted photons to the number of absorbed photons per unit time (Eq. 2.8).

$$\Phi_F = \frac{\text{No. of emitted photons}}{\text{No. of absorbed photons}} \qquad \text{(Eq. 2.8)}$$

It is therefore understandable that the fluorescence quantum yield is directly related to the radiative (k_f) and non-radiative (k_{nr}) rate constants of deactivation by the relationship (Eq. 2.9):

$$\Phi_F = \frac{k_F}{k_F + k_{nr}} \qquad \text{(Eq. 2.9)}$$

The measurement of absolute fluorescence quantum yield is critical and requires special equipment. It is necessary to know precisely the intensity of the exciting light as well as the intensity of fluorescence. The measurements are usually done by the use of scattering agents and integrating spheres or actinometers to calibrate the system [207,208]. For routine work, it is often satisfactory to determine the relative fluorescence quantum yields. The quantum yield of an unknown is then related to that of a standard by Eq. 2.10.

$$\Phi_{F(X)} = \Phi_{F(S)} \frac{F_X}{F_S} \frac{A_S}{A_X} \left(\frac{\eta_X}{\eta_S} \right)^2 \qquad \text{(Eq. 2.10)}$$

Φ_F is the fluorescence quantum yield; F, the area under the corrected emission curve; A, the absorbance at the excitation wavelength; and n the solvent's refractive index. When light passes from one medium to another, part of it is lost to reflection, which depends on the difference between the refractive indices of the two media. Hence it is necessary to introduce refractive index correction to the fluorescence quantum yield equation. Subscripts 'X' and 'S' denote the unknown substance and reference standard respectively.

2.3 Lifetimes

The lifetime (τ) of a chemical species, which decays in a first-order process, is the time needed for a concentration of this species to decrease to 1/e of its original value. Statistically, τ represents the mean life expectancy of an excited species. In a reacting system in which the decrease in concentration of a particular chemical species is governed by a first-order rate law, τ is equal to the reciprocal of the sum of the (pseudo) unimolecular rate constants of all processes, which cause the decay.

For any molecular entity which decays in a first order kinetics,

$$\text{Rate of decay} = \frac{-dA}{dt} = k_d[A] \qquad \text{(Eq. 2.11)}$$

k_d is the first order decay constant. Rearranging Eq 2.11 gives Eq. 2.12:

$$\frac{dA}{[A]} = -k_d dt \qquad \text{(Eq. 2.12)}$$

Integrating,

$$\int_{A_0}^{A} \frac{1}{[A]} dA = -k_d \int_0^t dt \qquad \text{(Eq. 2.13)}$$

and

$$\ln[A] - \ln[A]_o = -k_d t \qquad \text{(Eq. 2.14)}$$

$$\ln \frac{[A]}{[A]_0} = -k_d t \qquad \text{(Eq. 2.15)}$$

From the definition above,

$$t = \tau, \text{ when } [A] = \frac{[A]_0}{e} \qquad \text{(Eq. 2.16)}$$

Substituting Eq. 2.16 into equation 2.15 gives:

$$\ln\left(\frac{1}{e}\right) = -k_d \tau \qquad \text{(Eq. 2.17)}$$

$$\tau = \frac{\ln e}{k_d} \qquad \text{(Eq. 2.18)}$$

And

$$\tau = \frac{\log_e e}{k_d} = \frac{1}{k_d} \qquad \text{(Eq. 2.19)}$$

In the field of photochemistry, as already stated, two important excited states are known: the singlet and the triplet excited states. The lifetimes of these states are designated τ_F and τ_T respectively. The photophysical processes that deactivated the first excited singlet state are shown in Scheme 2.1: However, there exists a term called the radiative lifetime, designated as τ_0.

$S_0 + h\nu \longrightarrow S_1$	$Rate = I_{abs}$	Absorption
$S_1 \longrightarrow S_0 + h\nu_F$	$Rate = k_F[S_1]$	Fluorescence
$S_1 \longrightarrow S_0 + heat$	$Rate = k_{IC}[S_1]$	Internal conversion
$S_1 \longrightarrow T_1$	$Rate = k_{ISC}[S_1]$	Intersystem crossing

Scheme 2.1: The primary photophysical processes deactivating the excited singlet state

The radiative lifetime, τ_0, is a measure of the probability of emission, which is related to the probability of absorption. The radiative lifetime is represented by Eq. 2.20:

$$\tau_0 = \frac{1}{k_F} \qquad \text{(Eq. 2.20)}$$

By definition, τ_0 is the lifetime of an excited molecule in the absence of radiationless transitions. The radiative lifetime is not the actual lifetime of the excited state; it is the lifetime if fluorescence was the only process deactivating the excited state, and it is the reciprocal of the first order rate constant of fluorescence (Eq. 2.20). Following excitation, the molecule will also relax by internal conversion and intersystem crossing, in addition to fluorescence; so that the rate of decay of the singlet excited state is the sum of these three decay processes (Eq. 2.21).

$$\frac{-d[S_1]}{dt} = (k_F + k_{IC} + k_{ISC})[S_1] \qquad \text{(Eq. 2.21)}$$

The lifetime of the excited state is the reciprocal of the first order rate constant for decay.

$$\tau_F = \frac{1}{k_F + k_{IC} + k_{ISC}} \qquad \text{(Eq. 2.22)}$$

The triplet state formed can undergo further relaxation processes (Scheme 2.2):

T_1	$\longrightarrow$	$S_0 + h\nu_{Ph}$	Rate = $k_{Ph}[T_1]$	Phosphorescence
T_1	$\longrightarrow$	S_0	Rate = $k'_{ISC}[T_1]$	Intersystem crossing

Scheme 2.2: Photophysical processes deactivating the excited triplet state

Typically, the rate of triplet formation is much faster than the rate of triplet decay, i.e., $k_{ISC} > (k_{Ph} + k'_{ISC})$.

As in the case of the singlet state,

$$\frac{-d[T_1]}{dt} = (k_{Ph} + k'_{ISC})[T_1] \qquad \text{(Eq. 2.23)}$$

And the phosphorescence (triplet) lifetime is given by Eq. 2.24:

$$\tau_T = \frac{1}{(k_{Ph} + k'_{ISC})} \qquad \text{(Eq. 2.24)}$$

In all cases, the excited triplet state is longer lived than the singlet counterpart because the decay (radiative or non-radiative) of the T_1 to the S_0 state is forbidden.

In Fig. 2.1, a typical first order decay curve is simulated.

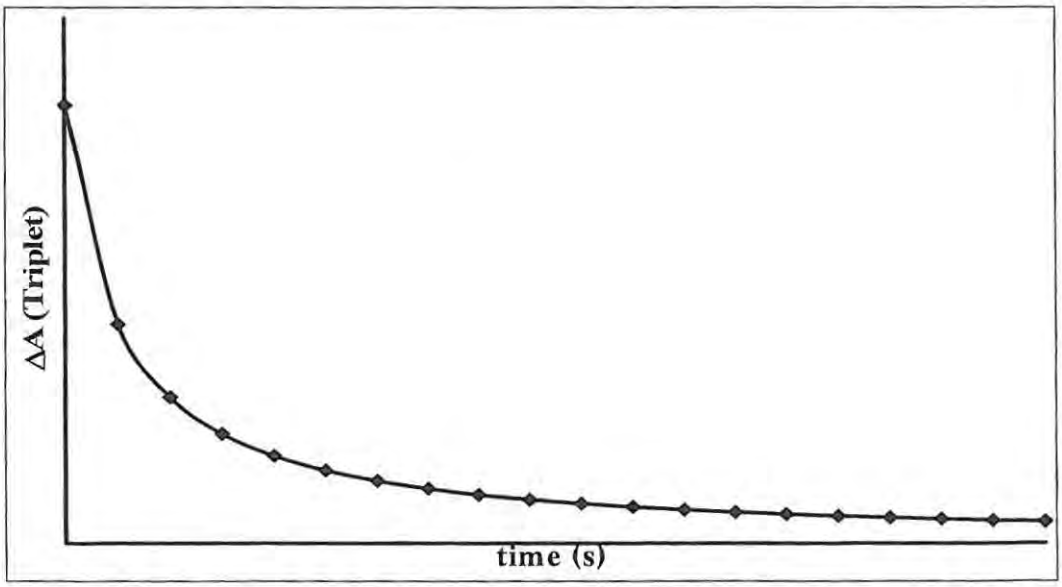

Fig. 2.1: A typical triplet absorption curve (simulated)

2.4 The triplet quantum yield

The quantum yield of triplet formation (Φ_T) is based on the absorption of the triplet state generated during a flash photolytic experiment. The measurement of MPc triplet absorption is possible because this state absorbs far away (~ 500 nm) from the region of ground singlet absorption (~ 680 nm). However, considering the depletion of the ground singlet state after photo-irradiation, one could make another estimate of the triplet absorption. For both methods, the change in absorbance of the triplet state molecules (ΔA) resulting from photo-irradiation is related to the triplet quantum yield (Φ_T).

2.4.1 Triplet absorption

The extent of attenuation of the analyzing light around 500 nm is a measure of the number of molecules in the excited triplet state.

Let $\mathbf{I_0}$ be the intensity of analyzing light in the absence of sample (maximum transmittance) at ~ 500 nm; $\mathbf{I_i}$, the intensity of the analyzing light in the presence of sample but with no ground state excitation (the excited singlet state not populated, hence no triplet formation); and $\mathbf{I_f}$, the intensity of the analyzing light in the presence of sample and with ground state excitation (excited singlet state populated and subsequently, the excited triplet state also becomes populated)

It should be noted that $\mathbf{I_f < I_i}$ $\therefore$ $\mathbf{A_f > A_i}$ ('i' and 'f' stand for 'initial' and 'final' respectively). **A** is the absorbance.

$$T_i \text{ (Initial transmittance)} = \frac{I_i}{I_0} \qquad \text{(Eq. 2.25)}$$

and

$$T_f \text{ (Final transmittance)} = \frac{I_f}{I_0} \qquad \text{(Eq. 2.26)}$$

Therefore,

$$A_i = -\log\frac{I_i}{I_0} = \log\frac{I_0}{I_i} \qquad \text{(Eq. 2.27)}$$

and

$$A_f = -\log\frac{I_f}{I_0} = \log\frac{I_0}{I_f} \qquad \text{(Eq. 2.28)}$$

$$\Delta A = A_f - A_i = \log\frac{I_0}{I_f} - \log\frac{I_0}{I_i} \qquad \text{(Eq. 2.29)}$$

$$\Delta A = \log\frac{I_0}{I_f}.\frac{I_i}{I_0} \qquad \text{(Eq. 2.30)}$$

$$\Delta A = \log\frac{I_i}{I_f} \qquad \text{(Eq. 2.31)}$$

However, Φ_T depends not only on ΔA of the excited triplet state (Fig. 2.1), but also on molar extinction coefficient of the excited triplet state (ε_T).

ε_T is determined using Eq. 2.32 [209]:

$$\varepsilon_T = \varepsilon_S.\frac{\Delta A_T}{\Delta A_S} \qquad \text{(Eq. 2.32)}$$

Where ΔA_T and ΔA_S are the changes in absorbance of excited triplet and ground singlet states, respectively. ε_S is the molar extinction coefficient of the ground singlet state.

The triplet quantum yield (Φ_T) is directly proportional to the change in triplet absorbance (ΔA_T) and inversely proportional to the triplet extinction coefficient (ε_T), as represented in Eq. 2.33; and is usually determined with reference to a standard whose value (Φ_T^{Std}) is known.

$$\Phi_T^S \propto \frac{\Delta A_T^S}{\varepsilon_T^S} \qquad \text{(Eq. 2.33)}$$

For the reference standard, we also have:

$$\Phi_T^{Std} \propto \frac{\Delta A_T^{Std}}{\varepsilon_T^{Std}} \qquad \text{(Eq. 2.34)}$$

Taking ratios of Eq. 2.33 over Eq. 2.34,

$$\Phi_T^S = \Phi_T^{Std} \cdot \frac{\Delta A_T^S \cdot \varepsilon_T^{Std}}{\Delta A_T^{Std} \cdot \varepsilon_T^S} \qquad \text{(Eq. 2.35)}$$

2.4.2 Singlet depletion

The extent of attenuation of the analyzing light around the Q band of the MPc is a measure of the number of molecules remaining in the singlet ground state. Two crucial assumptions are made while using this method: (i) that all non-fluorescing molecules in the excited singlet state automatically undergo intersystem crossing and (ii) that the absorptions of the excited singlet and triplet states at the working wavelength are negligible when compared to that of the ground singlet state.

Let $\mathbf{I_0}$ be the intensity of analyzing light in the absence of sample (the maximum transmittance of the analyzing light); $\mathbf{I_i}$, the intensity of the analyzing light in the presence of sample but with no ground state excitation (the excited singlet state not populated, hence all the molecules are in the ground state – low transmittance); and $\mathbf{I_f}$, the intensity of the analyzing light in the presence of sample and with ground state excitation (excited singlet state populated and subsequently, the excited triplet state also becomes populated; the number of molecules remaining in the ground singlet state has reduced – high transmittance).

It should be noted that $\mathbf{I_f > I_i}$ $\therefore$ $\mathbf{A_f < A_i}$

As in the triplet absorption method, Eqs. 2.25 – 2.31 hold, and Φ_T depends not only on ΔA_S, but also on ε_S. ε_S is determined using the Beer-Lambert relationship (Eq. 2.1). Φ_T here is also determined with reference to a known standard; and Eq. 2.36 [210] applies:

$$\Phi_T^S = \Phi_T^{Std} \cdot \frac{\Delta A_S^S \cdot \varepsilon_S^{Std}}{\Delta A_S^{Std} \cdot \varepsilon_S^S} \qquad \text{(Eq. 2.36)}$$

A typical singlet depletion curve is simulated in Fig 2.2.

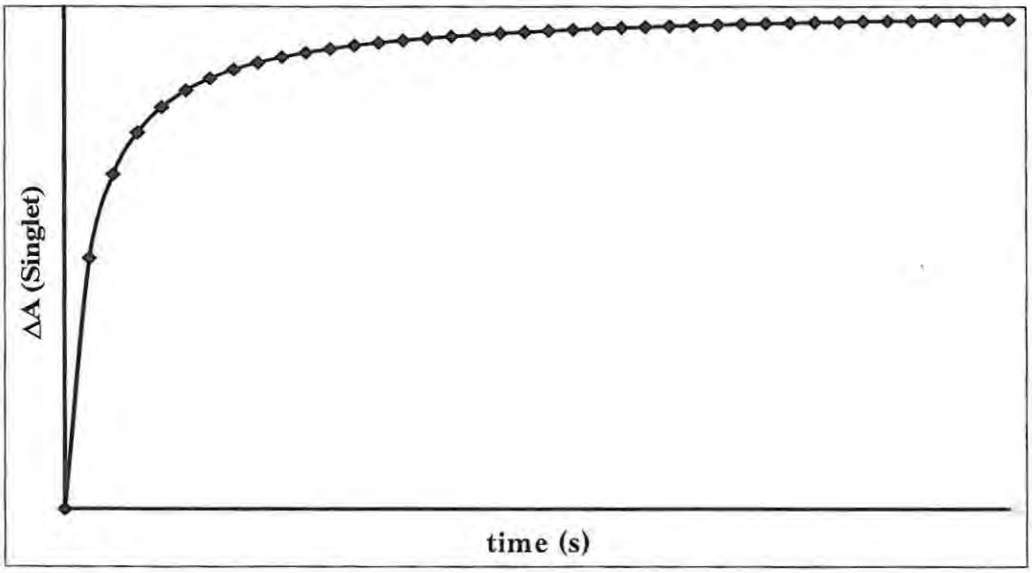

Fig 2.2: A typical singlet depletion curve (simulated)

2.5 Photodegradation quantum yield

Photodegradation (or photobleaching) is the photochemical transformation of a molecule into lower molecular-weight fragments, usually in an oxidative process. Photodegradation is identified by loss of absorption or emission intensity occurring as a result of absorption of light quanta by the substrate. The photodegradation quantum yield (Φ_{Pd}) is defined as the ratio of the number of moles of a substance degraded to

the number of moles of photons absorbed (Eq. 1.6). The differential photodegradation quantum yield is defined by Eq. 2.37:

$$\Phi_{Pd} = \frac{\Delta n/\Delta t}{I_{abs}} \qquad \text{(Eq. 2.37)}$$

Where $\Delta n/\Delta t$ is the rate of photodegradation and I_{abs} is the number of moles of photons absorbed per unit time.

According to Beer-Lambert law,

$$c = \frac{A}{\varepsilon} \text{ (For a cell of thickness 1 cm)} \qquad \text{(Eq. 2.38)}$$

Where c, A and ε are the concentration (M), absorbance and molar extinction coefficient (M^{-1} cm^{-1}) of the degrading substance, respectively.

Since

$$c = \frac{n}{V} \qquad \text{(Eq. 2.39)}$$

Where n is the number of moles of the degrading substance and V is the reaction volume (dm^3).

Combining Eqs. 2.38 and 2.39 and rearranging, we have Eq. 2.40:

$$n = \frac{AV}{\varepsilon} \qquad \text{(Eq. 2.40)}$$

Therefore, the rate of photodegradation ($\frac{\Delta n}{\Delta t}$) is given by Eq. 2.41:

$$\frac{\Delta n}{\Delta t} = \frac{\Delta A}{\Delta t} \cdot \frac{V}{\varepsilon} \qquad \text{(Eq. 2.41)}$$

The unit of I_{abs} depends on the unit of incident intensity (I). If a power meter is used, the intensity I′ is given in J cm^{-2} s^{-1}. For a monochromatic light, the Einstein relation gives the energy of one photon:

$$E = \frac{hc}{\lambda} \qquad \text{(Eq. 2.42)}$$

The number of photons present in I′ is therefore given by Eq. 2.43:

$$I\ (\text{photons}\ cm^{-2}s^{-1}) = \frac{I'}{E} \qquad \text{(Eq. 2.43)}$$

However, only a fraction of the incident light intensity is absorbed

$$\therefore I_{abs}\ (\text{photons}\ cm^{-2}\ s^{-1}) = \alpha I \qquad \text{(Eq. 2.44)}$$

In order to obtain I_{abs} in photon moles s^{-1}, it is necessary to introduce a factor $\frac{S}{N_A}$ into Eq. 2.44; where S is the irradiated cell area (cm^2) and N_A is the Avogadro's constant ($mole^{-1}$), i.e.

$$I_{abs}\ (\text{photon moles}\ s^{-1}) = \frac{\alpha SI}{N_A} \qquad \text{(Eq. 2.45)}$$

Substituting Eqs. 2.41 and 2.45 into Eq. 2.37 gives Eq. 2.46:

$$\Phi_{Pd} = \frac{\Delta A}{\Delta t} \cdot \frac{V}{\varepsilon} \cdot \frac{N_A}{\alpha SI} \qquad \text{(Eq. 2.46)}$$

2.6 Singlet oxygen quantum yield

Singlet oxygen is produced as a result of quenching of the excited triplet state of photosensitizers; the excitation energy is transferred to ground state oxygen molecule, generating the singlet oxygen. By definition, singlet quantum yield (Φ_Δ) is the ratio of

the number of singlet oxygen moles formed to the number of moles of photons absorbed by the photosensitizer (Eq. 1.7).

As earlier stated, $O_2(^1\Delta_g)$, once generated, can be trapped using an appropriate singlet oxygen scavenger (quencher). The disappearance of the quencher can then be determined spectroscopically, and thus serves as a monitor for singlet oxygen. The quencher (in this case DPBF or ADMA) is mixed with the photosensitizer solution and the mixture is irradiated. The following reactions lead to the disappearance of $O_2(^1\Delta_g)$ in the mixture, in the presence of DPBF (Scheme 2.3):

$O_2(^1\Delta_g)$	$\xrightarrow{k_d}$	$O_2(^3\Sigma_g)$	Natural decay	(i)
DPBF + $O_2(^1\Delta_g)$	$\xrightarrow{k_{Chem}}$	Products	Chemical quenching	(ii)
DPBF + $O_2(^1\Delta_g)$	$\xrightarrow{k_{Phys}}$	DPBF + $O_2(^3\Sigma_g^-)$	Physical quenching	(iii)
S + $O_2(^1\Delta_g)$	$\xrightarrow{k_{Prod}}$	Products	Chemical quenching	(iv)
S + $O_2(^1\Delta_g)$	$\xrightarrow{k_P}$	S + $O_2(^3\Sigma_g^-)$	Physical quenching	(v)

Scheme 2.3: Reactions leading to the decay of singlet oxygen in solution;

DPBF = quencher, S = photosensitizer; k_d, k_{Chem} and k_{Phys} are the rate constants for first order natural decay, chemical quenching and physical quenching by DPBF respectively; k_{Prod} and k_P are the rate constants for chemical and physical quenching of singlet oxygen by the photosensitizer. The singlet oxygen quenchers used in this work are DPBF.

Reaction (iii) is ignored because DPBF acts exclusively as chemical quenchers in organic solvents [211]; reaction (iv) is also ignored because the rate of reaction of singlet oxygen with the photosensitizer is negligible, compared to that with the quencher. Again, reaction (v) is disregarded because singlet oxygen quantum yield does not depend on the concentration of the photosensitizer, so physical quenching

can be overlooked. Therefore, the rate of disappearance of $O_2(^1\Delta_g)$ solely depends on reactions (i) and (ii) as given by Eq. 2.47:

$$R_{dis}\{O_2(^1\Delta_g)\} = k_d\,[O_2(^1\Delta_g)] + k_{Chem}\,[DPBF][O_2(^1\Delta_g)] \quad \text{(Eq. 2.47)}$$

However, using steady state approximation,

$$R_f\{O_2(^1\Delta_g)\} = R_{dis}\{O_2(^1\Delta_g)\} \quad \text{(Eq. 2.48)}$$

Where $R_f\{O_2(^1\Delta_g)\}$ and $R_{dis}\{O_2(^1\Delta_g)\}$ are the rates of formation and disappearance of $O_2(^1\Delta_g)$ respectively.

But singlet oxygen quantum yield (Φ_Δ) is given by Eq. 2.49:

$$\Phi_\Delta = \frac{R_f\{O_2(^1\Delta_g)\}}{I_{abs}} \quad \text{(Eq. 2.49)}$$

Combining Eqs. 2.47 - 2.49 results in Eq. 2.50:

$$\Phi_\Delta = \frac{k_d[O_2(^1\Delta_g)] + k_{Chem}[DPBF][O_2(^1\Delta_g)]}{I_{abs}} \quad \text{(Eq. 2.50)}$$

Rearranging, we have:

$$[O_2(^1\Delta_g)] = \frac{\Phi_\Delta \,.\, I_{abs}}{k_{Chem}[DPBF] + k_d} \quad \text{(Eq. 2.51)}$$

The rate of disappearance of the quencher $\left(-\frac{\Delta[DPBF]}{\Delta t}\right)$, is given by Eq. 2.52:

$$-\frac{\Delta[DPBF]}{\Delta t} = k_{Chem}[DPBF][O_2(^1\Delta_g)] \quad \text{(Eq. 2.52)}$$

Therefore, the quantum yield of disappearance of DPBF ($\Phi_{-[DPBF]}$) is:

$$\Phi_{-[DPBF]} = \frac{k_{Chem}[DPBF][O_2(^1\Delta_g)]}{I_{abs}} \quad \text{(Eq. 2.53)}$$

Substitution of Eq. 2.51 into Eq. 2.53 gives Eq. 2.54:

$$\Phi_{-[DPBF]} = \frac{k_{Chem}[DPBF].\Phi_\Delta}{k_{Chem}[DPBF] + k_d} \quad \text{(Eq. 2.54)}$$

At low DPBF concentrations, $k_d >>> k_{Chem}$

$$\Phi_{-[DPBF]} = \frac{k_{Chem}[DPBF].\Phi_{\Delta}}{k_d} \qquad \text{(Eq. 2.55)}$$

For a photosensitizer (S) and a reference standard (Std), Eqs. 2.56 and 2.57 hold:

$$\Phi^{S}_{-[DPBF]} = \frac{k_{Chem}[DPBF]^{S}.\Phi^{S}_{\Delta}}{k_d} \qquad \text{(Eq. 2.56)}$$

$$\Phi^{Std}_{-[DPBF]} = \frac{k_{Chem}[DPBF]^{Std}.\Phi^{Std}_{\Delta}}{k_d} \qquad \text{(Eq. 2.57)}$$

Dividing Eq. 2.56 by Eq. 2.57 results in Eq. 2.58:

$$\frac{\Phi^{S}_{-[DPBF]}}{\Phi^{Std}_{-[DPBF]}} = \frac{[DPBF]^{S}.\Phi^{S}_{\Delta}}{[DPBF]^{Std}.\Phi^{Std}_{\Delta}} \qquad \text{(Eq. 2.58)}$$

This can be rewritten as:

$$\Phi^{S}_{\Delta} = \Phi^{Std}_{\Delta}.\frac{\Phi^{S}_{-[DPBF]}.[DPBF]^{Std}}{\Phi^{Std}_{-[DPBF]}.[DPBF]^{S}} \qquad \text{(Eq. 2.59)}$$

But as in Eq. 2.46, $\Phi_{-[DPBF]}$ is defined by Eq. 2.60:

$$\Phi_{-[DPBF]} = \left(\frac{\Delta A}{\Delta t}\right)_{DPBF}.\frac{V}{\varepsilon_{DPBF}}.\frac{N_A}{\alpha SI} \qquad \text{(Eq. 2.60)}$$

Eq. 2.59 can then be written as:

$$\Phi^{S}_{\Delta} = \Phi^{Std}_{\Delta}.\frac{\left(\frac{\Delta A}{\Delta t}\right)^{S}_{DPBF}}{\left(\frac{\Delta A}{\Delta t}\right)^{Std}_{DPBF}}.\frac{\alpha_{Std}}{\alpha_{S}}.\frac{[DPBF]^{Std}}{[DPBF]^{S}} \qquad \text{(Eq. 2.61)}$$

V, ε_{DPBF}, N_A, S and I cancel out since they are the same for both the Sensitizer and the standard. Eq. 2.61 suggests that the singlet oxygen quantum yield is inversely proportional to the fraction of light absorbed and the initial concentration of the quencher. Eq. 2.61 was also employed for the calculation of Φ_{Δ} using ADMA as quencher.

2.7 Rate constants for excited state deactivation

An alternative description of the quantum yield of a process emanating from an excited state is in terms of the relationship between the rate constant for the specified process and the sum of rate constants of all processes deactivating the excited state. For example, Eq. 2.62 gives the quantum yield of fluorescence (Φ_F):

$$\Phi_F = \frac{k_F}{k_F + k_{IC} + k_{ISC}} \qquad \text{(Eq. 2.62)}$$

Substituting Eq. 2.22 into Eq. 2.62 give Eq. 2.63:

$$\Phi_F = k_F.\tau_F \qquad \text{(Eq. 2.63)}$$

If the lifetime of an excited state as well as the quantum yields of all processes deactivating it are known, it is possible to calculate the rate constants for the deactivating processes. Eqs. 2.64 a-c give the expressions for rate constants for the intrinsic processes (fluorescence, F; internal conversion, IC and intersystem crossing, ISC), which deactivate the excited singlet state of a molecule:

$$k_F = \frac{\Phi_F}{\tau_F} \qquad \text{(Eq. 2.64a)}$$

$$k_{IC} = \frac{\Phi_{IC}}{\tau_F} \qquad \text{(Eq. 2.64b)}$$

$$k_{ISC} = \frac{\Phi_{ISC}}{\tau_F} \qquad \text{(Eq. 2.64c)}$$

It is believed that photodegradation mostly takes place from the excited triplet state, since this state is sufficiently long-lived to encounter species that are responsible for the molecules' degradation; hence the rate constant for this process should be calculated from the value of Φ_{Pd} and τ_T (Eq. 2.64d).

$$k_{Pd} = \frac{\Phi_{Pd}}{\tau_T} \qquad \text{(Eq. 2.64d)}$$

2.8 Fluorescence quenching

Eq. 2.22 gives an expression for the fluorescence lifetime of a fluorophore when only the three intrinsic processes deactivate the excited singlet state, i.e., no external factor contributing to the singlet decay. Rearranging Eq. 2.22 gives Eq. 2.65:

$$\frac{1}{\tau_F^0} = k_F + k_{IC} + k_{ISC} \qquad \text{(Eq. 2.65)}$$

τ_F^0 is the fluorescence intensity in the absence of a quencher. However in the presence of a reactant (Q, also known as a quencher) that intercepts the S_1 state, the following excited state reaction takes place:

$$S_1 + Q \xrightarrow{k_Q} S_0 + Q^* \qquad \text{(Eq. 2.66)}$$

The rate law for this reaction is written as:

$$\text{Rate} = k_Q[S_1][Q] \qquad \text{(Eq. 2.67)}$$

Where k_Q is the bimolecular quenching constant; $[S_1]$ and $[Q]$ are the concentrations of the S_1 state and the quencher respectively.

Assuming that the reaction is pseudo-unimolecular with $[Q] >> [S_1]$, we can state that:

$$\text{Rate} = k'[S_1] \qquad \text{(Eq. 2.68)}$$

Where

$$k' = k_Q[Q] \qquad \text{(Eq. 2.69)}$$

As a result of this quenching reaction, the fluorescence lifetime of the fluorophore is lowered, and Eq. 2.65 is modified to give Eq. 2.70:

$$\frac{1}{\tau_F} = k_F + k_{IC} + k_{ISC} + k_Q[Q] \qquad \text{(Eq. 2.70)}$$

Taking ratios of Eqs. 2.65 and 2.70,

$$\frac{\tau_F^0}{\tau_F} = \frac{k_F + k_{IC} + k_{ISC} + k_Q[Q]}{k_F + k_{IC} + k_{ISC}} \qquad \text{(Eq. 2.71)}$$

Simplification of Eq. 2.71 gives Eq. 2.72:

$$\frac{\tau_F^0}{\tau_F} = 1 + k_Q[Q].\tau_F^0 \qquad \text{(Eq. 2.72)}$$

A vital assumption made in the treatment of fluorescence quenching data is that the rate constants for the intrinsic processes (Eq. 2.64) do not change in the presence of a quencher. This implies that for any system,

$$\frac{\tau_F^0}{\tau_F} = \frac{\Phi_F^0}{\Phi_F} = \frac{I_0}{I} \qquad \text{(Eq. 2.73)}$$

Eq. 2.72 can then be rewritten as:

$$\frac{I_F^0}{I_F} = 1 + k_Q[Q].\tau_F^0 \qquad \text{(Eq. 2.74)}$$

This is the familiar Stern-Volmer (S-V) equation, which is usually written as given in chapter 1 as Eq. 1.8.

$$\frac{I_0}{I} = 1 + K_{SV}[Q] \qquad \text{(Eq. 1.8)}$$

Where k_Q (M^{-1} s^{-1}) is the bimolecular quenching rate constant, the Stern-Volmer constant (K_{SV}, M^{-1}) is defined by Eq. 1.9 (from Chapter 1):

$$K_{SV} = k_Q \tau_F^0 \qquad \text{(Eq. 1.9)}$$

A plot of $\frac{I_0}{I}$ versus [Q] should give a straight line with intercept 1 and slope K_{SV}. The observation of a straight line from this plot would indicate that the quenching process is solely by a collisional mechanism (dynamic quenching).

2.8.1 Deviation from Stern-Volmer (S-V) relationship

A large number of reactions deviate from the S-V relationship. Positive deviations, recognized by an upward curvature of the S-V plot could be caused by a number of factors which include the presence of several excited states, the ionic strength of the solution and the formation of a non-fluorescent ground state complex between the fluorophore and the quencher (static quenching, represented by the static rate constant K_S). Negative deviation from the S-V relationship is usually due to fractional accessibility of the fluorophore to the quencher. Static quenching is responsible for most observed positive deviations from the S-V relationship. In order to accommodate static quenching, the S-V equation needs to be modified.

Assuming molecules of the fluorophore (M) and quencher (Q) as continually approaching and separating in the ground state (Eq. 2.75), the non-fluorescent ground state complex formed between them does not emit a photon, and the association (static) constant (K_S) for this complex is given by Eq. 2.76 [212]:

$$M + Q \rightleftharpoons M\cdots\cdots Q \qquad \text{(Eq. 2.75)}$$

$$K_S = \frac{[M....Q]}{[M][Q]} \qquad \text{(Eq. 2.76)}$$

In order to account for the positive deviation arising from this static quenching, the S-V equation is multiplied by a factor $\frac{M_0}{M}$, where M_0 is the total number of fluorophore molecules and M, the number of uncomplexed fluorophore molecules. Hence

$$\frac{M_0}{M} = \frac{[M] + [M....Q]}{[M]} \qquad \text{(Eq. 2.77)}$$

Combining Eqs. 2.76 and 2.77 yields Eq. 2.78:

$$\frac{M_0}{M} = 1 + K_S[Q] \qquad \text{(Eq. 2.78)}$$

Multiplying the S-V equation (Eq. 1.8) by Eq. 2.78 gives rise to the modified S-V equation (Eq. 2.79), which caters for both dynamic (collisional quenching of excited fluorophore) and static (ground state complex formation) quenching mechanisms (where in the presence of both dynamic and static quenching, the K_{SV} in Eq. 1.8 is replaced with K_D, giving Eq. 2.79).

$$\frac{I_0}{I} = (1 + K_D[Q])(1 + K_S[Q]) \qquad \text{(Eq. 2.79)}$$

K_D and K_S are the dynamic and static quenching constants respectively.

To obtain K_D for a reaction described by both (dynamic and static) quenching mechanisms, the values of K_{SV} are calculated by means of Eq. 1.8 and plotted against [Q]. The values of K_{SV} are then extrapolated to [Q] = 0. The dynamic quenching constant (K_D) is the value of K_{SV} when [Q] = 0 [212]. K_S can be determined by rearranging Eq. 2.79 to give Eq. 2.80.

$$\frac{I_0}{I(1 + K_D)[Q]} = 1 + K_S[Q] \qquad \text{(Eq. 2.80)}$$

Using the value of K_D obtained above, the plot of $\frac{I_0}{I(1 + K_D)[Q]}$ versus [Q] gives the static quenching constant K_S.

2.8.2 The Sphere of Action Quenching Model (SAQM)

Occasionally, positive deviations from S-V are observed even after all factors mentioned earlier have been eliminated, and there is no evidence of complexation between the fluorophore and the quencher. This type of apparent static quenching process is often interpreted in terms of the "sphere of action" quenching model (SAQM) [213-215]. Imagine fluorophore and quencher distributions at the instant of

excitation. There is a certain probability that at this instant, some fluorophore molecules are in contact with the quencher. Fluorophore molecules in contact with the quencher at the instant of excitation will not fluoresce; hence we again have a coexistence of both dynamic and static quenching mechanisms in the same system. The customized S-V equation that takes care of this scenario is given by Eq. 2.81 [213].

$$\frac{I_0}{I} = (1 + K_D[Q]).e^{K'_S[Q]} \qquad \text{(Eq. 2.81)}$$

This rearranges to Eq. 2.82:

$$\frac{I_0}{I(1+K_D[Q])} = e^{K'_S[Q]} \qquad \text{(Eq. 2.82)}$$

Where K'_S (= VN_A) is the 'sphere of action' static quenching constant, and is related to the sphere of action volume V (the volume of the sphere that surrounds the fluorophore within which the quencher is considered to be in contact with it) and Avogadro's constant (N_A).

K'_S is obtained from the plot of $\ln \frac{I_0}{I(1+K_D[Q])}$ against [Q].

2.8.3 Interpretation of the bimolecular quenching constant

The bimolecular quenching constant (k_Q) is indicative of the effectiveness of quenching and the accessibility of the fluorophores to the quencher. According to the Einstein-Smoluchowski approximation, diffusion-controlled quenching typically results in values of k_Q near 1×10^{10} M^{-1} s^{-1}, at room temperature. Smaller values of k_Q can result from steric shielding of the fluorophore, and larger apparent values of k_Q usually indicate some type of binding interaction [215]. The diffusion-controlled

bimolecular rate constant (k_R) may be calculated using the Einstein-Smoluchowski equation:

$$k_R = \frac{4\pi N_A (D_f + D_Q)(R_f + R_Q)}{1000} \qquad \text{(Eq. 2.83)}$$

N_A is the Avogadro's number, D_f and D_Q are the diffusion coefficients of the fluorophore and quencher respectively; R_f and R_Q are the radii of fluorophore and quencher respectively. k_R is similar in meaning to k_Q except that k_R is due to collision and not necessarily quenching; while k_Q is the rate constant due to collisional quenching.

The diffusion coefficient D is given by the Stokes-Einstein equation:

$$D = \frac{kT}{6\pi\eta R} \qquad \text{(Eq. 2.84)}$$

Where k is the Boltzman constant; T, the absolute temperature; η, the solvent's viscosity and R, the molecule's radius.

The bimolecular quenching constant k_Q is related to the diffusion-controlled bimolecular rate constant k_R by Eq. 2.85:

$$k_Q = f_Q.k_R \qquad \text{(Eq. 2.85)}$$

Where f_Q is the efficiency of collision.

2.8.4 Determination of fluorescence lifetime by fluorescence quenching technique

It is possible to determine the lifetime of an excited singlet state by monitoring the fluorescence emission intensity as a function of added quencher concentration. If the S-V quenching constant (K_{SV}, Eq. 1.8), and the bimolecular quenching constant (k_Q,

Eq. 2.83 – Eq. 2.85) are known, the fluorescence lifetime (τ_F) can then be calculated from Eq. 1.9.

2.8.5 Fluorescence quenching in multiporphyrin-phthalocyanine oligomers and mixtures

Under the assumption that only the intrinsic processes deactivate the excited singlet states of the monomeric phthalocyanine (Pc) and porphyrin (P), Eq. 2.86 holds; and the singlet excited state lifetime (τ_F^M) of Pc or P monomer (M) is given by Eq. 2.87 (similar to Eq. 2.65):

$$\bullet_F + \bullet_{ISC} + \bullet_{IC} = 1 \qquad \text{(Eq. 2.86)}$$

$$\tau_F^M = \frac{1}{k_F + k_{ISC} + k_{IC}} \quad (M = Pc \text{ or } P) \qquad \text{(Eq. 2.87)}$$

The quantum yields of intrinsic processes ($\bullet_F$, $\bullet_{IC}$ and $\bullet_{ISC}$) are related to their respective rate constants (k_F, k_{IC} and k_{ISC}) by Eq. 2.64 a-c.

Maintaining the assumption that the rate constants for intrinsic processes (k_F, k_{IC} and k_{ISC}) are the same in the monomer, oligomer and mixture (the mixture consists of free Pc and P monomers in solution without chemical coupling), it can be shown that for Pc or P in the monomer (M), oligomer (Olig) and mixture (Mix), Eq. 2.88 applies.

$$\frac{\Phi_{F,Pc}^{M}}{\tau_{F,Pc}^{M}} = \frac{\Phi_{F,Pc}^{Olig}}{\tau_{F,Pc}^{Olig}} = \frac{\Phi_{F,Pc}^{Mix}}{\tau_{F,Pc}^{Mix}} = k_{F,Pc} \qquad \text{(Eq. 2.88)}$$

Where $\Phi_{F,Pc}^{M}$, $\Phi_{F,Pc}^{Olig}$ and $\Phi_{F,Pc}^{Mix}$ are the fluorescence quantum yields of Pc in monomer, oligomer and mixture, respectively, and $\tau_{F,Pc}^{Pc}$, $\tau_{,F,Pc}^{Olig}$ and $\tau_{F,Pc}^{Mix}$ are the fluorescence

lifetimes of Pc in monomer, oligomer and mixture, respectively. Similar equations could be written for P by replacing the subscripts 'Pc' with 'P' in Eq. 2.88.

Using Eq. 2.88, the values of $\tau_{F,Pc}^{Olig}$ and $\tau_{F,Pc}^{Mix}$ can be calculated from the experimental values of $\Phi_{F,Pc}^{M}$, $\Phi_{F,Pc}^{Olig}$ and $\Phi_{F,Pc}^{Mix}$ respectively, and literature values of $\tau_{F,Pc}^{M}$. Eqs. 2.89 and 2.90, similar to Eq. 2.88 could also be written for k_{ISC} and k_{IC}, i.e.,

$$\frac{\Phi_{T,Pc}^{Pc}}{\tau_{F,Pc}^{Pc}} = \frac{\Phi_{T,Pc}^{Olig}}{\tau_{F,Pc}^{Olig}} = \frac{\Phi_{T,Pc}^{Mix}}{\tau_{F,Pc}^{Mix}} = k_{ISC,Pc} \qquad \text{(Eq. 2.89)}$$

And

$$\frac{\Phi_{IC,Pc}^{Pc}}{\tau_{F,Pc}^{Pc}} = \frac{\Phi_{IC,Pc}^{Olig}}{\tau_{F,Pc}^{Olig}} = \frac{\Phi_{IC,Pc}^{Mix}}{\tau_{F,Pc}^{Mix}} = k_{IC,Pc} \qquad \text{(Eq. 2.90)}$$

Here, it is assumed that $\Phi_{ISC} = \Phi_T$.

In the oligomer, an additional deactivation pathway is introduced for the Pc excited singlet state: charge transfer quenching. It is known [60] that porphyrins are more easily oxidized than phthalocyanines; hence an electronic charge gradient is set-up between these two components of the pentamer. The efficiency of this charge transfer is expressed in terms of charge transfer quantum yield ($\bullet_{CT}$). An expression for the singlet excited state lifetime of Pc in the oligomer (or in the mixture) is thus given by Eq. 2.91:

$$\tau_{F,Pc}^{Olig} = \frac{1}{k_F + k_{ISC} + k_{IC} + k_{CT}} \qquad \text{(Eq. 2.91)}$$

However for P (in the oligomer or mixture), the singlet excited state is being deactivated by further deactivation process (energy transfer), since the lowest unoccupied molecular orbital (LUMO) for porphyrins are higher in energy than for phthalocyanines. The expression for the fluorescence lifetime of P in the oligomer (or in the mixture) is thus given by Eq. 2.92:

$$\tau_{F,P}^{Olig} = \frac{1}{k_F + k_{ISC} + k_{IC} + k_{ExT}} \qquad \text{(Eq. 2.92)}$$

Where k_{ExT} is the sum of rate constants for charge transfer (k_{CT}) and energy transfer (k_{ET}).

Combining Eq. 2.87 with equations Eqs. 2.91 and 2.92 gives equations Eqs 2.93 and 2.94, respectively

$$k_{CT} = \frac{1}{\tau_{F,Pc}^{Olig}} - \frac{1}{\tau_{F,Pc}^{M}} \qquad \text{(Eq. 2.93)}$$

and

$$k_{ExT} = \frac{1}{\tau_{F,P}^{Olig}} - \frac{1}{\tau_{F,P}^{M}} \qquad \text{(Eq. 2.94)}$$

Maintaining the assumption that k_F is the same in both the monomer and the oligomer (or mixture), Eq. 2.95 applies:

$$\frac{\Phi_F^{Olig}}{\tau_F^{Olig}} = \frac{\Phi_F^{M}}{\tau_F^{M}} = k_f \qquad \text{(Eq. 2.95)}$$

and can be rearranged to Eq. 2.96

$$\frac{1}{\tau_F^{Olig}} = \frac{\Phi_F^{M}}{\tau_F^{M}.\Phi_F^{Olig}} \qquad \text{(Eq. 2.96)}$$

Substituting for $\frac{1}{\tau_F^{Olig}}$ in Eqs. 2.93 and 2.94 gives Eqs 2.97 and 2.98:

$$k_{CT} = \frac{1}{\tau_{F,Pc}^{M}}\left(\frac{\Phi_{F,Pc}^{M}}{\Phi_{F,Pc}^{Olig}} - 1\right) \qquad \text{(Eq. 2.97)}$$

$$k_{ExT} = \frac{1}{\tau_{F,P}^{M}}\left(\frac{\Phi_{F,P}^{M}}{\Phi_{F,P}^{Olig}} - 1\right) \qquad \text{(Eq. 2.98)}$$

Having obtained the rate constants for charge transfer and the combination of charge and energy transfer (k_{CT} and k_{ExT}, respectively), the corresponding quantum yields ($\bullet_{CT}$ and $\bullet_{ExT}$) may be calculated using the Eqs. 2.99 and 2.100 :

$$\Phi_{CT,Pc} = k_{CT}.\tau_{F,Pc}^{Olig} \qquad \text{(Eq. 2.99)}$$

$$\Phi_{Ext,P} = k_{ExT}.\tau_{F,P}^{Olig} \qquad \text{(Eq. 2.100)}$$

2.9 Binding of sulphonated metallophthalocyanines ($MPcs_{mix}$) complexes to bovine serum albumin (BSA)

2.9.1 $MPcS_{mix}$-BSA binding analysis

Since the inherent fluorescence of proteins is usually quenched upon binding to tetrapyrrolic compounds, [205], this spectroscopic behaviour provides a means of studying the interaction between metallophthalocyanines (MPcs) and bovine serum albumin (BSA).

The basic reaction between an MPc complex and BSA is represented as:

$$BSA + nMPc \rightarrow BSA:(MPc)_n \qquad \text{(Eq. 2.101)}$$

Then, the expression for the binding constant (K_b) in the above equation is given by Eq. 2.102:

$$K_b = \frac{[BSA:(MPc)_n]}{[BSA][MPc]^n} \qquad \text{(Eq. 2.102)}$$

If F_0 is the fluorescence intensity of BSA in the absence of MPc; F, the fluorescence intensity of BSA in the presence of MPc; F_∞, the fluorescence intensity of BSA saturated with MPc; and n, the number of binding sites on a BSA molecule, Eq. 2.102 could be rewritten as:

$$K_b = \frac{[F_0 - F]}{[F - F_\infty][MPc]^n} \qquad \text{(Eq. 2.103)}$$

Eq. 2.103 presupposes that fluorescence emission intensities of BSA are directly proportional to its concentrations.

Taking logs of both sides of Eq. 2.103 and rearranging yield Eq. 2.104:

$$\log\left[\frac{(F_0 - F)}{(F - F_\infty)}\right] = \log K_b + n\log[MPc] \qquad \text{(Eq. 2.104)}$$

Plots of $\log\left[\frac{(F_0 - F)}{(F - F_\infty)}\right]$ against log [MPc] should give a straight line with slope n and intercept log K_b.

2.9.2 Determination of $MPcS_{mix}$ fluorescence lifetimes from $MPcS_{mix}$ -BSA interaction

$MPcS_{mix}$ fluorescence lifetimes were determined by monitoring the fluorescence intensity as a function of quencher concentration. Here, two sets of data were obtained from: (i) quenching of BSA fluorescence by $MPcS_{mix}$ and (ii) quenching of $MPcS_{mix}$ fluorescence by BSA. For (i), the quenching of BSA by $MPcS_{mix}$, the changes in BSA fluorescence intensity were related to $MPcS_{mix}$ concentrations by the Stern-Volmer relationship (Eq. 2.105), similar to Eq. 1.8:

$$\frac{F_0^{BSA}}{F^{BSA}} = 1 + K_{SV}^{BSA}[MPcS_{mix}] \qquad \text{(Eq. 2.105)}$$

and K_{SV}^{BSA} is given by Eq. 2.106 (similar to Eq. 1.9):

$$K_{SV}^{BSA} = k_Q \tau_F^{BSA} \qquad \text{(Eq. 2.106)}$$

Where F_0^{BSA} and F^{BSA} are the fluorescence intensities of BSA in the absence and presence of $MPcS_{mix}$ respectively; K_{SV}^{BSA}, the Stern-Volmer quenching constant; k_Q, the bimolecular quenching constant; and τ_F^{BSA}, the fluorescence lifetime of BSA. τ_F^{BSA}

is known from literature, thus from the values K_{SV}^{BSA} obtained from the plots of $\frac{F_0^{BSA}}{F^{BSA}}$ versus [$MPcS_{mix}$], the value of k_Q may be determined from Eq. 2.106. For quenching of $MPcS_{mix}$ by BSA, Eqs. 2.107 and 2.108 apply.

$$\frac{F_0^{MPc}}{F^{MPc}} = 1 + K_{SV}^{MPc}[BSA] \qquad \text{(Eq. 2.107)}$$

$$K_{SV}^{MPc} = K_Q \tau_F^{MPc} \qquad \text{(Eq. 2.108)}$$

Where F_0^{MPc} and F^{MPc} are the fluorescence intensities of $MPcS_{mix}$ in the absence and presence of BSA respectively; K_{SV}^{MPc}, the Stern-Volmer quenching constant; k_Q, the bimolecular quenching constant; and τ_F^{MPc}, the fluorescence lifetime of $MPcS_{mix}$. In both cases, k_Q is assumed to be the same. Using K_{SV}^{MPc} from the plot generated by Eq. 2.107, and k_Q from Eq. 2.106, we can obtain the value of τ_F^{MPc} from Eq. 2.108.

3 EXPERIMENTAL

This chapter discusses the experimental procedures undertaken during the course of the study, leading to this thesis writing. It gives an experimental complement to the theoretical and mathematical portrayal of this study as discussed in the previous chapters.

3.1 EQUIPMENT

The various equipments used in this study are listed alongside the techniques for which each was used, as follows:

(i) Ground state electronic absorption spectra: Varian Cary 500 Scan UV-Vis-NIR spectrophotometer.

(ii) Infra-red spectra: Perkin Elmer Spectrum 2000 FT-IR Spectrometer.

(iii) ^{1}H nuclear magnetic resonance: Bruker EMX 400 NMR spectrometer.

(iv) X-ray powder diffraction: Philips PW 1012 diffractometer.

(v) Chromatographic separation: Quad-Gradient HPLC system, Agilent 1100 Series; fitted with an analytical column, μ Bondapak C18 (390 x 3.00 mm) and connected to a variable wavelength UV-Vis detector (set at λ = 365 nm). The mobile phase comprised of 50:50 methanol:water mixture, with a flow rate of 1 ml min^{-1} and sample injection volume of 20 μl.

(vi) Fluorescence excitation and emission spectra: Varian Cary Eclipse Fluorescence spectrophotometer.

(vii) Photo-irradiations were done using a General electric Quartz line lamp (300W). A 600 nm glass cut off filter (Schott) and a water filter were used to filter off ultraviolet and infrared radiations respectively. An interference filter (Intor, 670 nm with a band width of 20 nm) was additionally placed in the light path before the sample (Fig. 3.1).

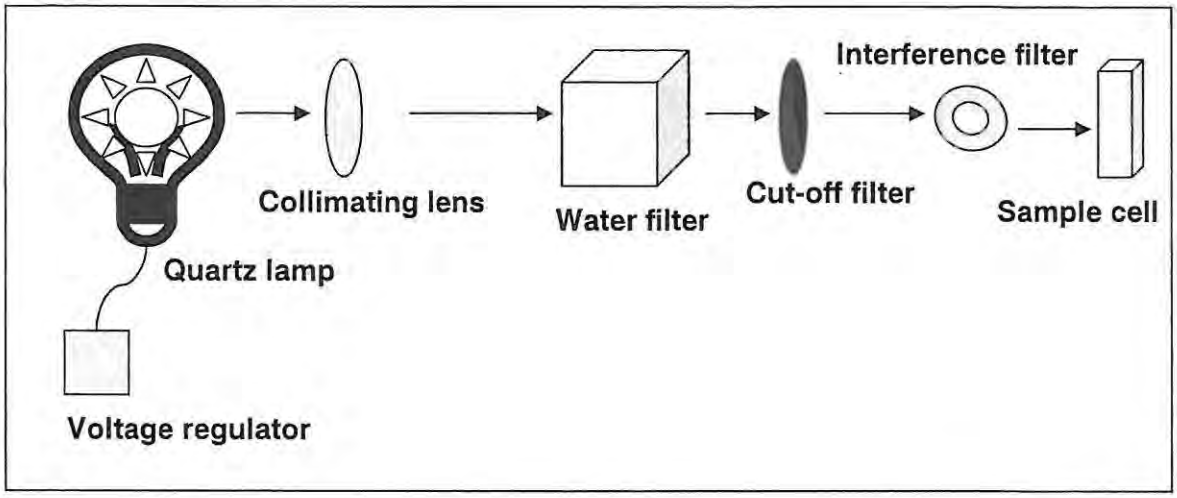

Fig. 3.1: The photo-irradiation set-up

(viii) Light intensities were measured with a POWER MAX 5100 (Molelectron detector incorporated) power meter.

(ix) Triplet absorption and decay kinetics were recorded on a laser flash photolysis system. The excitation pulses were produced by a Nd: YAG laser (Quanta-Ray, 1.5 J / 8 ns)- pumped tunable dye laser (Lambda Physic FL 3002, Pyridine 1 dye in methanol). The analyzing beam source was from a Thermo Oriel xenon arc lamp, and a photomultiplier tube (PMT) was used as detector. Signals were recorded with a Tektronix TDS 360 two-channel digital real-time oscilloscope.

A schematic representation of the laser flash photolysis set-up is shown in Fig. 3.2.

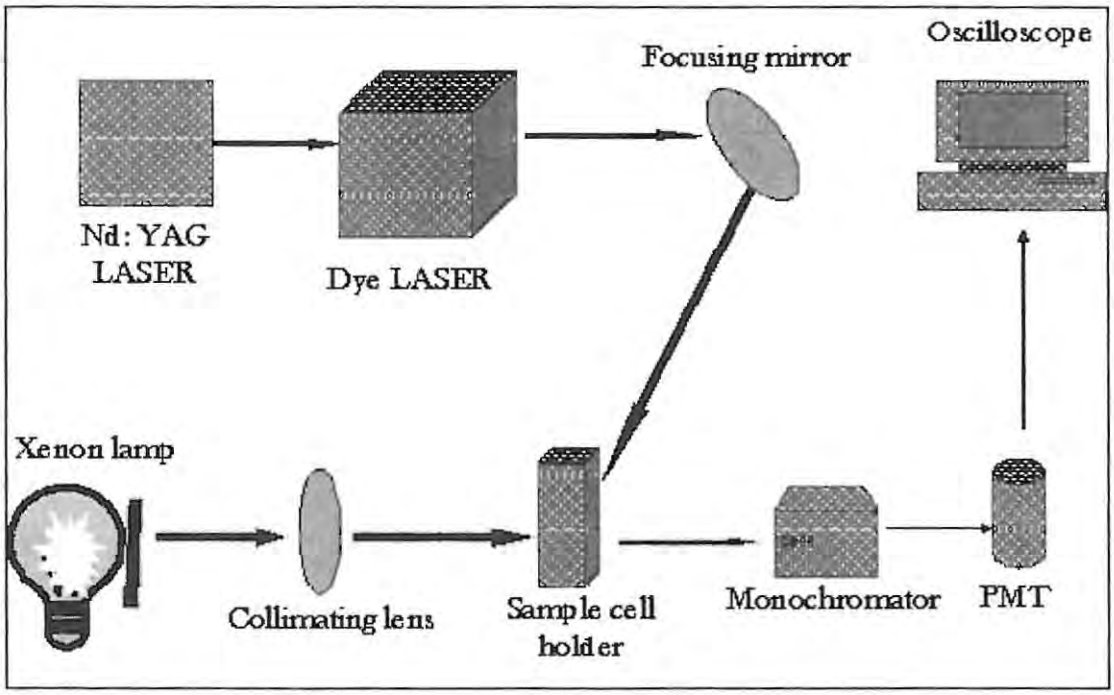

Fig. 3.2: Schematic diagram of the laser flash photolysis set-up.

3.2 MATERIALS

3.2.1 Solvents

All solvents used in this study were purchased from either Aldrich or SAARCHEM. A list of the solvents is given below:

Benzene, benzonitrile, n-butylamine, chlorobenzene, chloroform, 1-chloronaphthalene, deuterated chloroform ($CDCl_3$), dichloromethane, diethyl ether, *N,N'*-dimethylformamide (DMF), dimethylsulphoxide (DMSO), 1,4-dioxane, ethanol, ethyl acetate, methanol, nitrobenzene, propanol, pyridine, quinoline, tetrahydrofuran (THF), toluene, triehtylamine (TEA) and *o*-xylene. DMSO (SAARCHEM) was dried on alumina before use and DMF was freshly distilled. Phosphate buffer solution (PBS, pH 7.4) was prepared by mixing KH_2PO_4 (0.008695 mol) and Na_2HPO_4

(0.03043 mol) in 1 kg of milli-pore water. All other solvents were used as received without further purification.

3.2.2 Reagents

Aluminium chloride ($AlCl_3$), 1,4-benzoquinone (BQ), chloroaluminium phthalocyanine (ClAlPc, **33**), chlorophyll a (**34**), 1,3-diphenyl*iso*benzofuran (DPBF), napthalene dicarboxylic acid, 4-nitrophthalimide, 4-nitrophthalonitrile, phthalonitrile, sodium sulphide and zinc acetate were purchased form Aldrich; bovine serum albumin (BSA) and trifluoroacetic acid (TFA), from FLUKA; hydroquinone (HQ) and potassium cyanide, from May & Baker; germanium(IV) chloride and piperidine, from Riedel-de-haën AG; sodium hydroxide (NaOH) and concentrated sulphuric acid, from SAARCHEM; and alumina, β-cyclodextrin (β-CD), hydroxypropyl-γ-cyclodextrin (HPγ-CD) and Triton X-100 (TX), from Sigma. Tetrasodium anthracene-9,10-bis-methylmalonate (ADMA) was a gift from Dr N. Kuznetsova.

3.2.3 Methallophthalocyanine (MPc) substrates

The MPc substrates used in this study were either bought or synthesized according to the referenced literature methods:

Unsubstituted zinc phthalocyanine (ZnPc, **15**) and tetraphenylzinc porphyrin (ZnTPP) were bought from Aldrich; tetrasulphozinc phthalocyanine (ZnTSPc, **18** [78]), (*tert*-butylphenoxy)zinc phthalocyanine (ZnTBPPc, **19** [77]), octaestronezinc phthalocyanine (ZnOEPc, **21** [77]), octaphenoxyzinc phthalocyanine (ZnOPPc, **22** [77] and octamethylphenoyzinc phthalocyanine (ZnOMPPc, **23** [77], dichlorosilicon(IV) phthalocyanine (Cl_2SiPc, **35** [140]) and dichlorotin(IV)

phthalocyanine (Cl_2SnPc, **36** [76) were synthesized in our laboratory as referenced; Phthalocyanine-tetraporphyrin heteropentamer : zinc(II) *tetrakis*(5-phenoxy-10,15,20-triphenylporphyrin)zinc(II) phthalocyanine ($ZnPc\text{-}(O\text{-}ZnTPP)_4$, **20**), ZnPc with axial ligands: cyanozinc phthalocyanine {(CN)ZnPc, **24**}, piperidinozinc phthalocyanine {(pip)ZnPc, **25**} and pyridinozinc phthalocyanine {(py)ZnPc, **26**}; mixtures of differently sulphonated metallophthalocyanines: $AlPcS_{mix}$ (**27**), $ZnPcS_{mix}$ (**28**), $SiPcS_{mix}$ (**29**), $GePcS_{mix}$ (**30**) and $SnPcS_{mix}$ (**31**); and zinc naphthalocyanine (ZnNPc, **32**), dichlorogermanium(IV) phthalocyanine (Cl_2GePc, **37**), dihydroxygermanium(IV) phthalocyanine ($GePc(OH)_2$, **38**), dihydroxysilicon(IV) phthalocyanine ($SiPc(OH)_2$, **39**) and dihydroxytin(IV) phthalocyanine ($SnPc(OH)_2$, **40**) were synthesized and characterized according to established literature methods as described in the following sections.

3.2.3.1 Syntheses of tetranitrozinc phthalocyanine ZnTNPc (17, [216]) and tetraaminozinc phthalocyanine (ZnTAPc (16, [216]) – Scheme 4.1.

ZnTNPc (17)

4-Nitrophthalimide (**41**, 1.81 g, 9.45 mmol), zinc chloride (0.3529 g, 2.59 mmol), ammonium chloride (0.2474 g, 4.63 mmol), ammonium molybdate (0.0282 g, 0.02 mmol) and excess urea (3 g) were finely ground and added to nitrobenzene (10 cm^3) in a 500 cm^3 flask. The mixture was refluxed for 5 hrs at 190 ºC after a gradual temperature increase from 25 to 190 ºC over 30 min. After filtration and washing with methanol to remove the nitrobenzene, the deep purple solid was added to sodium chloride-saturated 1M hydrochloric acid (30 cm^3). This suspension was boiled for about 5 min and filtered after cooling. The solid was added to 1M sodium hydroxide (30 cm^3) containing sodium chloride (11 g) and heated at 90 ºC for 30 min. After

filteration, the solid product was treated with sodium chloride-saturated 1M hydrochloric acid (30 cm^3) and 1M sodium hydroxide (30 cm^3) containing excess sodium chloride (as before) twice alternatively and separated each time by centrifugation. The green compound obtained was washed with water (100 cm^3) and dried overnight at 135 ºC to yield ZnTNPc (**17**) (0.79 g, 45%); IR [(KBr) ν_{max}/cm^{-1}]: 3098w, 1521s (NO_2 asym), 1338vs (NO_2 sym), 1118w, 1091m, 1060w, 936w, 857w, 765s; UV-Vis [DMSO, λ_{max}/nm (log ε)]: 682 (4.88), 645 (4.66), 347 (4.79).

(ZnTAPc (16)

ZnTNPc (**17**, 0.74 g, 0.98 mmol)) was finely ground and suspended in water (20 cm^3). Sodium sulphide nonahydrate (3.7 g, 15.41 mmol) was added and the mixture stirred at 50 ºC for 5 hrs. The dark green product was separated by centrifugation and treated with 1M hydrochloric acid (60 cm^3). After removal of residual solids by centrifuging, the acidic solution was stirred in 1M sodium hydroxide (40 cm^3) for 1 hr and centrifuged again. The green product was washed with water (40 cm^3) and dried overnight at 140 ºC to yield the green amine, ZnTAPc (**16**) (0.59 g, 95%); IR [(KBr) ν_{max}/cm^{-1}]: 3350w (N–H str), 3187w, 1618s (NH_2 def), 1411m, 1341w, 1306w, 1252w, 1133m, 1095m, 1052m, 949w, 865w, 832w, 746w, 731m; UV-Vis [DMSO, λ_{max}/nm (log ε)]: 727 (4.75), 647 (4.40), 354 (4.75).

3.2.3.2 Syntheses of cyanozinc phthalocyanine {(CN)ZnPc, 24}, piperidinozinc phthalocyanine {(pip)ZnPc, 25} and pyridinozinc phthalocyanine {(py)ZnPc, 26} [108,109]

For (pip)ZnPc (**25**) and (py)ZnPc (**26**), ZnPc was refluxed, respectively in piperidine and pyridine for 3 hrs. The solvents were then evaporated in air; the solid dried at 60

°C and washed with hexanes. In the case of (CN)ZnPc (**24**) synthesis, 4.6 x 10^{-4} M ZnPc was mixed with excess potassium cyanide and the mixture refluxed in DMF for 3 hrs. The resulting solution was evaporated to dryness; the solid washed in water and recrystallized from absolute ethanol. The axially ligated ZnPc derivatives are known to be five-coordinate [47] and are thus represented as {(pip)ZnPc}, {(py)ZnPc} and {(CN)ZnPc}, respectively. These complexes gave satisfactory spectroscopic data as reported in literature [108,109].

(CN)ZnPc (24): IR [(KBr) ν_{max}/cm^{-1}]: 3411m, 2108s (C≡N), 1608w, 1488m, 1461m, 1440m, 1349m, 1209m, 1283s, 1207w, 1166m, 1139s, 948s, 860w, 790w, 761s; UV-Vis [DMF, λ_{max}/nm (log ε)]: 672 (5.38), 640 (4.61), 605 (4.64), 390 (4.65), 330 (4.79).

(pip)ZnPc (25): IR [(KBr) ν_{max}/cm^{-1}]: 3409m, 1609w, 1491m, 1460m, 1438m, 1348m, 1467m, 1450m, 1346m, 1217m, 1279s, 1210w, 1169m, 1144s, 959s, 849w, 800w, 755s; UV-Vis [DMF, λ_{max}/nm (log ε)]: 670 (5.40), 639 (4.62), 603 (4.66), 352 (4.82).

(py)ZnPc, (26): IR [(KBr) ν_{max}/cm^{-1}]: 3414m, 1605w, 1490m, 1464m, 1441m, 1348m, 1466m, 1449m, 1334m, 1220m, 1277s, 1211w, 1171m, 1143s, 961s, 844w, 803w, 751s; UV-Vis [DMF, λ_{max}/nm (log ε)]: 669 (5.44), 639 (4.63), 604 (4.68), 350 (4.84).

3.2.3.3 Dichlorogermanium(IV) phthalocyanine (Cl_2GePc, 37) [217] (Same as Scheme 1.3a with R = H)

Germanium(IV) chloride (3.55 g, 10 mmol) was added under nitrogen to 20 ml of quinoline and brought quickly to reflux. When the temperature of the solution reached

200 ºC, phthalonitrile (**10**) (6 g, 39 mmol) was added to the mixture. The solution was next refluxed for 4 hrs and then allowed to cool slowly to room temperature over 2 hrs. The purple microcrystalline product was filtered off, washed with DMF and ether, and dried in air (Yield: 90%). The product gave satisfactory spectroscopic data as reported in the literature [217]. IR [(KBr) ν_{max}/cm^{-1}]: 1612m, 1591w, 1514s, 1423s, 1331s, 1288s, 1165m, 1125s, 1095w, 1080w, 961w, 900s, 885m, 868m, 801w, 784s, 768w, 752s, 723s, 689m, 643w, 611w, 577m, 510m and 435w (Ge–Cl), 423w; UV-Vis [DMSO, λ_{max}/nm]: 676, 644, 608, 358.

3.2.3.4 Dihydroxygermanium(IV) phthalocyanine ($GePc(OH)_2$, 38) [218]

Cl_2GePc (**37**) (0.3 g, 0.21 mmol) was refluxed in 1:1 pyridine:conc. ammonia solution (20 ml) for 6 hrs. The blue hydroxide was dried at 110 ºC. IR [(KBr) ν_{max}/cm^{-1}]: 3204br (O–H), 1606m, 1584w, 1503s, 1423m, 1349m, 1334s, 1293s, 1197w, 1177w, 1169m, 1136s, 1125s, 1099w, 1071s, 1001w, 988w, 951m, 900s, 872w, 798w, 780m, 770m, 759s, 709s, 675w, 648s (Ge–O), 641w 610w, 571m, 504m; UV-Vis [DMSO, λ_{max}/nm]: 676, 645, 609, 357.

3.2.3.5 Dihydroxysilicon(IV) phthalocyanine ($SiPc(OH)_2$, 39) [219]

Cl_2SiPc (**35**) (0.44 g, 0.72 mmol), NaOH (0.11 g, 2.75 mmol), H_2O (20 ml) and pyridine (5 ml) were refluxed for 1 hr. The product was recovered by filteration, washed with water and dried in vacuo. Spectroscopic data for the compound were satisfactory. IR [(KBr) ν_{max}/cm^{-1}]: 3201br (O–H), 1610m, 1599w, 1516s, 1430s, 1333s, 1291s, 1222w, 1168m, 1133m, 1120s, 1075s, 1071s, 1023w, 990w, 976w, 947w, 910m, 873w, 831s (Si–O), 779s, 776w, 759s, 730s, 701w, 675w, 641m, 618w, 573m, 530m, 448w; UV-Vis [DMSO, λ_{max}/nm]: 672, 641, 602, 341.

3.2.3.6 Dihydroxytin(IV) phthalocyanine ($SnPc(OH)_2$, 40) [217]

Cl_2SnPc (**36**) (0.13 g, 0.18 mmol) was hydrolysed by mixing with NaOH (0.1 g, 2.5 mmol), pyridine (5 ml) and H_2O (20 ml). The mixture was refluxed for 5 hrs and then allowed to cool slowly. The blue solid was filtered off, washed with water and dried in a vacuum desiccator. IR [(KBr) ν_{max}/cm^{-1}]: 3208br (O–H), 1614m, 1406m, 1342s, 1331s, 1294w, 1285s, 1187w, 1164m, 1136m, 1112s, 1081s, 1049s, 1005w, 981w, 953w, 893s, 805w, 779m, 766m, 756s, 715s, 701m, 678w, 638w, 564s (Sn–O), 505m, 435m; UV-Vis [DMSO, λ_{max}/nm]: 698, 630, 358.

3.2.3.7 Syntheses of $AlPcS_{mix}$ (27), $ZnPcS_{mix}$ (28), $SiPcS_{mix}$ (29), $GePcS_{mix}$ (30) and $SnPcS_{mix}$ (31) [79] (As in Scheme 1.6).

These complexes, containing differently substituted sulphophthalocyanines were synthesized from ClAlPc (**33**), ZnPc (**15**), $(OH)_2SiPc$ (**39**), $(OH)_2GePc$ (**38**) and $(OH)_2SnPc$ (**40**) respectively, using fuming sulphuric acid (30% SO_3) according to the reported procedures for $AlPcS_{mix}$ [79,174]. The respective precursor (named above, 8 mmol) was stirred and heated to 100 °C. Oleum (25 ml, containing 30% SO_3) was added and the mixture stirred vigorously and maintained at 100 °C for 25 mins. The reaction was quenched by pouring unto crushed ice (200 g) and the resulting mixture was adjusted to pH 7.0-7.5 by addition of NaOH solution. The resulting solution was evaporated to dryness and the residue was Soxhlet extracted with methanol (200 ml) for 12 hrs. The solvent was removed by evaporation. The $MPcS_{mix}$ complexes are known [9] to contain a mixture of the di-, tri-, and tetra- sulphonated derivatives with an average of three sulphonate groups per molecule.

AlPcS$_{mix}$ (27): IR [(KBr) ν_{max}/cm^{-1}]: 3200br (O–H), 1730m, 1637m, 1497w, 1399w, 1332m, 1231m, 1175m, 1111s, 1031s (S=O), 916m, 753m, 721m; UV-Vis: [pH 7.4, λ_{max}/nm (log ε)]: 674 (5.18), 607 (4.40), 349 (4.78)].

ZnPcS$_{mix}$ (28): IR [(KBr) ν_{max}/cm^{-1}]: 3210br (O–H), 1734m, 1624m, 1545w, 1391s, 1222m, 1203w, 1145m, 1091w, 1040s (S=O), 977w, 905w, 745m, 716w; UV-Vis: [pH 7.4, λ_{max}/nm (log ε)]: 673 (4.89), 630 (4.55)].

SiPcS$_{mix}$ (29): IR [(KBr) ν_{max}/cm^{-1}]: 3211br (O–H), 1642m, 1618w, 1572m, 1389m, 1287w, 1191m, 1133m, 1037s (S=O), 897w, 830w (Si–O), 621w; UV-Vis: [pH 7.4, λ_{max}/nm (log ε)]: 678 (5.11), 641 (4.83), 605 (4.62), 339 (5.00)].

GePcS$_{mix}$ (30): IR [(KBr) ν_{max}/cm^{-1}]: 3217br (O–H), 1647m, 1621m, 1577m, 1391m, 1288w, 1193m, 1138m, 1042s (S=O), 905w, 815w, 647w (Ge–O), 627w; UV-Vis: [pH 7.4, λ_{max}/nm (log ε)]: 680 (5.01), 610 (4.29), 354 (4.65)].

SnPcS$_{mix}$ (31): IR [(KBr) ν_{max}/cm^{-1}]: 3206br (O–H), 1728m, 1586m, 1397w, 1305w, 1202m, 1136w, 1079s, 1036s (S=O), 887m, 850w, 803w, 745m, 713m, 638w, 566w (Sn–O); UV-Vis: [pH 7.4, λ_{max}/nm (log ε)]: 688 (4.57), 640 (4.39)].

3.2.3.8 Synthesis of ZnNPc (32) [220] – Scheme 4.2

Naphthalene-2,3-dicarboxylic acid (**42**, 2 g, 9.3 mmol) was mixed with urea (3 g, 50 mmol), and zinc acetate (1 g, 5.5 mmol); the mixture was heated to 310 ºC for 40 mins. Purification of the crude product was first achieved by sublimation of volatile impurities and then by extraction with pyridine for 48 hrs.

IR [(KBr) ν_{max}/cm^{-1}]: 3049w, 2927m, 1709m, 1606m, 1517m, 1425m, 1365m, 1162s, 1088s, 1020m, 891m, 756m cm^{-1}; UV-Vis: [DMSO, λ_{max}/nm (log ε)]: 766 (5.20) and 332 (4.62).

3.2.3.9 Synthesis of (ZnPc-(O-ZnTPP)$_4$, (20) – Scheme 4.3

This molecule has not been reported in the literature; hence full characterization details are provided.

Preparation of 5-[4-(3,4-dicyanophenoxy)phenyl],10,15,20-triphenylporphyrin (CNOTPP, 45)

5-hydroxyphenoxy-10,15,20-triphenylporphyrin, (P-OH)TPP, **43**, was synthesized according to literature methods [221]. A mixture of (P-OH)TPP (**43**, 0.23 g, 0.365 mmol), 4-nitrophthalonitrile (**44**, 0.104 g, 0.6mmol) and K_2CO_3 (0.276 g, 2 mmol) in dry DMSO (20 ml) was heated at 70 ºC for 5 hrs with stirring under a nitrogen atmosphere. The reaction progress was monitored by thin layer chromatography (TLC). After cooling to room temperature, the purple reaction mixture was poured into 100 ml dichloromethane and washed three times with 100 ml water. The dichloromethane was removed by evaporation. Column chromatography on silica gel with dichloromethane as eluent gave two bands; the first band was found to be the product. The second band was the starting material. Evaporation of the dichloromethane afforded 0.20g (72.3%) of purple solid. The purple crude product (**45**) was recrystallized from dichloromethane with absolute methanol. ^{1}H NMR (400 MHz, $CDCl_3$), δ 8.89 (d, 2H, phenyl H), 8.85 (d, 6H, phenyl H), 8.30 (d, 2H, phenyl-H), 8.23 (d, 6H, phenyl-H), 7.88 (d, 1H, J = 8.6 Hz, phthalonitrile), 7.77-7.83 (m, 9H, pyrrole-H (8) & phenyl-H(1)), 7.63 (s, 1H, J = 2.4 Hz, phthalonitrile H), 7.56 (d, 1H, J = 8.63, Hz, phthalonitrile H), 7.46 (d, 2H, phenyl-H), -2.78 (s, 2H, N-H); IR [(KBr) ν_{max}/cm^{-1}]: 3316w, 2231m (C≡N), 1473w, 1207 (C-O-C), 966m ; UV-Vis [$CHCl_3$, λ_{max}/nm (log ε)]: 306 (3.18), 417 (5.52), 515 (4.23), 550 (3.85), 590 (3.66), 645 (3.51).

***Preparation of 5-[4-(3,4-dicyanophenoxy)phenyl],10,15,20-triphenylporphyrin zinc (II) (ZnCNOTPP, 46)* – Scheme 4.3**

A mixture of CNOTPP (**45**, 0.12 g, 0.159 mmol) and hydrous zinc acetate (0.171 g, 0.75 mmol) in chloroform (10 ml) was heated at reflux for 5 hrs with stirring. After cooling to room temperature, the mixture was washed with 100 ml water three times to remove excess zinc acetate and acetic acid. Column chromatography on silica gel with dichloromethane as eluent gave one band. Removal of dichloromethane by evaporation afforded 0.115 g (88.2%) of a purple-red solid. The purple-red crude product (**46**) was recrystallized from dichloromethane with absolute methanol. ^{1}H NMR (400 MHz, $CDCl_3$), δ 8.99 (d, 2H, phenyl H), 8.96 (d, 6H, phenyl H), 8.31 (d, 2H, phenyl-H), 8.22 (d, 6H, phenyl-H), 7.88 (d, 1H, J = 8.67 Hz, phthalonitrile), 7.67 -7.83 (m, 9H, pyrrole-H (8) & phenyl-H(1)), 7.63 (s, 1H, J = 3.0 Hz, phthalonitrile H), 7.56 (d, 1H, J = 8.43 Hz, phthalonitrile H), 7.46 (d, 2H, phenyl-H); IR [(KBr) ν_{max}/cm^{-1}]: 2229m (C≡N), 1484w, 1205s (C-O-C) ; UV-Vis [$CHCl_3$, λ_{max}/nm (log ε)]: 306 (3.80), 419 (5.57), 556 (4.14), 595 (3.29);

***Preparation of the tetra(5-phenoxy-10,15,20-triphenylporphyrin zinc (II)) zinc(II) phthalocyanine (ZnPc-(O-ZnTPP)$_4$)* (20, Scheme 4.3)**

A mixture of ZnCNOTPP (**46**, 20 mg, 0.025 mmol) and sodium methoxide (5 mg) was added to distilled methanol (5 ml). Anhydrous ammonia gas was bubbled through the strirred suspension for 1 hr. The suspension was then refluxed for 6 hrs with continued addition of ammonia gas, giving an imido internediate, which was not isolated. The methanol was removed, then hydrous zinc acetate (11 mg, 0.05 mmol), DBU (2 drops) and propan-1-ol (2 ml) was added. The mixture was heated at 95°C for 2hrs with stirring under a nitrogen atmosphere. The reaction procedure was monitored

by UV-Vis spectroscopy. After cooling to room temperature, the blue-purple solution was poured into 20 ml dichloromethane, washed three times with 100 ml water. The dichloromethane layer was collected, evaporated and the solid applied to a silica gel column. A series of purple bands was eluted by dichloromethane. The desired compound (blue bands) was eluted using dichloromethane with 5% methanol. Removal of dichloromethane and methanol by evaporation afforded 3.3 mg (15.8%) of a dark-purple solid (**20**), which was recrystallized from dichloromethane with hexane. ^{1}H NMR (400 MHz, DMSO-d_6), δ 9.05 (d, 4H, phthalocyanine H), δ 8.89 (d, 4H, phthalocyanine H), 8.55 –8.78 (m, 32H, pyrrole H), 8.31 (broad s, 4H, phthalocyanine H), 7.86 -8.17 (m, 32H, phenyl-2, 6 H), 7.72, 7.45 –7.58 (m, 44 H, phenyl-3, 4, 5 H); IR [(KBr) ν_{max}/cm^{-1}]: 2923s, 2851s, 1587m, 1472s, 1205s (C-O-C), 1165m, 1092w, 881w, 751w ; UV-Vis [DMSO, λ_{max}/nm (log ε)]: 682 (5.04), 602 (4.10), 561 (4.63), 429 (5.59), 365 (4.83);

3.3 PROTONATION OF ZnPc DERIVATIVES

Protonation of the MPc ring was performed (in different solvents, Table 4.18) by the addition of the protonating agent (trifluoroacetic acid (TFA), concentrated sulphuric acid or aluminium chloride) in increasing concentrations to a fixed concentration of the ZnPc derivative, and observing the spectral changes that accompanied the addition of the protonating agent. Protonation is achieved when the intensities of the new red-shifted bands reach their maxima. Only the mono- and di-protonation were obtained using TFA. With concentrated H_2SO_4, however, tetra-protonation was achieved. The substituted ZnPc derivatives degraded on addition of H_2SO_4.

3.4 CYCLODEXTRIN INCLUSION OF ZnPc DERIVATIVES

DMSO was employed as solvent for the inclusion process. The inclusion of the complexes into cyclodextrins (CDs) was performed using a 1:6 (ZnPc:CD) molar ratio. The ZnPc:cyclodextrin mixture (1:6) was dissolved in DMSO and heated at 80 ºC for 24 hrs. The solution was then cooled in an ice bath and kept at 5 ºC for a further 24 hrs. Uncomplexed CD precipitated out during this time and the precipitate was removed by filteration. Ethyl acetate was added to the solution to precipitate out the inclusion complex, which was then obtained by filteration. β-CD was employed for the inclusion of ZnPc (**15**), ZnTAPc (**16**), ZnTNPc (**17**) and ZnNPc (**32**), while ZnTBPPc (**19**) was included in HPγ-CD, due to the large cavity of this CD which can accommodate the large tertiary butyl substituents of **19**. Formation of the complexes was confirmed by X-ray powder diffraction and ^{1}H NMR spectroscopy. The resulting inclusion complexes were used for photochemical and fluorescence studies. For comparison, compounds **15** and **32** were additionally included into β-CD by cogrinding method as follows: β-CD (29.2 mg, 2.57 x 10^{-5} mol) was placed in a small mortar, and the mortar placed in a closed vessel containing water to encourage the entrapment of water molecules into the CD cavity. After 12 hrs, **15** (3.71 mg, 4.8 x 10^{-6} mol) or **32** (5 mg, 8.7 x 10^{-6} mol) was added, the mixture thoroughly milled in the mortar and dried in the oven at 100 ºC for 12 hrs. The inclusion complex formation happens by replacement of water molecules in the CD cavity with a guest molecule [222].

The stoichiometry of the inclusion complexes with CD was evaluated by Job's method. Various dilutions of solutions of the MPc derivatives (2.0 x 10^{-6} M) and the

CDs (2.0×10^{-5} M) were mixed to standard volumes to make the mole fractions shown in the appropriate figures. After an equilibration period of 24 hrs, the absorption spectra of each solution measured, and Job's plot was constructed for the absorbance differences at the Q band maximum.

3.5 $MPcS_{mix}$ BINDING TO BOVINE SERUM ALBUMIN

The binding of the $MPcS_{mix}$ complexes to BSA was studied by spectrofluorometry at 25 ºC. A solution of BSA in PBS 7.4 was titrated with increasing concentrations of the respective $MPcS_{mix}$ solution. BSA fluorescence was excited at 280 nm and recorded between 290 nm and 500 nm, with excitation and emission bandwidths of 5 nm. The steady diminution in BSA fluorescence with increase in $MPcS_{mix}$ concentration were noted and used in the determination of the binding constant and the number of binding sites on BSA, according to Eq. 2.104.

3.6 MPc PHOTOPHYSICS

3.6.1 Fluorescence quantum yields

The determination of fluorescence quantum yield begins with the choice of the right standard. Then solutions of the MPc complex under investigation and the standard (concentration ~ 1×10^{-6} M) were prepared, the absorbance of each determined, and finally the emission spectra of these solutions were recorded in order to measure the

area under the curves. Where different solvents were used for the MPc and the standard, a correction for the refractive indices was done. Absorbances were measured at the wavelengths that were later used for excitation. These wavelengths were lower than those of the absorption maxima, as exciting at wavelengths very close to the absorption maxima did not yield the full emission spectra of the MPcs. The absorbances used for the measurements ranged between 0.04 and 0.05. The solutions with absorbances around 0.04 - 0.05 were not prepared directly, due to lack of precision of most instruments in this range [207]. Instead, absorbances of ~ 0.4 - 0.5 were recorded and the solutions diluted by a factor of 10.

The excitation bandwidth was kept small on the instrument, since excitation is assumed to be monochromatic. The settings on the instrument remained unchanged until the end of the experiment, so that the spectra of the MPc and the standard were comparable. During the experiments, it was ascertained that the baseline returned to zero in the red region. Fluorescence quantum yields were calculated using Eq. 2.10, and chlorophyll a in ether ($\Phi_F = 0.32$, [223]) was used as standard.

3.6.2 Triplet quantum yields and lifetimes

Triplet absorption and decay kinetics were recorded with the flash photolysis system described above (Section 3.1). The solution of the MPc under investigation (abs ~ 3.5 in a 1cm cell) was introduced into a 2 mm x 10 mm spectrophotometric cell, nitrogen bubbled through for 20 mins and the solution irradiated at the Q band maximum using the Nd: YAG laser-pumped dye laser. Triplet quantum yields (Φ_T) were determined by triplet absorption (Eq. 2.35) or singlet depletion (Eq. 2.36). Depending on the solvent in which the determination was being made, the following reference standards

were employed: ZnPc in DMSO (Φ_T = 0.65, [167]); ZnPc in toluene (Φ_T = 0.65, [224]) and ZnTSPc in H_2O (Φ_T = 0.56 [158]).

The kinetic curves obtained were averaged over 256 laser pulses using an oscilloscope. Triplet lifetimes were determined by exponential fitting of the kinetic curves using the OriginPro 7.5 software, and Eq. 2.19.

For ZnPc(-OZnTPP)$_4$ (**20**), photophysical studies were performed for the pentamer, the individual components and for the mixture of the components (ZnPc/4ZnTPP).

3.6.3 MPc fluorescence quenching by benzoquinone (BQ) and hydroquinone (HQ)

Fluorescence quenching experiments were carried out by adding increasing concentrations of the quencher (BQ or HQ) to a fixed concentration of the MPc complex. The quencher concentrations in the resulting mixtures were 0, 0.008, 0.016, 0.024, 0.032, 0.040 and 0.048 M. The fluorescence spectra of the MPc substrate in the absence and presence of the various quencher concentrations were recorded, and the changes in fluorescence intensity with quencher concentration analysed by the Stern-Volmer (S-V) equation (Eq. 1.8). The ratios $\frac{I_0}{I}$ were calculated at each quencher concentration and plotted against [Q], the quencher concentrations.

3.6.4 Fluorescence lifetimes

MPc fluorescence lifetimes were determined from steady-state measurements; using the S-V fluorescence quenching technique described above. The diffusion-controlled

bimolecular rate constant (k_R) for the reaction between the excited MPc and the quencher was calculated from Eqs. 2.83 and 2.84, and k_R was related to the bimolecular quenching constant, k_Q, by Eq. 2.85. A knowledge of k_Q (from Eq. 2.85) and K_{SV} (from Eq. 1.8) afforded the calculation of fluorescence lifetime (τ_F) by Eq. 1.9.

3.7 MPc PHOTOCHEMISTRY

3.7.1 Photodegradation quantum yields

Photodegradation quantum yield (Φ_{Pd}) determinations were carried out using the experimental set-up described in Section 3.1(vii), Fig. 3.1 [77,140,225] and Eq. 2.46. A 2 ml portion of the respective MPc solution (absorbance ~ 1.0 at the Q band maximum) in a spectrophotometric cell was irradiated at the Q band maximum using the General electric quartz lamp as described in Section 3.1. The intensity of light used for photodegradation experiments was 4.82×10^{16} photons s^{-1} cm^{-2}.

The absorbances of the MPc solution and the interference filter were converted to transmittances. The interference filter chosen was one whose transmittance overlaps with the absorbance of the respective MPc. A differential computation was performed to determine the value of α (the fraction of incident light absorbed), for use in Φ_{Pd} determination (Eq. 2.46). An illustration of the computation is shown in Table 3.1.

Table 3.1: Computation of α (fraction of incident light absorbed) for ZnPc in DMSO (Abs ~ 1.0)

Wavelength (nm)	Transmittance of filter (T_F)	Transmittance of MPc (T_{MPc})	$1-T_{MPc}$	$T_F(1-T_{MPc})$
655	0.575	0.642	0.358	0.206
656	0.597	0.597	0.403	0.241
660	0.625	0.404	0.536	0.335
665	0.663	0.230	0.770	0.511
670	0.663	0.114	0.883	0.587
675	0.625	0.118	0.882	0.551
680	0.579	0.242	0.758	0.439
685	0.575	0.481	0.519	0.298
686	0.539	0.539	0.461	0.249
	$\Sigma T_F = 5.441$			$\Sigma T_{F(1-TMPc)} = 3.417$

α was then calculated using Eq. 3.1:

$$\alpha = \frac{\Sigma T_F (1 - T_{MPc})}{\Sigma T_F} \qquad \text{(Eq. 3.1)}$$

The steady reduction in Q absorption intensity with irradiation time is recorded and used for the calculation of Φ_{Pd} according to Eq. 2.46.

According to Eq. 3.1, $\alpha = \frac{3.417}{5.441} = 0.628$ from the above illustration.

3.7.2 Singlet oxygen quantum yields

For singlet oxygen quantum yield (Φ_Δ) determination, a 2 ml portion of the respective MPc solution (absorbance ~ 0.2 at the irradiation wavelength) containing the singlet oxygen quencher (DPBF or ADMA) was irradiated in the Q band region with the

same set up as in the photodegradation experiment. The radiant light intensity used for Φ_Δ determination was ~ 5 x 10^{15} photons s^{-1} cm^{-2} (using the setup in Fig. 3.1). α values in Eq. 2.61 were calculated as illustrated above (Section 3.7.1). The relative method shown by Eq. 2.61 was employed for calculations of Φ_Δ. The initial quencher concentrations (corresponding to absorbance ~ 1.0) were kept the same for both the standard and the MPcs. Table 3.2 shows the molar extinction coefficients of quenchers and the Φ_Δ values of standards used in various solvents.

Table 3.2: Standards for Φ_Δ determination in different solvents

Solvent	Singlet oxygen Quencher	λ_{max} (nm)	ε (dm^3 mol^{-1} cm^{-1})	Standard	Φ_Δ
DMF	DPBF	417	23,000	ZnPc	0.56 [226]
DMSO	DPBF	417	23,000	ZnPc	0.67 [227]
Benzene	DPBF	416	18,000	Chlorophyll a	0.60 [30]
Pyridine	DPBF	417	27,500	Chlorophyll a	0.59 [30]
Toluene	DPBF	416	18,000	Chlorophyll a	0.60 [228]
PBS 7.4	ADMA	380	12,600	$ZnPcS_{mix}$	0.45 [229]

4 RESULTS AND DISCUSSION

This chapter dwells in the general discussion and explanation of observations made during experiments in this study.

The spectral, photophysical and photochemical properties of monomeric, aggregated or mixed MPc complexes are presented. For the monomeric species, these properties are well defined, but for the aggregated species, the measured parameters are those for the monomeric components. $MPcS_{mix}$ complexes (containing mixtures of mono-, di-, tri- and tetra-sulpho MPcs) were not separated, but studied as mixtures. It is important to study them in this form since $AlPcS_{mix}$ has been applied in photodynamic therapy (PDT). A comparative study of the photophysical and photochemical parameters of $MPcS_{mix}$ complexes containing different central metal ions is of value; this would give vital information as to the relevance of other $MPcS_{mix}$ complexes (apart from $AlPcS_{mix}$) in PDT and other photosensitizing applications.

The photophysical and photochemical parameters presented here are the averages for the different components of the mixtures.

4.1 SPECTROSCOPIC CHARACTERIZATION OF COMPLEXES

4.1.1 IR spectra of MPc derivatives

4.1.1.1 Peripherally substituted ZnPc derivatives

ZnTAPc (**16**) and ZnTNPc (**17**) were synthesized following literature methods [216] as explained in Section 3.2.3.1. Scheme 4.1 shows the well-established synthetic route [216] to **16** and **17**.

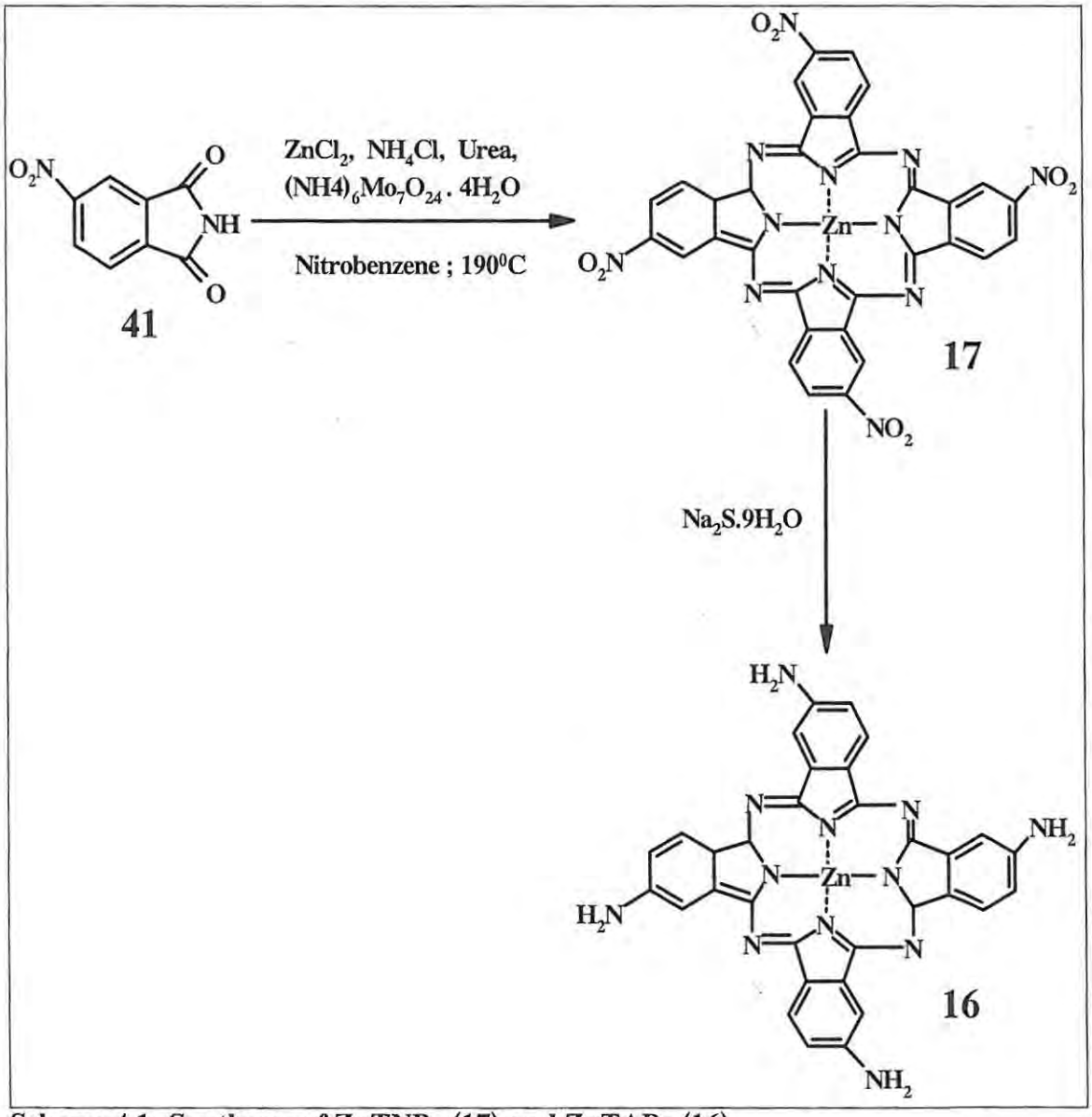

Scheme 4.1: Syntheses of ZnTNPc (17) and ZnTAPc (16)

ZnTAPc (**16**) showed two weak vibrational bands at 3350 and 3187 cm^{-1} in the IR spectrum. These bands are assigned to the symmetric and asymmetric stretching vibrations of the amino groups. The intense absorption band at 1618 cm^{-1} is due to the $-NH_2$ in-plane bending vibrations. The other bands at 1133, 1095, 1052, 949, 865 and 746 cm^{-1} are due to the phthalocyanine skeletal vibrations.

ZnTNPc (**17**) showed the vibrations due to the phthalocyanine skeleton in addition to characteristic bands assigned to the NO_2 symmetric (1338 cm^{-1}) and asymmetric (1521 cm^{-1}) bending vibrations.

ZnNPc (**32**) was also synthesized following literature methods as shown in Scheme 4.2:

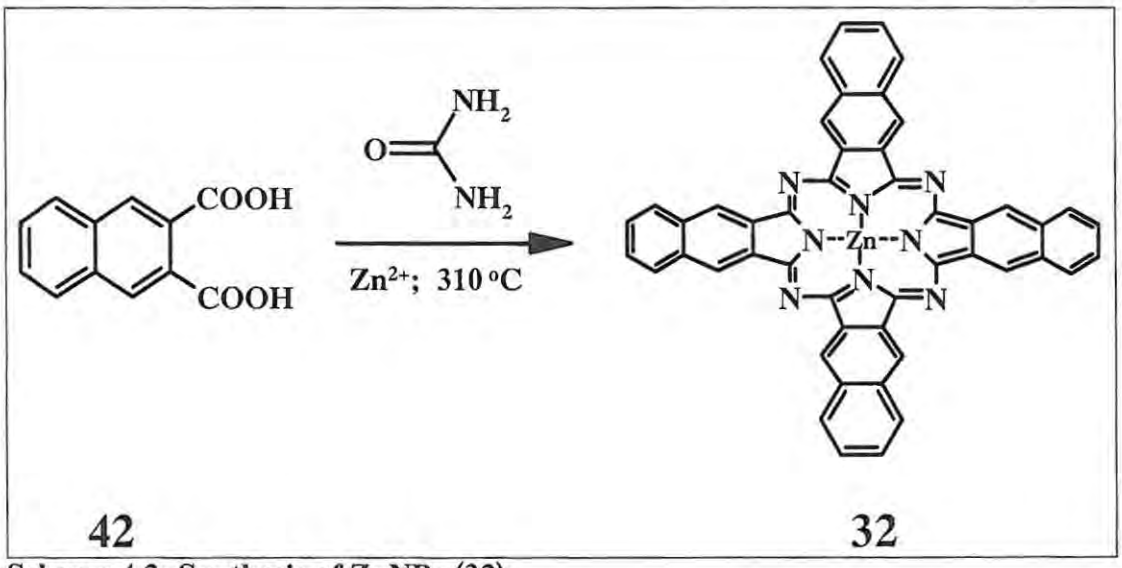

Scheme 4.2: Synthesis of ZnNPc (32)

The IR bands of the naphthalocyanine, **32**, are the usual bands for phthalocyanines and naphthalocyanines. The band at 3049 cm^{-1} is assigned to the outer benzene ring C-H stretching, while that at 1709 cm^{-1} could be due to the macrocycle's C=C or C=N vibration. The pyrrolic C=C vibration is assigned at 1517 cm^{-1}.

4.1.1.2 Axially ligated MPc complexes

The infrared (IR) spectra of (CN)ZnPc (**24**), (pip)ZnPc (**25**) and (py)ZnPc (**26**) are typical of non-ring-substituted MPc complexes. For **24**, the vibration at 2108 cm^{-1} is attributed to C≡N stretching. This vibration band is conspicuously absent in the spectra of **25** and **26**.

There is an extensive literature on the dichlorometallophthalocyanine (Cl_2MPc) and dihydroxymetallophthalocyanine (OH_2MPc) vibrational spectra [217]. The most important signals here are those attributed to the axial ligands. Metal complexes containing M–X (X = halogen) bonds give rise to relatively intense IR bands in the region below 650 cm^{-1}. The frequencies of these bands could be related to the mass and oxidation states of the metal ions, among other parameters. The bands observed for Cl_2GePc (**37**) at 435 and 510 cm^{-1} could be assigned to Ge–Cl vibration. Most of the vibrations in OH_2GePc (**38**) are also observed in Cl_2GePc (**37**). The band at 648 cm^{-1} in **38** is assigned to Ge–O stretching, which is typical of germanols [217]. The Sn–O stretch has been assigned at 562 cm^{-1} [217]; in this work, the Sn-O bond in OH_2SnPc (**40**) is assigned at 564 cm^{-1}. In OH_2SiPc (**38**), the band at 831 cm^{-1} is assigned to Si–O stretch; such transitions generally occur in the 830 – 950 cm^{-1} region on silanes [217].

4.1.1.3 Sulphonated MPc complexes

For the $MPcS_{mix}$ complexes (**27 – 31**), the distinctive bands are those associated with S=O vibrations. The characteristic bands of the S=O vibrations appeared in the 1030 – 1060 cm^{-1} region. The other bands are MPc regular bands: aromatic C-C stretching (1475 – 1600 cm^{-1}) and aromatic C-H out-of-plane bending (690 – 900 cm^{-1}). The bands due to M–O vibrations still occurred weakly in the $MPcS_{mix}$ complexes as

follows: Si–O (830 cm^{-1}), Ge–O (647 cm^{-1}) and Sn–O (566 cm^{-1}). These spectral assignments are in concordance with literature reports [217], and suggest that $MPcS_{mix}$ (M = Si, Ge, Sn) have OH groups axially coordinated. However throughout the thesis, the OH group is not shown for simplicity.

4.1.2 IR and NMR spectra of ZnPc(O-ZnTPP)$_4$ (20)

The synthetic route to the heteropentamer (ZnPc(O-ZnTPP)$_4$, **20**) is shown in Scheme 4.3; since this is a new compound, a detailed characterization is provided.

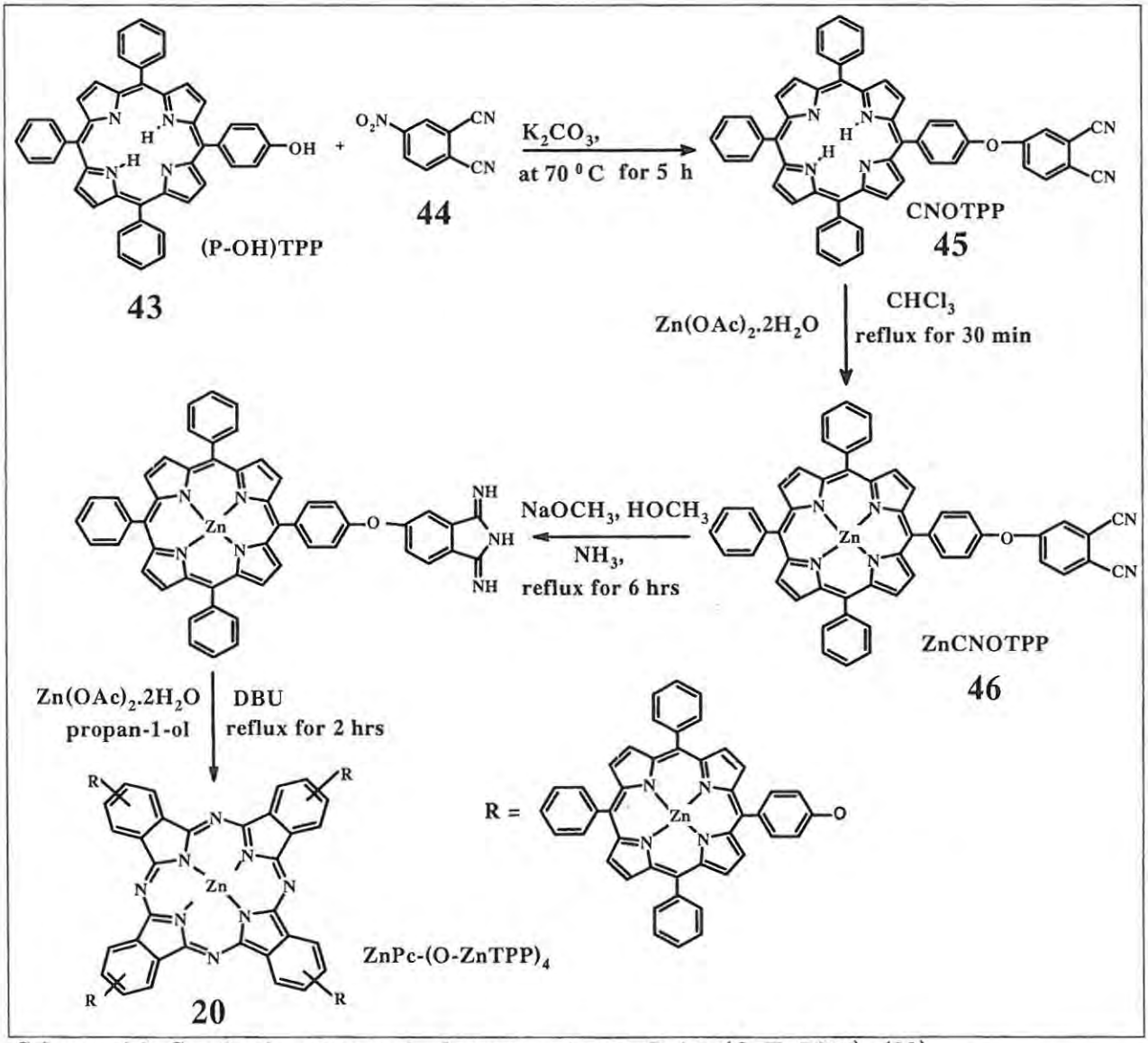

Scheme 4.3: Synthetic route to the heteropentamer ZnPc-(O-ZnTPP)$_4$ (20)

The compounds are abbreviated as indicated in the experimental section. CNOTPP (**45**) was characterized by IR (C≡N stretch at 2231 cm^{-1} and aromatic ether at 1207 cm^{-1}) as well as ^1H NMR spectroscopy as shown in Fig. 4.1. The proton resonances may be compared to the structure given. The reference protons used for integral measurement were the two N-H protons in the porphyrin (H_j in Fig. 4.1). The attachment of the phthalonitrile group onto one of the phenyl rings splits the resonances at 8.3 ppm and 8.9 ppm into two sets of doublets with the smaller doublets integrating for a third of the larger doublets, indicating a 2:6 proton ratio (Compare H_a to H_b and H_c to H_d).

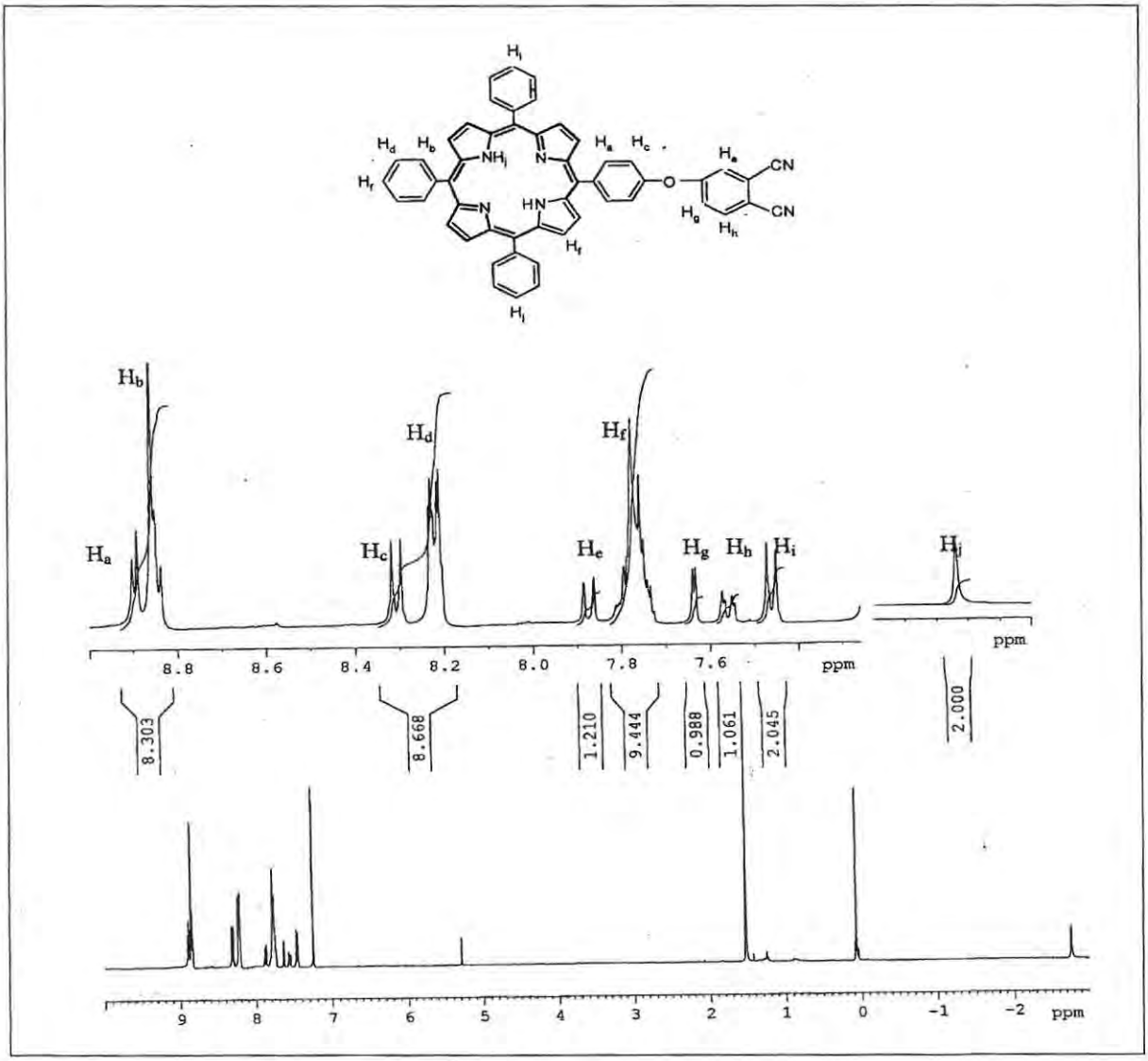

Fig. 4.1: ^1H NMR spectrum of CNOTPP

The three protons on the phthalonitrile ring (H_e, H_g and H_h) are present in the correct ratios. Finally, the multiplet at ~7.8 may appear anomalous with 9 protons but it actually consists of 8 overlapping pyrrole doublets with one terminal phenyl proton (H_f) which differs in environment from the other two terminal phenyl protons (H_i). The IR and NMR spectra of ZnCNOTPP (**46**) are the same as those of CNOTPP (**45**), except for the absence of N-H resonances in the NMR spectra of the former.

The infrared spectrum of ZnPc-(O-ZnTPP)$_4$ (**20**) did not have a cyano peak at ~ 2230 cm^{-1} but retained the phenyl ether peak at 1207 cm^{-1}. The ^1H NMR resonances for **20** were generally broad due to the complex mixture of isomers formed, typical of a tetrasubstituted phthalocyanine species.

4.1.3 Ground state electronic absorption spectra

4.1.3.1 MPc complexes with single Q bands

The ground state electronic absorption spectra of ZnPc (**15**), ZnTBPPc (**19**) and ZnNPc (**32**) in DMSO are typical for monomeric phthalocyanines, Fig. 4.2.

The Q band of ZnTBPPc (**19**) in DMSO is not as sharp as those of **15** and **32**; the former exhibits some broadening, even at very low concentrations. The broadening of bands and formation of an extra band called the "X" band, have been attributed to a slight reduction of symmetry of the molecule due to the presence of bulky groups at the non-peripheral positions [230]. The observation of slight broadening of spectra for complexes containing bulky peripheral substituents may suggest that steric effects of the substituents in this position could also cause some lowering in symmetry. A flexible σ bond connects the phenyl rings to the local MPc ring. Twisting of the

phenyl ring about this σ bond distorts the molecule and so a slight loss of symmetry occurs [230].

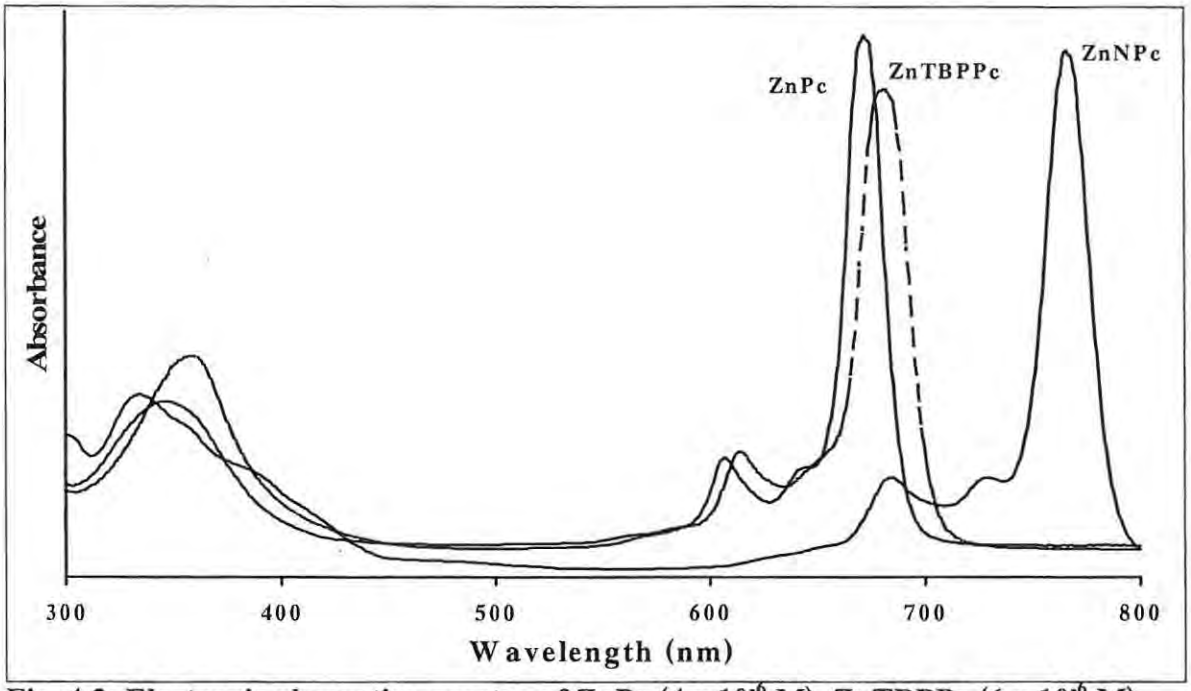

Fig. 4.2: Electronic absorption spectra of ZnPc (4 x 10^{-6} M), ZnTBPPc (6 x 10^{-6} M) and ZnNPc (6 x 10^{-6} M) in DMSO.

The electronic absorption spectra of ZnOPPc (**22**) and ZnOMPPc (**23**) (spectra not shown) are also typical of monomeric MPcs, with strong Q bands around 680 nm.

The effect of axial ligands on the electronic absorption spectra of ZnPc is very slight, with a shift of a few nanometers from that of unsubstituted ZnPc (Fig. 4.3, Table 4.1). The presence of axial ligands prevents aggregation, thus (CN)ZnPc (**24**), (pip)ZnPc (**25**), and (py)ZnPc (**26**) show monomeric behaviour in solution. MPc complexes containing cyanide axial ligands are identified by a split B band as shown in Fig. 4.3.

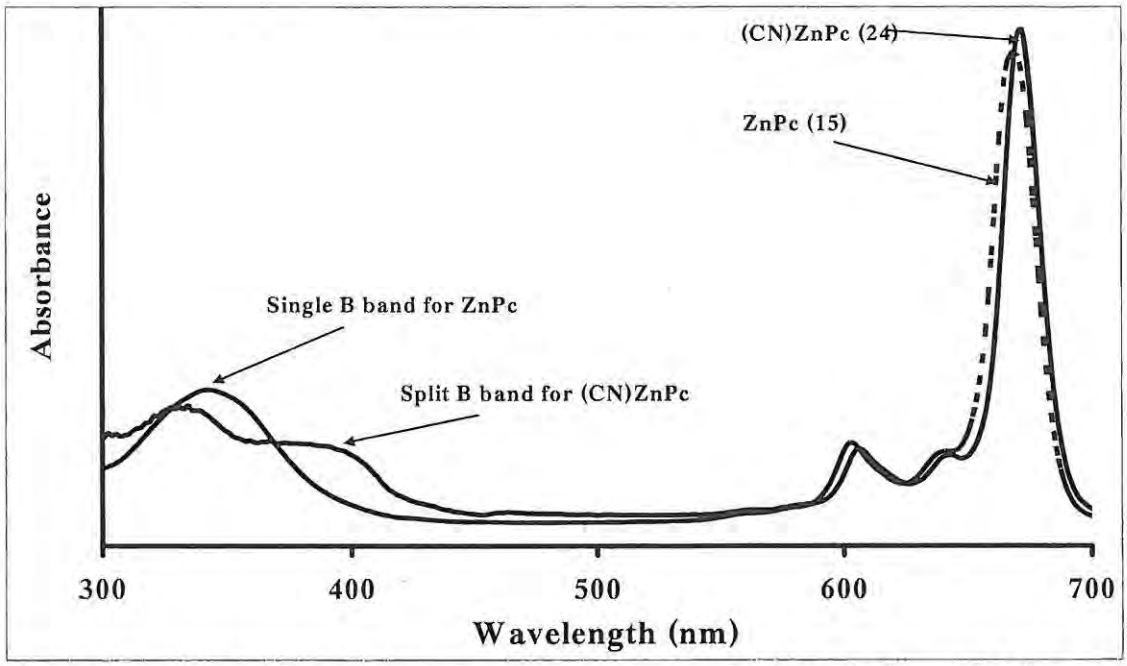

Fig. 4.3: Ground state electronic absorption spectra of ZnPc (15) and (CN)ZnPc (24) in DMF, showing the spectral effects of axial ligation.

Beer's law was obeyed for all the monomeric MPc complexes at concentrations up to 2×10^{-5} M (Fig. 4.4).

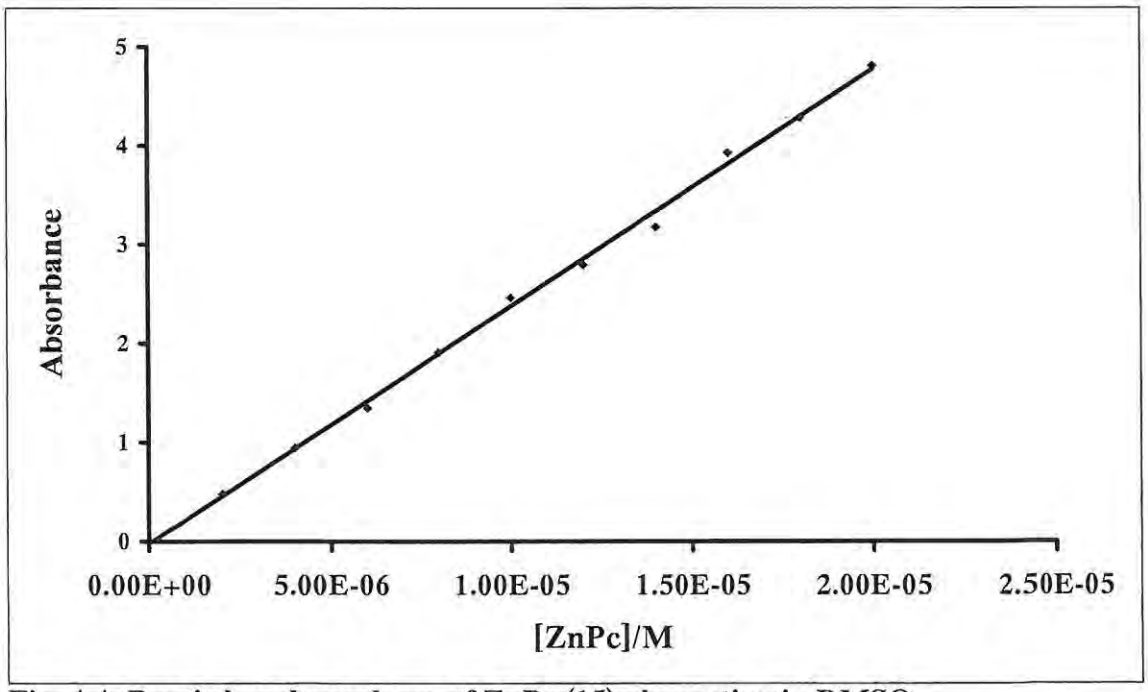

Fig. 4.4: Beer's law dependence of ZnPc (15) absorption in DMSO

Table 4.1: UV-Vis absorption and emission band positions of MPc derivatives in DMSO (or PBS 7.4).

Compound	Solvent	λ_{max} (Q_{Abs}, nm)	Log ε	λ_{max} (Q_{Em}, nm)
ZnPc (15)	DMSO	672	5.38	679
ZnTAPc (16)	DMSO	727	4.75	732
ZnTNPc (17)	DMSO	682[a]	4.88	691
ZnTSPc (18)	DMSO	680	4.54	686
ZnTBPPc (19)	DMSO	681	5.15	692
ZnPc(OZnTPP)$_4$ (20)	DMSO	682	5.26	682
ZnOEPc (21)	DMSO	681[a]	5.44	689
ZnOPPc (22)	DMSO	674	5.13	687
ZnOMPPc (23)	DMSO	679	5.12	686
ZnNPc (32)	DMSO	766	5.24	773
(CN)ZnPc (24)	DMSO	673	5.39	680
(pip)ZnPc (25)	DMSO	672	5.40	678
(py)ZnPc (26)	DMSO	673	5.42	679
AlPcS$_{mix}$ (27)	PBS 7.4	674	5.18	677
ZnPcS$_{mix}$ (28)	PBS 7.4	673	4.89	677
SiPcS$_{mix}$ (29)	PBS 7.4	678	5.11	682
GePcS$_{mix}$ (30)	PBS 7.4	680	5.01	686
SnPcS$_{mix}$ (31)	PBS 7.4	688	4.57	699

[a]Only monomeric peak shown.

4.1.3.2 MPcs with broad or split Q bands

The UV-visible spectrum of ZnTNPc (**17**, Fig. 4.5) shows cofacial aggregation in DMSO, as is typical for such complexes [84,231,232]. This is seen by the presence of two non-vibrational peaks in the Q band region. The lower energy (red-shifted) band at 682 nm is due to the monomeric species, while the higher energy (blue-shifted) band at 645 nm is due to the aggregated species. Fig. 4.5 also shows the UV-Vis spectra of ZnTAPc (**16**) and ZnOEPc (**21**); the spectrum of **16** is broad (hence still aggregated), but with only one defined Q-band, showing less aggregation than **17**. The absorption spectrum of **21** can be likened to that of **17** because it shows an additional band around 630 nm, which is attributable to the presence of aggregates in solution. As will be discussed later, this aggregation tendency if **21** is solvent-dependent, as it is observed only in DMSO.

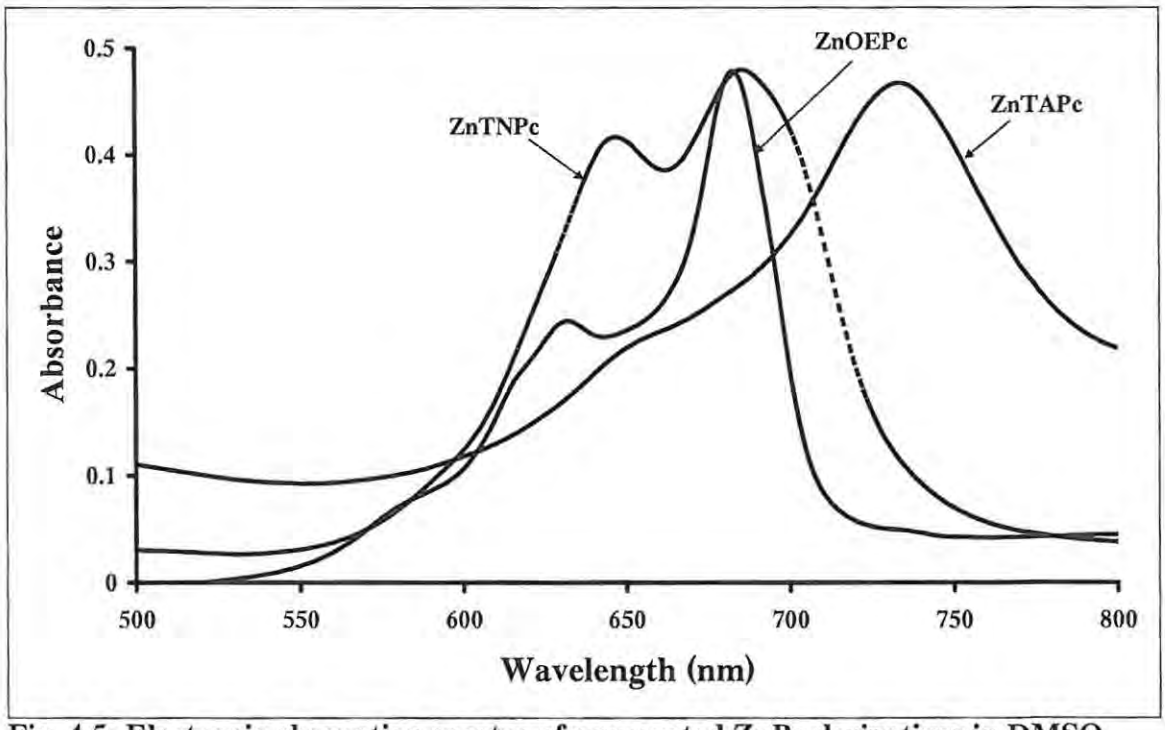

Fig. 4.5: Electronic absorption spectra of aggregated ZnPc derivatives in DMSO

For the highly aggregated compounds (**16**, **17**, **18** and **21**), deviations from Beer's law were observed at concentrations higher than 4 x 10^{-6} M (Fig. 4.6).

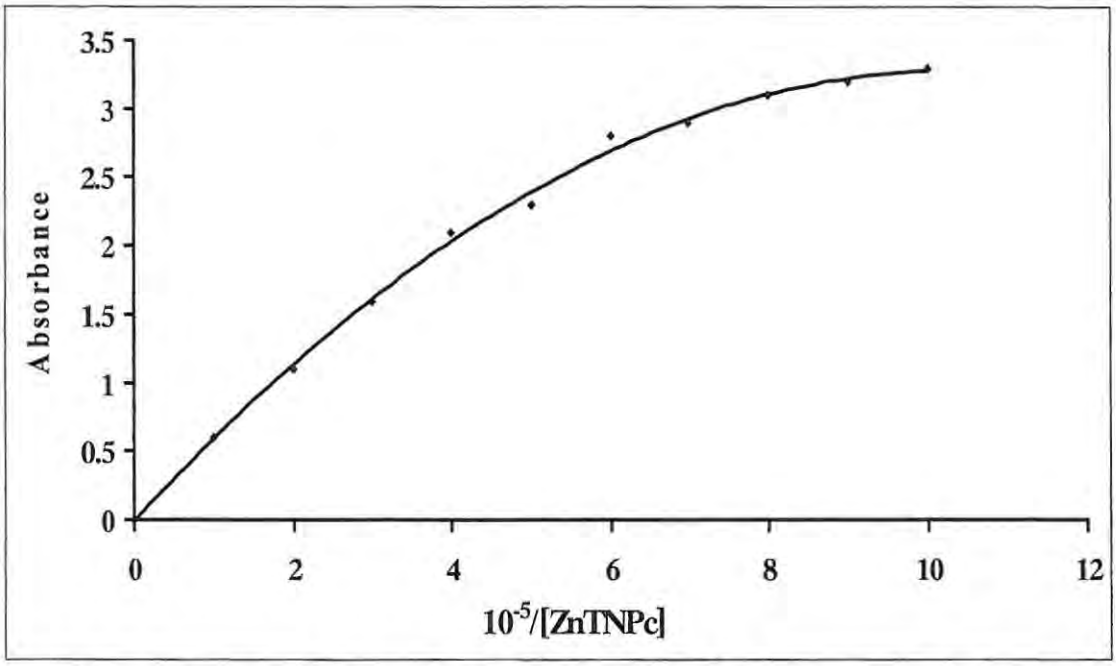

Fig. 4.6: Deviation from Beer's law of ZnTNPc (17) absorption in DMSO at concentrations higher than 4 x 10^{-6} M.

4.1.3.3 Sulphonated MPc complexes

The spectrum of dilute solution of ZnTSPc (**18**) in DMSO shows a strong Q band at 680 nm, implying that monomeric species are predominant. A similar spectrum is being exhibited by $ZnPcS_{mix}$ (**28**) in the same solvent. Fig. 4.7 shows the electronic absorption spectra of $AlPcS_{mix}$ (**27**), $ZnPcS_{mix}$ (**28**), $SiPcS_{mix}$ (**29**) and $SnPcS_{mix}$ (**31**) in PBS 7.4. The formation of aggregates in sulphophthalocyanines is characterized by broadening in the visible region spectra and the presence of a low energy band near 630 nm due to sandwich type dimer formation. Addition of a surfactant (Triton X-100) to the solutions of **27**, **29** and $GePcS_{mix}$ (**30**) in PBS 7.4 did not bring about any noticeable change in shape and intensity of the spectra. The lack of change in the intensity of the spectra on addition of Triton X-100 (TX) suggests that these complexes are in monomeric states.

The degree of aggregation in PBS increases with lipophilicity [10] hence, the prevalence of the less sulphonated fractions in solution is expected to increase aggregation.

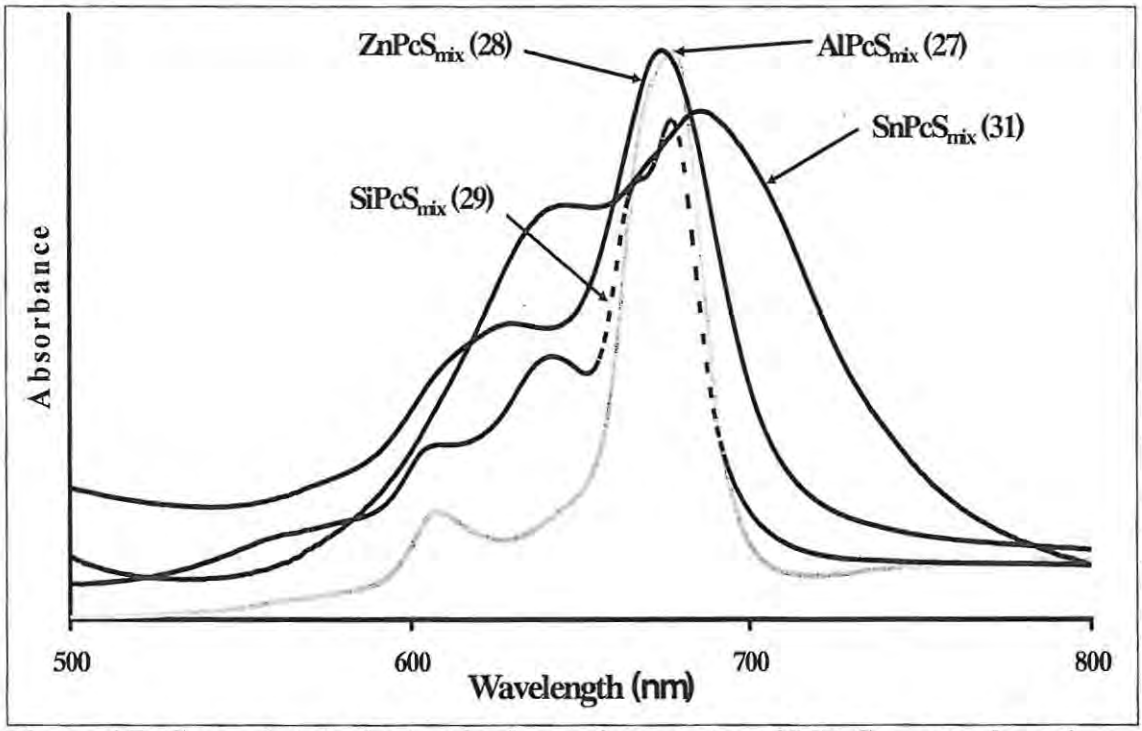

Figure 4.7: Ground state electronic absorption spectra of MPcS$_{mix}$ complexes in PBS 7.4. (~ 5.0 x10^{-6} M for 27 and 29; ~ 1.2 x 10^{-5} M for 28 and 31).

Thus the lack of aggregation in AlPcS$_{mix}$ (**27**), SiPcS$_{mix}$ (**29**) and GePcS$_{mix}$ (**30**) could be due to the prevalence of fractions with higher degree of sulphonation. This was attested by HPLC results discussed below, which showed the presence of mainly the highly sulphonated derivatives in the mixture for complexes **27**, **29** and **30**. It is known [9] that sulphonated aluminium phthalocyanine containing three sulphonate substituents is not aggregated in solution. The split in the Q band observed in Fig. 4.7 for the **29** (and also for **30**, not shown in Fig. 4.7, and a slight broadening for **27**) are assigned to unsymmetrical species in solution [9], since aggregation has been ruled out by the addition of TX, or the different sulpho species absorbing at diferent wavelengths.

Addition of TX to solutions of $ZnPcS_{mix}$ (**28**) and $SnPcS_{mix}$ (**31**) brought about considerable increase in intensity of the low energy side of the Q band (Fig. 4.8), suggesting that the molecules are aggregated and that addition of TX breaks up the aggregates.

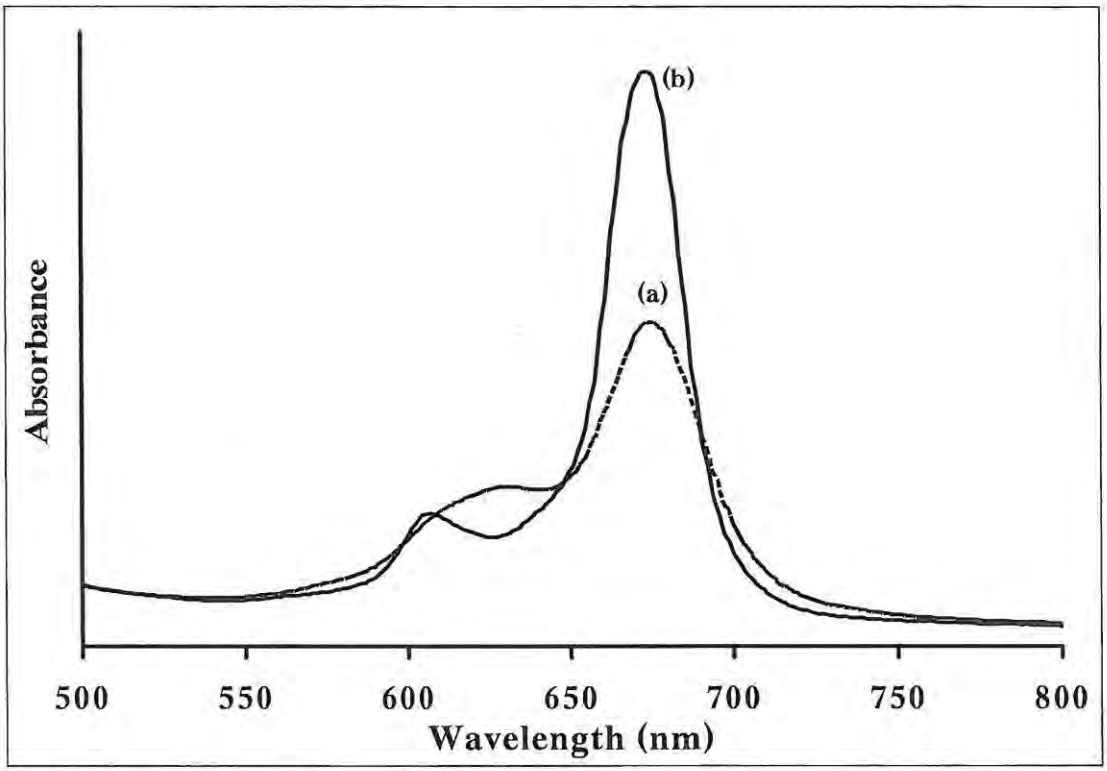

Fig. 4.8: Electronic absorption spectra of $ZnPcS_{mix}$ (28) in PBS 7.4 (a) and in the presence of Triton X-100 (b). [28] = 5 x 10^{-6} M and [TX] = 0.02 M.

Following the discussion above, the observed aggregation for **28** and **31** could reflect the dominance of fractions with lower degree of sulphonation compared to the rest of the complexes under investigation in this work. As will be established by HPLC studies below, fractions with lower degree of sulphonation are prevalent in complexes **28** and **31**. The degree of aggregation was 49% for **28** and 35% for **31**. It is important to point out that the degree of aggregation and the Q band maxima reported (Table 4.1) in this work are slightly different from those reported in pH 7 [174]. The spectra of sulphonated MPc complexes are known to be affected by slight changes in the

medium such as the ionic strength [233]. Also different batches of $MPcS_{mix}$ may contain different mixtures of isomers, affecting spectral and other physical properties [174].

Chromatographic (analytical) separation of $MPcS_{mix}$ complexes

Based on the different degrees of sulphonation in the component fractions in the various $MPcS_{mix}$ complexes, the most highly sulphonated (most soluble) fraction comes out of the column first, and so gave the lowest retention time, Figs. 4.9 and 4.10. For the five $MPcS_{mix}$ samples, the HPLC signals with the lowest retention times (~ 1 min) are assigned to the tetrasulphonated fractions, using tetrasulphozinc phthalocyanine (ZnTSPc, **18**) as reference. The assignment of other signals on the HPLC trace were done based on the idea that the higher the degree of sulphonation, the lower the retention time [79], such that the monosulphonated fractions gave the highest retention times.

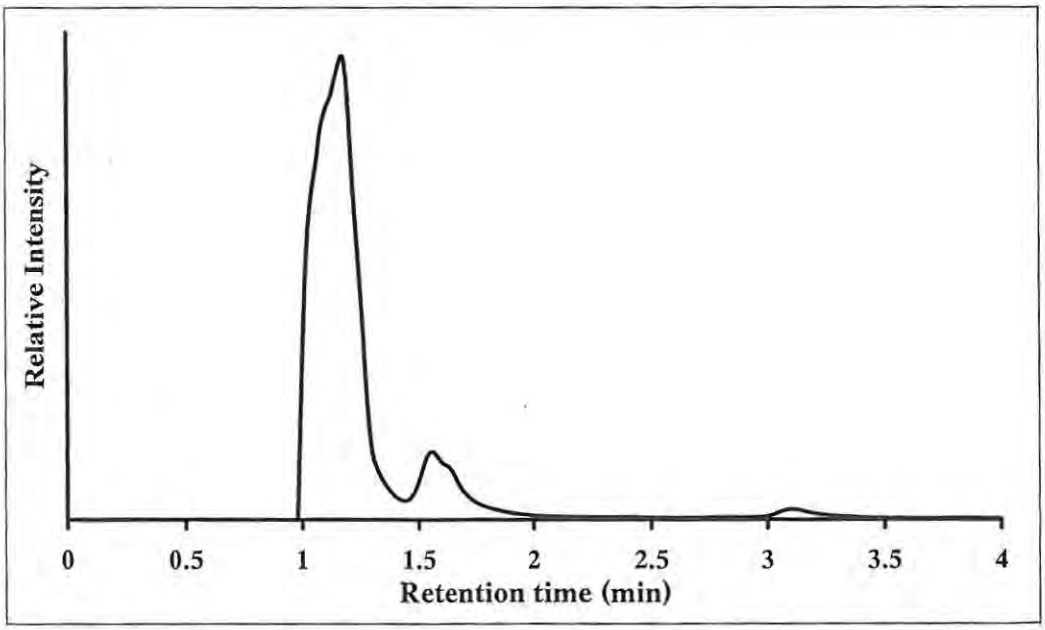

Fig. 4.9: HPLC trace for $GePcS_{mix}$ (30)

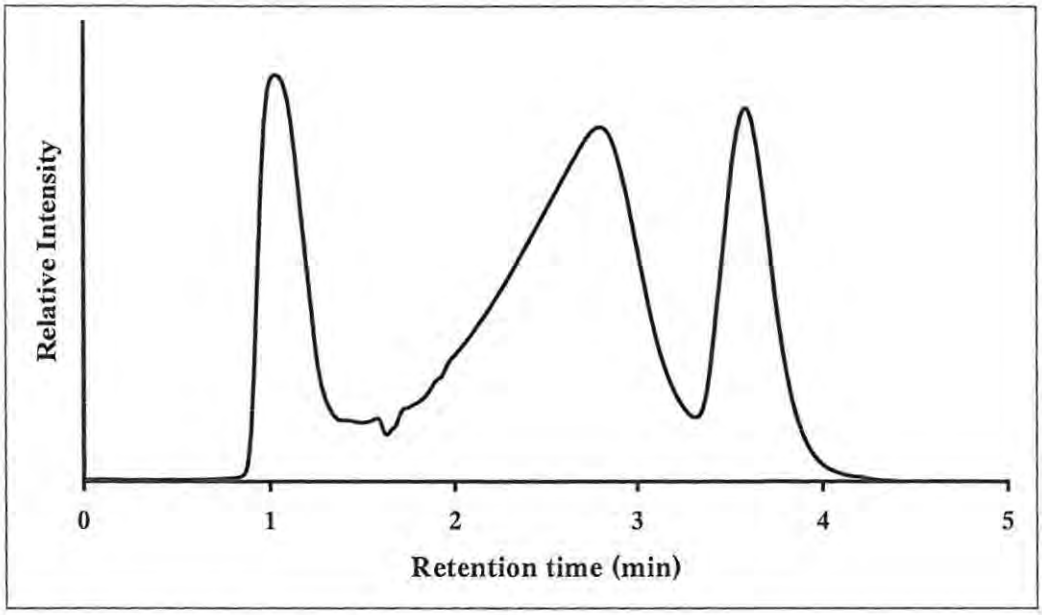

Fig. 4.10: HPLC trace for $ZnPcS_{mix}$ (28)

For $AlPcS_{mix}$ (**27**), $SiPcS_{mix}$ (**29**) and $GePcS_{mix}$ (**30**), there is clustering of signals in the low-retention-time part of the HPLC traces (Fig. 4.9), which implies the prevalence of fractions with higher degree of sulphonation in these species. In the case of $ZnPcS_{mix}$ (**28**) and $SnPcS_{mix}$ (**31**) however, the signals are appreciable in the relatively high retention time regions of the HPLC traces (Fig. 4.10).

These observations suggest the prevalence of the highly sulphonated fractions in $AlPcS_{mix}$ (**27**), $SiPcS_{mix}$ (**29**) and $GePcS_{mix}$ (**30**), while in $ZnPcS_{mix}$ (**28**) and $SnPcS_{mix}$ (**31**), the less sulphonated fractions are prevalent.

4.1.3.4 Tetraporphyrin-phthalocyanine pentamer

The ground state absorption spectra of monomeric ZnTPP and ZnPc, respectively in toluene are shown in Fig. 4.11. The spectra are typical of these complexes in solution. The spectrum of $ZnPc(O\text{-}ZnTPP)_4$ (**20**) (Fig. 4.12) is however not just a simple combination of these two monomeric spectra; the Q band maximum of ZnPc (**15**) is shifted bathochromically by 8 nm for the pentamer (678 nm) compared to the

monomer (670 nm), due to the presence of bulky peripheral substituents. It is known [234] that the presence of electron donating bulky peripheral substituents gives rise to bathochromic shifts in the Q absorption wavelengths of phthalocyanines.

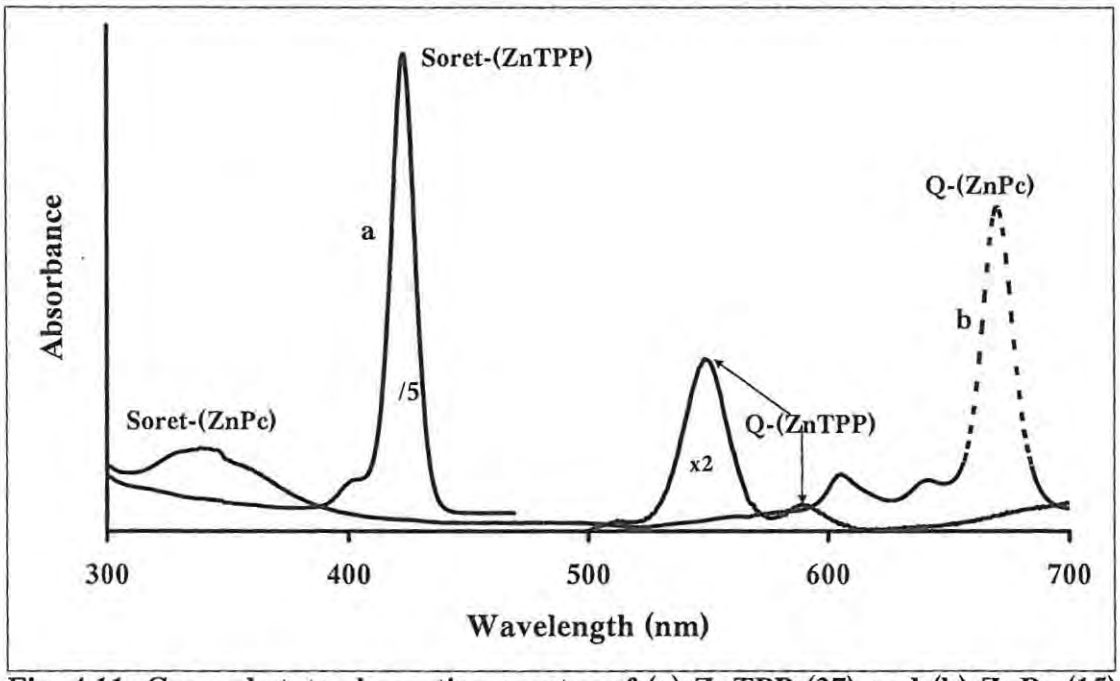

Fig. 4.11: Ground state absorption spectra of (a) ZnTPP (37) and (b) ZnPc (15) in toluene. Concentration = 4 x 10^{-6} M for both complexes.

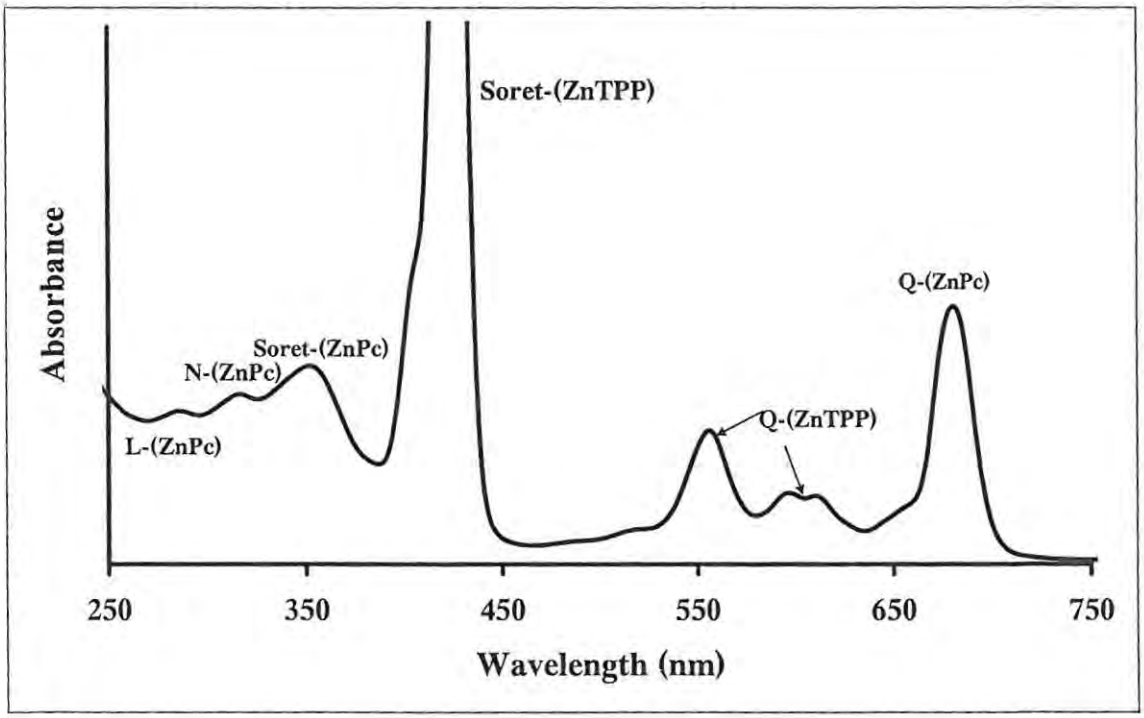

Fig. 4.12: Ground state absorption spectrum of ZnPc(OZnTPP)$_4$ (20) (4 x 10^{-6} M) pentamer in toluene.

4.1.3.5 Solvent effects on ground state electronic absorption spectra

The ground state absorption spectra of ZnOEPc (**21**) was found to show aggregation in DMSO even at very low concentrations < 4 x 10^{-6} M; this is evidenced by broadening of the Q band and the appearance of the band associated with aggregates at the higher energy side (629 nm) of the Q band, Fig. 4.13a. Conversely in other solvents (e.g., THF, pyridine and benzene) investigated for **21**, such broadening was not observed, Fig. 4.13b. The ZnOPPc (**22**) species showed the presence of an extra band at low energy (698 nm) in THF, Fig. 4.13c.

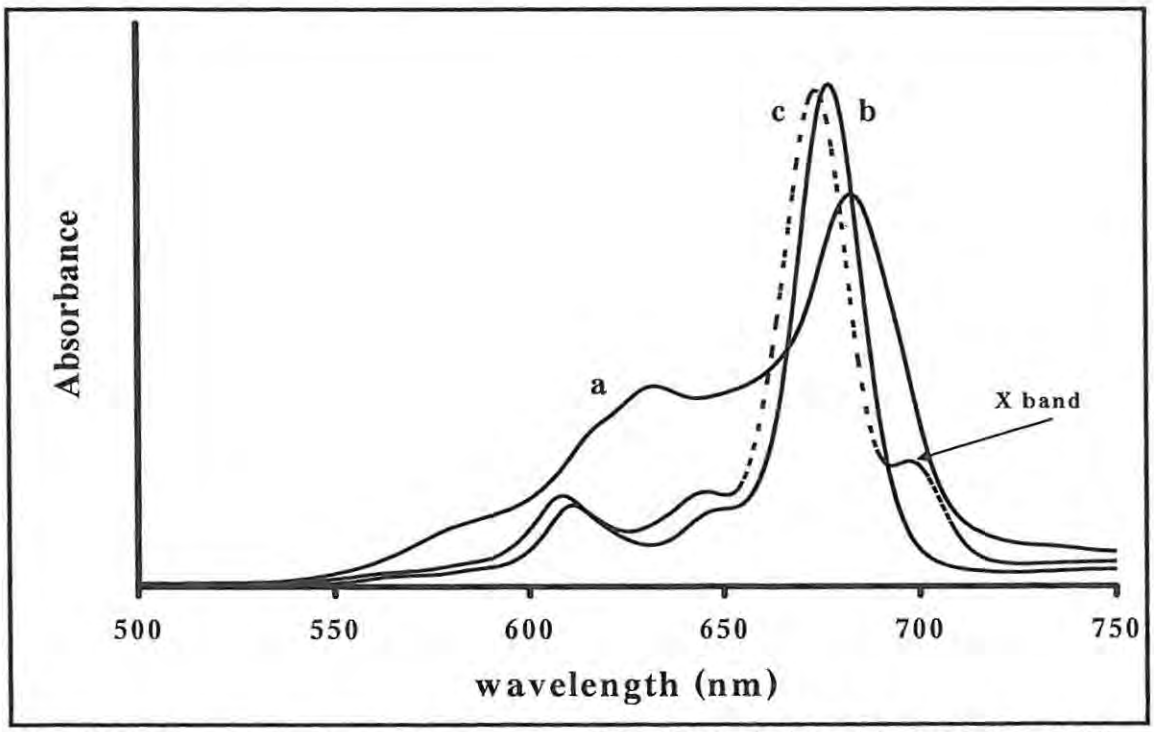

Fig. 4.13: Electronic absorption spectra of ZnOEPc (21) in (a) DMSO and (b) THF. (c) Electronic absorption spectra of ZnOPPc (22) in THF. Concentration = ~ 1 x 10^{-6} M.

Observation of two bands in the Q band region of MPc complexes is normally associated with the presence of monomeric (low energy) and aggregated (high energy) species (as earlier stated) as observed for ZnOEPc (**21**) in DMSO. However, comparison of the spectrum of **22** with the spectra for systems where monomer/dimer

equilibrium exists (e.g. Fig 4.13a) shows that the main Q band at 674 nm in Fig. 4.13c is due to the monomer, there is no dimer peak evident to the higher energy side of this peak. The band at 698 nm needs some explanation. Charge transfer bands involving the central metal are not expected in ZnPc complexes. A similar band termed the "X" band has been observed before is substituted ZnPc complexes [230]. This band was observed in non-polar or less polar solvents such as benzene and chloroform, but not in more polar solvents such as DMF, acetone and DMSO [230]. This band was observed more clearly only in THF in this work. The origin of the "X" band was explained in terms of the distortion of the Pc ring in substituted ZnPc complexes. Thus the presence of an extra band at 698 nm for the ZnOPPc (**22**) complex in THF, suggests loss of symmetry in this molecule due to the distortion of the MPc molecule. Such departure from planarity is common in tetraphenyl porphyrins [235]. It is also known that the presence of eight phenyl groups on the peripheral positions of the phthalocyanine ring results in high distortion of the ring [236]. This distortion may be more pronounced in **22** due to the more flexible nature of the phenoxy rings compared to the estrone group. Also, the presence of substituents on the phenyl ring (as in ZnTBPPc (**19**) and ZnOMPc (**23**) is expected to reduce the flexibility of the ring, thereby lowering the extent of the distortion. The reason why the 698 nm was clearly observable in THF may be due to the observation [230] that the presence of oxygen at the axial position of ZnPc complexes results in the distortion of the Pc ring. THF contains oxygen which may interact with the central Zn metal of the ZnOPPc (**22**) molecule, enhancing the distortion. However solvents such as DMF and DMSO also contain oxygen, but the latter may be S-bonded in MPc complexes [237].

4.1.4 Fluorescence Spectra

4.1.4.1 Monomeric ZnPc derivatives

The absorption and fluorescence excitation spectra of the monomeric ZnPc species were similar and bear mirror-image resemblance to their fluorescence emission spectra. This shows that the molecules remain the same (in their monomeric forms) prior to and after excitation. ZnPc (**15**) and its axially ligated derivatives - (CN)ZnPc (**24**), (pip)ZnPc (**25**) and (py)ZnPc (**26**) showed monomeric absorption and emission spectra (figure not shown). As earlier stated, the absorption spectra of ZnTBPPc (**19**), ZnOMPc (**23**) and ZnNPc (**32**) also show monomeric behaviour in DMSO; therefore, their monomeric fluorescence behaviours exemplified by Fig. 4.14 (for ZnNPc) are not unexpected.

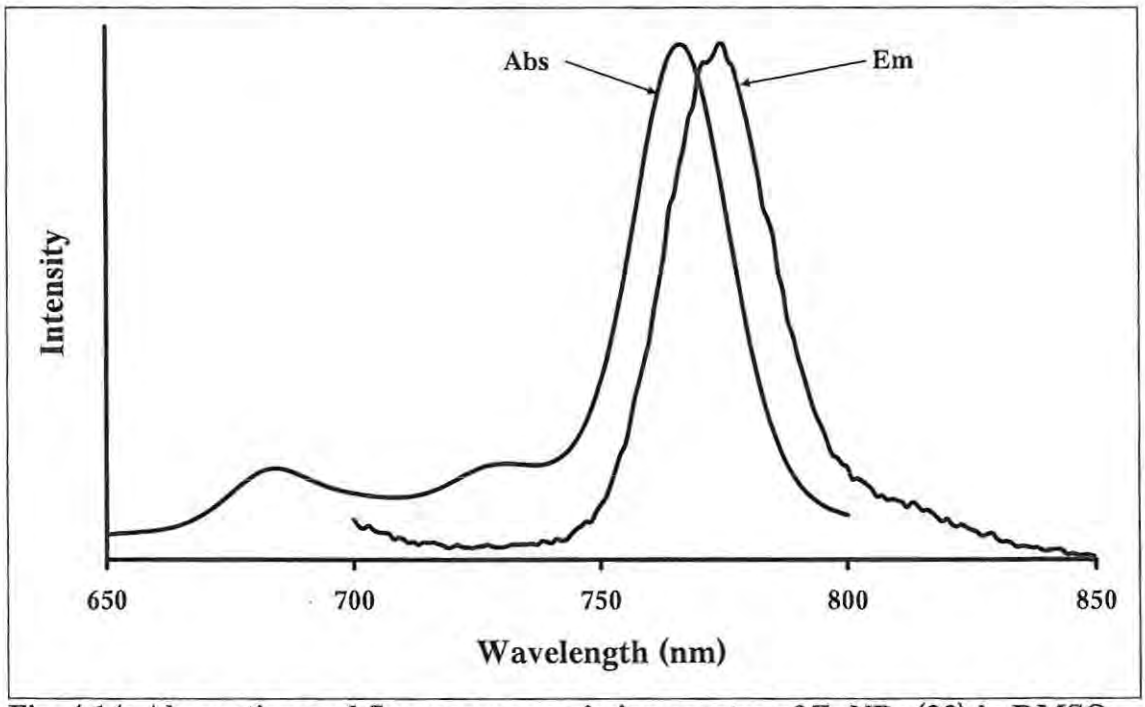

Fig. 4.14: Absorption and fluorescence emission spectra of ZnNPc (32) in DMSO.

The fluorescence excitation spectrum (not shown) of ZnNPc (**32**) is similar to the absorption spectrum, implying that it is the absorbing species (monomeric), which also fluoresce. This similarity between fluorescence excitation and absorption spectra were also observed for the monomeric species (**15**, **19**, **23**, **24**, **24** and **26**) mentioned above.

4.1.4.2 Aggregated and non-symmetrical ZnPc derivatives

The absorption and emission spectra of ZnTNPc (**17**) in DMSO are shown in Fig. 4.15. The ground state absorption spectrum of this complex shows considerable aggregation even at low concentrations. It is widely known that aggregates generally do not fluoresce, thus the fluorescence in Fig. 4.15 can be attributed to the monomeric species of compound **17**. A similar monomeric fluorescence was observed for ZnTAPc (**16**), which showed a broad Q band (in the absorption spectrum) due to aggregation. These fluorescence spectra are typical of monomeric MPc species.

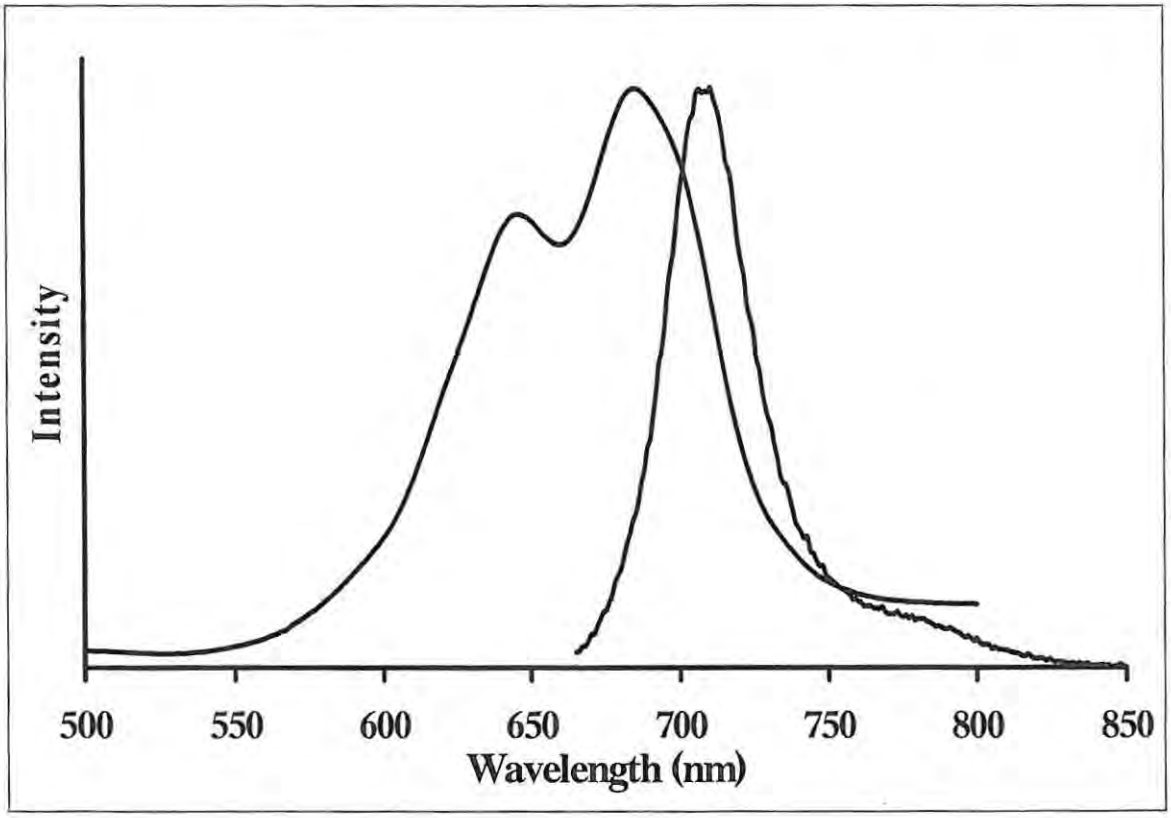

Fig. 4.15: Normalized absorption and fluorescence emission spectra of ZnTNPc (17) in DMSO.

Fig. 4.16 shows the absorption, fluorescence excitation and emission spectra of ZnOEPc (**21**) in DMSO. It is shown here that the fluorescing species are monomeric.

The fluorescence excitation and emission spectra of **21** (in DMSO) shown in Fig.4.16 were also observed in DMF, pyridine, benzonitrile, benzene, toluene and THF; and this confirmed that it is the monomeric species which fluoresces. The slight difference (in Q band positions) in the absorption and fluorescence excitation spectra of ZnOEPc (**21**) indicates that the molecule undergoes some structural rearrangement in-between absorption and fluorescence.

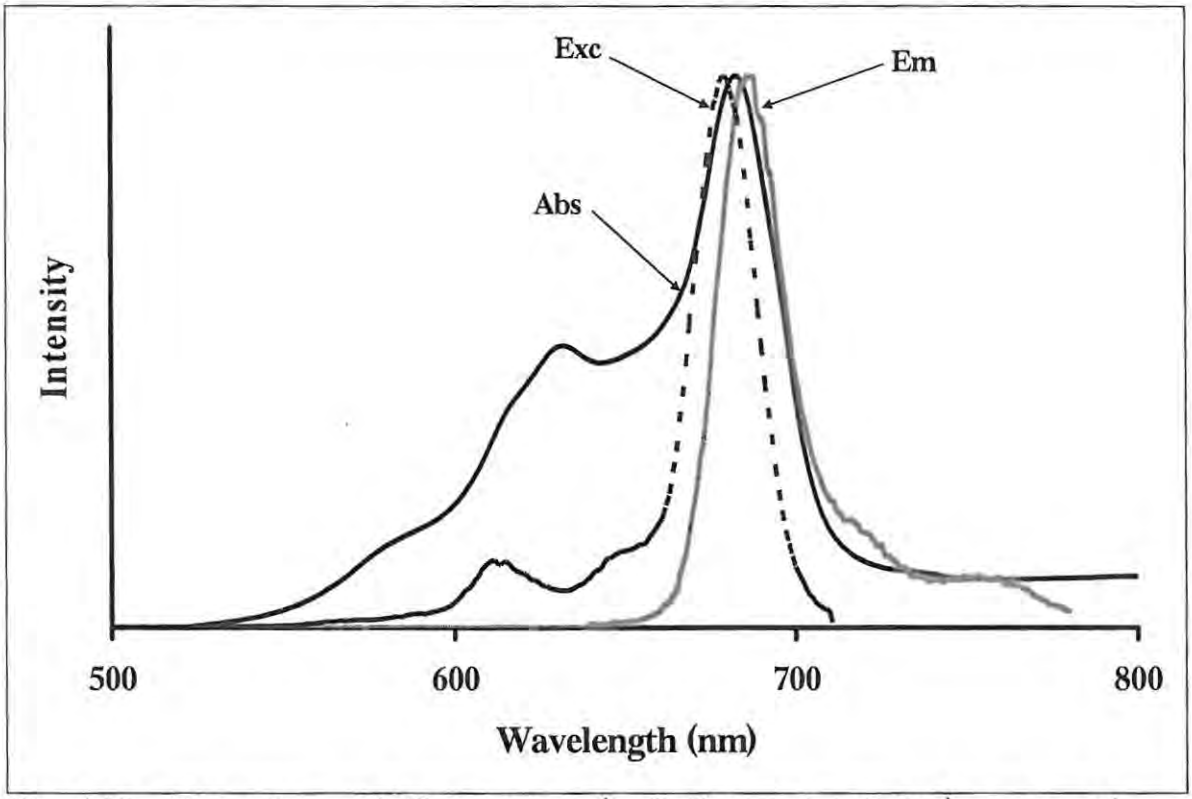

Fig. 4.16: Absorption and Fluorescence (excitation and emission) spectra of ZnOEPc (21) in DMSO, Excitation wavelength (λ_{Exc}) = 630 nm.

The fluorescence excitation and emission spectra for the ZnOPPc (**22**) showed two bands, Fig. 4.17, associated with the loss of symmetry as discussed in Section 4.1.3.5, Fig. 4.13.

The presence of two peaks in the excitation and fluorescence spectra was observed not only in THF, but also in pyridine, benzene and toluene, and not in the more polar solvents such as DMF or DMSO. This observation suggests that in the former group

of solvents, loss of symmetry occurs following excitation. This loss of symmetry was observed only for THF in the ground state of **22** (Section 4.1.3.5).

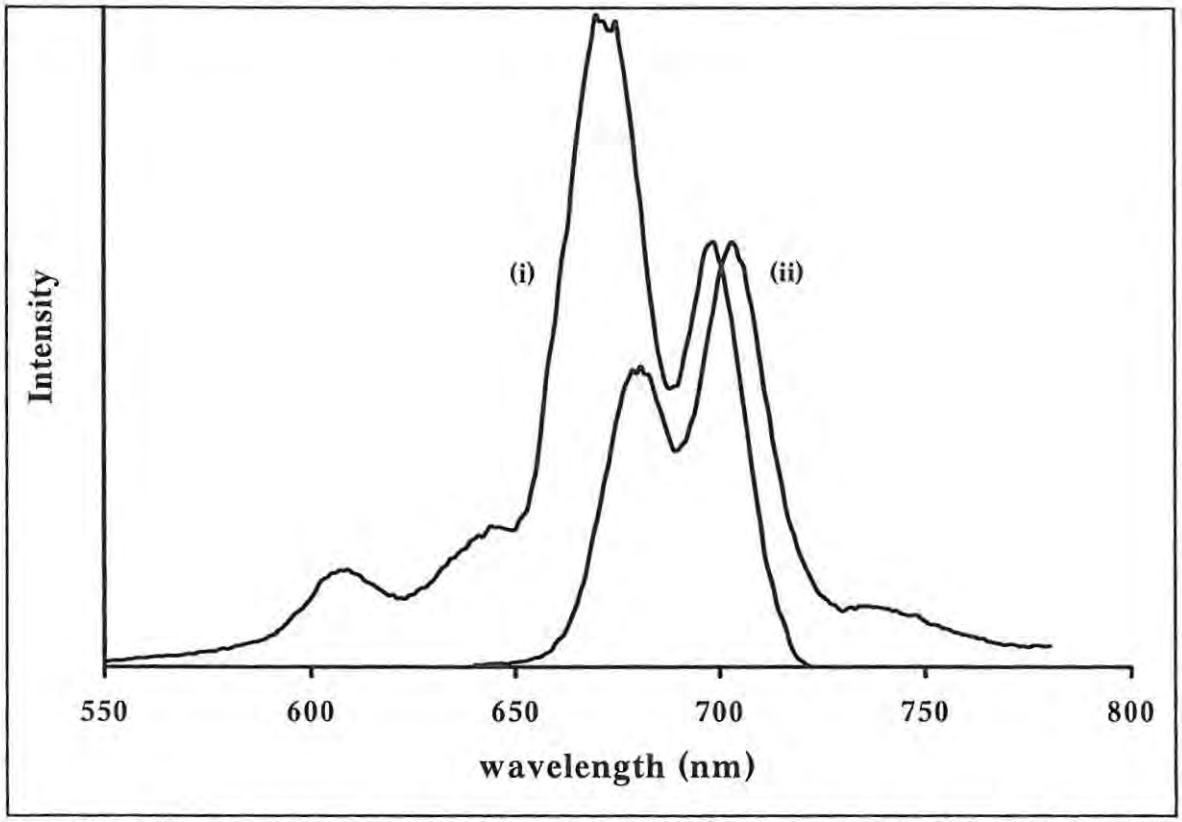

Fig. 4.17: Fluorescence excitation (i) and emission (ii) spectra of ZnOPPc (22) in THF, Excitation wavelength (λ_{Exc}) = 630 nm.

4.1.4.3 Sulphonated MPc derivatives

In PBS 7.4, the absorption and fluorescence excitation spectra (not shown) of $AlPcS_{mix}$ (**27**) are in close agreement, suggesting that the absorbing species is also the fluorescing species. Also, the emission spectrum of **27** was found to be a mirror image of its absorption spectrum. For $SiPcS_{mix}$ and $GePcS_{mix}$, absorption and fluorescence excitation spectra are similar, but not mirror images of the fluorescence emission spectrum, Fig. 4.18, in PBS 7.4. The differences could be due to the non-fluorescence of some of the species in solution.

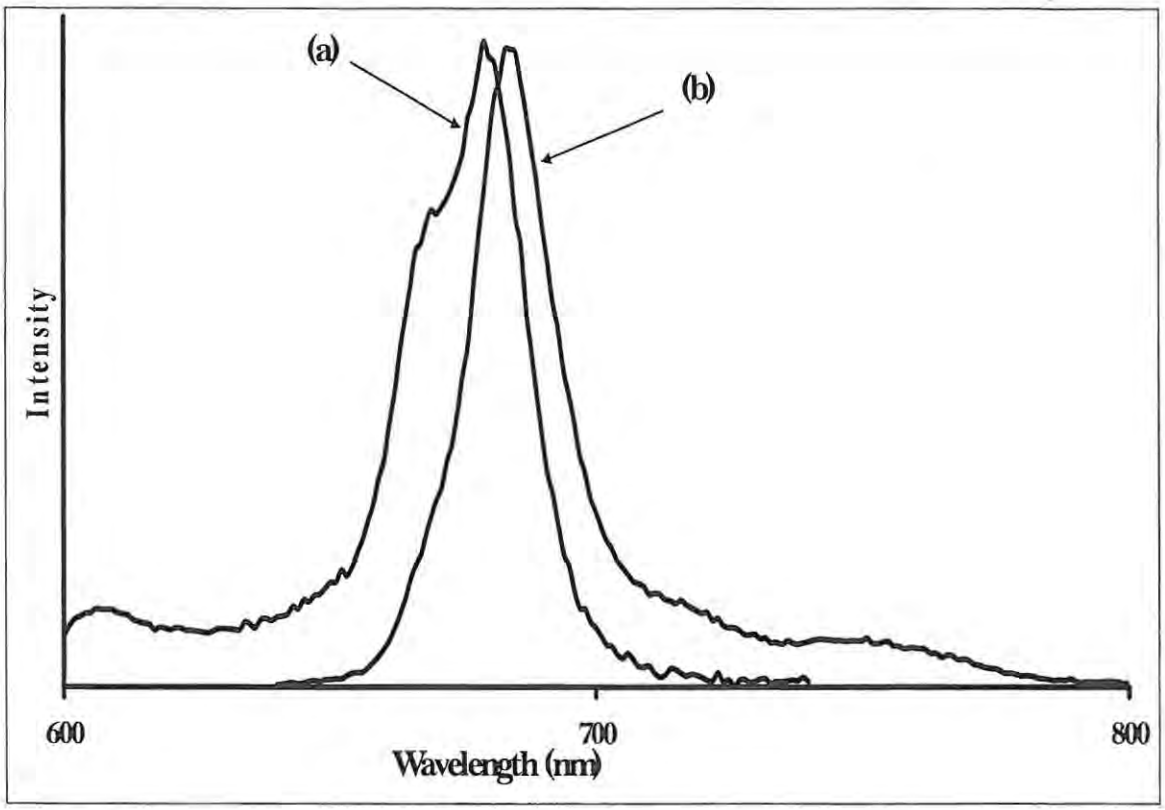

Fig. 4.18: Fluorescence excitation (a) and emission (b) spectra of $SiPcS_{mix}$ in PBS 7.4.

Fig. 4.19 shows the UV-Vis absorption and fluorescence (excitation and emission) spectra of $ZnPcS_{mix}$ (**28**) in PBS 7.4. Obviously, there is a lack of agreement between the absorption and fluorescence excitation spectra. The band around 630 nm, associated with the dimer is not seen in the fluorescence excitation spectrum; which suggests that it is only the monomer that fluoresces. Similar scenarios were observed for ZnTSPc (**18**) and $SnPcS_{mix}$ (**31**), which are extensively aggregated in aqueous solutions. In these cases, the λ_{max} of absorption are different from those of fluorescence excitation, which implies that the absorbing species are somewhat different from the fluorescing species.

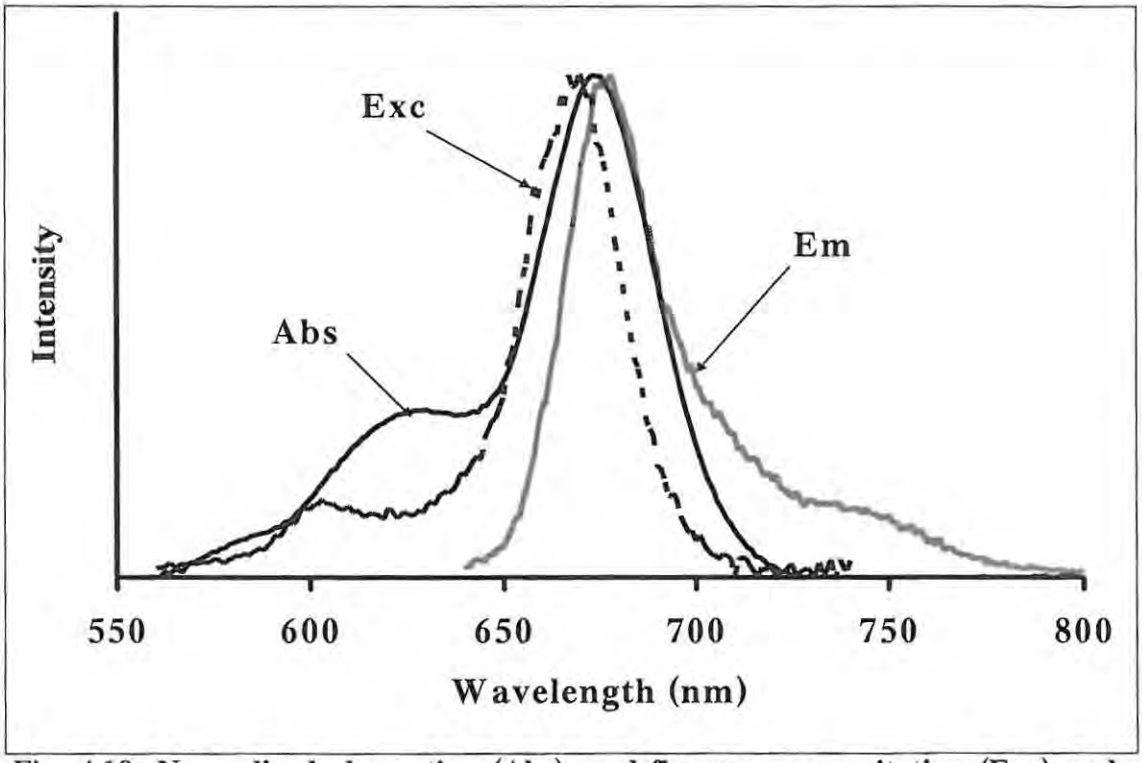

Fig. 4.19: Normalized absorption (Abs), and fluorescence excitation (Exc) and emission (Em) spectra of $ZnPcS_{mix}$ in PBS 7.4.

In DMSO, the absorption and fluorescence excitation spectra of $AlPcS_{mix}$ (**27**) and $ZnPcS_{mix}$ (**28**) are similar and are mirror images of their emission spectra. However for $SiPcS_{mix}$, $GePcS_{mix}$ and $SnPcS_{mix}$, single Q bands were observed in the fluorescence excitation spectra, in contrast with the split Q bands in these complexes' absorption spectra; probably suggesting that not all components of each mixture are equally fluorescent.

4.1.4.4 Tetraporphyrin-phthalocyanine heteropentamer (20)

Excitation of $ZnPc(O\text{-}ZnTPP)_4$ (**202**) could be carried out on ZnPc (at 640 nm) or ZnTPP (at 550 nm) part of the molecule. Excitation at 640 nm resulted in fluorescence only from ZnPc, while 550 nm excitation resulted in fluorescence not only from ZnTPP, but also from ZnPc, as will be discussed later.

In toluene (with 640 nm excitation), the absorption and fluorescence excitation spectra of the pentamer (**20**) were similar, and bore a mirror image resemblance to the emission spectrum (Fig. 4.20).

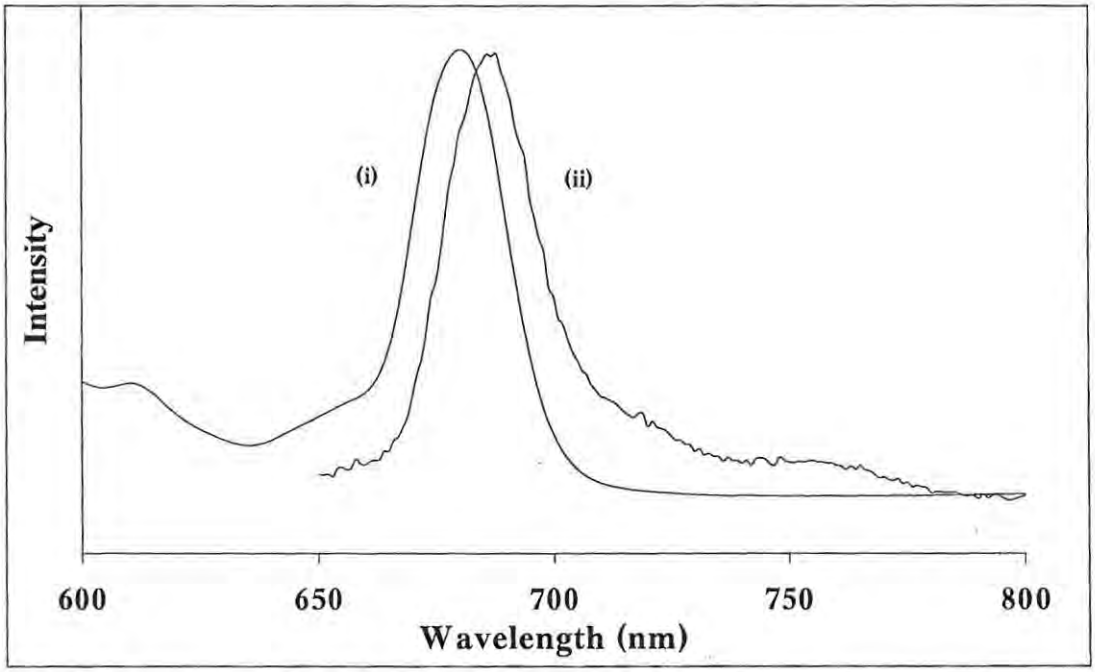

Fig. 4.20: Ground state electronic absorption (i) and fluorescence emission (ii) spectra of ZnPc(O-ZnTPP)$_4$ (20) (1 x 10^{-6} M) in toluene (λ_{Exc} = 640 nm).

This type of fluorescence spectrum (Fig. 4.20) is typical of monomeric MPc complexes. Fig. 4.21 shows the absorption and emission spectra of **20** in DMSO ; a different behaviour from that in toluene is observed.

With ZnPc excitation at 640 nm, the pentamer molecule reaches an excited state that is localized on the phthalocyanine component of the system. This is called the locally excited state (LES). Since electron transfer (internal charge transfer, ICT) is possible between excited phthalocyanine and porphyrin, a charge transfer state (CTS) is formed soon after excitation (Scheme 4.4).

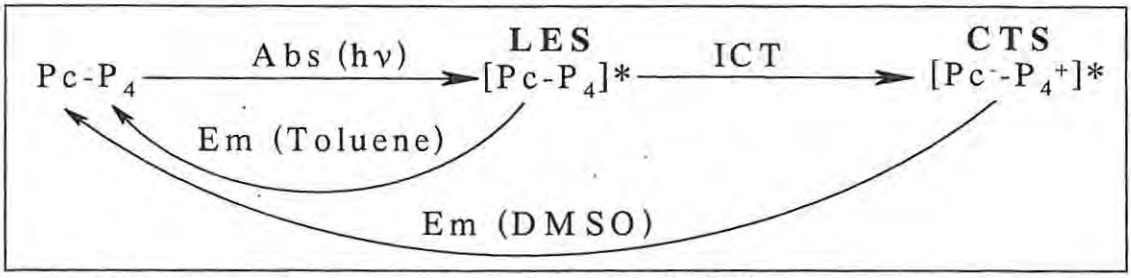

Scheme 4.4 : Electronic states of ZnPc(-OZnTPP)$_4$ (20). **Abs ≡ absorption; Em ≡ Emission ; ICT ≡ Internal charge trancfer ; LES ≡ Locally excited state and CTS ≡ Charge transfer state.**

In toluene (with low polarity and viscosity), the LES is the fluorescent species (see explanation below), with ZnPc fluorescence shown in Fig. 4.20 and a Stokes' shift of about 10 nm.

In DMSO (with high polarity and viscosity) however, the CTS becomes the fluorescent species. Charge transfer is favoured in highly polar solvents, hence CTS is reached in DMSO. It is thus expected that fluorescence occurs from CTS in DMSO. In toluene (with less polarity, hence not favouring charge transfer), only the LES state is attained, and fluorescence occurs from this state. Little or no Stokes' shift was obtained in DMSO (Fig. 4.21). This may be explained as follows: the formation of the CTS results in an increased dipole moment. Consequently, a strain is created in the solvent molecules with respect to both orientations and positions. Relaxation of the solute-solvent system into equilibrium with a new charge distribution therefore involves reorientation of the solvent molecules. The reorientation (relaxation) of the solvent molecules depends on temperature and viscosity [136]. In viscous solvents like DMSO, equilibrium around the CTS is not reached prior to emission, and so emission occurs during relaxation. The effect of this partially relaxed emission under steady state conditions is the observation of little or no Stokes' shift in the emission spectrum (Fig. 4.21).

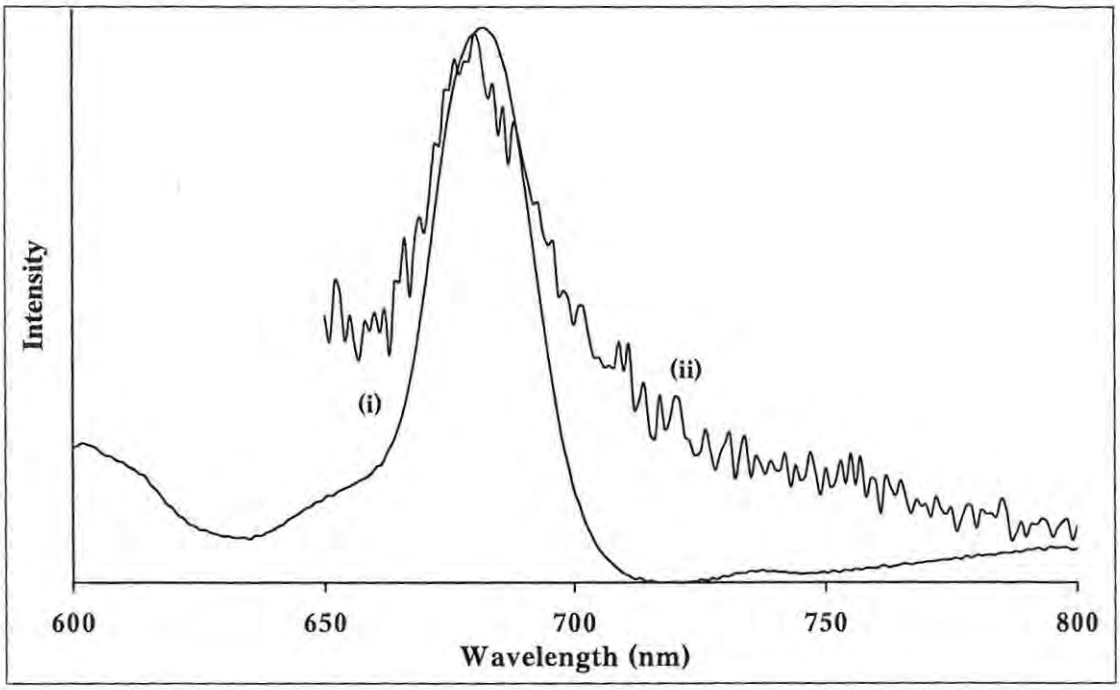

Fig. 4.21: Ground state electronic absorption (i) and fluorescence emission (ii) spectra of ZnPc(-OZnTPP)$_4$ (1 x 10^{-6} M) in DMSO (λ_{Exc} = 640 nm).

A comparison of the absorption and fluorescence excitation spectra of the heteropentamer (**20**) in DMSO (figure not shown) showed that the two spectra are not entirely similar suggesting changes in the nature of the molecules following excitation. The lack of agreement between the ground state absorption and fluorescence excitation spectra of the pentamer in DMSO also substantiates the fact that the LES (which is expected not to have a different structure in the excited state) is not the fluorescent species in this solvent.

The fluorescence of the pentamer (**20**) with 550 nm excitation (in DMSO and toluene) is discussed fully in Section 4.2.1.4.

In the mixture containing ZnPc and 4 molar equivalents of ZnTPP, the components behave as individual entities ; they both adopt their monomeric behaviours. The absorption and fluorescence spectra are simply a sum of those of the monomeric species.

4.1.5 Quantitative interpretation of solvent effects

Table 4.2 shows that with the exception of chloroform, larger red shifts of the Q band were observed for ZnPc (**15**) in aromatic solvents, the largest red shift being observed in 1-chloronaphthalene. The shift to longer wavelength could be due to either the destabilization of the highest occupied molecular orbital (HOMO) or the stabilization of the lowest unoccupied molecular orbital (LUMO).

Table 4.2: Polarization red shifts of ZnPc (15) in various solvents. $\lambda_{Q\ band}$ for ZnPc (15) vapour = 660 nm [47].

Solvent	Dipole Moment, μ	Refractive Index, n_D	Q-band λ_{max} (nm)	Polarization red shift, $\Delta\lambda$ (nm)
Triethylamine	0.72	1.401	666	6
1,4-Dioxane	0.45	1.422	666	6
THF	1.69	1.406	668	8
***n*-Butylamine**	1.3	1.401	669	9
DMF	3.79	1.43	670	10
Dichloromethane	1.36	1.445	671	11
DMSO	3.96	1.479	672	12
Toluene	0.38	1.097	672	12
Benzene	0	1.501	672	12
***o*-Xylene**	0.62	1.505	672	12
Chloroform	1.9	1.438	673	13
Chlorobenzene	1.72	1.524	673	13
Pyridine	2.21	1.509	674	14
Benzonitrile	3.5	1.528	674	14
1-Chloronaphthalene	1.55	1.633	677	17

It has been suggested [133] that the interaction between coordinating solvents and the phthalocyanine molecule stabilises the LUMO of the complexes. The observed red shift suggests that aromatic solvents stabilise the LUMO in MPc complexes, with 1-chloronaphthalene containing a more extend π system stabilizing the LUMO to a larger extent. It is known [238] that the Q band shifts to longer wavelengths with enlargement of π conjugated system of the phthalocyanine ring. This work suggests that the presence of conjugation in solvents also shifts the Q band to the red.

It has been reported before [133] that Q band positions in Ti(IV)Pc complexes were red-shifted as the polarity of the solvent increased for non-coordinating solvents, with the magnitude of the red shift following the order hexane < toluene < chloroform < 1-chloronaphthalene. The trend observed in Table 4.2 for these solvents is as follows: benzene = toluene ~ chloroform < 1-chloronaphthalane.

Table 4.2 shows that in general, as the refractive index of the solvent increased the red shift of the Q band increased. The electronic absorption spectra of ZnPc (**15**) in the various solvents was analysed by using the method described originally by Bayliss [133,135]. The plot of $\frac{n^2-1}{2n^2+1}$ (where n is the refractive index) versus the red shift in the Q band (the polarization red shift) is shown in Fig. 4.22. The linear nature of the plot suggests that the red shifts in the Q band are mainly a result of solvation rather than coordination. The relationship for the solvents evaluated can be expressed by Eq. 4.1:

$$\Delta\lambda_Q = -7.298\ F - 44.73 \qquad \text{(Eq. 4.1)}$$

With $R^2 = 0.945$

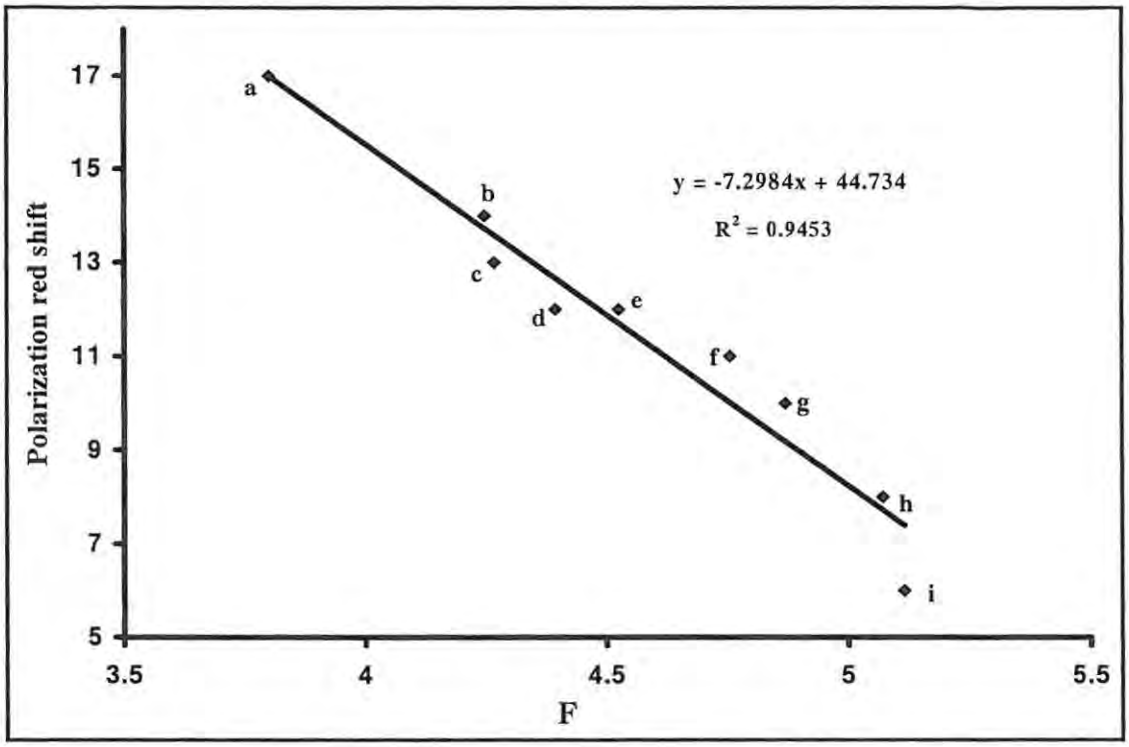

Fig. 4.22: Plot of polarization red shift vs. F where $F = \frac{n^2 - 1}{2n^2 + 1}$, **and n is the refractive index of the solvent for ZnPc (15) - (a) 1-chloronaphthalene, (b) benzonitrile, (c) chlorobenzene, (d) benzene, (e) DMSO, (f) dichloromethane, (g) DMF, (h) THF, (i) triethylamine.**

There is no correlation in Table 4.2 between the coordinating strength of the solvent and the red shift. A coordinating solvent such as DMSO gives the same red shift as, for example, dichloromethane, a non-coordinating solvent; confirming that coordination of the solvent does not play a significant role in the red shift. There was also no clear trend in the variation of the Q band positions with dipole moments considering all the solvents in Table 4.2.

4.2 PHOTOPHYSICAL STUDIES

4.2.1 Fluorescence

4.2.1.1 Fluorescence quantum yields of ZnPc derivatives

Table 4.3 shows the fluorescence quantum yield (Φ_F) values of the ZnPc derivatives in different solvents. ZnPc (**15**), ZnOEPc (**21**), ZnOPPc (**22**) and $ZnPcS_{mix}$ (**28**) were studied in a wider variety of solvents than the rest of the complexes. For complexes **15** and **22**, the highest Φ_F values were obtained in THF. The high Φ_F values in THF could reflect the low quenching abilities of THF for the excited singlet states. Toluene consistently showed the lowest Φ_F values for ZnPc (**15**), (py)ZnPc (**26**) and ZnOPPc (**22**), and a relatively low value for ZnOEPc (**21**), Table 4.3. Factors like temperature, solvent parameters (polarity, viscosity, refractive index and the presence of heavy atoms in the solvent molecule) are widely known to influence the yield of fluorescence. Toluene has a low viscocity of 0.61 cP [239] compared to 2.1 cP, 1.24 cP and 0.974 cP for DMSO, benzonitrile and pyridine, respectively.

Table 4.3: Fluorescence data for ZnPc derivatives in organic solvents.

Complex	Solvent	λ_{Em} (nm)	Stokes' Shift (nm)	Φ_F (±0.01)
ZnPc (15)	DMSO	679	7	0.20
	DMF	675	5	0.17
	THF	672	5	0.23
	Pyridine	681	7	0.20
	n-Butylamine	674	5	0.12
	Benzonitrile	681	7	0.13
	Benzene	676	4	0.06
	Toluene	676	4	0.07

Table 4.3 contd.

Complex	Solvent	λ_{Em} (nm)	Stokes' Shift (nm)	Φ_F (±0.01)
ZnTAPc (16)	DMSO	732	5	<0.02
ZnTNPc (17)	DMSO	691	9	0.022
	DMF	690	8	0.12
ZnTSPc (18)	DMSO	686	6	0.07
ZnTBPPc (19)	DMSO	692	11	0.14
	DMF	689	10	0.13
ZnOEPc (21)	DMSO	689	8	0.15
	DMF	684	4	0.19
	THF	682	5	0.13
	Pyridine	692	8	0.21
	n-Butylamine	687	6	0.15
	Benzonitrile	691	8	0.16
	Benzene	687	5	0.20
	Toluene	687	6	0.17
ZnOPPc (22)	DMSO	687	8	0.21
	DMF	684	7	0.17
	THF	680, 703	6, 4	0.31
	Pyridine	689	8	0.23
	n-Butylamine	683	5	0.12
	Benzonitrile	688	8	0.26
	Benzene	686, 704	7, 5	0.21
	Toluene	684, 704	5, 5	0.10

Table 4.3 contd.

Complex	Solvent	λ_{Em} (nm)	Stokes' Shift (nm)	Φ_F (±0.01)
ZnOMPPc (23)	DMSO	686	7	0.24
	DMF	684	7	0.20
(CN)ZnPc (24)	DMSO	680	7	0.18
	DMF	678	6	0.14
(pip)ZnPc (25)	DMSO	678	6	0.19
	DMF	677	7	0.16
(py)ZnPc (26)	DMSO	679	6	0.19
	DMF	676	7	0.22
	Benzene	676	4	0.16
	Toluene	677	5	0.08
[a]ZnPcS$_{mix}$ (28)	DMSO	682	7	0.14
	DMF	679	6	0.18
	Pyridine	684	7	0.23
	n-Butylamine	679	6	0.27
	H_2O	680	6	0.16
	D_2O	680	6	0.19
ZnNPc (32)	DMSO	773	7	0.07

[a]Average Φ_F for the mixture.

A decrease in viscosity of the solvent increases the possibility of deactivation of the excited state by external conversion. A chromophore could be rigid in the ground state, but loosens up after excitation in low-viscosity solvents. Φ_F values in Table 4.3 demonstrate that fluorescence is influenced by the environment of the fluorescing

molecule. In DMSO, ZnPc (**15**) and its axially ligated counterparts – (CN)ZnPc (**24**), (pip)ZnPc (**25**) and (py)ZnPc (**26**), have almost the same Φ_F within experimental error. However in DMF, (py)ZnPc (**26**) showed higher Φ_F than ZnPc (**15**), (CN)ZnPc (**24**) and (pip)ZnPc (**25**).

The variation of Φ_F values for $ZnPcS_{mix}$ (**28**) with solvent type is shown by Table 4.3. The highest value of Φ_F was observed in n-butylamine in which the complex exists mainly in the more fluorescent monomeric forms, as judged by the UV-Vis spectrum. One would expect the amine part of the solvent molecules to quench the complex's fluorescence, but it is known [240] that organic amines are inactive as quenchers of the singlet excited states of MPc complexes.

As earlier stated (Fig. 4.15), it is mainly the monomeric species which fluoresce, for aggregated species. Aggregation lowers the photo-activity of molecules through dissipation of energy by the aggregates. In light of this, aggregated species like ZnTAPc (**16**) and ZnTNPc (**17**) have unsurprisingly low Φ_F values, Table 4.3.

4.2.1.2 Fluorescence quantum yields of $MPcS_{mix}$ complexes

Table 4.4 lists the fluorescence quantum yield (Φ_F) and emission wavelengths for the $MPcS_{mix}$ complexes (**27 – 31**) in aqueous and non-aqueous media. It is a familiar understanding that aggregation usually leads to quenching of fluorescence [241,242]; this is again demonstrated by the low values of Φ_F for $ZnPcS_{mix}$ (**28**) and $SnPcS_{mix}$ (**31**) in PBS, which show aggregation in PBS compared to those of the monomeric $AlPcS_{mix}$ (**27**), $SiPcS_{mix}$ (**29**) and $GePcS_{mix}$ (**30**), Table 4.4. The trend observed among the monomeric $MPcS_{mix}$ complexes for Φ_F could be explained in terms of the heavy atom effect. The order observed for Φ_F is **27** > **29** > **30**, in either DMSO or PBS, which corresponds to the increase in atomic masses of the central metals. Germanium,

being a heavier metal, induces a greater propensity to undergo intersystem crossing than Si and Al, resulting in lower Φ_F for $GePcS_{mix}$ (**30**), and a correspondingly higher triplet state quantum yield (Φ_T) value, as will be discussed later.

Table 4.4: Fluorescence data for $MPcS_{mix}$ complexes in aqueous and non-aqueous solutions (Φ_F average for the mixture).

Complex	Solvent	λ_{Emm} (nm)	Stokes' Shift (nm)	Φ_F (±0.01)
$AlPcS_{mix}$ (27)	PBS 7.4	677	3	0.44
	DMSO	690	5	0.39
$ZnPcS_{mix}$ (28)	PBS 7.4	677	4	0.16
	PBS + TX	683	10	0.21
	DMSO	682	7	0.14
$SiPcS_{mix}$ (29)	PBS 7.4	682	4	0.34
	DMSO	685	5	0.29
$GePcS_{mix}$ (30)	PBS 7.4	686	6	0.30
	DMSO	692	7	0.21
$SnPcS_{mix}$ (31)	PBS 7.4	699	11	0.05
	PBS + TX	684	4	0.19
	DMSO	701	5	0.13

Any procedure that results in the monomerization of aggregates will ultimately give rise to an enhanced fluorescence. This is seen in the notable increase in Φ_F values of $ZnPcS_{mix}$ (**28**) and $SnPcS_{mix}$ (**31**) (in PBS 7.4) in the presence of Triton X-100. Contrary to what might be expected on grounds of DMSO's higher viscosity than water, Φ_F values were found to be lower in DMSO than in PBS 7.4, except for

$SnPcS_{mix}$. This observation may be ascribed to the presence of relatively heavier atoms in DMSO than in water, which would tend to favour intersystem crossing rather than fluorescence. As will be seen shortly, quantum yields of triplet formation are consistently higher in DMSO than in aqueous solutions.

4.2.1.3 Fluorescence parameters for ZnPc(O-ZnTPP)$_4$ and ZnPc/4ZnTPP (Excitation at 640 nm)

For the pentamer or mixture, where excitation can be either on the ZnPc (represented as Pc) or ZnTPP (represented as P) component of the system, excitation was done at both 640 nm (Pc excitation, since there is no P absorption at this wavelength) and at 550 nm (P excitation, since there is no Pc absorption at this wavelength). Φ_F values were determined using Eq. 2.10, by monitoring either the Pc or P emission spectrum, and are listed in Table 4.5.

Values of quantum yield of charge transfer (Φ_{CT}) between Pc and P units were calculated and also listed in Table 4.5. However, a separate value of Φ_{CT} could only be determined for Pc and not for P, since for P, energy transfer (ET) is also possible, in addition to charge transfer (CT). Hence the term excitation transfer (ExT), which implies a combination of both CT and ET, is used in the case of P singlet excited state deactivation.

Eq. 2.99 (now written as Eq. 4.2) shows how Φ_{CT} was determined.

$$\Phi_{CT} = k_{CT}.\tau_{F,Pc}^{Pc\text{-}P_4} \qquad \text{(Eq. 4.2)}$$

Where k_{CT} is the rate constant for charge transfer; $\tau_{F,Pc}^{Pc\text{-}P_4}$, the lifetime of ZnPc in the pentamer or mixture and Pc-P_4 represents either pentamer or mixture. The mixture is a 1:4 (molar proportions) mixture of ZnPc:ZnTPP in solution.

Quantum yields of excitation transfer (Φ_{ExT}) were calculated using Eq. 2.100 (now written as Eq. 4.3):

$$\Phi_{ExT} = k_{ExT}.\tau_{F,P}^{Pc\text{-}P_4} \qquad \text{(Eq. 4.3)}$$

Where k_{ExT} is the rate constant for excitation transfer and $\tau_{F,P}^{Pc\text{-}P_4}$, the lifetime of ZnTPP in the pentamer or mixture.

The fluorescence lifetimes of ZnPc ($\tau_{F,Pc}^{Pc\text{-}P_4}$) or ZnTPP ($\tau_{F,P}^{Pc\text{-}P_4}$) in the pentamer or mixture were determined using Eq. 4.4a and b, which are modifications of Eq. 2.88:

$$\tau_{F,Pc}^{Pc-P_4} = \frac{\Phi_{F,Pc}^{Pc-P_4}.\tau_{F,Pc}^{Pc}}{\Phi_{F,Pc}^{Pc}} \qquad \text{(Eq. 4.4a)}$$

$$\tau_{F,P}^{Pc-P_4} = \frac{\Phi_{F,P}^{Pc-P_4}.\tau_{F,P}^{Pc}}{\Phi_{F,P}^{Pc}} \qquad \text{(Eq. 4.4b)}$$

Where $\Phi_{F,Pc}^{Pc}$ and $\Phi_{F,Pc}^{Pc-P_4}$ are the fluorescence quantum yields of ZnPc monomer and ZnPc in the pentamer (or mixture) respectively, while $\tau_{F,Pc}^{Pc}$, the fluorescence lifetime of ZnPc monomer. Likewise, $\Phi_{F,P}^{P}$ and $\Phi_{F,P}^{Pc-P_4}$ are the fluorescence quantum yields of ZnTPP monomer and ZnTPP in the pentamer (or mixture) respectively; while $\tau_{F,P}^{P}$ is the fluorescence lifetimes of ZnTPP monomer.

The values of $\Phi_{F,Pc}^{Pc}$ and $\Phi_{F,Pc}^{Pc-P_4}$ (or $\Phi_{F,P}^{P}$ and $\Phi_{F,P}^{Pc-P_4}$) were determined experimentally, while $\tau_{F,Pc}^{Pc}$ (or $\tau_{F,P}^{P}$) value was obtained from literature. $\tau_{F,Pc}^{Pc\text{-}P_4}$ and $\tau_{F,P}^{Pc\text{-}P_4}$ values calculated here are listed in Table 4.5.

k_{CT} and k_{ExT} were calculated from the lifetimes determined above using Eqs. 4.5 and 4.6 (similar to Eqs. 2.93 and 2.94):

$$k_{CT} = \frac{1}{\tau_{F,Pc}^{Pc\text{-}P_4}} - \frac{1}{\tau_{F,Pc}^{Pc}} \qquad \text{(Eq. 4.5)}$$

$$k_{ExT} = \frac{1}{\tau_{F,P}^{Pc\text{-}P_4}} - \frac{1}{\tau_{F,P}^{P}} \qquad \text{(Eq. 4.6)}$$

The values of k_{CT} and $\tau_{F,Pc}^{Pc\text{-}P_4}$ were substituted in Eq. 4.2 ; while the values of k_{ExT} and $\tau_{F,P}^{Pc\text{-}P_4}$ were substituted in Eq. 4.3 to give Φ_{CT} and Φ_{ExT} respectively (listed in Table 4.5). The significance of the observed values of k_{CT} and k_{ExT} will be discusses later.

Table 4.5: Fluorescence data for ZnPc and ZnTPP as monomers and in the pentamer (or in the mixture of monomers)

(A) ZnPc parameters using 640 nm excitation, unless otherwise stated				
		τ_F (ns)	**Φ_F (± 0.01)**	**Φ_{CT}**
DMSO	**ZnPc monomer**	4.73 [84]	0.20	-
	ZnPc in Pentamer	0.71	0.03; <0.01[a]	0.85
	ZnPc in Mixture	3.07	0.13	0.35
Toluene	**ZnPc monomer**	3.80 [243]	0.07	-
	ZnPc in Pentamer	1.09	0.02; 0.02[a]	0.69
	ZnPc in Mixture	3.78	0.07	< 0.01
(B) ZnTPP parameters using 550 nm excitation				
		τ_F (ns)	**Φ_F (± 0.01)**	**[b]Φ_{ExT}**
DMSO	**ZnTPP monomer**	1.80 [244]	0.04 [244]	-
	ZnTPP in Pentamer	0.63	0.01	0.65[c]
	ZnTPP in Mixture	1.67	0.04	0.08[c]
Toluene	**ZnTPP monomer**	2.70 [167]	0.03 [167]	-
	ZnTPP in Pentamer	0.41	< 0.01	0.85[d]
	ZnTPP in Mixture	1.64	0.02	0.39[d]

[a]Excitation at 550 nm; [b]Combination of charge transfer and energy transfer; [c]Major contribution from charge transfer; [d]Major contribution from energy transfer.

The Φ_F values of ZnPc and ZnTPP in different forms - monomer, pentamer (ZnPc(O-ZnTPP)$_4$) and mixture (ZnPc/4ZnTPP); and in two different solvents (DMSO and toluene) are shown in Table 4.5. Excitation of the pentamer at 640 nm resulted in fluorescence exclusively from the phthalocyanine (Pc) component of the system, Fig. 4.20. This is expected since 640 nm photons would not excite the porphyrin (P) component, which absorbs at a higher energy. However, the Φ_F value of ZnPc in the pentamer (0.03 in DMSO) is several times smaller than that in the monomer (0.20 in DMSO, Table 4.5-A). The same situation applies in toluene where Φ_F = 0.02 in the pentamer and 0.07 in the monomer. This implies that ZnPc fluorescence is quenched in the presence of the porphyrin substituents. Such quenching could have resulted from either energy transfer (ET) or charge transfer (CT). The possibility of ET is however ruled out because energy transfer from Pc to P is not possible (since the LUMO of Pcs is lower in energy than that of Ps). The Pc component of the pentamer absorbs and emits photons at lower energies than the P component. Consequently, the observed lower Φ_F values of ZnPc in the pentamer compared to ZnPc alone (Table 4.5-A) may only be due to CT interaction between the P and Pc following excitation (Φ_{CT} = 0.85 and 0.69 in DMSO and toluene respectively, in the pentamer; and Φ_{CT} = 0.35 and < 0.01 in DMSO and toluene respectively, in the mixture). As already discussed (Section 4.1.4.4), normal fluorescence is observed in toluene (Stokes' shift = 10 nm), which was assigned to the locally excited state (LES). In DMSO however, fluorescence was from a charge transfer state (CTS); Scheme 4.4. This explains the higher Φ_{CT} values in DMSO than in toluene. These observations could be attributed to the differing abilities of the solvents to support and sustain charge transfer, which in turn depends on the solvent's dielectric constant and polarity. While DMSO is supposed to promote charge transfer, toluene is expected to inhibit it.

4.2.1.4 Fluorescence parameters for ZnPc(O-ZnTPP)$_4$ and ZnPc/4ZnTPP (Excitation at 550 nm)

550 nm excitation of the pentamer or mixture populates only the singlet excited state of P in the system, since the Pc component does not absorb at this wavelength. As a result, no Pc fluorescence is expected with 550 nm (porphyrin Q band) excitation. The observation of an intense Pc fluorescence at 688 nm when the pentamer is excited at 550 nm in toluene (Fig. 4.23b, which could not have resulted from CT, as CT would not result in any enhancement of fluorescence), suggests energy transfer from P to Pc, since as already stated, P energy lies higher than that of Pc. The fluorescence peaks of ZnTPP in the pentamer in toluene are observed at 598 nm and 650 nm, with a Φ_F value of < 0.01, compared to 0.03 for ZnTPP alone. These results demonstrate that ET is favoured in toluene, which results in the observed high Φ_{ExT} of 0.85 for ZnTPP within the pentamer (and 0.39 within the mixture) in this solvent (Table 4.5-B).

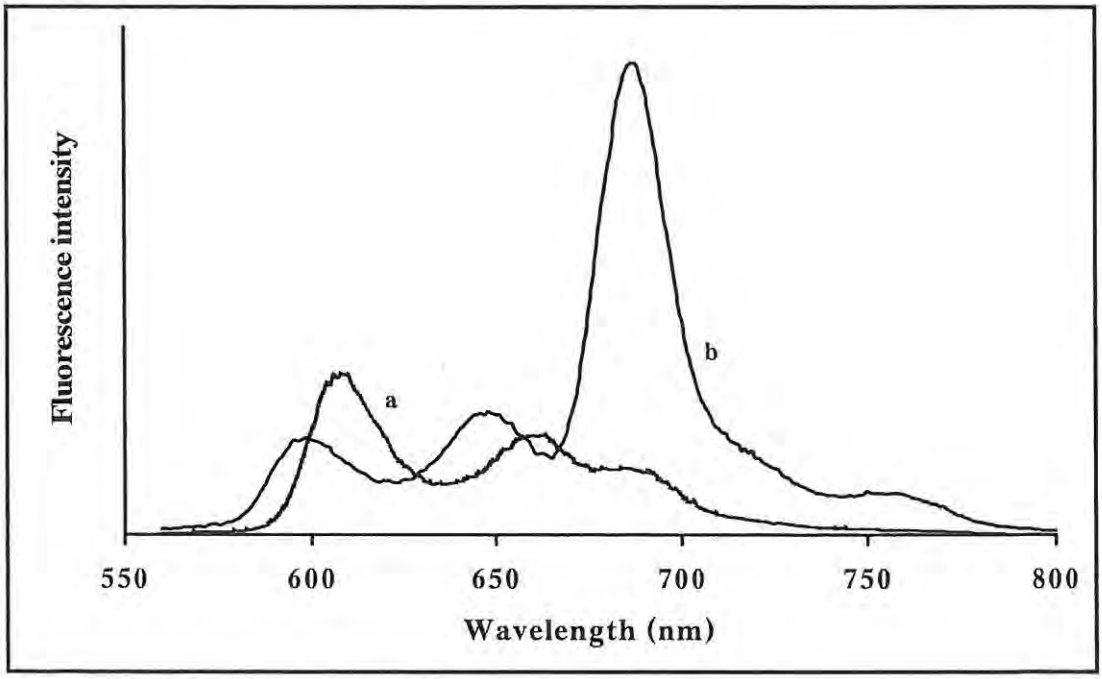

Figure 4.23: Fluorescence emission spectra of ZnPc within the pentamer in (a) DMSO and (b) toluene. Excitation wavelength in both cases was 550 nm.

In DMSO, a very weak Pc fluorescence (Φ_F < 0.01) is observed at 691 nm on excitation at 550 nm, Fig. 4.23a. This weak Pc fluorescence relative to that of P (at 609 nm and 663 nm), when compared with the intense Pc fluorescence in toluene suggests that different mechanisms operate in DMSO and toluene; ET is not dominant in DMSO, as it is in toluene. The Φ_F value of ZnTPP within the pentamer in DMSO is 0.01, compared to 0.04 for ZnTPP alone in DMSO. The lower value in the pentamer may suggest a combination of CT and ET, with ET being less efficient than CT (unlike in toluene, where ET is dominant).

In polar solvents like DMSO, it is known that the Pc fluorescence is drastically reduced when the P moiety of a heteroligomer is selectively excited, which is attributed to conformational change of the heteroligomer due to the nature of solvent interactions [167]. Since the possibility of ET being the major pathway for the ZnTPP singlet excited state decay has been ruled out in DMSO (Fig. 4.23a), it follows that the calculated Φ_{ExT} value for ZnTPP in DMSO (0.65 in the pentamer and 0.08 in the mixture) should be largely due to CT between the ZnTPP and ZnPc moieties in the system, with very little contribution being due to ET. As earlier stated, the difference in the prevailing mechanisms on going from DMSO to toluene (CT and ET respectively) is associated with the physical properties of the solvents.

4.2.1.5 Pentamer versus mixture (versus monomer)

The appreciable Φ_{CT} value (= 0.35) for the mixture in DMSO with 640 nm excitation (Table 4.5-A) shows that there is CT in this solvent even though the molecules are not chemically bound. However in toluene, there is virtually no CT, judging from the value of Φ_{CT} in this solvent (< 0.01).

For 550 nm excitation in toluene, $\Phi_{ExT} = 0.39$ in the mixture, compared to the value (0.08) in DMSO. The data confirms that DMSO does not support ET, which results on excitation at 550 nm. Both Φ_{CT} and Φ_{ExT} are lower in the mixture than in the pentamer; suggesting the significance of chemical bonding in CT and ET interactions in molecular arrays. It is known [245,246] that the efficiency of energy transfer in molecular photonic systems is directly related to the proximity of the donor and acceptor in the system. It is believed that ET occurs whenever the donor-acceptor distance is close to the Förster distance. The Förster distance is the distance between the donor and the acceptor at which energy transfer efficiency is 0.5 [246]. It is supposed that the donor-acceptor distance in the ZnPc/4ZnTPP exceeds that recommended by Förster, hence lower values of Φ_{ExT} and Φ_{CT} are expected in the mixture than in the pentamer. It can be concluded therefore that intramolecular CT or ET is more efficient than intermolecular CT or ET.

In DMSO, the values of Φ_{CT} for ZnPc in the pentamer and mixture (0.85 and 0.35 respectively) are greater than the corresponding Φ_{ExT} values of ZnTPP in the same systems (0.65 and 0.08 respectively); these imply that ZnPc experiences a greater excited state quenching than ZnTPP in the pentamer and in the mixture. This could be due to the fact that the central ZnPc moiety is being quenched by four equivalents of ZnTPP in the same system; while on the other hand, only one one ZnPc unit quenches four of ZnTPP.

Φ_F values for Pc or P in the mixture are the same as for the respective monomers (except for DMSO, with 640 nm excitation), and are larger than for the pentamer, showing that the components of the mixture behave as individual entities.

Similarly, τ_F values are consistently less for both ZnPc (Table 4.5-A) and ZnTPP (Table 4.5-B) in the pentamer compared to the mixture, implying a more efficient singlet excited state quenching in the pentamer than in the mixture.

4.2.1.6 Rate constants for ZnPc and ZnTPP excited single state deactivation processes

Table 4.6 shows values for the rate constants for all processes deactivating the excited singlet states of ZnPc and ZnTPP in the monomer, pentamer or mixture. These values were calculated using Eqs. 2.64a-c for k_F, k_{IC} and k_{ISC} respectively; and Eqs. 4.5 and 4.6 for k_{CT} and k_{ExT} respectively.

k_F = rate constant for fluorescence – radiative decay from the singlet excited state to the ground state;

k_{IC} = rate constant for internal conversion – non-radiative decay from the singlet excited state to the ground state;

k_{ISC} = rate constant for intersystem crossing – non-radiative energy transfer from singlet excited state to triplet excited state;

k_{CT} = rate constant for charge transfer between P and Pc in the pentamer or mixture, and

k_{ExT} = rate constant for the combination of charge transfer and energy transfer between P and Pc in the pentamer or mixture.

The rate constant values indicate the efficiency of the respective deactivating process from a kinetic point of view. The rate constants for the inherent processes (k_F, k_{ISC} and k_{IC}, each of which is assumed to be the same in the monomer, pentamer and mixture) are consistently lower in toluene compared to DMSO, with 550 nm

excitation. However, the value of k_{ExT} (550 nm excitation) is higher in toluene compared to DMSO.

Table 4.6: Rate constants for excited singlet state deactivation processes in ZnPc and ZnTPP within pentamer in DMSO and toluene.

	k_F ($x\ 10^{-7}\ s^{-1}$)	k_{ISC} ($x\ 10^{-7}\ s^{-1}$)	k_{IC} ($x\ 10^{-7}\ s^{-1}$)	k_{CT} ($x\ 10^{-7}\ s^{-1}$)	k_{ExT} ($x\ 10^{-7}\ s^{-1}$)
Kinetic data for ZnPc (640 nm excitation)					
DMSO	4.23	13.7	3.17	120 (11.4)	
Toluene	1.84	17.1	7.37	63.3	
Kinetic data for ZnTPP (550 nm excitation)					
DMSO	2.22	48.9	4.44		103 (4.3)
Toluene	1.11	32.6	3.33		207 (23.8)

Concentrations of ZnTPP and ZnPc in the mixture were 2×10^{-6} and 5×10^{-7} M respectively; Values for ZnPc/4ZnTPP mixture in brackets.

With 640 nm excitation, there is no clear trend in the values of the rate constants when comparing DMSO with toluene.

The conspicuously high values of k_{CT} and k_{ExT} for both ZnPc and ZnTPP in the pentamer compared to those in the mixture (Table 4.6), is an indication of the effect of chemical bonding on the efficiency of CT and ET.

4.2.2 The triplet quantum yield and lifetime

4.2.2.1 MPc derivatives

In aqueous media, due to the weak triplet absorption in the 450 – 550 nm region, singlet depletion (Eq. 2.36) was employed in the determination of Φ_T and τ_T values.

However in organic solvents, where triplet absorption was appreciable, triplet absorption (Eq. 2.35) was employed. Due to lack of suitable reference standards, Φ_T values could only be determined in DMSO and aqueous solutions.

Table 4.7 gives the values of triplet quantum yield, Φ_T and triplet lifetime (τ_T) for some MPc derivatives. Fig. 4.24 shows the triplet decay curve for ZnTBPPc (**19**). The presence of certain substituents on ZnPc encourages intersystem crossing from excited singlet to triplet state, since they have larger Φ_T values (in DMSO) than the unsubstituted ZnPc (**15**), e.g., ZnTSPc (**18**), ZnTBPPc (**19**) and $ZnPcS_{mix}$ (**28**). The increase in Φ_T values is complemented by a decrease (going from ZnPc to substituted ZnPc) in fluorescence quantum yield (Φ_F, in DMSO) values for all the derivatives except ZnOMPPc (**23**), Table 4.3 (also included in Table 4.7). In the case of ZnNPc (**32**), both the excited singlet and triplet states probably suffer serious internal conversion, such that the rate constant for internal conversion would be high for both states, resulting in low Φ_T. Also **32** (as will be seen later) degrades fast on photolysis, hence reducing the number of molecules in the excited state.

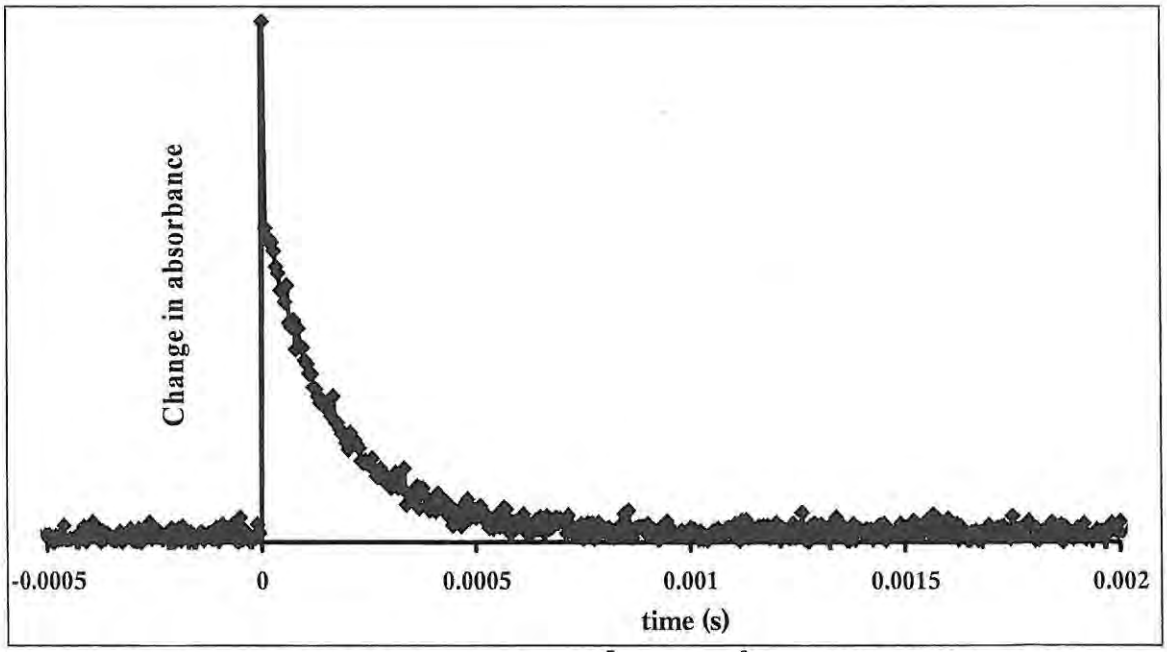

Figure 4.24: Triplet decay curve for 2 x 10^{-5} mol dm^{-3} ZnTBPPc (19) in DMSO. λ_{exc} = 680 nm; $\lambda_{Triplet\ Abs}$ = 520 nm.

Table 4.7: Triplet quantum yields and lifetimes MPcs in different solvents.

	Solvent	[a]Φ_T	τ_T(μs)	[a]Φ_{IC}	Φ_F
ZnPc (15)	DMSO	0.65 [167]	350	0.15	0.20
	DMF		330		0.17
	THF		230		0.23
	Benzonitrile		260		0.13
	n-Butylamine		300		0.12
	Pyridine	0.65 [224]	340	0.15	0.20
	Toluene	0.65 [224]	340	0.28	0.07
ZnTNPc (17)	DMSO	0.62	310	0.36	0.022
ZnTSPc (18)	DMSO	0.88	470	0.05	0.07
ZnTBPPc (19)	DMSO	0.85	160	0.01	0.14
ZnOMPPc (23)	DMSO	0.63	370	0.13	0.24
[b]**AlPcS$_{mix}$ (27)**	DMSO	0.52	800	0.09	0.39
	PBS 7.4	0.44	2.93	0.12	0.44
[b]**ZnPcS$_{mix}$ (28)**	DMSO	0.86	530	0.01	0.14
	DMF		290		0.18
	n-Butylamine		200		0.27
	Pyridine		250		0.23
	H_2O	0.55	190	0.29	0.16
	D_2O		420		0.19
	PBS 7.4	0.53	2.95	0.31	0.16
	PBS + TX	0.61	2.37	0.18	0.21
[b]**SiPcS$_{mix}$ (29)**	DMSO	0.58	430	0.13	0.29
	PBS 7.4	0.45	2.9	0.21	0.34

Table 4.7 contd.

	Solvent	$^{a}\Phi_T$	$\tau_T(\mu s)$	$^{a}\Phi_{IC}$	Φ_F
$^{b}GePcS_{mix}$ **(30)**	DMSO	0.79	760	0.01	0.21
	PBS 7.4	0.67	2.76	0.03	0.30
$^{b}SnPcS_{mix}$ **(31)**	DMSO	0.87	120	0.01	0.13
	PBS 7.4	0.59	2.52	0.36	0.05
	PBS + TX	0.68	2.32	0.13	0.19
ZnNPc (32)	DMSO	0.37	126	0.56	0.07

[a]Due to lack of suitable references in different solvents, Φ_T (and Φ_{IC}) values are compared for just a few solvents; [b]average parameters for the mixture.

Φ_T values depended on the heavy atom effect as well as on aggregation. In PBS 7.4 where they are aggregated, $ZnPcS_{mix}$ (**28**) and $SnPcS_{mix}$ (**31**) have lower Φ_T values (0.53 and 0.59 respectively) than in DMSO (0.86 and 0.87 respectively), where they are monomeric. The values in PBS are lower than are expected on the premise of heavy atom effect; for example, Φ_T value for **31** is lower than that of $GePcS_{mix}$ (**30**) in PBS 7.4 (Table 4.7), which is attributed to the aggregation of the former in aqueous solutions.

However in DMSO, where all five $MPcS_{mix}$ complexes are monomeric, $ZnPcS_{mix}$ (**28**) and $SnPcS_{mix}$ (**31**) gave the highest Φ_T values among the five. In DMSO, the Φ_T values for $AlPcS_{mix}$ and $SiPcS_{mix}$ are consistently lower than for $ZnPcS_{mix}$ (**28**), $GePcS_{mix}$ (**30**) and $SnPcS_{mix}$ (**31**); this observation is indicative of the smaller atomic masses of Al and Si compared to Ge, Sn and Zn.

An evaluation of Φ_T values in different media shows that higher values were obtained in DMSO than in PBS 7.4 (or PBS 7.4 plus Triton X-100); this observation reinforces the earlier proposition that intersystem crossing is favoured in DMSO than in aqueous

solution. As expected, the presence of Triton X-100 resulted in increased Φ_T values for the hitherto aggregated $SnPcS_{mix}$ and $ZnPcS_{mix}$ in aqueous solutions, as monomers have greater tendencies to undergo intersystem crossing because less energy is lost through internal conversion.

There is no particular trend in the variation of τ_T with substituent type. However, it is striking from Table 4.7 that sulphonation brings about a longer triplet lifetime compared to the corresponding unsubstituted derivatives. For example, ZnTSPc (**18**) and $ZnPcS_{mix}$ (**28**) have τ_T values of 470 and 530 μs respectively in DMSO (Table 4.7), compared to a value of 350 μs for ZnPc (**15**) in the same solvent. This implies that the anionic complexes are less efficient at dissipating energy of the excited triplet state. Of interest is the relatively low τ_T value (160 μs) for ZnTBPPc (**19**) in DMSO. It appears that the σ C-H bonds of the *tert*-butyl substituents may exhibit the so called "loose bolt" effect [247], associated with the vibration of bonds set off by the parent molecule in a similar manner as a loose bolt in a moving part of the machine, which tends to be set into motion by other moving parts of the machine. The "loose bolt" effect accelerates internal conversion, since electronic energy "leaks out" through C-H vibrations. The "loose bolt" effect is expected to be less pronounced in ZnOMPPc (**23**) molecules since there are less C-H bonds than in **19**. The fact that τ_T value of **23** is more than twice that of **19** in DMSO suggests that the triplet state of the former is probably being stabilized by some other factors. ZnNPc (**32**) gave the shortest triplet lifetime in DMSO compared to other ZnPc derivatives. Naphthalene itself is known to be an efficient triplet state quencher [248,249]. The triplet lifetimes for ZnPc (**15**) in Table 4.7 do not change much as the solvent is changed, with ZnPc (**15**) in THF and benzonitrile showing marginally shorter lifetimes than in other solvents.

$ZnPcS_{mix}$ (**28**) is of current interest in PDT and its photophysical and photochemical studies in aqueous media are essential. Table 4.7 shows that τ_T value for **28** is very low in water compared to the non-aqueous solvents or D_2O. The reason for this can be explained in terms of the near IR spectra of the solvents. Fig. 4.25 shows the near IR absorption spectra of three solvents: DMSO, DMF and H_2O, and how these affect the triplet and singlet oxygen lifetimes in solution. The triplet energy of ZnPc (**15**) and many of its derivatives in solution is ~ 1.12 eV [158,250], which corresponds to an absorption wavelength of ~ 1108 nm. The intensity and broadness of the solvent's absorption in this wavelength region should have considerable effect on the triplet lifetime of the ZnPc derivative. H_2O shows a very broad absorption near 1108 nm, which implies that non-radiative decay and quenching of the sensitizer's triplet state would be more rapid in H_2O than in DMSO or DMF where the 1108 nm absorption in minimal. Thus τ_T values are lower in water when compared to DMSO or DMF, Table 4.7.

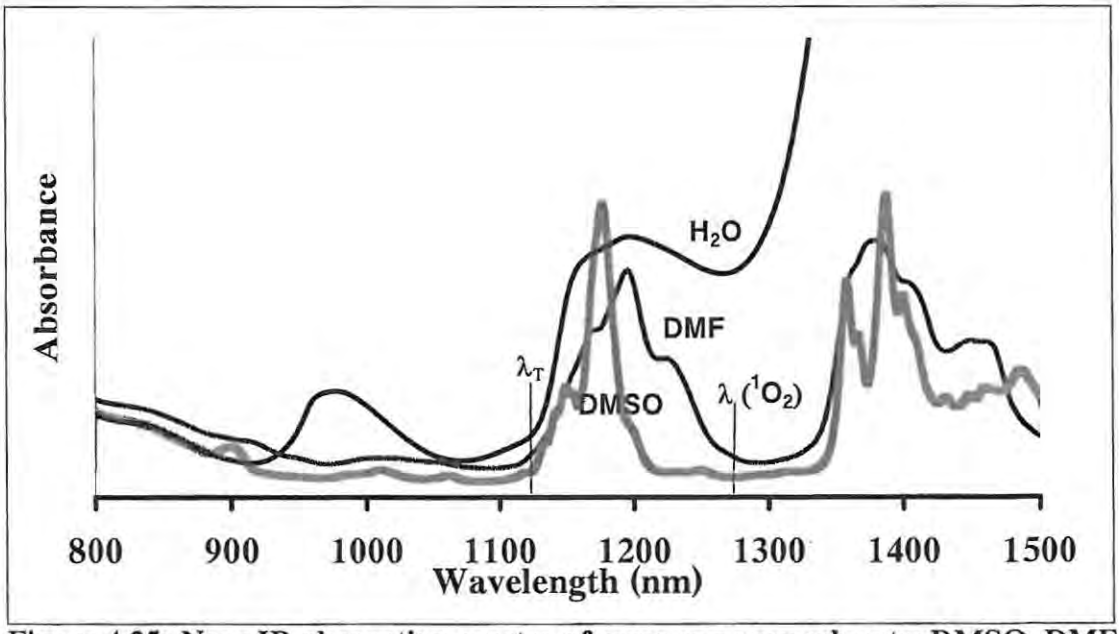

Figure 4.25: Near IR absorption spectra of some common solvents; DMSO, DMF and water.

The low value of τ_T for $ZnPcS_{mix}$ (**28**) in *n*-butylamine could be a result of the quenching of the triplet state by the amine group.

Triplet lifetimes (τ_T) among the $MPcS_{mix}$ complexes do not vary in a well-defined fashion in Table 4.7. Ordinarily, one would expect lower τ_T values for complexes containing heavy metals; although this is manifested to some extent in DMSO (Table 4.7), with $AlPcS_{mix}$ (**27**, 800 μs) showing the highest and $SnPcS_{mix}$ (**31**, 120 μs) showing the lowest τ_T values, the observed trend among the five $MPcS_{mix}$ species does not strictly conform to that predicted on the basis of heavy atom effect.

There is a striking increase in τ_T values on going from PBS 7.4 (or PBS 7.4 plus Triton X-100) to DMSO among all the complexes. Also, triplet lifetimes for $SnPcS_{mix}$ (**28**) and $SnPcS_{mix}$ (**31**) are slightly lower in the presence of Triton X-100, in spite of monomerization. It is possible that molecular vibrations in Triton X-100 could accelerate triplet quenching, suggesting that solvent effects in this case overrides that of monomerization by Triton X-100. These observations demonstrate that the effect of solvents on the triplet lifetimes of MPc complexes cannot be overstressed.

In PBS 7.4, triplet lifetimes of the $MPcS_{mix}$ complexes ranged from 2.52 μs ($SnPcS_{mix}$) to 2.95 μs ($ZnPcS_{mix}$), with an average value of 2.81 μs. These values are almost equal, considering a 10% error margin. The explanation for this observation could be that the triplet quenching of these complexes in PBS 7.4 is so severe that the heavy atom effect on intersystem crossing (from the triplet state to the ground singlet state) becomes insignificant in this solvent.

The determination of Φ_F and Φ_T values for the MPc complexes paved the way for the calculation of internal conversion quantum yield (Φ_{IC}), Eq. 4.7.

$$\Phi_{IC} = 1 - (\Phi_F + \Phi_T) \qquad \text{(Eq. 4.7)}$$

It is obvious in Table 4.7 that solvent effects on Φ_{IC} values are significant. For example, Φ_{IC} value of ZnPc (**15**) in toluene is greater than those in DMSO and pyridine, which are more viscous solvents. In low-viscosity toluene, the rate constant for fluorescence is lower than the rate of internal conversion; hence internal conversion is favoured above fluorescence. In the same vein, Φ_{IC} values of the $MPcS_{mix}$ complexes are higher in aqueous solutions than in DMSO, which suggests that the molecules are more photo-active in DMSO than in aqueous solutions. This could again be attributed to the lower viscosity of water than DMSO as well as the aggregation tendencies of $MPcS_{mix}$ complexes in PBS. As earlier stated, aggregation hinders fluorescence and intersystem crossing; hence most of the electronic energy of the excited singlet state is lost through internal conversion to the ground singlet state. Φ_{IC} is drastically reduced for $SnPcS_{mix}$ and $ZnPcS_{mix}$ in PBS 7.4 in the presence of Triton X-100, due to the monomerizing effect of this surfactant. In DMSO, Φ_{IC} values for the $MPcS_{mix}$ with heavier atoms (M = Ge, Sn and Zn) are close to zero.

4.2.2.2 ZnPc(O-ZnTPP)$_4$ heteropentamer

Triplet quantum yield and lifetimes for ZnPc in the pentamer or mixture were carried out in DMSO with excitation at 682 nm. The triplet states of Pcs normally absorb in the 450 – 550 nm wavelength range; therefore, triplet absorption could not be monitored for the Pc because the P component of the system absorbs in this region. As a result, Pc triplet quantum yields and lifetimes were determined by singlet depletion method (Eq. 2.36), following excitation at 682 nm, and are listed in Table 4.8. The porphyrin Q band excitation (550 nm) could not be carried out because the wavelength of the available laser light was > 650 nm. Consequently, all the values for ZnTPP in Table 4.8 were either calculated or obtained from literature.

Table 4.8: Triplet data for ZnPc and ZnTPP as monomers and in the pentamer (or mixture).

		τ_T(μs)	[a]Φ_T	[b]Φ_{IC}
(A) ZnPc parameters using 640 nm excitation				
DMSO	**ZnPc monomer**	350	0.65 [167]	0.15
	ZnPc in Pentamer	230	0.12 (0.10)	0.02
	ZnPc in Mixture	230	0.39 (0.42)	0.10
Toluene	**ZnPc monomer**	340	0.65 [224]	0.28
	ZnPc in Pentamer	240	0.23 (0.19)	0.11
	ZnPc in Mixture	250	0.63 (0.65)	0.28
(B) ZnTPP parameters (from literature or calculated)[c]				
		τ_T (μs)	[b]Φ_T	Φ_{IC}
DMSO	**ZnTPP monomer**		0.88 [244]	0.08
	ZnTPP in Pentamer		(0.31)	0.03
	ZnTPP in Mixture		(0.81)	0.07
Toluene	**ZnTPP monomer**	1400 [167]	0.88 [167]	0.09
	ZnTPP in Pentamer		(0.13)	0.01
	ZnTPP in Mixture		(0.54)	0.05

[a]Values in brackets ( ) were calculated using Eq. 4.8; [b]calculated using Eq. 4.7; [c]no experimental values obtained; [c]not determined experimentally due to laser wavelength limitations. References given in square brackets.

For comparison, Φ_T values were also calculated for Pc in the pentamer or mixture, and the values were compared with experimentally determined values.

Φ_T values were calculated using Eq. 2.89 (now written as Eq. 4.8)

$$\frac{\Phi_{T,Pc}^{Pc}}{\tau_{F,Pc}^{Pc}} = \frac{\Phi_{T,Pc}^{Pc-P_4}}{\tau_{F,Pc}^{Pc-P_4}} \qquad \text{(Eq. 4.8)}$$

Where $\Phi_{T,Pc}^{Pc}$ and $\Phi_{T,Pc}^{Pc-P_4}$ are the triplet quantum yields of ZnPc monomer and ZnPc in the pentamer (or mixture) respectively; while $\tau_{F,Pc}^{Pc}$ and $\tau_{F,Pc}^{Pc-P_4}$ are the fluorescence lifetimes of ZnPc monomer and ZnPc in the pentamer (or mixture) respectively. Pc-P_4 represents the monomer or mixture.

$\Phi_{T,Pc}^{Pc}$ was obtained from literature, while $\tau_{F,Pc}^{Pc}$ and $\tau_{F,Pc}^{Pc-P_4}$ are given in Table 4.5, using these values, $\Phi_{T,Pc}^{Pc-P_4}$ values were determined from Eq. 4.8, and are listed in Table 4.8.

Triplet quantum yields and lifetimes for ZnPc and ZnTPP monomers (Table 4.8) were lowered in both the pentamer and the mixture, compared to the monomer. The lower values of Φ_T could be as a result of the increase in the number of processes competing with intersystem crossing in deactivating the excited singlet state. Again here, the extent of lowering in Φ_T value was greater in the pentamer than in the mixture, supporting the earlier conclusion about the higher efficiency of intramolecular CT or ET transfer than intermolecular CT or ET.

In DMSO and toluene, the experimental Φ_T values of ZnPc in the pentamer and mixture (Eq. 2.36) agree well (within error limits) with those calculated (Table 4.8). Triplet lifetimes (τ_T) of ZnPc were almost similar in both the pentamer and mixture, but lower than those of the monomers.

Table 4.8 shows that quantum yields of internal conversion (Φ_{IC}) for ZnPc and ZnTPP are greater in the monomer than in the pentamer. This is not unexpected because in the pentamer, the singlet excited states of ZnPc and ZnTPP are quenched by CT or CT, rather than undergoing internal conversion. However in the mixture, Φ_{IC} values are almost the same as in the monomer. This observation constitutes a further

evidence in support of the fact that CT and ET are more efficient in the pentamer than in the mixture.

4.2.3 Fluorescence quenching

4.2.3.1 Fluorescence Quenching of $MPcS_{mix}$ complexes by benzoquinone (BQ)

Fig. 4.26 shows the fluorescence emission spectra of $GePcS_{mix}$ (**30**) in the presence of varying concentrations of benzoquinone (BQ), in PBS 7.4. There is a progressive decrease in fluorescence intensity as the concentration of BQ increases. A similar trend was observed for $AlPcS_{mix}$ (**27**), $ZnPcS_{mix}$ (**28**), $SiPcS_{mix}$ (**29**) and $SnPcS_{mix}$ (**31**).

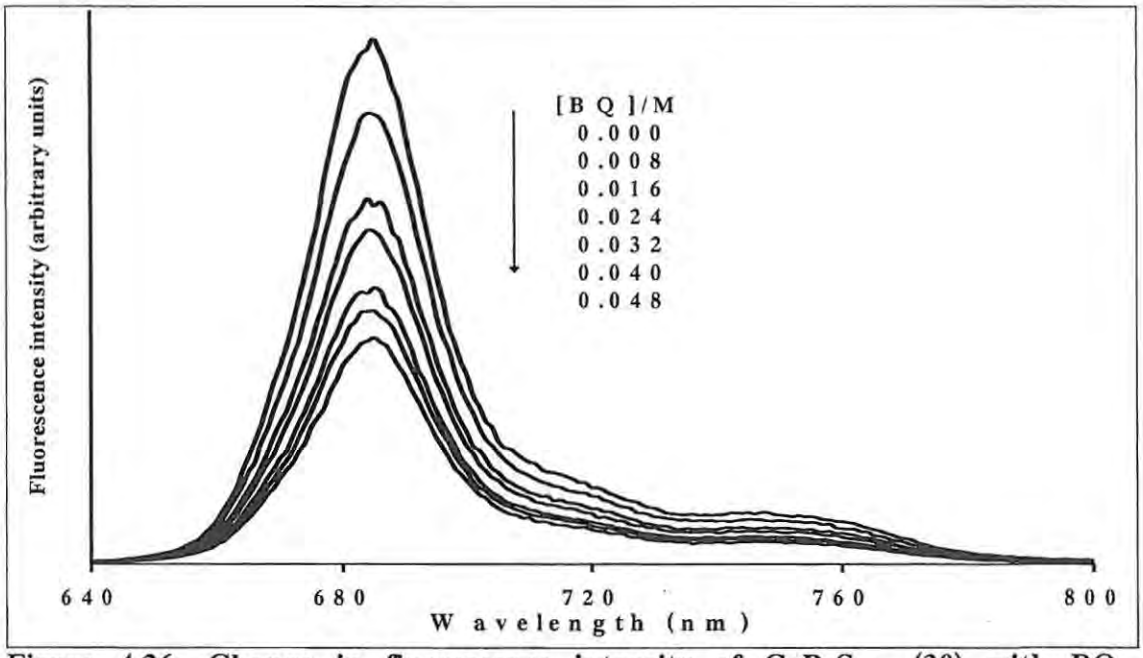

Figure 4.26: Change in fluorescence intensity of $GePcS_{mix}$ (30) with BQ concentration. [BQ] = 0, 0.008, 0.016, 0.024, 0.032, 0.040 and 0.048 M. [30] = 6 x 10^{-7} M.

The plot of $\frac{I_0}{I}$ versus concentration of BQ (using Eq. 1.8) gave a positive deviation from Stern-Volmer (S-V) relationship (Fig. 4.27a), which is recognized by an upward

curvature in the plot. The positive deviation is an indication of the coexistence of both static and dynamic quenching mechanisms.

As earlier explained in Chapt. 2, The linear S-V plot was obtained by calculating the apparent values of K_{SV} using Eq. 4.9 (similar to Eq.1.8):

$$\frac{I_0}{I} = 1 + K_{SV}[BQ] \qquad \text{(Eq. 4.9)}$$

The apparent K_{SV} values were then plotted against [BQ] and extrapolated to [BQ] = 0 to obtain K_D, the dynamic quenching constant.

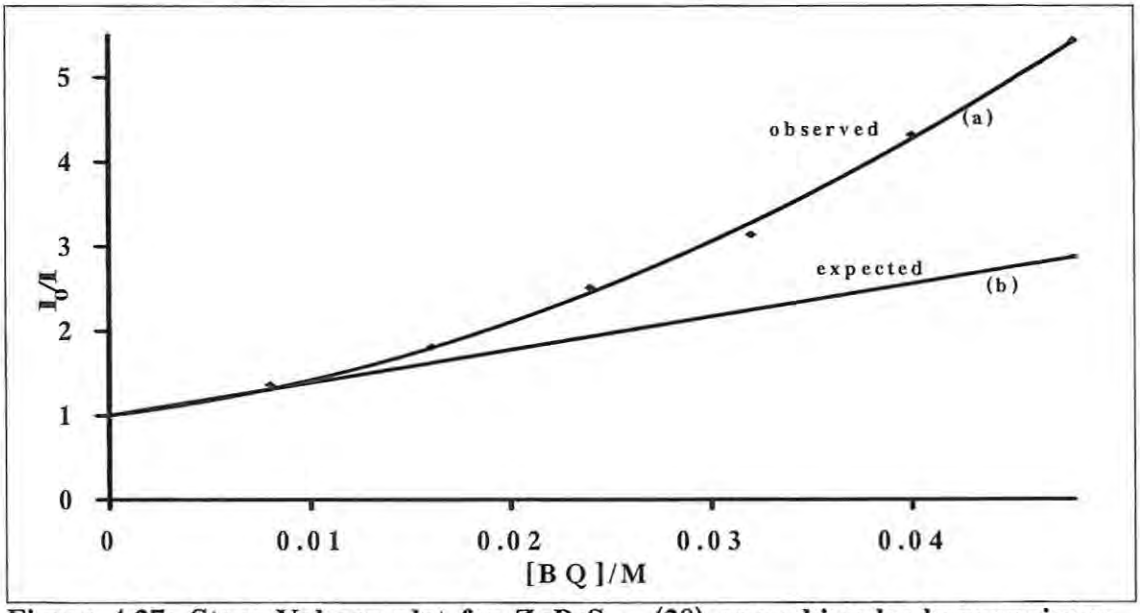

Figure 4.27: Stern-Volmer plot for $ZnPcS_{mix}$ (28) quenching by benzoquinone showing positive deviation (a) and the expected Stern-Volmer plot (b).

A straight line from $\frac{I_0}{I} = 1$ of slope K_D represents the expected S-V plot, Fig. 4.27b.

The static quenching constant (K_S) was determined using Eq. 4.10 (similar to Eq. 2.80):

$$\frac{I_0}{I(1+K_D)[BQ]} = 1 + K_S[BQ] \qquad \text{(Eq. 4.10)}$$

Using the value of K_D obtained above, the plot of $\frac{I_0}{I(1+K_D)[BQ]}$ versus [BQ] gives the constant K_S.

The values of K_D and K_S for the various $MPcS_{mix}$ complexes are listed in Table 4.9. K_S values range from 3.27 to 8.08 M^{-1} for the $MPcS_{mix}$ complexes.

Eq. 4.10 could be rewritten as Eq. 4.11 (similar to Eq. 2.79):

$$\frac{I_0}{I} = (1+K_D[BQ])(1+K_S[BQ]) \qquad \text{(Eq. 4.11)}$$

Considering only the static component of Eq. 4.11 gives Eq. 4.12:

$$\frac{I_0}{I} = (1+K_S[BQ]) \qquad \text{(Eq. 4.12)}$$

Using Eq. 4.12, the concentrations of the quencher required to quench half of the fluorophore molecules (that is to decrease the fluorescence intensity by half), via static quenching (complex formation), ranges from 0.12 to 0.27 M for the range of K_S values shown in Table 4.9.

Table 4.9: Variation of quenching constants (BQ quenching) with metal ionic radii.

	[a]R (pm)	K_D (M^{-1})	K_S (M^{-1})	K'_S (M^{-1})	τ_F (ns)	k_Q (M^{-1} s^{-1})
$AlPcS_{mix}$ (27)	67.5	22.09	3.27	12.04	5.00 [159]	4.42×10^9
$ZnPcS_{mix}$ (28)	88	31.20	8.08	18.84	2.90 [158]	1.08×10^{10}
$SiPcS_{mix}$ (29)	54	10.18	4.77	7.10		
$GePcS_{mix}$ (30)	67	17.71	4.81	10.64		
$SnPcS_{mix}$ (31)	83	27.48	5.00	15.42		

[a]R is the radius of a central metal ion; References in square brackets.

Thus an average BQ concentration of ~ 0.2 M is required to quench half of the $MPcS_{mix}$ complexes by the type of static quenching resulting from formation of a

ground complex between the fluorophore and the quencher. This concentration is large compared to the quencher concentrations (ranging from 0.0008 to 0.0048 M, Fig. 4.26) employed in this work, implying that the $MPcS_{mix}$ complexes do not actually form ground state complexes with BQ. This is supported by the fact that the wavelength of the Q bands in the absorption spectra of the $MPcS_{mix}$ complexes did not change on addition of BQ. Thus, the positive deviation of the S-V plot in Fig. 4.27a must due to another form of static quenching, which is often interpreted in terms of the proximity of the fluorophore to the quencher at the moment of excitation - the "sphere of action quenching model" (SAQM) (Fig. 4.28) [213-215]. This model limits the number of fluorophore ($MPcS_{mix}$) molecules, which can fluoresce and be quenched by molecules of BQ via the dynamic quenching process.

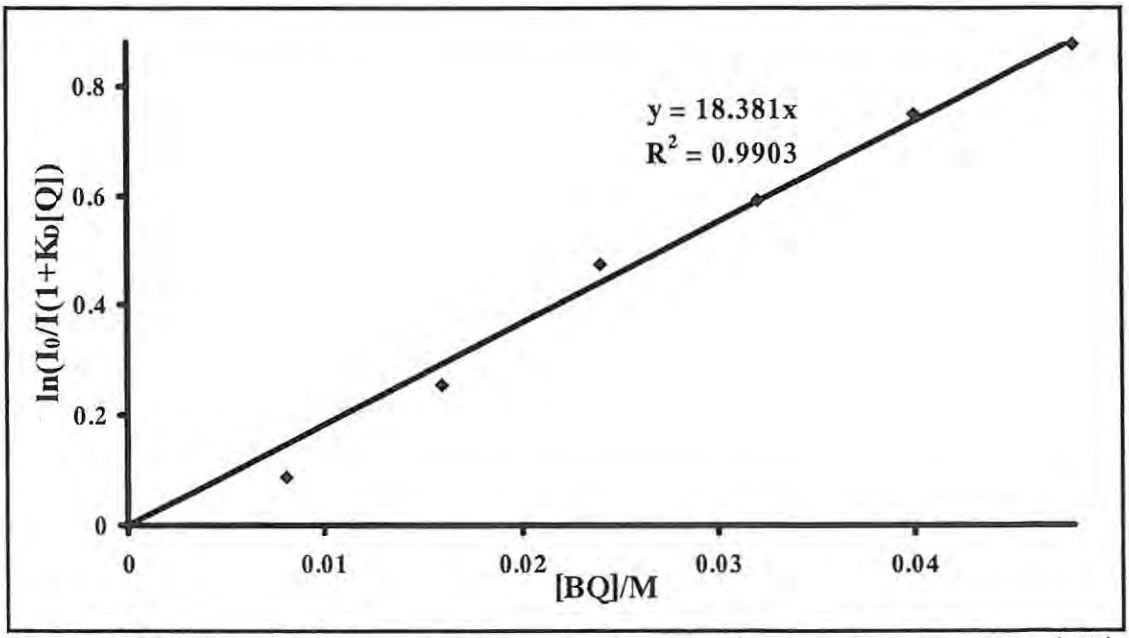

Figure 4.28: Determination of sphere-of-action static quenching constant (K'_S) for $ZnPcS_{mix}$ (1.2×10^{-6} M) with benzoquinone quencher.

Values of the sphere-of-action static quenching constant (K'_S) obtained from Eq. 4.13 (similar to Eq. 2.82), are listed in Table 4.9.

$$\frac{I_0}{I(1+K_D[BQ])} = e^{K's[BQ]} \qquad \text{(Eq. 4.13)}$$

k_Q (bimolecular quenching constant) values were calculated (Eq. 4.14) for only $AlPcS_{mix}$ (**27**) and $ZnPcS_{mix}$ (**28**) (where literatures values fluorescence lifetimes were available) and are listed in Table 4.9. k_Q values for **27** and **28** are 4.42 $x10^9$ and 1.08 x 10^{10} M^{-1} s^{-1}, respectively. k_Q values near 1 x 10^{10} M^{-1} s^{-1} are in agreement with the theoretical Smoluchowski-Stokes-Einstein approximation at 298 K [224].

$$k_Q = \frac{K_D}{\tau_F} \qquad \text{(Eq. 4.14)}$$

Influence of central metal ion on BQ quenching of $MPcS_{mix}$ complexes

It is interesting to note in Table 4.9 that an increase in the radius of the central metal ion resulted in increase in the values of the quenching constants: K_D (dynamic), K_S (static) and K'_S (sphere of action). $ZnPcS_{mix}$ (**28**) showed the highest values, while $SiPcS_{mix}$ (**29**) showed the lowest values. It is known [251] that since ionic radii differ for different metals, their spatial molecular structures would differ slightly. While some MPc complexes are flat, some have protruding metals because of the big ionic radii of the coordinating metals. Such metals are bigger than the cavity in the phthalocyanine's backbone. For example in zinc phthalocyanines [43,44], zinc is displaced 45 pm from the plane of the aromatic ring, with Zn-N bond lengths of 206.1 pm, to form a domed shape. Also in tin phthalocyanine [46,251], tin is protruded out of the Pc cavity due to its ionic size. It is logical therefore to conclude that the higher the radius of a metal ion, the greater the extent of displacement from the planar Pc ring, which amounts to a greater molecular volume of the respective MPc complex. In

the foregoing discussion, differences in molecular volume could be responsible for the observed trend in the variation of the quenching constants - K_D, K_S and K'_S among the $MPcS_{mix}$ complexes. It is proposed here that the greater the molecular volume of the fluorophore, the larger the K'_S values and hence the more efficient the apparent static quenching, which occurs at the moment of excitation. The same applies to the dynamic quenching constant, K_D and the association (static) constant K_S. Thus the K_D, K'_S and K_S values are most pronounced in $ZnPcS_{mix}$ (**28**), with the largest molecular volume.

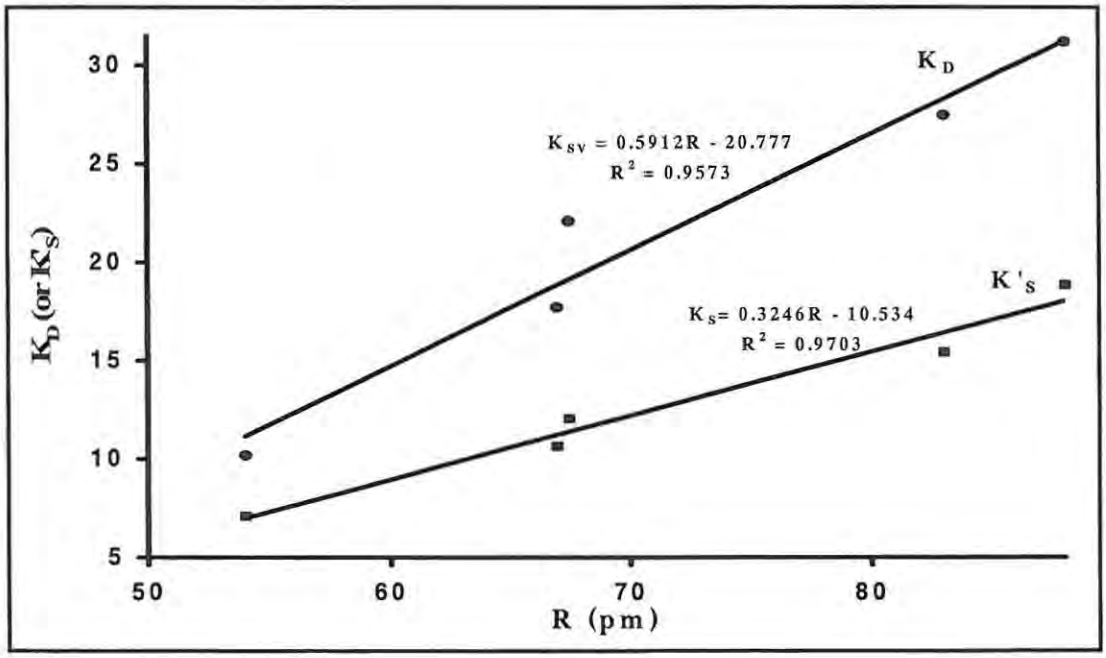

Figure 4.29: Dependence of quenching constants of $MPcS_{mix}$ complexes on central metal ionic radii.

Fig. 4.29 relates quenching constants (K_D and K'_S) to the radii of central metal ions [252-255]. The frequency of collision of the quencher with the fluorophore should increase with the size of the molecule. The quencher molecules travel a little distance before encountering a fluorophore molecule for the larger molecules.

4.2.3.2 Fluorescence Quenching of $MPcS_{mix}$ complexes by Hydroquinone (HQ)

In the presence of HQ quencher, a reaction takes place between the excited $MPcS_{mix}$ and the HQ molecules. According to Darwent et al.[159], the following mechanism holds for the reaction:

$$MPcS_{mix}^{*} + BQH_2 \rightarrow (MPcS_{mix}^{\bullet-} \ldots BQ^{\bullet-}) + 2H^{+} \qquad \text{(Eq. 4.15)}$$

(Where BQH_2 represents HQ and BQ is benzoquinone).

The $MPcS_{mix}^{*}$ molecule interacts with HQ by diffusional collision, hence dynamic quenching applies.

The fluorescence quenching of $MPcS_{mix}$ by hydroquinone (HQ) in PBS 7.4 was found to obey S-V kinetics (Eq. 4.9, with [BQ] replaced by [HQ]; Fig. 4.30). Such behaviour was not observed in the case of BQ (Fig. 4.27), which did not obey S-V kinetics. Only the Stern-Volmer dependence of quenching of $AlPcS_{mix}$ (**27**) by HQ in aqueous solution has been reported before [159].

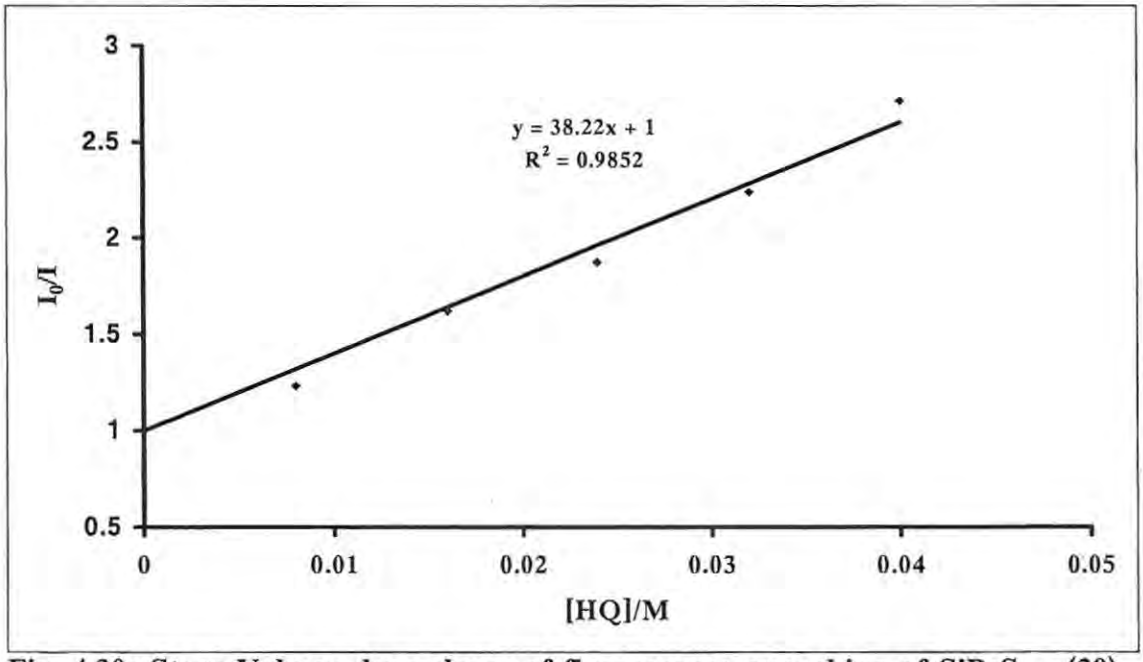

Fig. 4.30: Stern-Volmer dependence of fluorescence quenching of $SiPcS_{mix}$ (29) by hydroquinone.

K_{SV} values for the HQ quenching of $MPcS_{mix}$ are listed in Table 4.10. The observed order of the values is **27 > 29> 30 > 28 > 31**. It is interesting to note that this is the

exact order of molar extinction coefficients of the respective complexes. The molar extinction coefficient value is an indication of the probability of light absorption by ground state molecules; and since the interaction of the excited molecules with HQ is diffusion-controlled, it follows from collision theory of reaction rates that the higher the probability of absorption, the higher the likelihood of collision; and the more collisions there are, the greater the quenching constant (K_{SV}).

Table 4.10: Rate constants for various excited state deactivation processes of $MPcS_{mix}$ complexes in PBS 7.4; $k_D = 8.4 \times 10^9\ M^{-1}\ s^{-1}$.

	[a]λ_Q (nm) (log ε)	K_{SV} (M^{-1})	τ_F (ns)	[b]k_F (s^{-1})	[b]k_{IC} (s^{-1})	[b]k_{ISC} (s^{-1})	[b]k_{Pd}(s^{-1})
$AlPcS_{mix}$ (27)	674 (5.18)	44.86	5.34	8.24×10^7	2.25×10^7	8.24×10^7	1.37
$ZnPcS_{mix}$ (28)	673 (4.89)	23.35	2.78	5.76×10^7	1.12×10^8	1.91×10^8	12.37
$SiPcS_{mix}$ (29)	678 (5.11)	38.22	4.55	7.47×10^7	4.62×10^7	9.89×10^7	2.45
$GePcS_{mix}$ (30)	680(5.01)	36.29	4.32	6.94×10^7	6.94×10^6	1.55×10^8	1.63
$SnPcS_{mix}$ (31)	688 (4.57)	17.05	2.03	2.46×10^7	1.77×10^8	2.91×10^8	6.31

[a]Q band maxima shown for the low energy band only where bands are split. [b]Values calculated using Eqs. 2.64a-d: $k_F = \frac{\Phi_F}{\tau_F}$; $k_{IC} = \frac{\Phi_{IC}}{\tau_F}$; $k_{ISC} = \frac{\Phi_{ISC(T)}}{\tau_F}$; $k_{Pd} = \frac{\Phi_{Pd}}{\tau_T}$. **$\Phi_F$ taken from Table 4.4; Φ_T and Φ_{IC} from Table 4.7, Φ_{Pd} from Table 4.12 (next Section).**

The rate of movement of materials by diffusion can be predicted mathematically using the Fick's law of diffusion, given by Eq. 4.16:

$$J_0 = -D_0\left(\frac{\partial C_0}{\partial x}\right) \qquad \text{(Eq. 4.16)}$$

Where J_0 is the diffusional flux (rate of movement of material by diffusion); D_0, the diffusion coefficient; and $\left(\frac{\partial C_0}{\partial x}\right)$, the concentration gradient. It is expected that the

aggregated species ($SnPcS_{mix}$ and $ZnPcS_{mix}$), would give lower J_0 values, since aggregation slows down molecular motion. Aggregation, coupled with the relatively low molar extinction coefficients of these molecules results in their low K_{SV} values. Fig. 4.31 shows the variation of K_{SV} with the log of molar extinction coefficients (log ε).

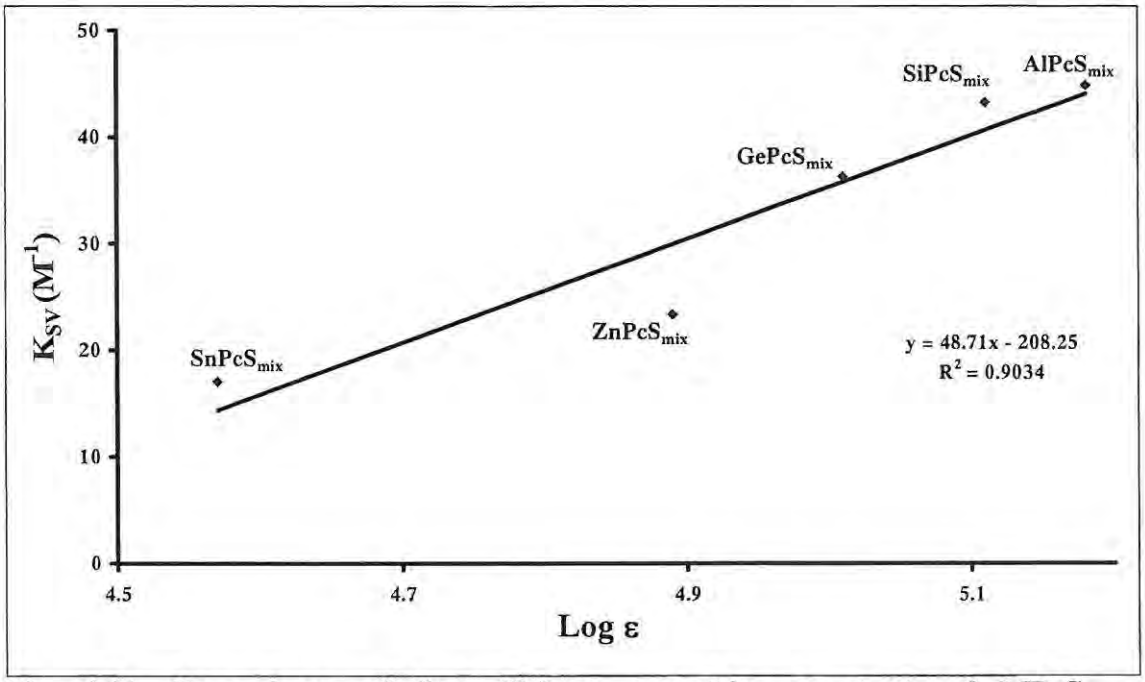

Fig. 4.31: Dependence of Stern-Volmer quenching constants of $MPcS_{mix}$ complexes on molar extinction coefficients

Determination of $MPcS_{mix}$ fluorescence lifetimes from HQ-quenching data

This work presents a simple route to determining the fluorescence lifetimes of fluorophores from fluorescence quenching data. This however, could only be possible if the bimolecular quenching constant (k_Q) is known (Eq. 4.14). k_Q values for the MPc_{Smix} complexes were calculated according to Eqs. 2.83 - 2.85 (from k_R, the diffusion-controlled bimolecular rate constant), assuming that the efficiency (f) of $MPcS_{mix}$-HQ collision is unity (HQ quenches the fluorescence of $MPcS_{mix}$ complexes effectively) [159]. Using the values of ~ 7.7×10^{-10} m and 3.9×10^{-10} m for molecular radii of an MPc molecule [256] and HQ [257] respectively (assuming that a change of

the central metal ion has little effect on the molecular radius of the MPc backbone); the bimolecular rate constant (k_R) value for the HQ-quenching of each $MPcS_{mix}$ species was found to be 8.4 x 10^9 M^{-1} s^{-1}. From the values of K_{SV} (slope in Fig. 4.30) and k_Q, the fluorescence lifetimes (τ_F) could be calculated according to Eq. 4.14 (K_D replaced with K_{SV} when only diffusion-controlled quenching is present).

This procedure for the determination of τ_F for the $MPcS_{mix}$ complexes could however not be used when BQ was used as quencher; this is because quenching in this case is not absolutely diffusion-controlled, and such treatment would definitely lead to erroneous results.

The determination of τ_F afforded the calculation of the rate constants for the intrinsic processes from quantum yield values of the respective processes (Eq. 2.64a-c) – See Table 4.10.

The rate constant values of processes deactivating the excited states of the $MPcS_{mix}$ complexes are listed in Table 4.10. Rate constants for fluorescence (k_F) ranged from 2.46 x 10^7 s^{-1} ($SnPcS_{mix}$, **31**) to 8.24 x 10^7 s^{-1} ($AlPcS_{mix}$, **27**); while k_{ISC} values range from 8.24 x 10^7 s^{-1} ($AlPcS_{mix}$, **27**) to 2.91 x 10^8 s^{-1} ($SnPcS_{mix}$, **31**).

Among the $MPcS_{mix}$ species, $AlPcS_{mix}$ (**27**) showed the highest value of k_F, while $SnPcS_{mix}$ (**31**) showed the lowest. Obviously, the lower values for **28** and **31** compared to the rest could be due to their aggregated nature in aqueous solution.

The values of k_{ISC}, as expected, increased with the mass of the central metal ion, which is a manifestation of the heavy atom effect that promotes intersystem crossing.

As expected, **28** and **31** gave the highest value of k_{IC}, which is again readily attributed to aggregation. $GePcS_{mix}$ (**30**) gave the lowest value of k_{IC}, indicating that this species is perhaps the most photoactive in the list.

4.3 PHOTOCHEMICAL STUDIES

4.3.1 Photodegradation (photobleaching) quantum yields

4.3.1.1 Solvent and substituent effects

Table 4.11 gives the photodegradation (photobleaching) quantum yield (Φ_{Pd}) values for ZnPc (**15**), ZnOEPc (**21**) and ZnOPPc (**22**) in the various solvents. Photobleaching is identified by a reduction in the spectral intensity without the formation of new peaks (Fig. 4.32).

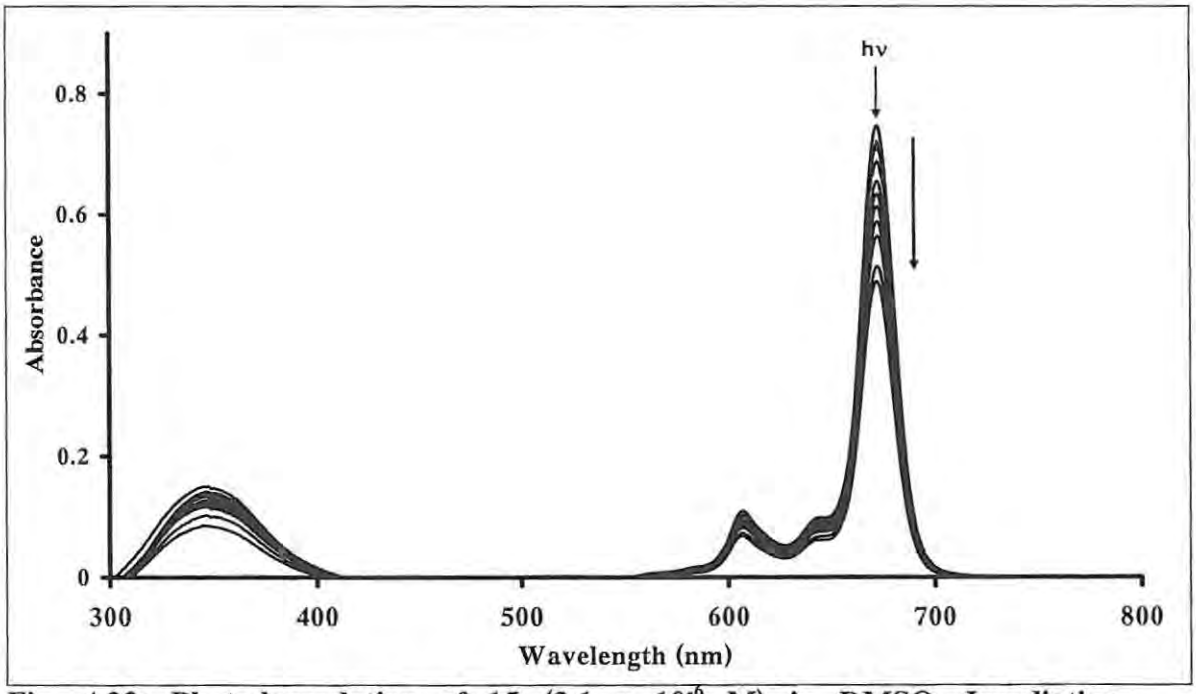

Fig. 4.32: Photodegradation of 15 (3.1 x 10^{-6} M) in DMSO. Irradiation wavelength 670 ± 20 nm.

Phthalocyanine molecules in general photodegrade oxidatively via attack by singlet oxygen generated by them (see Scheme 1.14). However, reductive photodegradation has also been reported [225] for phthalocyanines containing pyridine rings (porphyrazines). It is believed that photodegradation takes place at the excited triplet

state of a photosensitizer; it therefore follows that the higher the population of molecules in this state, the higher the probability of photodegradation.

In general, Table 4.11 shows that photodegradation is more pronounced in pyridine, DMF and DMSO for all the ZnPc derivatives, with the exception of ZnPc (**15**) in benzonitrile. For all the ZnPc derivatives, the lowest photobleaching quantum yields were observed when *n*-butylamine or THF were employed as solvents. *N*-butylamine is highly basic with solvent basicity (SB) = 0.944 [258], compared to SB = 0.581 for pyridine, hence the basicity of *n*-butylamine may prevent the oxidative degradation of MPc complexes. Pyridine (SB = 0.581), DMSO (SB = 0.647) and DMF (SB = 0.613) are less basic than *n*-butylamine (SB = 0.944), Table 4.11. Thus pyridine, DMSO and DMF will be less efficient in stabilising the ring against oxidative attack than *n*-butylamine, resulting in higher photodegradation rates. THF (SB = 0.591, Table 4.11) is less basic than DMSO and DMF, hence it would be expected to show high photodegradation quantum yield using the argument that low donor number (low basicity) of solvent gives rise to less stabilization of the ring against oxidative attack.

Different substituents exhibit different effects on the $\bullet_{Pd}$ values of ZnPc. While some substituents stabilize the ring against photodegrdation, some make it more vulnerable to oxidative attack. For example, it has been observed before [77] that phthalocyanine molecules containing biological molecules on the peripheral positions are more easily degraded compared to other octasubsitituted MPc complexes.

Table 4.11: Photodegradation quantum yields of ZnPc (15), ZnOEPc (21) and ZnOPPc (22) in different solvents.

Compound	Solvent	Solvent Basicity (SB)	$10^{-5}/\varepsilon$ ($dm^3\ M^{-1}\ cm^{-1}$) Q band	$10^5/\Phi_{Pd}$
ZnPc (15)	DMSO	0.647	2.38	2.61

	DMF	0.614	2.35	2.23
	Pyridine	0.581	2.65	5.85
	THF	0.591	3.05	0.152
	n-Butylamine	0.944	2.9	0.543
	Benzonitrile	0.281	2.5	4.99
ZnOEPc (21)	DMSO	0.647	1.74	3.51
	DMF	0.614	2.76	6.21
	THF	0.591	2.62	0.121
	Pyridine	0.581	2.18	6.15
	Benzonitrile	0.281	2.78	1.71
	Benzene	0.124	2.91	1.89
	n-Butylamine	0.944	2.35	0.643
ZnOPPc (22)	DMSO	0.647	1.34	2.53
	DMF	0.614	1.26	12.1
	Pyridine	0.581	1.58	4.93
	Benzonitrile	0.281	1.67	2.16
	Benzene	0.124	1.7	1.39
	n-Butylamine	0.944	2.08	0.699

Axial ligands impart some extra photostability on the Pc ring compared to ring substituted or unsubstituted derivatives containing no axial ligands, as judged by the low $\bullet_{Pd}$ values for (CN)ZnPc (**24**), (pip)ZnPc (**25**) and (py)ZnPc (**26**) compared to the rest of ZnPc derivatives in Table 4.12.

Table 4.12: Effects of substituents and solvents on photodegradation quantum yields of MPc complexes.

Compound	$10^5/\Phi_{Pd}$ (DMSO)	[a]$10^5/\Phi_{Pd}$ (PBS)7.4	[b]$10^5/\Phi_{Pd}$ (PBS + TX)
ZnTSPc (18)	4.03		
ZnTBPPc (19)	3.33		
ZnOMPPc (23)	2.12		
(CN)ZnPc (24)	0.21		
(pip)ZnPc (25)	0.24		
(py)ZnPc (26)	0.51		
[c]**$AlPcS_{mix}$ (27)**	5.79	0.40	
[c]**$ZnPcS_{mix}$ (28)**	13.65	3.65	7.02
[c]**$SiPcS_{mix}$ (29)**	7.35	0.71	
[c]**$GePcS_{mix}$ (30)**	9.74	0.45	
[c]**$SnPcS_{mix}$ (31)**	14.01	1.59	4.13
ZnNPc (32)	16.35		

[a]Only the $MPcS_{mix}$ complexes were studied in aqueous media; the non-suphonated derivatives were insoluble in water, hence no data in aqueous solutions for these complexes.
[b]TX = Triton X-100; only the aggregated $ZnPcS_{mix}$ (28) and $SnPcS_{mix}$ (31) showed spectral changes in the presence of TX. [c]average fothe mixture.

Among the $MPcS_{mix}$ derivatives (**27-31**) in PBS, the aggregated complexes - $ZnPcS_{mix}$ (**28**) and $SnPcS_{mix}$ (**31**) show higher Φ_{Pb} values (Table 4.12). These species have lower Φ_{Δ} values than $GePcS_{mix}$ (**30**) (as will be seen later); this implies that $MPcS_{mix}$ photodegradation is probably not initiated by singlet oxygen alone. The excited triplet state of a photosensitizer is sufficiently long-lived to intercept other species in solution. Φ_{Pb} values are consistently higher in DMSO than in aqueous solution for the $MPcS_{mix}$ complexes, and this could be a reflection of the higher Φ_T (hence high Φ_{Δ}) values in DMSO.

A study of the solvent effects on the photostability of $ZnPcS_{mix}$ **(28)** revealed that photostability of this species increases with solvent basicity, as already discussed (Fig. 4.33). This is attributed to the differing extents of screening of the MPc ring from oxidative attack, by the solvents' donor abilities. The solvent basicities of DMSO, DMF, pyridine and *n*-butylamine [258] correlate well with the observed Φ_{Pd} values for **28** in these solvents (13.65, 15.97, 16.38 and 9.03 x 10^{-5} respectively).

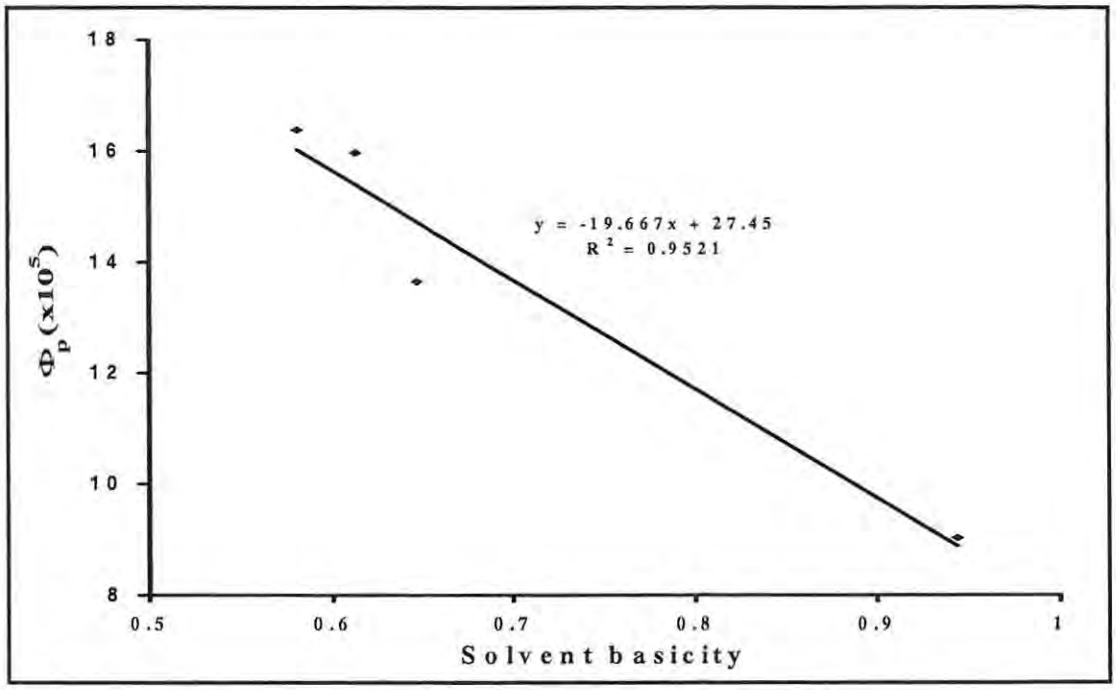

Fig. 4.33: Dependence of of photostability of ZnPcSmix (28) on solvent basicity.

4.3.1.2 Phototransformation

Symmetry

In THF, ZnOPPc **(22)** species underwent phototransformation rather than photobleaching, Fig. 4.34. The phototransformation process involved an increase in

the low energy band at 698 nm and a very slow decrease in the main Q band for **22** in THF. As discussed earlier, the observation of the band at 698 nm may reflect loss of symmetry by distortions of the MPc molecule as photolysis progressed.

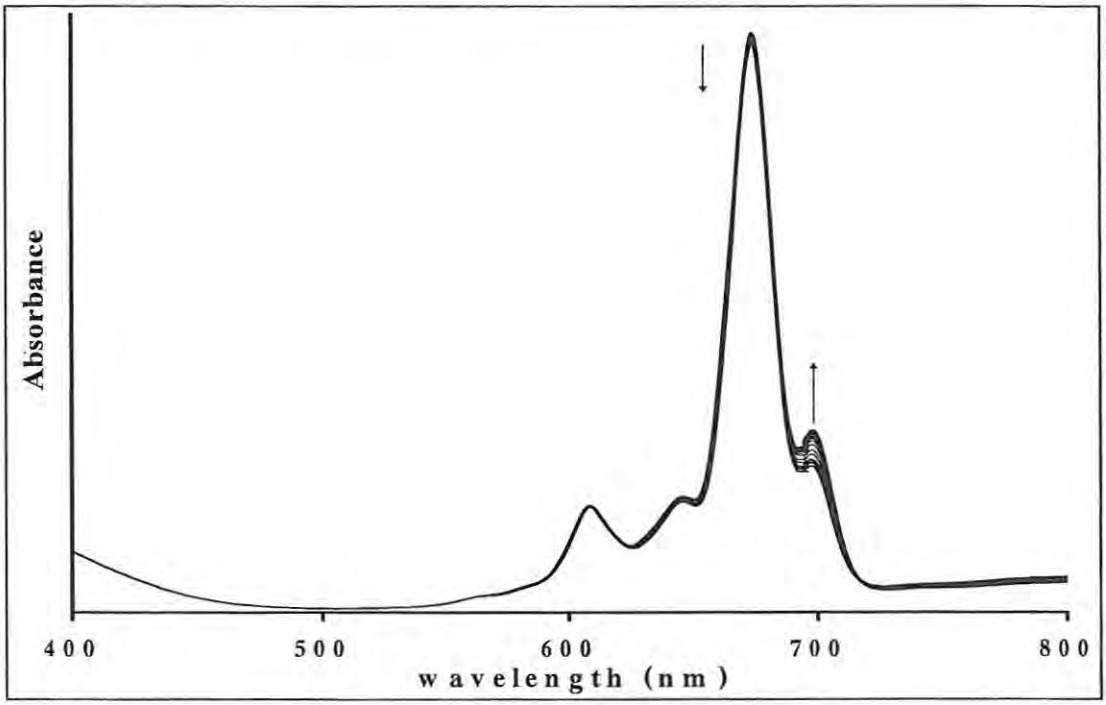

Fig. 4.34: Electronic absorption spectra observed during photo-irradiaton of ZnOPPc (22) in THF.

Disaggregation

Upon irradiation of ZnTNPc (**17**) in DMSO solution, the intensity of the absorbance peak corresponding to the monomeric units (longer wavelength) increases, while that corresponding to the aggregated species decreases (Fig. 4.35). A valid explanation for this observation is that photo-irradiation disturbs the monomer to aggregate equilibrium, the re-establishment of which is in favour of the monomer due to the presence of coordinating DMSO molecules. Thus, disaggregation is obtained upon irradiation. For both of the highly aggregated complexes ZnTAPc (**16**) and ZnTNPc (**17**), photodegradation (i.e. disappearance of the Q band) was not observed; only slow

phototransformation from the dimer to the monomer were seen, hence Φ_{Pd} values could not be determined for these complexes.

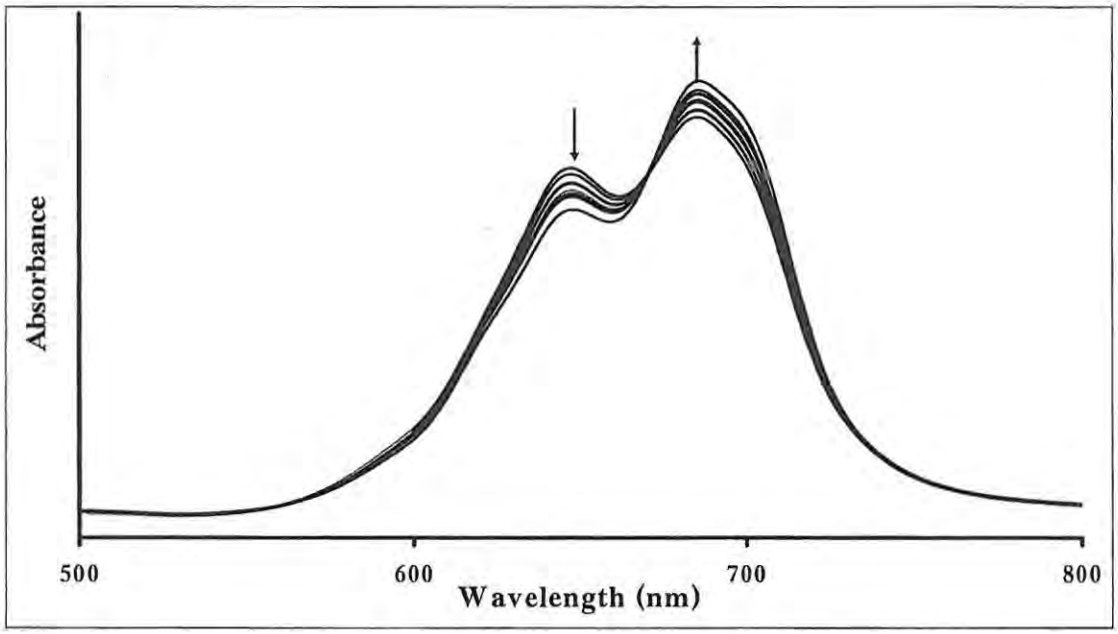

Fig. 4.35: Photo-disaggregation of ZnTNPc (17, 1 x 10^{-5} M) in DMSO.

4.3.2 Singlet oxygen quantum yields

Figs. 4.36 and 4.37 show the decay of DPBF and ADMA respectively, in the presence of singlet oxygen generated from the photo-excited MPc complexes studied. There were no significant changes in the intensities of the Q bands within the timescale of the photo-irradiation. The decrease in DPBF and ADMA absorbances were monitored at 417 nm and 380 nm respectively, in order to avoid any interference from the B bands of the MPc complexes, which ranged between 330 nm and 250 nm.

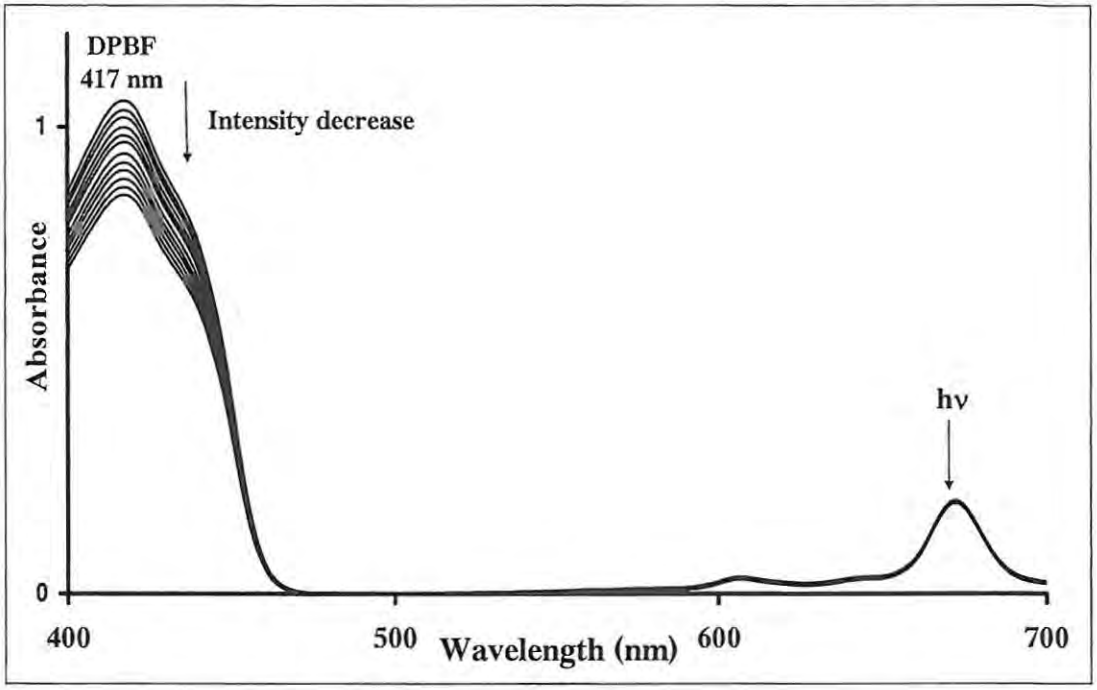

Fig. 4.36: Photodegradation of DPBF in the presence of ZnPc (15). [ZnPc] = 8.4 x 10^{-7} M and the starting concentration of ADMA = 4.8 x 10^{-5} M. Irradiation wavelength = 670 nm ± 20 nm, solvent is DMSO.

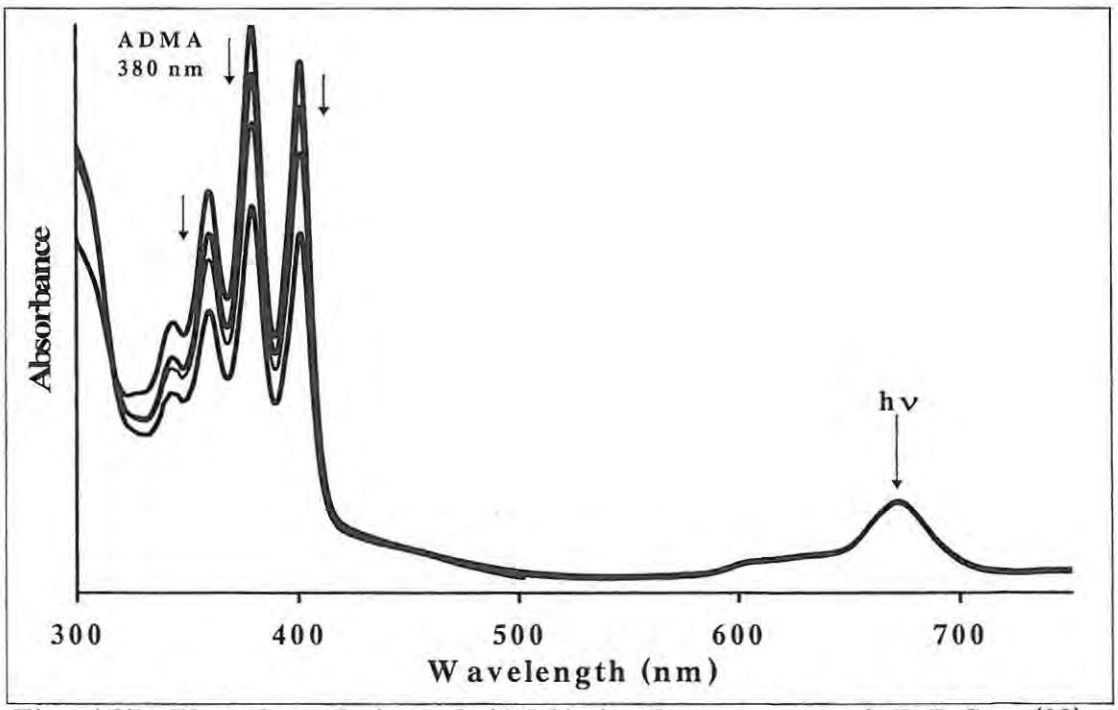

Fig. 4.37: Photodegradation of ADMA in the presence of $ZnPcS_{mix}$ (28). [$ZnPcS_{mix}$] = 1 x 10^{-6} M and the starting concentration of ADMA = 8 x 10^{-5} M. Irradiation wavelength = 670 nm ± 20 nm, solvent is PBS 7.4.

The singlet oxygen quantum yield (Φ_Δ) is a measure of a photosensitizer's ability to generate singlet oxygen. In a particular solvent, the value of Φ_Δ could depend on a number of factors: (i) triplet quantum yield, Φ_T, (ii) triplet lifetime, τ_T, (iii) triplet energy, E_T, (iv) ability of substituents to quench singlet oxygen and (v) the efficiency of energy transfer from the excited triplet state to ground state molecular oxygen. It is difficult to actually identify which of these factors is predominant in explaining the observed trends in Φ_Δ values.

4.3.2.1 Ring-substituted derivatives

The unsubstituted ZnPc (**15**) shows a higher singlet oxygen quantum yield than most of its substituted derivatives, Table 4.13, despite its lower triplet quantum yield than those of some of the complexes studied.

Table 4.13: Singlet oxygen quantum yields and related parameters of ZnPc and its ring-substituted derivatives in DMSO.

	Φ_T	τ_T (μs)	Φ_Δ	S_Δ
ZnPc (15)	0.65 [167]	350	0.67 [227]	1.03
ZnTNPc (17)	0.62	310	0.11	0.18
ZnTSPc (18)	0.86	470	0.46	0.52
ZnTBPPc (19)	0.85	160	0.60	0.71
ZnOMPPc (23)	0.63	370	0.51	0.81
[a]ZnPcS$_{mix}$ (28)	0.86	530	0.72	0.84
ZnNPc (32)	0.37	126	0.19	0.51

References in square brackets;

[a]average for the mixture.

For the substituted ZnPc derivatives, it is possible that intramolecular vibrations associated with the introduction of certain subsituents quench singlet oxygen as soon as it is formed. The effects of aggregation in ZnTAPc (**16**, Φ_Δ = 0.11), ZnTNPc (**17**, Φ_Δ = 0.11), ZnTSPc (**18**, Φ_Δ = 0.46) and ZnOEPc (**21**, Φ_Δ = 0.43) cannot be ruled out. As already stated, aggregates take up electronic energy and convert it into vibrational motion i.e., shortens the triplet lifetimes of photosensitizers. As a result, molecular interaction with singlet oxygen is reduced drastically, thereby bringing about low Φ_Δ values. ZnNPc (**32**) in particular has a low Φ_Δ value due to its low values of Φ_T and τ_T. Also because the triplet energy of **32** is very low compared to that of ZnPc (**15**), this may result in a less efficient energy transfer from this state to ground state molecular oxygen.

The high value of Φ_Δ for $ZnPcS_{mix}$ (**28**) in Table 4.13 could reflect the relative monomeric nature of this molecule in DMSO. Table 4.13 shows that in DMSO the value of Φ_Δ for **28** is higher than that of ZnPc (**15**). This suggests that **28** should be a better sensitizer than **15** in all applications involving singlet oxygen.

Interaction between vibrational levels of the solvent molecules and the electronic or vibrational levels of singlet oxygen results in the deactivation of singlet oxygen in some solvents, especially protic ones such as water and methanol [30]. Table 4.14 shows that Φ_Δ values for ZnPc (**15**) do not vary much with changes in solvent, with values ranging from 0.56 (DMF) to 0.67 (DMSO).

In Table 4.14, a large variation in Φ_Δ values is observed for the octa-substituted ZnPc derivatives – ZnOEPc (**21**) and ZnOPPc (**22**). Considering different solvents, Φ_Δ for **21** ranged from 0.43 (DMSO) to 0.64 (pyridine), and for **22**, the Φ_Δ ranged from 0.45 (toluene) to 0.60 in DMSO. These complexes are known [77] to show aggregation at concentrations as low as 1 x 10^{-5} M in DMSO. The variation in Φ_Δ values with solvent

for each complex may reflect different extents of aggregation in this complex in the various solvents. Pyridine as a solvent (containing a nitrogen donor) does not seem to quench singlet oxygen significantly since Φ_Δ values in pyridine are not lower than in the other solvents listed in Table 4.14.

Table 4.14: Singlet oxygen quantum yields (Φ_Δ) of ZnPc derivatives in five different solvents.

	DMSO	DMF	Pyridine	Benzene	Toluene
ZnPc (15)	0.67 [227]	0.56 [226]	0.61	0.62	0.58
ZnOEPc (21)	0.43	0.60	0.64	0.51	0.54
ZnOPPc (22)	0.60	0.53	0.52	0.47	0.45

S_Δ (Eq. 4.17, [142]), the fraction of triplet state quenched by triplet state oxygen, leading to formation of singlet state oxygen is less than unity for the substituted ZnPc derivatives, Tables 4.13, but unity of ZnPc.

$$S_\Delta = \frac{\Phi_\Delta}{\Phi_T} \qquad \text{(Eq. 4.17)}$$

This suggests that not all triplet quenching by ground state oxygen leads to singlet oxygen formation, but the quenching is efficient since the values are not too far from unity with the exception of ZnTSPc (**18**) and ZnNPc (**32**), Table 4.13. The low value of S_Δ for the latter may be attributed to either the fast degradation of **32** (Table 4.12) or the inefficient transfer of energy to oxygen by this molecule, as discussed above.

4.3.2.2 Axially ligated ZnPc derivatives

(CN)ZnPc (**24**), (pip)ZnPc (**25**) and (py)ZnPc (**26**) are more soluble than the ZnPc species without axial ligands. Therefore, it is expected that the Φ_Δ values would be

higher based on solubility alone. However, there is a general lowering of the Φ_Δ values for **24**, **25** and **26** in DMSO and DMF, compared to ZnPc (**15**), Table 4.15. This can only be explained by the possible quenching of the singlet oxygen by the axial ligands when attached to the ZnPc complex, in a similar manner to singlet oxygen quenching by other electron donors.

Table 4.15: Singlet oxygen quantum yield (Φ_Δ) values for axially ligated ZnPc derivatives in DMSO and DMF.

	DMSO	DMF
ZnPc (15)	0.67 [227]	0.56 [226]
(CN)ZnPc (24)	0.61	0.51
(pip)ZnPc (25)	0.59	0.31
(py)ZnPc (26)	0.63	0.48

References is square brackets.

4.3.2.3 $MPcS_{mix}$ complexes

Singlet oxygen absorbs at ~ 1267 nm, and as earlier argued, the solvent's absorption around this wavelength should have great effect on singlet oxygen lifetime, Fig. 4.25. For example, the short lifetime of singlet oxygen in H_2O (4.2 μs [259]) could be due to the broad absorption of water near 1267 nm. Singlet oxygen lifetimes (τ_Δ), are longer in DMSO (30 μs [260]), pyridine (20 μs [261]) and DMF (19μs [262]), than in H_2O because the former solvents exhibit little absorption in the 1267 nm region. D_2O does not have the O-H vibration, hence singlet oxygen suffers less quenching from D_2O than from H_2O. Thus Φ_Δ values of $ZnPcS_{mix}$ (**28**) are higher for pyridine, DMSO, DMF and D_2O than in aqueous media (H_2O and PBS 7.4), Table 4.16.

Table 4.16: Singlet oxygen quantum yields (average) and related parameters of $MPcS_{mix}$ complexes in aqueous and non-aqueous solutions.

	Solvent	[a]Φ_T	τ_T (μs)	Φ_Δ	S_Δ
AlPcSmix (27)	PBS 7.4	0.44	2.93	0.42	0.95
	DMSO	0.52	800	0.48	0.92
$ZnPcS_{mix}$ (28)	PBS 7.4	0.53	2.95	0.45	0.85
	PBS + TX	0.61	2.37	0.54	0.89
	DMSO	0.86	530	0.72	0.84
	DMF		290	0.58	
	H_2O	0.55	190	0.48	0.87
	D_2O		420	0.53	
	Pyridine		250	0.62	
$SiPcS_{mix}$ 29	PBS 7.4	0.45	2.90	0.49	1.09
	DMSO	0.58	430	0.52	0.90
$GePcS_{mix}$ 30	PBS 7.4	0.67	2.76	0.68	1.01
	DMSO	0.79	760	0.78	0.99
$SnPcS_{mix}$ 31	PBS 7.4	0.59	2.52	0.42	0.71
	PBS + TX	0.68	2.32	0.52	0.77
	DMSO	0.87	120	0.65	0.75

[a]**Due to lack of reference standards, Φ_T values could not be determined in DMF, D_2O and pyridine.**

The relatively low Φ_Δ value for $SnPcS_{mix}$ (**31**) (0.42) compared to $GePcS_{mix}$ (**30**) (0.68) in PBS is not unexpected since, even though the former will have a greater probability of undergoing intersystem crossing to the triplet excited state, due to the heavy atom effect, its aggregated nature results in the dissipation of triplet energy. Within experimental error, Φ_Δ values for the Al (**27**), Zn (**28**), Si (**29**) and Sn (**31**) $MPcS_{mix}$

complexes are not too different in PBS 7.4 (but are different in DMSO). $GePcS_{mix}$ (**30**) on the other hand has a comparatively larger Φ_Δ value, considering the same solvent. This could be due to both the lower degree of aggregation (compared to **31** and **28**) and the increase in excited state triplet yield through the heavy atom effect, compared to $AlPcS_{mix}$ (**27**) and $SiPcS_{mix}$ (**29**). Also, the composition of each $MPcS_{mix}$ complex could influence the values of Φ_Δ. Comparing **27** and **28**, one would expect the latter to have a substantially larger value of Φ_Δ, on grounds of the heavy atom effect. However, the values are not too different in PBS due to the aggregated nature of **28** in aqueous solution. Except for **29**, the Φ_Δ values in PBS shown in Table 4.16 (for **27**, **28** and **31**), are similar to those reported [174] before, within experimental error. The larger value of Φ_Δ for **29** (Φ_Δ = 0.49) compared to Φ_Δ = 0.16 reported before [174], could reflect the known [9] fact that the average number of sulphonate groups per molecule varies with different preparations of $MPcS_{mix}$ complexes, and that the Φ_Δ values vary with number of sulphonate groups [9]. The value of Φ_Δ for **30** is reported for the first time in this work.

4.4 PROTONATION of ZnPc DERIVATIVES

4.4.1 Effects of protonation on the ground state electronic absorption spectra

Spectral changes accompanying the protonation of MPc complexes have been reported [263] and as explained in the introduction, the spectra consists of shifting of the Q band to the red, with successive protonation, Fig. 4.38. The Q band is split for the mono-, di- and tri-protonated derivatives due to loss of symmetry as seen in Fig.

4.38. The tetra-protonated species regains symmetry, hence the Q band spectra is not split. *Cis* di-protonation is of C_{2v} symmetry and is expected to show a single Q band [119]. The fact that we see a split Q in Fig. 4.38 for di-protonated species, suggests that *trans* (of D_{2h} symmetry) protonation occurs.

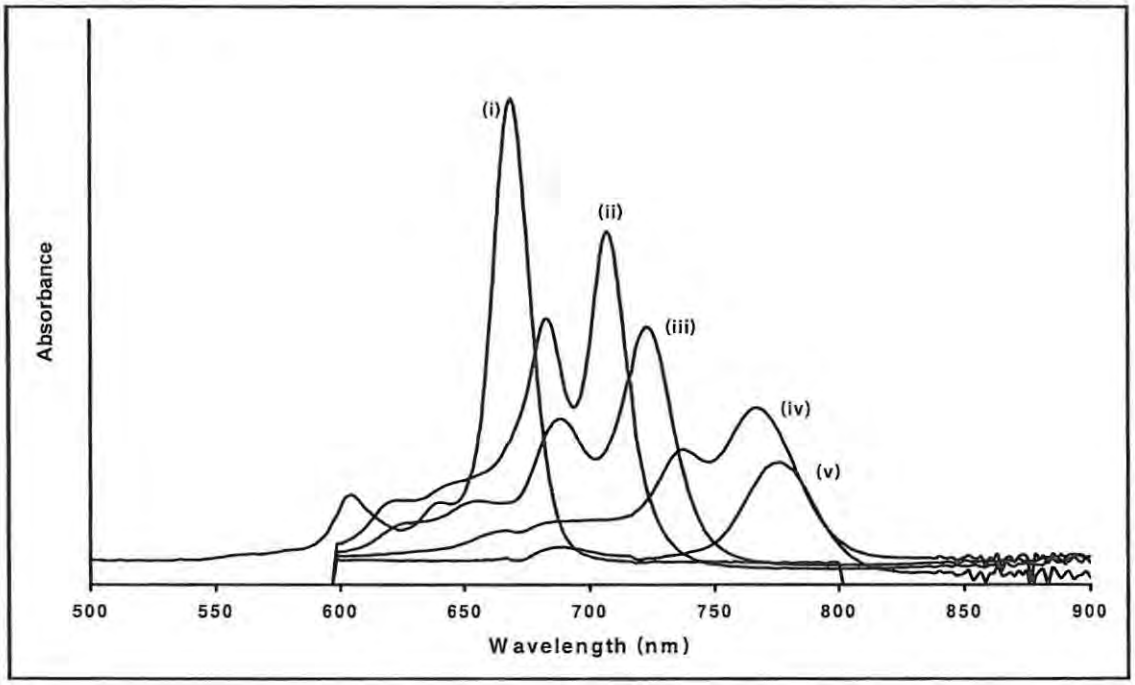

Fig. 4.38: Absorption spectral changes observed on addition of sulphuric acid (98%) to ZnPc (15) in DMF. Spectrum (i) is for ZnPc (15) before addition of acid, (ii) 1st, (iii) 2nd, (iv) 3rd and (v) 4th protonations. Sulphuric acid concentrations = 1.84, 7.36, 11.04, 12.88 M, for (ii), (iii), (iv) and (v), respectively.

The protonations occured with isosbestic points as shown in Fig. 4.39. Tri- and tetra-protonation could only be obtained for non-ring substituted ZnPc derivatives, including axially ligated (CN)ZnPc (**24**), (pip)ZnPc (**25**) and (py)ZnPc (**26**) species using a strong acid such as sulphuric acid, and not when trifluoroacetic acid (TFA) was employed. Ring substituted ZnPc derivatives decomposed on addition of sulphuric acid.

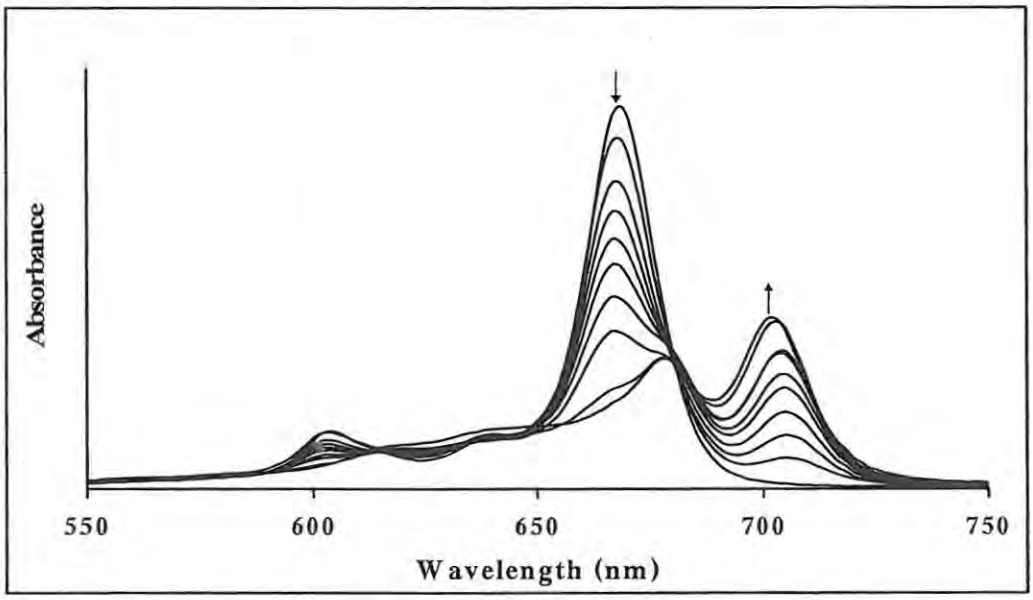

Fig. 4.39: Isosbestic spectral changes observed for the first protonation of ZnPc (15) in DMF, using increasing concentrations of TFA. TFA concentrations increase as follows: 0.5, 1.0, 1.5, 2.0, 2.5, 3.0, 3.5, 5.2 and 7.0 M.

Formation constants for the first protonation (K_f) were determined from the absorption spectra of the solutions using Eq. 4.18 [123]:

$$A = (\varepsilon_{Pc} - \varepsilon_{PcH^+}).\frac{C_T}{1+K_f[H^+]} + (\varepsilon_{PcH^+})C_T \qquad \text{(Eq. 4.18)}$$

Where A is the absorbance of the protonated derivative, ε_{Pc} and ε_{PcH^+}, the extinction coefficients of the unprotonated and protonated ZnPc derivative respectively, C_T, the total concentration of the ZnPc derivative and $[H^+]$, the concentration of TFA. K_f values (Table 4.17), for the ZnPc derivatives in DMF ranged from 0.23 to 0.63. These values are comparable to those reported in the literature for protonation of phthalocyanines [123,264].

Protonation occurred more readily in the presence of electron donating peripheral substituents as expected, Fig. 4.40. Thus ZnTBPPc (**19**) (K_f = 0.63) containing phenoxy ring substituted with $C(CH_3)_3$ groups was easier to protonate than ZnPc (**15**)

(K_f = 0.23). The axially ligated complexes – (CN)ZnPc (**24**), (pip)ZnPc (**25**) and (py)ZnPc (**26**), with K_f ~ 0.3 gave similar plots as the one for **24** in Fig. 4.40.

It has also been reported [119] that annulation or extension of the π conjugated system tends to increase the basicity of the ring, hence enhancing protonation. Thus on this basis alone, ZnOPPc (**22**) is more readily protonated than ZnPc (**15**).

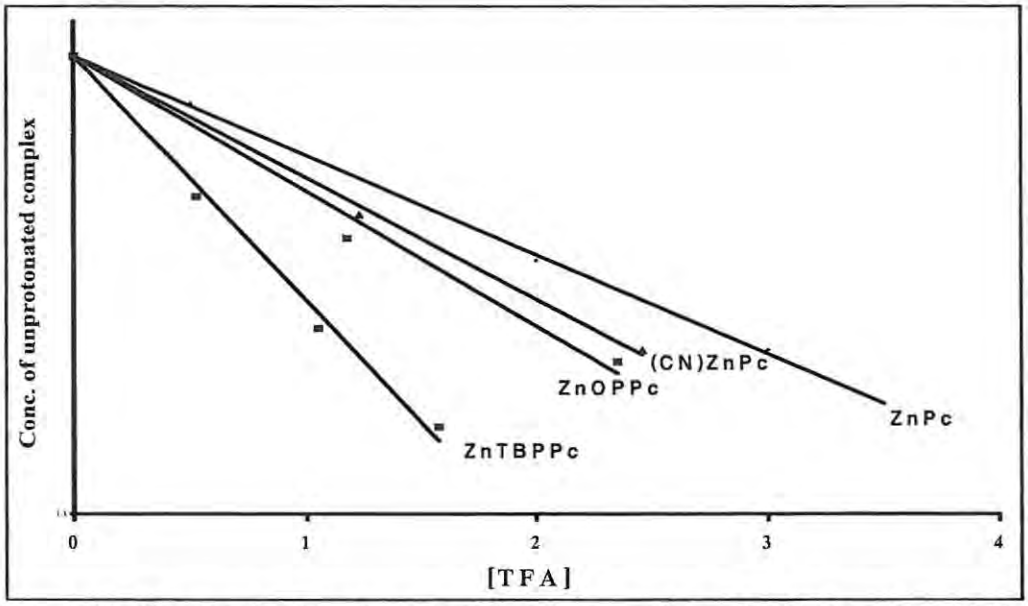

Fig. 4.40: Change in absorbance with concentration of TFA for selected ZnPc complexes in DMF.

Considering only the low energy component of the split Q band, the magnitude of the shift of the Q band to the red compared to the corresponding unprotonated species (second number in brackets) was larger for the ZnPc species containing electron-donating substituents – ZnTBPPc (**19**) and ZnOPPc (**22**) than for ZnPc (**15**), which in turn had a larger shift than ZnTNPc (**17**) containing electron-withdrawing substituents, Table 4.17. Smaller red shifts have been reported for porphyrins substituted with electron-withdrawing compared to electron-donating substituents [265].

Table 4.17: Q band shifts following protonation of ZnPc in DMF, using TFA.

	$\lambda_{Q\ band}$ (nm)			
	Unprotonated (log ε in brackets)	First proton[a]	Second proton[a]	K_f (1st protonation)
ZnPc (15)	666 (5.37)	678,701 (10,33)	685, 713 (17,45)	0.23
ZnTAPc (16)[b]	720 (3.02)	–	–	–
ZnTNPc (17)	647, 683 (4.45, 4.67)	685, 712 (2, 29)[c]	–	–
ZnTBPPc (19)	679 (5.02)	688, 717 (9,38)	710, 744 (31,65)	0.63
ZnOEPc (21)[b]	679 (5.44)	–	–	–
ZnOPPc (22)	677 (5.10)	688, 715 (11,38)	702, 732 (25,55)	0.42
(CN)ZnPc (24)	672 (5.38)	679, 702 (7,30)	684, 714 (12,42)	0.30
(pip)ZnPc (25)	670 (5.40)	678, 702 (8,32)	684, 714 (14,44)	0.31
(py)ZnPc (26)	669 (5.44)	680, 701 (11,32)	685, 713 (16,44)	0.34

[a]Numbers in brackets are the wavelength numbers by which the Q band of the protonated species has red-shifted compared to the neutral species; the first number is the shift of the first peak and second number for the second peak. [b]Aggregated in solution and did not protonate. [c]Wavelength shifts based on the Q band associated with the monomeric peak at 683 nm.

Q band positions of protonated species vary as the protonating agent is changed as follows for first protonation of ZnPc (**15**): TFA (678,701) < H_2SO_4 (684,707) ~ Lewis acid ($AlCl_3$) (685,708), suggesting that the Q band red-shifting is proportional to the strength of the acid, since this trend follows the order of the strength of the acid. $AlCl_3$ undergoes hydrolysis in solution forming a complex acid H^+-$[AlCl_4]^-$ [119]. It has been reported [266] that complexes are formed between the protonated species and the undissociated acid, and this could result in the observed shift in the spectra with different acids.

ZnTNPc (**17**) gave spectral changes shown in Fig. 4.41 on addition of TFA. Before addition of TFA, the complex showed aggregation as evidenced by the presence of a

broad high energy band at 647 nm (dimer or aggregate) in addition to the sharper band at 685 nm (monomer).

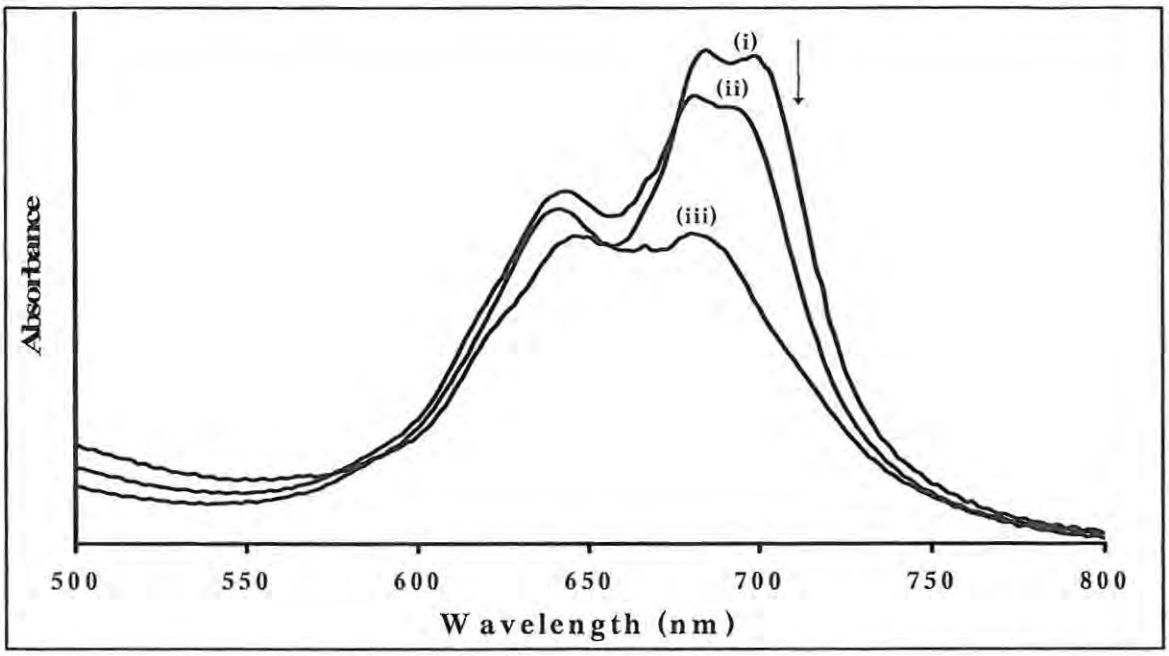

Fig. 4.41: Spectral changes observed on addition of TFA to ZnTNPc (17) (3.2 x 10^{-5} M) in DMF. (i) No TFA (ii) [TFA] = 1.18 M, (iii) [TFA] = 2.35 M.

The spectral changes observed on addition of acid to solutions of **17** consisted of a decrease in the monomer peak and an initial increase in the peak due to the aggregated (dimeric) species. The latter then began to decrease in intensity. These changes suggest that addition of protonating agents results in the shift of the monomer-dimer equilibrium towards the dimeric species, followed finally by protonation as shown in Fig. 4.42.

Only the first protonation could be achieved for this complex (**17**), and the protonation required a very large concentration of TFA. Spectral changes observed for ZnTAPc (**16**) and ZnOEPc (**21**) on addition of protonating agents were similar to those shown in Fig. 4.41. However, protonation was not achieved for **16** and **21** even at very high TFA concentrations. Addition of large concentrations of TFA resulted in

the degradation of both of these complexes (**16** and **21**). The aggregated natures of **16** [265], ZnTNPc (**17**) [265] and **21** [77] complexes have been reported before.

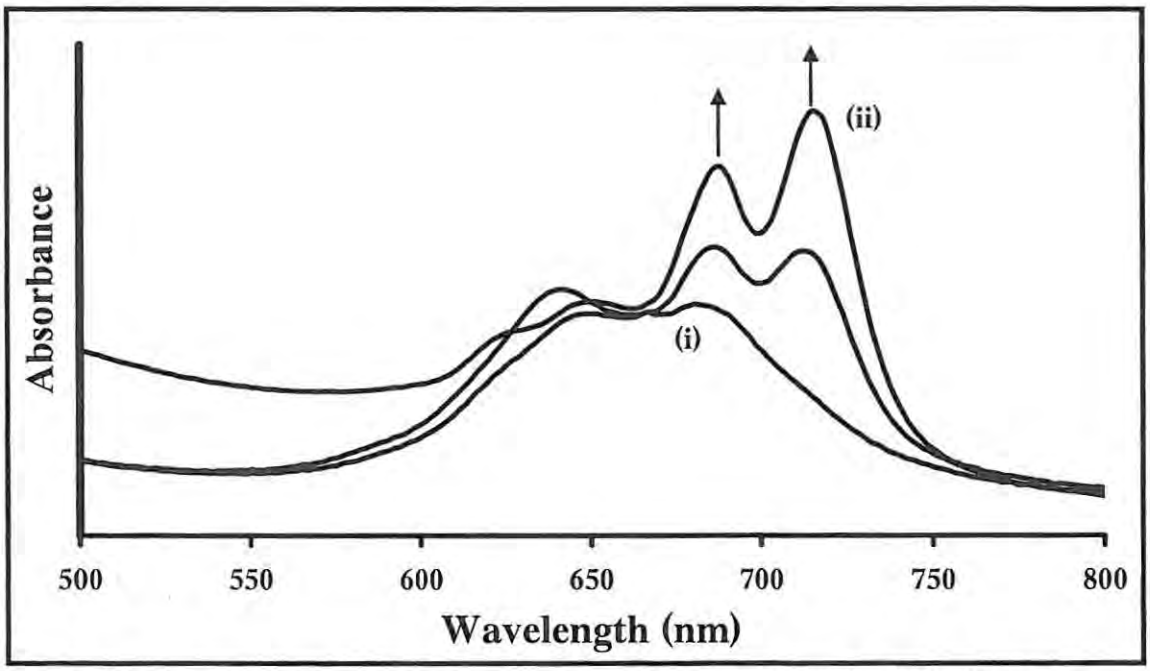

Fig. 4.42: Evolution of spectra due to protonation of ZnTNPc (17). (i) the last spectrum (iii) in Fig. 4.37 and (ii) final spectrum obtained following addition of acid (1.2×10^{1} mol dm^{-3} of TFA).

Aggregation in phthalocyanines occurs via intermolecular π-π interactions [267,268]. For this type of aggregates, the monomers are not chemically bonded but exist as loosely associated species. The presence of axial ligands prevents aggregation. Thus, the observation of increased aggregation on addition of acids to these complexes may suggest possible weak coordination of the solvent to the axial position, which may be lost on addition of acid, thereby enhancing aggregation. The observation also suggests that the aggregated species is not readily protonated as judged by the lack of red shit for **16** and **21**, and by the large concentration of TFA which was required to complete the first protonation of **17**.

Fig. 4.43 shows that protonation of ZnPc containing axial ligands – (CN)ZnPc (**24**), (pip)ZnPc (**25**) and (py)PZnPc (**26**) proceeds by the loss of the axial ligands as judged by the small blue shift of the Q band on addition of the acid. Also MPc complexes containing cyanide axial ligand are identified with a split B band. In Fig. 4.43, the B band collapses into one on protonation, hence confirming the loss of the axial ligand. However, as the observations stated below will demonstrate, axial ligands still have an effect on the protonation, suggesting that axial ligands are probably lost simultaneously with the protonation process. Immediately after addition of acid, peaks due to the protonated species were observed at the same time as the blue shift in the Q band. The axial ligands employed in this work are electron-donating and all show easier protonation than ZnPc (**15**) in DMF (which is presumably (DMF)ZnPc), (See Fig. 4.40 for the (CN)ZnPc (**24**) derivative, and K_f values in Table 4.17). Thus this work also suggests that the basicity of the Pc ring is enhanced by the axially coordinated ligands.

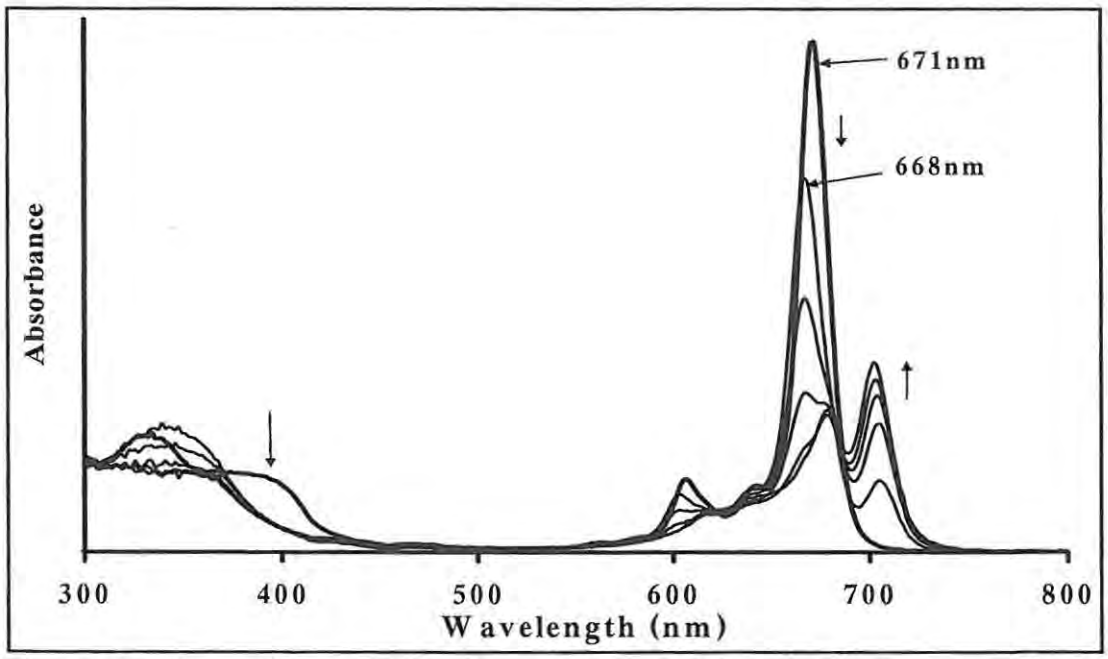

Fig. 4.43: Absorption spectral changes observed for the first protonation of (CN)ZnPc (24) (4.26×10^{-6} M) in DMF, using TFA. [TFA] = 1.18 M to 6.0 M.

4.4.2 Solvent effects on protonation

Q-band positions of protonated derivatives of ZnPc species are almost the same, Table 4.18, irrespective of solvent type (except in the case of chloroform). The concentration of TFA needed to effect protonation increased linearly with solvent basicity as shown in Fig. 4.44, hence confirming that the less basic solvents encourage protonation more than the more basic solvents. Chloroform being an acidic solvent, may add to the acid strength of TFA, resulting in a larger red shift. This is in agreement with the argument presented above that extent of red-shifting is proportional to acid strength.

Table 4.18: Effect of solvent on the Q band maxima of protonated $(ZnPc\text{-}H)^+$.

Solvent	Dipole moment, μ	Solvent Basicity, SB[a]	Q-band[b] λ_{max} (nm)	λ_{max}/nm 1st proton[c]	λ_{max}/nm 2nd proton[c]	[TFA]/M 1st proton[d]	K_f[e]
Chloroform	1.90	0.071	670	683, 708	690, 720	0.75	2.7
Benzonitrile	3.50	0.281	673	677, 703	683, 713	1.80	0.95
1,4-Dioxane	0.45	0.444	665	678, 703	683, 712	3.41	0.45
THF	1.69	0.591	666	677, 703	683, 712	5.11	0.32
DMF	3.79	0.613	668	678, 701	685, 713	6.71	0.23
DMSO	3.96	0.647	670	678, 703	685, 713	6.11	0.27
n-Butylamine	1.30	0.944	668	678, 703	684, 711	7.13	0.21
Triethylamine	0.72	0.885	664	-	-	-	-
Pyridine	2.21	0.581	673	-	-	-	-

[a]Values from reference 258; [b]Q band maxima of the unprotonated species. [c] Q band maxima of protonated species. [d] Concentration of TFA required to complete first protonation. [e]K_f = stability constants for monoprotonated species.

There was no protonation when pyridine and triethylamine were used as solvents. Pyridine formed a white precipitate of pyridinium trifluoroacetate with TFA. Thus, TFA reacted with the solvent instead of the ring. Amines are basic; hence the formation of a quaternary salt on adding TFA to an amine solution is not unexpected. Protonation in the highly basic *n*-butylamine was accompanied by a great loss of heat and effervescence.

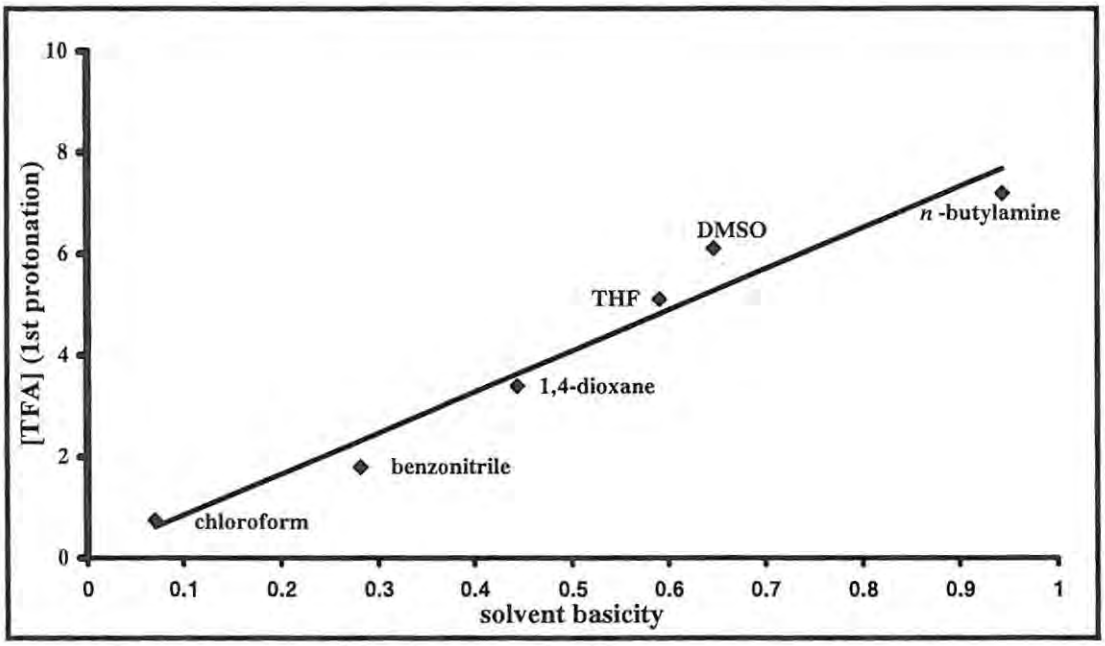

Fig. 4.44: Variation of solvent basicity with the concentration of TFA required completing the first protonation of ZnPc (15).

Two factors (basicity and coordinating strength of solvent) may be competing in determining the relative ease of protonation of the Pc ring. While solvent basicity impedes ring protonation, axial coordination of the solvent may aid it by increasing the basicity of the ring. Table 4.18 shows that DMSO, with a relatively high dipole moment of 3.96 hence more strongly coordinated to the central zinc ion, results in easier protonation of the ring (slightly higher K_f value) than for DMF with a lower dipole moment.

In spite of the higher basicity of *n*-butylamine compared to triethylamine, protonation was observed in the former instead of precipitation observed for the latter. This could be attributed to the higher polarity (coordinating strength) of *n*-butylamine, which is responsible for its coordination to the central ZnPc metal. As observed above for the axially ligated ZnPc derivatives (**24 – 26**), the axial *n*-butylamine will be lost on protonation. Broadening of the Q band of the neutral species was observed on addition of TFA to solutions of ZnPc (**15**) in *n*-butylamine, suggesting that the loss axially coordinated *n*-butylamine ligand is accompanied by aggregation.

Stepwise deprotonation of the protonated ZnPc derivaties was achieved on addition of hydrazine to the solution of the protonated species, as evidenced by reversal of spectral changes.

4.4.3 Effects of protonation on photochemical and fluorescence properties

4.4.3.1 Singlet oxygen quantum yields

Table 4.19 shows singlet oxygen quantum yield (Φ_Δ) values for the unprotonated and mono-protonated ZnPc complexes under discussion. Φ_Δ values for the unprotonated ZnPc derivatives are all higher than for the corresponding protonated derivatives as has been reported before for tetra-*tert*-butylzinc phthalocyanine [123]. The lowering of Φ_Δ values following protonation is attributed to the lowering of the triplet energy to the level where transfer of energy to ground state oxygen is no longer favourable, as suggested before [123].

For the ZnTAPc (**16**) and ZnOEPc (**21**), Φ_Δ for the protonated species were not obtained since these species did not protonate.

4.4.3.2 Photodegradation quantum yields

The quantum yields of photobleaching (Φ_{Pd}) were found to decrease for ring substituted ZnPc derivatives and for unsubstituted ZnPc containing no axial ligands following protonation, Table 4.19. Phthalocyanine molecules in general photodegrade oxidatively via attack by singlet oxygen generated by them.

Table 4.19: Photochemical data for neutral and protonated ZnPc derivatives. Results refer to first protonation only. Solvent: DMF.

Complex	Φ_{Δ}	$10^5/\Phi_{Pd}$	Φ_F
ZnPc (15)	0.56 [226]	2.23	0.18
[15-H]$^+$	0.39	0.23	0.12
ZnTNPc (17)	0.24	-	0.12
[17-H]$^+$	0.11	-	-
ZnTBPPc (19)	0.42	9.41	0.13
[19-H]$^+$	0.12	2.33	0.076
ZnOPPc (22)	0.53	12.1	0.17
[22-H]$^+$	0.26	2.62	0.042
(CN)ZnPc (24)	0.51	0.12	0.14
[24-H]$^+$	0.37	1.38	0.11
(pip)ZnPc (25)	0.31	0.14	0.16
[25-H]$^+$	0.25	1.63	0.18
(py)ZnPc (26)	0.48	1.32	0.22
[26-H]$^+$	0.41	2.09	0.19

As suggested stated, protonation impedes singlet oxygen generation, hence it is expected that Φ_{Pd} values of protonated species would be generally lower than for

corresponding unprotonated derivatives, and this is the case in Table 4.19 for non-axially ligated ZnPc derivatives. However for the axially ligated ZnPc derivatives, protonation resulted in an increase in Φ_{Pd} value. Considering unprotonated derivatives, axial ligands impart some extra photostability on the Pc ring compared to ring substituted or unsubstituted derivatives containing no axial ligands, as judged by the low Φ_{Pd} for the axially ligated derivatives compared to the rest, Table 4.19.

As earlier suggested however, protonation leads to the loss of these axial ligands, which amounts to the removal of this extra photostability. As a result, the Φ_{Pd} values increase when the axially ligated ZnPc derivatives are protonated. For the protonated form of **17** ($[ZnTNPc-H]^+$), no spectral changes were observed on photo-irradiation, showing that this complex is stable to photodegradation.

4.4.3.3 Fluorescence quantum yield

As observed before [123], the fluorescence quantum yield (Φ_F) is lowered on protonation. This was generally observed in Table 4.19. The fluorescence excitation spectrum of the monoprotonated complex (Fig. 4.45) was similar to the absorption spectrum, consistent with the fact that the absorbing species is also the fluorescing species under the conditions used in this work.

The difference in shape between the fluorescence excitation and emission spectra (Fig. 4.45) suggests a change in symmetry after excitation and prior to emission. For ZnTnPc (**17**), Φ_F could not be obtained since very dilute solutions are required for fluorescence studies, and dilution of protonated **17** resulted in its deprotonation back to the neutral species, hence confirming the ease of reduction of this species.

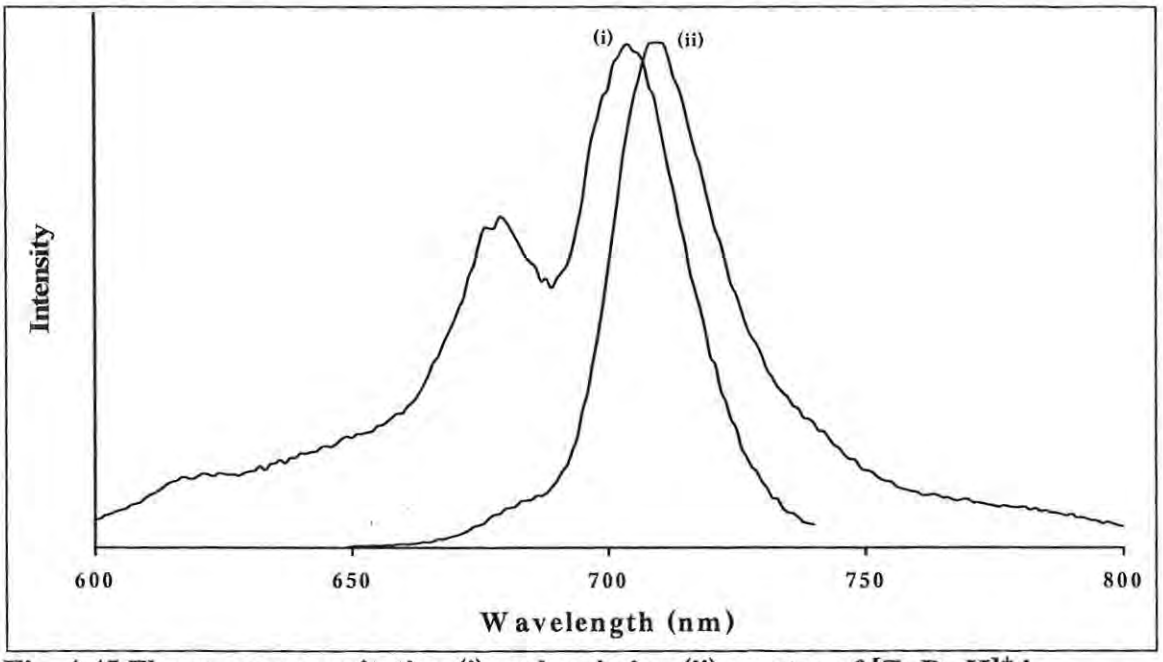

Fig. 4.45 Fluorescence excitation (i) and emission (ii) spectra of $[ZnPc\text{-}H]^+$ in DMF. Excitation wavelength (λ_{Exc}) = 630 nm.

4.5 CYCLODEXTRIN INCLUSION COMPLEXES OF ZnPc DERIVATIVES

4.5.1 Spectroscopic studies on inclusion complexes

These studies were done for ZnPc (**15**), ZnTAPc (**16**), ZnTNPc (**17**) and ZnTBPPc (**19**), and ZnNPc (**32**), as representative complexes.

Inclusion complexes between cyclodextrins (CDs) and the ZnPc derivatives resulted in a significant increase in the intensity of the complexes' Q band absorption peaks, but no noticeable peak shifts were obtained, (Fig. 4.46) for **15**, **19** and **32**.

For the highly aggregated complexes e.g. ZnTNPc (**17**), there was an increase in the intensity of both peaks. There was no disappearance of the high energy band associated with the dimeric species for compound **17**, showing that addition of CD does not

disaggregate the dimeric species of this molecule. Furthermore for this compound, a reduction in the background intensity was observed as well as a slight narrowing of the absorption bands. The increase in intensity for ZnPc (**15**), ZnTBPPc (**19**) and ZnNPc (**32**), and the narrowing of the bands for ZnTAPc (**16**) and ZnTNPc (**17**) suggest the formation of an inclusion complex between CD and the studied compounds.

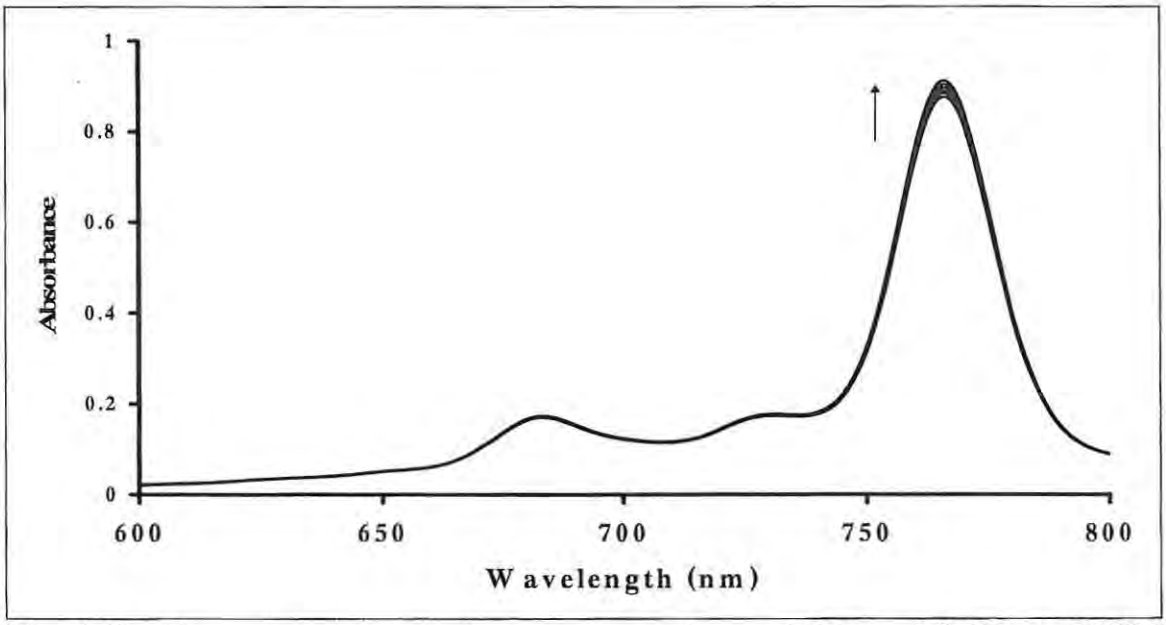

Fig. 4.46: Absorption spectral changes observed on addition of β-CD to DMSO solution of ZnPc (15). Ratio 15:CD starting from 1:0 to 1:4.

Changes such as enhancement or decrease in the intensity of the absorption and fluorescence bands have been associated with the formation of an inclusion complex between CDs and porphyrins [182,184]. Fig. 4.47 shows that there was improvement in the Beer's law behaviour for the aggregated ZnTNPc (**17**) following formation of the inclusion complex, even though this was not evident from the spectra, i.e. there was no observable decrease in the dimeric peak for **17** upon addition of CD.

Job's plots for the formation of the inclusion complexes between CDs and ZnPc derivatives were obtained. For ZnPc (**15**), ZnTAPc (**16**), ZnTBPPc (**19**) and ZnNPc (**32**), which showed only one peak in the Q band region, the changes in the intensity of this peak were monitored following addition of CD, and allowing an equilibration time of 24

hr. For compound **17**, the low energy band (due to monomeric species) in the Q band region was followed.

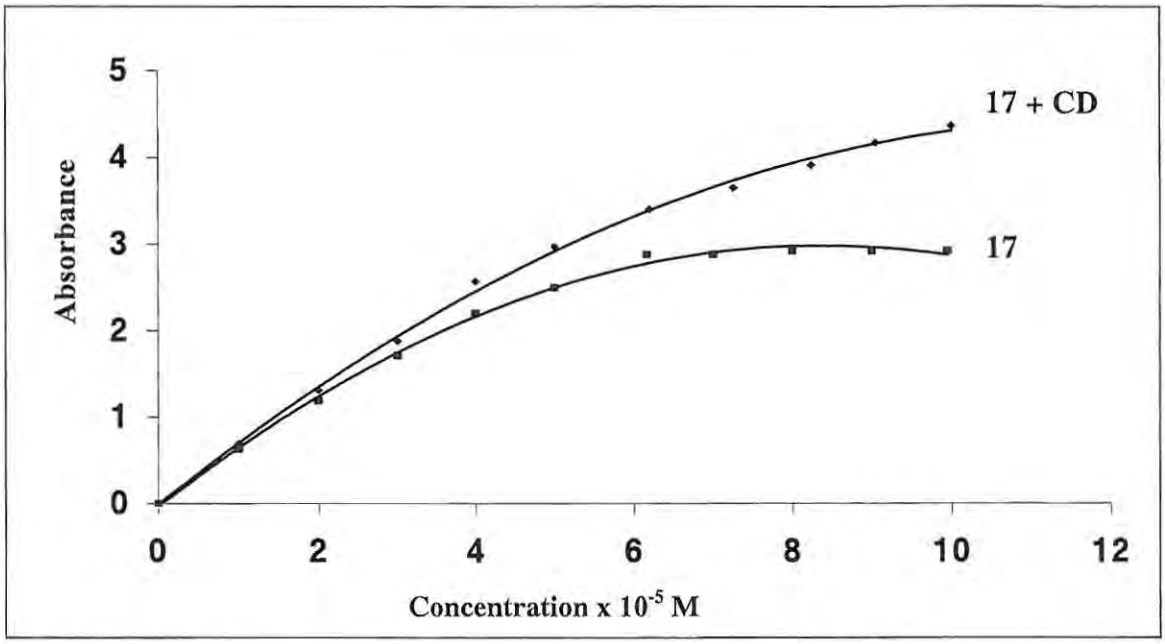

Fig. 4.47: Deviation from Beer's law for ZnTNPc (17) and its inclusion complex with β-cyclodextrin in DMSO.

Fig. 4.48 shows a Job's plot for the monomeric ZnTBPPc (**19**); a maximum was observed at an inclusion ratio of about 1.5:1 (or ~ 2:1; CD:**19**).

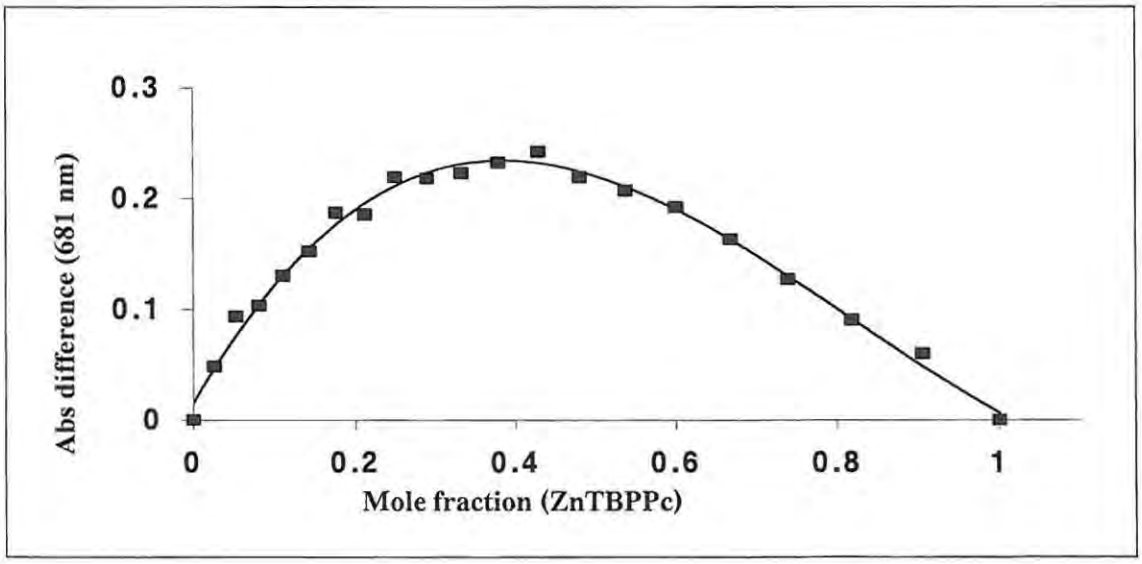

Fig. 4.48: Job's plot for the inclusion of compound ZnTBPPc (19) into hydroxypropyl-γ-cyclodextrin using DMSO as solvent.

For ZnTNPc (**17**), the Job's plot showed some interesting behaviour as a maximum was observed at 4:1 (CD:**17**) and at a ratio of 1.5: 1 (~ 2:1; CD:**17**) (Fig. 4.49). This behaviour is most likely due to the coordination of CD to the aggregated as well as non-aggregated components of the molecule, with the 4:1 (CD:**17**) being coordination of 4 CDs to the aggregates and 2:1 (CD:**17**) to the monomeric species. The binding of CDs to porphyrins is known to be a two-step process involving first the formation of a 1:1 complex, which evolves into a 2:1 complex [185]. The cyclodextrin molecule coordinates in a stepwise manner to the porphyrin ring substituents such as the phenyl groups in tetraphenylporphyrin molecules. A 2:1 (CD:MPc) complex was also formed for the unsubstituted ZnPc (**15**). The coordination of the CD to **15** and its derivatives is expected to involve the outer benzene ring and the substituents attached to it. Coordination of CD to the unsubstituted compound **15** confirms that it is not only the phthalocyanine ring substituents which coordinate to the CD, but also the fused benzene part of the phthalocyanine.

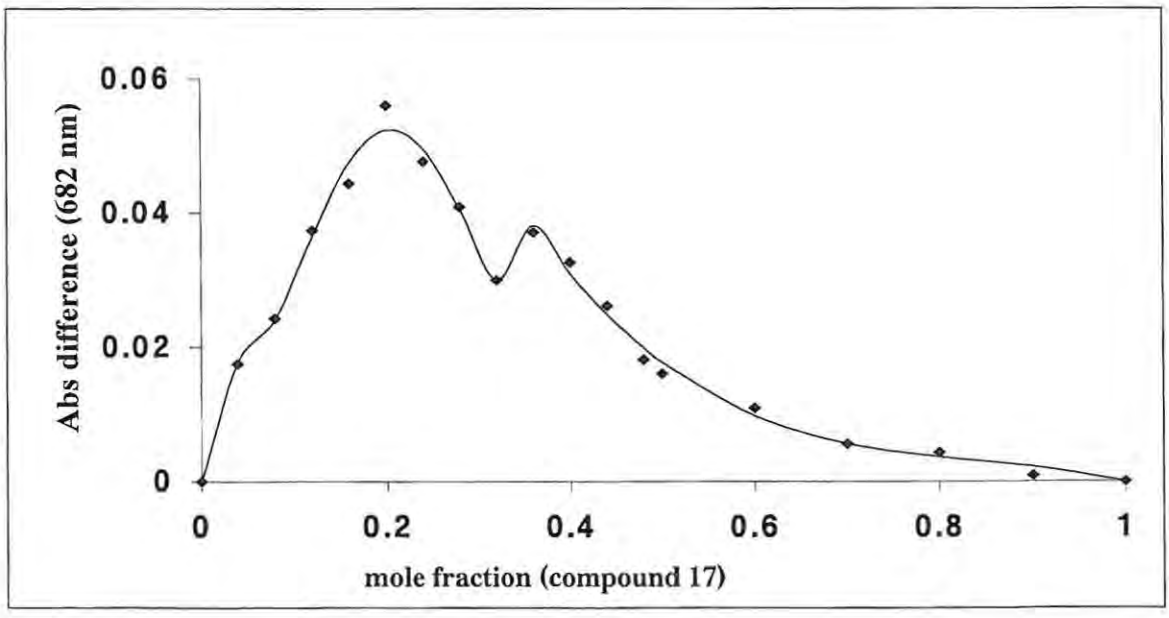

Fig. 4.49: Job's plot for the inclusion of ZnTNPc (17) into β-cylcodextrin in DMSO.

The formation of the solid complex between CD and ZnPc derivatives was confirmed by X-ray powder diffraction (XRD) (Fig. 4.50) peaks of the inclusion compound of ZnPc (15) when compared to peaks due to CD or the phthalocyanine compounds alone. The XRD pattern change upon inclusion suggests formation of inclusion complexes.

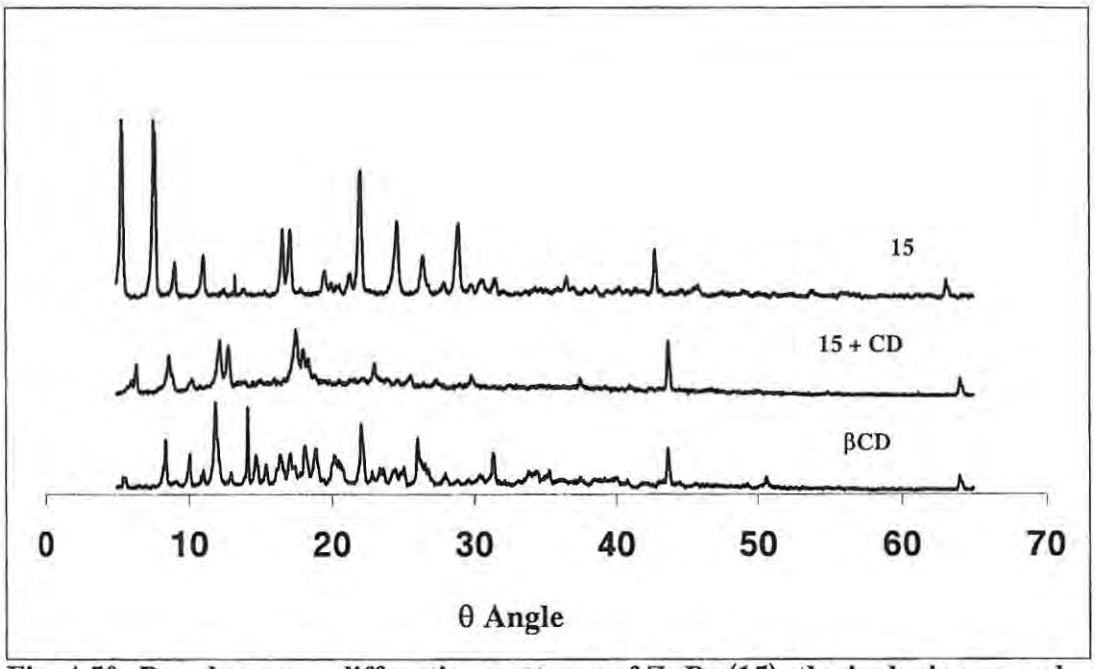

Fig. 4.50: Powder x-ray diffraction patterns of ZnPc (15), the inclusion complex and β-cyclodextrin.

4.5.2 Fluorescence and photochemical studies on MPc-cyclodextrin inclusion complexes

The increase in fluorescence intensity upon addition of CD has been reported for porphyrin complexes [182]; but a decrease in fluorescence intensity has also been reported for some porphyrins [184]. In both cases, these changes were attributed to the formation of inclusion complexes. The fluorescence quantum yields (Φ_F) for the MPc derivatives were however not significantly affected by addition of CD for all the complexes (Table 4.20), except for ZnNPc (**32**) where Φ_F decreased on inclusion.

Singlet oxygen quantum yields (Φ_Δ) for the MPc derivatives and the naphthalocyanine, compound **32**, are also given in Table 4.20.

On addition of CDs to the ZnPc derivatives, there was a general increase in the Φ_Δ values for ZnPc (**15**), ZnTNPc (**17**), ZnTBPPc (**19**) and ZnNPc (**32**), but not for ZnTAPc ZnTAPc (**16**), considering experimental error. The increase in Φ_Δ values for these complexes may suggest that CD removes aggregation which may be present to some extent even in the complexes which appear to be monomeric from their spectra (e.g. ZnTBPPc, **19**), resulting in an increase in absorption intensity on addition of CD.

Table 4.20: Singlet oxygen (Φ_Δ), photodegradation (Φ_{Pd}) and fluorescence (Φ_F) quantum yields for ZnPc derivatives and their inclusion complexes in DMSO.

Complex	$\lambda_{Q\ band}$, nm	λ_F, nm	Φ_F	Φ_Δ	[a]Φ_{Pd} (x 10^5)
ZnPc (15)	672	678	0.20	0.67	2.61
15-βCD	672	681	0.18	0.74	0.68
ZnTAPc (16)	727	732	<0.01	0.11	-
16-βCD	727	732	<0.01	0.11	-
ZnTNPc (17)	682	691	0.022	0.11	-
17-βCD	682	691	0.022	0.21	-
ZnTBPPc (19)	681	692	0.14	0.60	3.33
19-HP-γCD	681	692	0.14	0.75	2.75
ZnNPc (32)	766	773	0.065	0.19	16.35
32-βCD	766	772	0.059	0.27	20.40

[a]Φ_{Pd} values could not be obtained for 16 and 17 (and their inclusion complexes) because these complexes did not photobleach; rather, they underwent phototransformation.

Photobleaching studies were undertaken in order to determine the effects of CD on the stability of the ZnPc derivatives in the presence of light. The presence of CD decreased

the Φ_{Pd} values (for **15** and **19**) compared to the values in the absence of CDs, the notable exception being ZnNPc (**32**). The decrease in Φ_{Pd} may be due to the partial protection of the phthalocyanine ring (by CD) from attack by singlet oxygen.

4.6 MPc BINDING TO BOVINE SERUM ALBUMIN (BSA)

4.6.1 Interaction of $MPcS_{mix}$ with BSA

The binding constants (K_b) obtained for $MPcS_{mix}$-BSA binding, together with the binding stoichiometry of the complex formed were obtained as described by Eq. 2.104, given below as Eq. 4.19 (Fig. 4.51); and the results are presented in Table 4.21. The values are typical for MPc-albumin interactions in aqueous solutions [190].

$$\log\left[\frac{(F_0 - F)}{(F - F_\infty)}\right] = \log K_b + n\log[MPcS_{mix}] \qquad \text{(Eq. 4.19)}$$

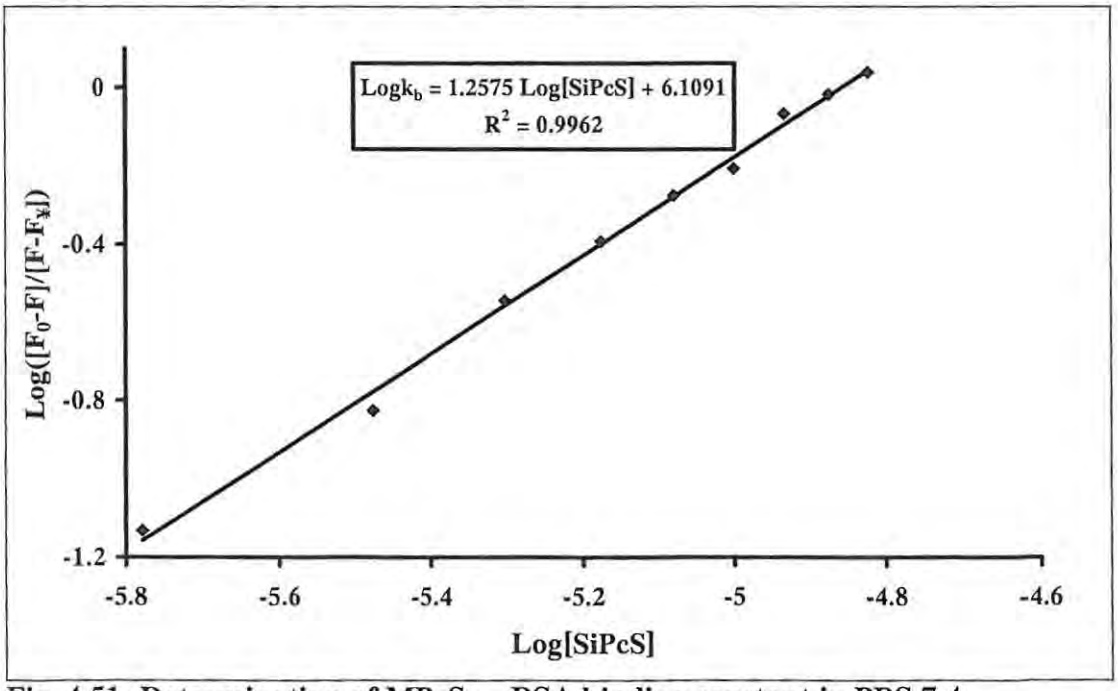

Fig. 4.51: Determination of $MPcS_{mix}$-BSA binding constant in PBS 7.4.

The highest value of K_b was obtained for $AlPcS_{mix}$ (**27**) which is particularly monomeric while the aggregated $ZnPcS_{mix}$ (**28**) and $SnPcS_{mix}$ (**31**) complexes gave the lowest values. This shows that aggregation plays an important role in the binding. The involvement of a dimer in BSA binding is indirect, via dissociation into monomers. Consequently, K_b values for aggregated species are expected to depend largely on, and be limited by the inherent dimer dissociation constants.

Table 4.21: Binding and quenching data for $MPcS_{mix}$-BSA interaction in PBS 7.4.

Complex	K_b $x10^{-6}$ (M^{-1})	n	K_S^{BSA} $x10^{-4}$ (M^{-1})	K_S^{MPcS} $x10^{-3}$ (M^{-1})	k_Q $x10^{-12}$ ($M^{-1}s^{-1}$)	$^a\tau_F$ ns
$AlPcS_{mix}$ (27)	17.21	1.396	11.45	58.43	11.40	5.13 (5.34)
$ZnPcS_{mix}$ (28)	0.10	1.008	7.36	-	7.36	[b]2.9 (2.78)
$SiPcS_{mix}$ (29)	1.29	1.258	6.90	34.36	6.90	4.98 (4.55)
$GePcS_{mix}$ (30)	0.81	1.077	4.54	18.48	4.54	4.07 (4.32)
$SnPcS_{mix}$ (31)	0.08	1.004	1.98	-	1.98	(2.03)

[a]Values in brackets obtained from hydroquinone quenching data, [b]value from reference 158. K_S and hence τ_F coukd not be determined for the aggregated species (28 and 31), as the fluorescence quenching of theses species by BSA was overridden by the effects of monomerization.

The variation of K_b with the nature of the complex in Table 4.21 could also be a reflection of the relative affinity of BSA for the respective $MPcS_{mix}$ species. Again, the observed variation in the values of K_b could suggest the predominance of species containing a larger number of negatively charged sulphonate groups in some of the $MPcS_{mix}$ mixtures, since it is known that serum albumins have high affinities for negatively charged molecules [269]. As HPLC studies have shown (compare Fig. 4.9 and Fig. 4.10), $AlPcS_{mix}$ (**27**), $SiPcS_{mix}$ (**29**) and $GePcS_{mix}$ (**30**) have derivatives

containing more of the highly sulphonated derivatives in the mixture (more negatively charged groups), hence higher affinities for BSA than $ZnPcS_{mix}$ (28) and $SnPcS_{mix}$ (31), which contain more of the less sulphonated derivatives in the mixture. The number of binding sites on BSA (n) obtained from the experiments is ~ 1 (Table 4.21), which suggests a 1:1 stoichiometry for all the $MPcS_{mix}$:BSA adducts.

4.6.2 $MPcS_{mix}$-BSA fluorescence quenching analysis

BSA and each of the $MPcS_{mix}$ species display mutual quenching on one another. These reciprocative fluorescence quenching could have arisen from either dynamic (no complexation) or static (due to non-fluorescent ground state complex) quenching.

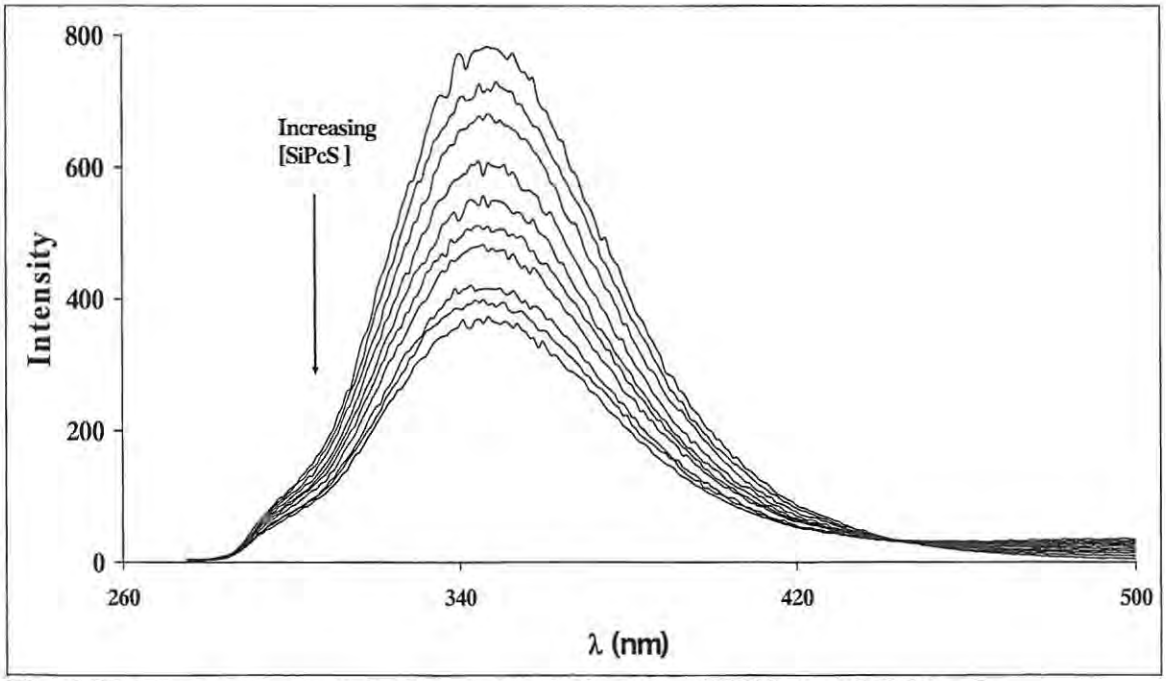

Fig. 4.52: Fluorescence emission spectral changes of BSA on addition of increasing concentrations of $SiPcS_{mix}$ (29).

The Stern-Volmer analysis (Eq. 4.9) of fluorescence data was used to discern the actual quenching mechanism. Figs. 4.52 and 4.53 show the quenching of BSA by $SiPcS_{mix}$ and of $GePcS_{mix}$ by BSA in PBS, respectively. The slopes of the plots shown

in Figs. 4.54 and 4.55 gave K_{SV}^{BSA} and $K_{SV}^{MPcS_{mix}}$, respectively. Fig. 4.53 shows the quenching behaviour of $MPcS_{mix}$ by BSA, typical of the un-aggregated complexes (Al, Si and Ge complexes). For the Zn and Sn complexes, there were increases in fluorescence intensities (rather than quenching) upon addition of BSA, hence the $K_{SV}^{MPcS_{mix}}$ values could not be determined (see Section 4.6.3); whereas all five $MPcS_{mix}$ complexes (**27 – 31**) quenched BSA, with K_{SV}^{BSA} values shown in Table 4.21 as K_S^{BSA} (see below).

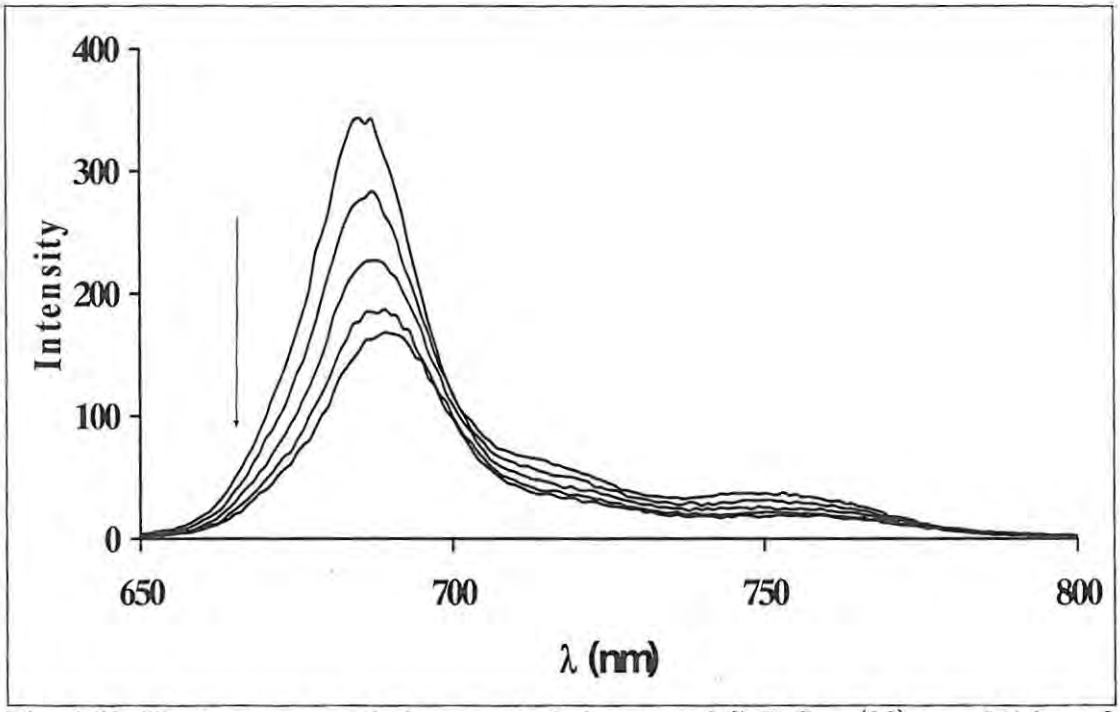

Fig. 4.53: Fluorescence emission spectral changes of $GePcS_{mix}$ (30) on addition of increasing concentrations of BSA.

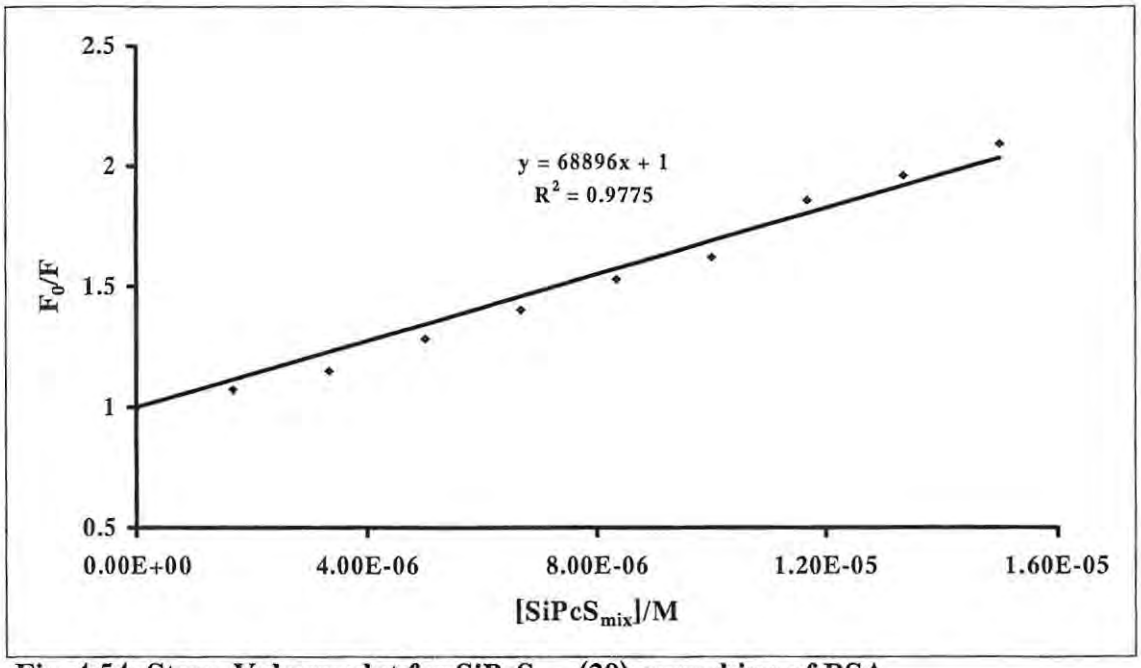

Fig. 4.54: Stern-Volmer plot for SiPcS$_{mix}$ (29) quenching of BSA.

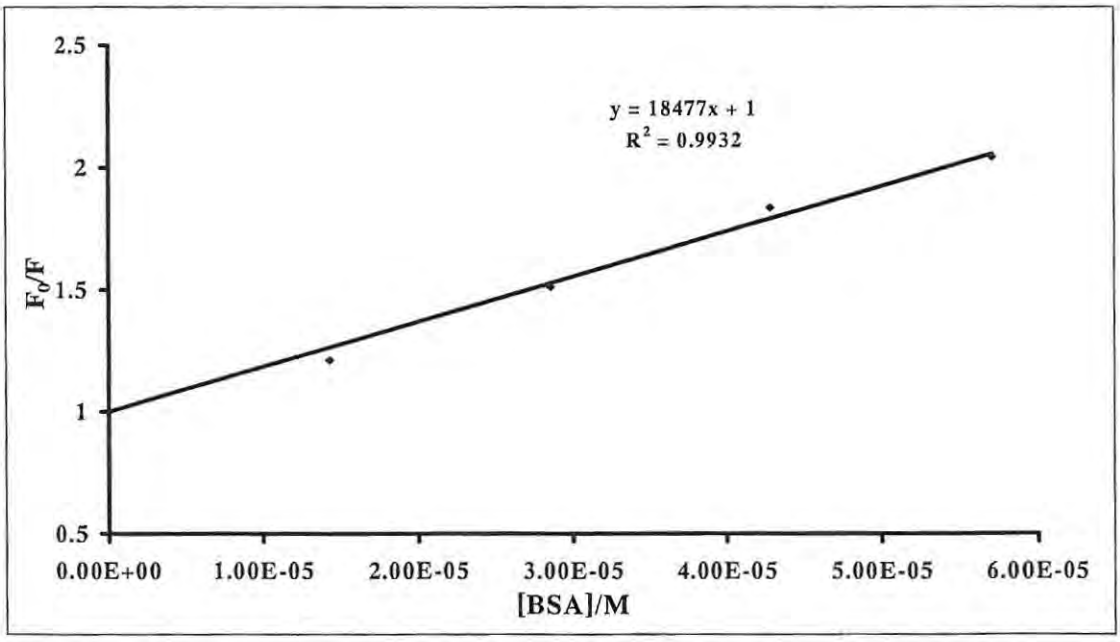

Fig. 4.55: Stern-Volmer plot for BSA quenching of GePcS$_{mix}$ (30).

Values of k_Q (bimolecular quenching constant) were determined from Eq. 4.20 (similar to Eq. 2.106) for quenching of BSA by MPcS$_{mix}$, using a value of 10^{-8} s [270] for the fluorescence lifetime of the BSA biopolymer (τ_F^{BSA}); and are listed in Table

4.21. The k_Q values from Eq. 4.20 were then used to calculate the MPc fluorescence lifetime $\tau_F^{MPcS_{mix}}$, according to Eq. 4.21 (similar to Eq. 2.108).

$$K_{SV}^{BSA} = k_Q \tau_F^{BSA} \qquad \text{(Eq. 4.20)}$$

$$K_{SV}^{MPcS_{mix}} = k_Q \tau_F^{MPcS_{mix}} \qquad \text{(Eq. 4.21)}$$

k_Q values are of the order of 10^{12} M^{-1} s^{-1}, Table 4.21. However, the acceptable value of k_Q for dynamic quenching according to Einstein-Smoluchowski approximation [224] at room temperature is of the order of 10^{10} M^{-1} s^{-1}. The high values of k_Q observed in Table 4.21, suggests that the fluorescence quenching of BSA by $MPcS_{mix}$ is not initiated by dynamic quenching, but by static quenching (Eq. 2.78, shown here as Eq. 4.22), and the K_{SV}^{BSA} and $K_{SV}^{MPcS_{mix}}$ values in equation Eqs. 4.20 and 4.21 are due to static quenching, hence may be represented by K_S^{BSA} and $K_S^{MPcS_{mix}}$, respectively.

$$\frac{I_0}{I} = 1 + K_S[Q] \qquad \text{(Eq. 4.22)}$$

Where Q is either BSA or MPS_{mix}.

The static quenching constants (K_S^{BSA} and $K_S^{MPcS_{mix}}$; Table 4.21) for BSA and the $MPcS_{mix}$ complexes reveal the relative degrees of interaction between BSA and the $MPcS_{mix}$ complexes. Both constants are highest for $AlPcS_{mix}$ (**27**). From these values, it could be inferred that **27** (K_S^{BSA} = 11.45 x 10^4 M^{-1}) possesses the highest degree of interaction with BSA while $SnPcS_{mix}$ (**31**, K_S^{BSA} = 1.98 x 10^4 M^{-1}) has the lowest. The observed lower values of K_S^{BSA} for $ZnPcS_{mix}$ (**28**) and $SnPcS_{mix}$ (**31**) are not unconnected with their aggregation in aqueous solution; and the relatively higher values for the former (**28**) could imply the lower aggregation tendency of **28** compared to **31**. The high K_S^{BSA} and $K_S^{MPcS_{mix}}$ values for **27** compared to the other

monomeric complexes - $SiPcS_{mix}$ (**29**) and $GePcS_{mix}$ (**30**), suggests that the latter two have lower affinities for BSA than the former.

$MPcS_{mix}$ fluorescence lifetimes from BSA binding data

A crucial assumption was made in this study; that k_Q values are the same for both $MPcS_{mix}$-quenching of BSA and BSA-quenching of $MPcS_{mix}$. Making this assumption, it was possible to calculate the fluorescence lifetimes ($\tau_F^{MPcS_{mix}}$) of the $MPcS_{mix}$ complexes, using Eq. 4.21, knowing the value of $K_S^{MPcS_{mix}}$. The fluorescence lifetimes (Table 4.21) calculated for the $MPcS_{mix}$ complexes, using this method, are quite close to the typical MPc fluorescence lifetimes [79,158]. The procedure described here could however not be employed in the case of $ZnPcS_{mix}$ (**28**) and $SnPcS_{mix}$ (**31**), whose fluorescence intensities increased on BSA addition (see discussion below).

Among the three complexes: $AlPcS_{mix}$ (**27**), $SiPcS_{mix}$ (**29**) and $GePcS_{mix}$ (**30**) which are monomeric, fluorescence lifetime decreases as the atomic mass of central metal ion increases, most probably due to an enhanced intersystem crossing. The literature value for **28** [158] is notably less than those calculated for **27**, **29** and **30**, which is attributable to the aggregated nature of this species in aqueous solution. Comparing the lifetime values (for **27**, **29** and **30**) obtained using this procedure with those obtained from HQ quenching of $MPcS_{mix}$, one can say that the values are the same, considering a 5 % error margin (Table 4.21).

4.6.3 Effects of BSA binding on photophysical and photochemical properties of $MPcS_{mix}$ complexes.

BSA shows a strong absorption around 280 nm (log ε = 4.65) which is characteristic of tryptophan residues [200,271]. Fig. 4.56 shows the ground state electronic absorption and fluorescence emission spectra of BSA in PBS 7.4.

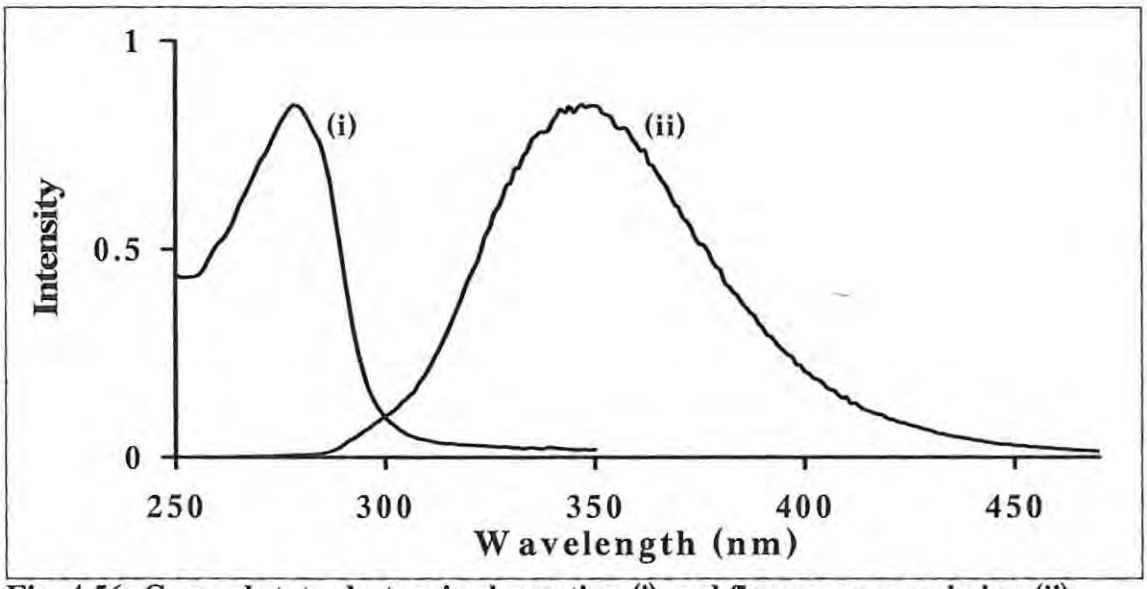

Fig. 4.56: Ground state electronic absorption (i) and fluorescence emission (ii) spectra of BSA in PBS 7.4.

In Fig. 4.57, one can observe the small bathochromic shift (~ 2 nm) in Q band position of $AlPcS_{mix}$ (**27**) when bound to BSA. This implies that a complex is actually being formed between the photosensitizer and the biopolymer. A similar subtle change in Q band position was observed for $SiPcS_{mix}$ (**29**), but not for $ZnPcS_{mix}$ (**28**), $GePcS_{mix}$ (**30**) and $SnPcS_{mix}$ (**31**).

This observation could be an indication of the varying degrees of feasibility of binding to BSA, with **27** and **29** showing the highest probability. HPLC showed that $ZnPcS_{mix}$ (**28**) and $SnPcS_{mix}$ (**31**) have more of the less sulphonated derivatives, hence will show lower tendencies to bind with BSA.

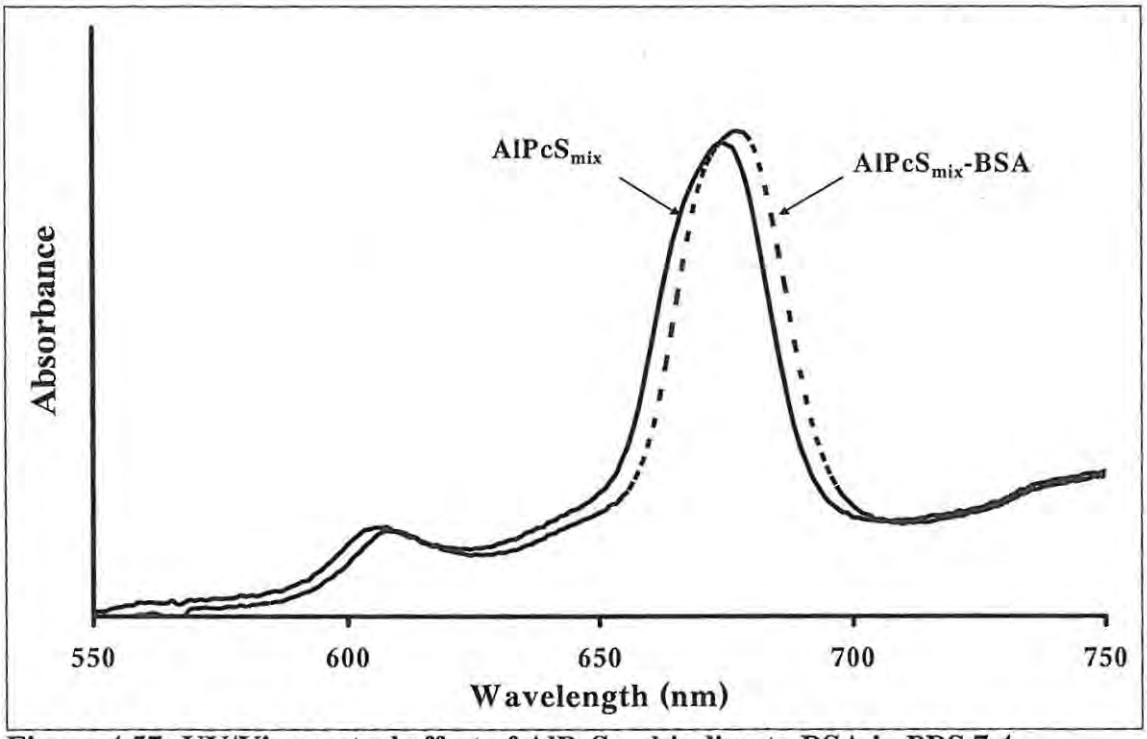

Figure 4.57: UV/Vis spectral effect of AlPcS$_{mix}$ binding to BSA in PBS 7.4.

Fig. 4.58 shows the fluorescence emission spectra of mainly monomeric AlPcS$_{mix}$ (**27**) and mainly aggregated ZnPcS$_{mix}$ (**28**) (free and BSA-bound).

For the monomeric MPcS$_{mix}$ species, BSA binding resulted in reasonable fluorescence quenching which is manifested in decrease in spectral intensity in the presence of BSA. For ZnPcS$_{mix}$ (**28**), an increase in emission intensity is observed in the presence of BSA (Fig. 4.58). The fluorescence quantum yield (Φ_F) values of AlPcS$_{mix}$ (**27**), SiPcS$_{mix}$ (**29**) and GePcS$_{mix}$ (**30**) (Table 4.22), are larger than those of their BSA-bound counterparts. On the other hand, BSA binding resulted in increase in Φ_F values for the aggregated ZnPcS$_{mix}$ (**28**) and SnPcS$_{mix}$ (**31**) (Table 4.22), which suggests that BSA actually monomerizes the aggregated species.

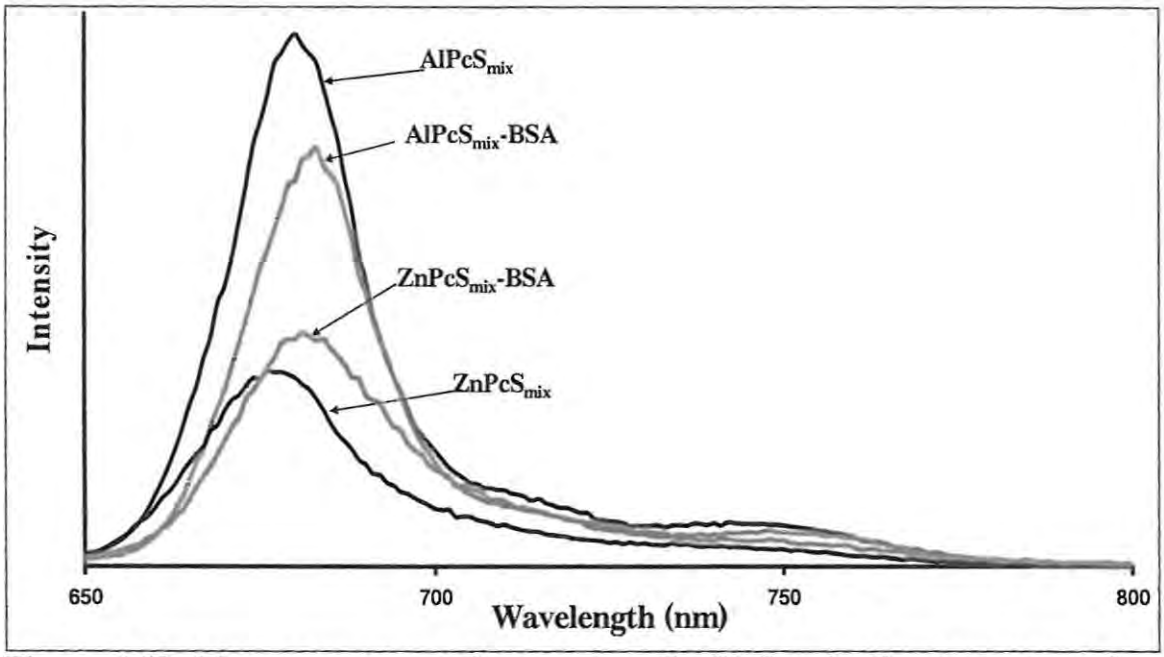

Figure 4.58: Fluorescence emission spectra of $MPcS_{mix}$ in the presence and absence of BSA in PBS 7.4.

Table 4.22: Photophysical and photochemical parameters of $MPcS_{mix}$ complexes in PBS 7.4.

	λ_Q (nm)	λ_F (nm)	Φ_F	Φ_T	Φ_{IC}	$10^5/\Phi_{Pd}$	Φ_Δ	$\frac{\Phi_{OP}}{\Phi_{OP}^{SnPcS_{mix}}}$
$AlPcS_{mix}$ (27)	674	677	0.44	0.44	0.12	0.40	0.42	
	(677)	**(683)**	**(0.34)**			**(0.59)**		**(0.59)**
$ZnPcS_{mix}$ (28)	673	677	0.16	0.53	0.31	3.65	0.45	
	(676)	**(681)**	**(0.20)**			**(17.1)**		**(0.37)**
$SiPcS_{mix}$ (29)	678	682	0.34	0.45	0.21	0.71	0.49	
	(679)	**(682)**	**(0.30)**			**(0.86)**		**(0.40)**
$GePcS_{mix}$ (30)	680	686	0.30	0.67	0.03	0.45	0.68	
	(680)	**(686)**	**(0.24)**			**(0.44)**		**(0.57)**
$SnPcS_{mix}$ (31)	688	699	0.05	0.59	0.36	1.59	0.42	
	(685)	**(688)**	**(0.07)**			**(1.77)**		**(1.00)**

Values in brackets are in the presence of 10 molar proportions of BSA.

4.6.4 Photosensitized oxidation of BSA

MPc photodegradation is believed to be a singlet oxygen-mediated process [180], and so its efficiency should be related to the rate of singlet oxygen generation, among other factors. With the exception of $GePcS_{mix}$ (**30**) for which the value of Φ_{Pd} did not change (Table 4.22), $MPcS_{mix}$ photobleaching was enhanced in the presence of BSA. This is attributed to the formation of active oxidative albumin species which could additionally react with the $MPcS_{mix}$.

In the photobleaching experiment on BSA-bound $MPcS_{mix}$, $MPcS_{mix}$ photobleaching was accompanied by substantial intensity increase in the UV region of the spectrum (Fig. 4.59), implying that BSA competes with the $MPcS_{mix}$ for singlet oxygen. It is difficult to identify which species is responsible for the UV region intensity increase, but it could be due to some BSA photo-oxidation products, which absorb in the UV region.

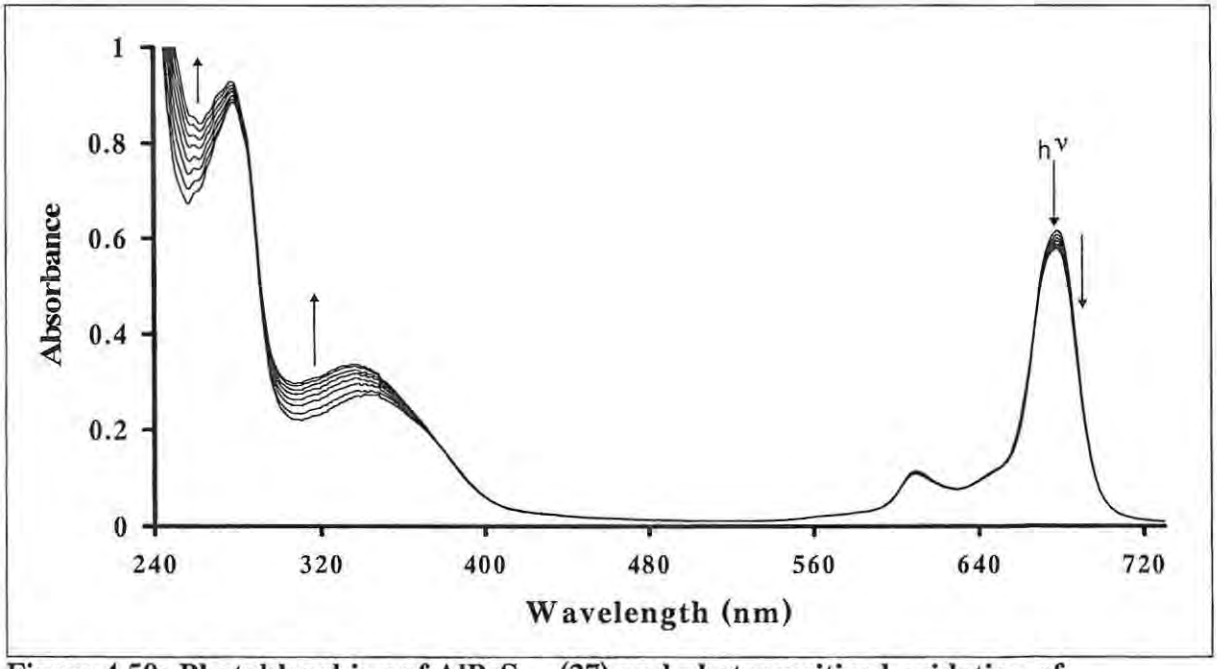

Figure 4.59: Photobleaching of $AlPcS_{mix}$ (27) and photosensitized oxidation of BSA in PBS 7.4. Irradiaiton at 27's Q band maximum. Light intensity used was 4.82×10^{16} photons s^{-1} cm^{-1}.

Due to the relatively large concentration of BSA used in the experiments and the high rate constants for reaction of singlet oxygen with some amino acid side chains [272], it is logical to think that BSA would be a target for singlet oxygen. A series of endoperoxides and hydroperoxides have been indicated as products of oxidation of amino acid side chains in proteins [272].

In order to quantify the efficiency of BSA photooxidation, the intensity increase in the UV region (305 nm) was used, and this is related to the photooxidation quantum yield (Φ_{OP}), by Eq. 4.23:

$$\Phi_{OP} = \frac{(A_t - A_0)V/\varepsilon}{I_{abs}.t} \qquad \text{(Eq. 4.23)}$$

Where A_t and A_0 are the absorbances at 305 nm after irradiation for t secs and before irradiaiton respectively; V, the reaction volume; ε, the molar extinction coefficient of oxidation product; and I_{abs}, the intensity of absorbed light in photon mol s^{-1}.

But

$$R = \frac{(A_t - A_0)V/\varepsilon}{t} \qquad \text{(Eq. 4.24)}$$

Where R is the rate of formation of oxidation product. It therefore follows that

$$\Phi_{OP} = \frac{R}{I_{abs}} \qquad \text{(Eq. 4.25a)}$$

For another photosensitizer, we can write a similar equation:

$$\Phi'_{OP} = \frac{R'}{I'_{abs}} \qquad \text{(Eq. 4.25b)}$$

Taking ratios,

$$\frac{\Phi'_{OP}}{\Phi_{OP}} = \frac{R'.I_{abs}}{R.I'_{abs}} \qquad \text{(Eq. 4.26)}$$

Values of BSA photooxidation quantum yields were obtained relative to that in $SnPcS_{mix}$ (**31**), which is given an arbitrary value of 1.00. The relative values of Φ_{OP} for all $MPcS_{mix}$ complexes studied are listed in Table 4.22.

Singlet oxygen quantum yield experiments in the presence of BSA yielded no results, as the singlet oxygen trap employed (ADMA) was not bleached during the experiment. However, slight spectral changes (similar to those attributed to photooxidation) were observed for BSA. BSA is probably more susceptible to singlet oxygen oxidation than ADMA.

4.6.5 Kinetic data from $MPcS_{mix}$-BSA binding (fluorescence lifetimes)

The rate constants for the excited singlet state deactivation processes (k_F, k_{IC} and k_{ISC}) were calculated from the determined values of $MPcS_{mix}$ fluorescence lifetimes and the quantum yields of the respective singlet excited state deactivation processes (Φ_F, Φ_{IC} and Φ_{ISC}), and are listed in Table 4.23.

Table 4.23: [a]Rate constants for $MPcS_{mix}$ intrinsic processes in PBS 7.4.

Complex	τ_F (ns)	k_F (x10^{-7}) (s^{-1})	k_{ISC} (x10^{-7}) (s^{-1})	k_{IC} (x10^{-7}) (s^{-1})
$AlPcS_{mix}$ (27)	[b]5.13	8.58	8.58	2.34
$ZnPcS_{mix}$ (28)	[c]2.78	5.76	19.10	11.20
$SiPcS_{mix}$ (29)	[b]4.98	6.83	9.04	4.22
$GePcS_{mix}$ (30)	[b]4.07	7.37	16.71	0.74
$SnPcS_{mix}$ (31)	[c]2.03	2.46	29.10	17.70

[a]Values calculated using Eqs. 2.64a-c: $k_F = \frac{\Phi_F}{\tau_F}$; $k_{IC} = \frac{\Phi_{IC}}{\tau_F}$; $k_{ISC} = \frac{\Phi_{ISC\,(T)}}{\tau_F}$. **$\Phi_F$ taken from Table 4.4; Φ_T and Φ_{IC} from Table 4.7; [b]Values obtained from BSA quenching data (Table 4.21); [c]Values from HQ quenching data (Table 4.10).**

The superior photo-activity of this species is also shown in Table 4.22, where its values of Φ_F, Φ_T and Φ_Δ are consistently high.

The values of k_F, k_{ISC} and k_{IC} determined from BSA binding are within the same order or magnitude as those determined from HQ quenching (Section 4.2.3.2), Table 4.10.

5 CONCLUSION

This thesis has presented a comprehensive investigation of the effects of peripheral substituents, axial ligands, central metal ions and solvents on the photophysical and photochemical properties of non-transition metallophthalocyanine derivatives. The variation of fluorescence quantum yield (Φ_T) with substituent type is slight; this parameter was found to be more responsive to change of solvent than to change of substituents.

The presence of sulpho substituents leads to the enhancement of intersystem crossing, as evident from the higher values of triplet quantum yields (Φ_T) compared to that of unsubstituted ZnPc. Most of the substituted ZnPc derivatives gave lower singlet oxygen quantum yield (Φ_Δ) values than the unsubstituted ZnPc, due to the probable quenching of singlet oxygen by vibrations in the substituents. The anionic sulphonated ZnPc derivatives again gave longer triplet lifetimes (τ_T) and higher triplet state quantum yields compared to the rest of the complexes, probably due to the poor ability of anionic species to dissipate excitation energy non-radiatively. The low triplet lifetimes of some of the complexes, e.g., ZnTBPPc (**19**), was interpreted in terms of the flexibility of the substituents, the motion of which accelerates non-radiative decay of the excited states. Since it is desirable for molecules to have reasonably high values of Φ_T and τ_T for efficient photosensitization, the design of new photosensitizers should take into consideration the charge and flexibility of the molecules.

This work stresses the importance of solvent consideration in the spectral, photophysical and photochemical studies of MPc complexes. The largest red shift of Q band of ZnPc (**15**) was observed in aromatic solvents, the highest shift being

observed for 1-chloronaphthalene. Split Q band in the emission and excitation spectra of ZnOPPc (**22**) was observed in some solvents and this was explained in terms of the lowering of symmetry following excitation. THF proved to be a solvent which behaves quite differently from the rest of the solvents; for example, higher Φ_F values were obtained in this solvent for ZnPc (**15**) and ZnOPPc (**22**); also, phototransformation, rather than photodegradation, was observed for **22** in this THF. Solvent studies revealed that strong near-IR absorption of some solvents is responsible for the short singlet oxygen and triplet lifetimes in such solvents, and that photostability of the complexes is a function of solvent basicity.

The Φ_T and Φ_Δ values of $MPcS_{mix}$ complexes, where M = Al, Zn, SI, Ge or Sn, suggest efficient sensitization for the production of singlet oxygen, the chief cytotoxin in PDT. $ZnPcS_{mix}$ (**28**) and $SnPcS_{mix}$ (**31**) showed aggregation in PBS 7.4 and this is explained in terms of the preponderance of the relatively lipophilic low-sulphonated MPc fractions present in solution, as proved by HPLC studies. Among the non-aggregated complexes, **30** gave the largest value of Φ_Δ compared to **27** and **29**, and this is explained in terms of the heavy atom effect. Low values of Φ_F were observed for the aggregated **28** and **31**, as aggregation leads to severe quenching of fluorescence.

The departure from linearity of the S-V plots for the fluorescence quenching of the complexes by BQ was ascribed to the coexistence of both dynamic and static quenching mechanisms, and the latter was interpreted according the "sphere of action quenching model". Quenching efficiency was found to vary directly as the size of the central metal ions of the complexes. On the contrary, $MPcS_{mix}$ fluorescence quenching by HQ was found to be diffusion-controlled (obeyed the Stern-Volmer relationship) and so was used to estimate the fluorescence lifetimes of the $MPcS_{mix}$

complexes. In-depth photophysical studies of photosensitizers are usually hampered by the lack of fluorescence lifetime data; determination of fluorescence lifetimes involves the use of high-level equipment which are beyond the reach of many researchers. The fluorescence quenching analysis in this work is of great academic interest; it provides a simple route to the determination of fluorescence lifetimes of photosensitizers from simple fluorescence quenching experiments. The fluorescence lifetime values obtained compared well with typical MPc fluorescence lifetime literature values.

Qualitative and quantitative interpretations of the interaction of $MPcS_{mix}$ mixtures with bovine serum albumin (BSA) were also discussed in this thesis. Results of binding experiments showed that each of the $MPcS_{mix}$ mixtures formed a 1:1 adduct with BSA. However, the binding feasibilities varied markedly, as evident from the values of binding constant (K_b) for the $MPcS_{mix}$-BSA adduct; with $AlPcS_{mix}$ (**27**) giving the highest K_b value, while $SnPcS_{mix}$ (**31**) gave the lowest. The observed trend in the values of K_b was explained in terms of aggregation and the greater affinities of some of the species for BSA, than others. The spectral as well as photophysical and photochemical properties of the complexes were altered in the presence of BSA, thus providing a justification for this study. As in the case of HQ quenching, fluorescence lifetimes of the $MPcS_{mix}$ complexes were determined from $MPcS_{mix}$-BSA binding data (which also obeyed the Stern-Volmer relationship), which is a simple but unique route to the determination of fluorescence lifetimes of MPc complexes from steady-state measurements. Fluorescence lifetime values obtained in both cases mentioned above are closely comparable, within a 5 % error margin.

This work also showed that ZnPc derivatives containing different peripheral substituents can form inclusion complexes with cyclodextrins. The resulting inclusion

complexes generally showed larger Φ_Δ values when compared to the complexes before inclusion. Jobs plots showed that 2:1 and 4:1 (CD:MPc) complexes may be formed. Photobleaching is decreased after inclusion of the MPc derivatives into CD, while fluorescence quantum yields generally remained unchanged following inclusion into CDs.

Protonation of ZnPc derivatives is dependent on the presence of axial ligands ring substituents; electron-donating axial ligands and ring substituents enhance the ease of protonation, while electron-withdrawing substituents make protonation more difficult. Ring-substituted ZnPc complexes which were aggregated in solution were not readily protonated. Addition of protonating agents resulted in enhanced aggregation, as axial ligands were lost on protonation. The ease of protonation decreased with the increase in the basicity of the solvent, because a highly basic solvent competes with the MPc for protonation. In all cases protonation decreases the singlet oxygen and fluorescence quantum yields. Photobleaching quantum yields decreased for the protonated derivatives except when axial ligands were present, where protonation resulted in decrease in stability (increase in Φ_{Pd}).

Photophysical studies on the tetraporphyrin-phthalocyanine heteropentamer, **20**, revealed that there was a mutual quenching of the singlet excited states of both ZnPc and ZnTPP moieties when each was selectively excited in the pentamer. Quenching in the case of ZnPc was attributed to charge transfer while ZnTPP quenching was due to a combination of both charge transfer (CT) and energy transfer (ET). A ZnPc charge transfer state (CTS) was identified as the fluorescent species in DMSO (high dielectric constant), while the locally excited state (LES) was the fluorescent species in toluene; an observation that was related to the viscosity and polarity of the respective solvents. Comparison of the data for the pentamer and a 1:4 molar mixture of ZnPc and ZnTPP showed greater efficiencies of charge transfer and

energy transfer in the pentamer, which was attributed to the proximity of the donor and acceptor in the pentamer.

REFERENCES

1. Madej SL, Okajima S and Lim EC, *J. Chem. Phys.,* 1976; **65**: 1219.
2. Kanamaru N and Lim EC, *J. Chem Phy.,* 1975; **62**: 3252.
3. Li R and Lim EC, *J. Chem. Phys.,* 1972; **57**: 605.
4. Wassam WA and Lim EC, *J. Phys. Chem.,* 1978; **68**: 433.
5. Lim EC. In *Excited states* Vol. 3, Lim EC (Ed). Academic Press: New York, 1977.
6. Jablonski A, *Z. Phys.,* 1935; **94**: 38.
7. Lakowicz, JR and Balter A., *Biophys. Chem.,* 1982; **16**:117.
8. Stern O and Volmer M, *Z. Physik,* 1919; **20**: 183.
9. Kuznetsova NA, Gretsova NS, Derkacheva VM, Kaliya OL and Lukyanets EA, *J. Porphyrins Phthalocyanines,* 2003; **7**: 147.
10. Edrei R, Gottfried V, Van Lier J.E and Kimel S, *J. Porphyrins Phthalocyanines,* 1998; **2**: 191.
11. Sokolov VV, Stranadko EF, Zharkova NN, Iakubovskaia RI, Filonenko EV and Astrakhankina TA, *Voprosy Onkologii,* 1995; **41**: 134.
12. Lim YM, Park SH, Song SH, Park CJ, Ryu H, Jee JG and Yang HS, *Bull. Korean Chem. Soc.,* 1999; **20**: 701.
13. Casstevens M, Samok M, Pfleger J and Prasad PN, *J. Chem. Phys.,* 1996; **92**: 2019.
14. Leznoff CC and Lever ABP (Eds). In *Phthalocyanines, Properties and Apllications*, Vols 1-3, VCH: New York, 1989-1993.
15. Wöhrle D, Gitzel J Krawczyk G, Tsuchida E, Ohno H and Nishisaka T, *J. Macromol. Sci. Chem: A,* 1998; **25**: 1227.

16. Wöhrle D and Meissner D, *Adv. Mater.,* 1991; **3**: 129.

17. Gan F, *Chinese Sci. Bull.,* 2000; **45**: 572.

18. Hagen R and Bieringer T, *Adv. Mater.,* 2001; **13**: 1805.

19. Kuder JE, *Imag. Sci.,* 1988; **32**: 51.

20. Gregory P. In *High-Technology Applications of Organic Colourants,* Plenum Press: New York, 1991; p 759.

21. Maya EM, Snow AW, Shirk JS, Pong RG, Flom SR and Roberts GL. *J. Mat. Chem.* 2003; **13:** 1603.

22. Nalwa NS and Shirk JS. In *Phthalocyanines: Properties and Applications*, Vol. 4, Lever APB and Leznoff CC (Eds). Willey-VCH: New York, 1996; Chapt. 3.

23. Radhakrishnann S and Deshpande SD, *Sensors,* 2002; **2**: 185.

24. Oni J, Westbroek P and Nyokong T. *Electroanalysis,* 2002; **14**: 1165.

25. Robert GG, Petty MC, Baker S, Flowler MT and Thomas NJ, *Thin Solid films,* 1985; **132**: 113.

26. Cook, MJ, Dunn AJ, Daniel FM, Hart RCO, Richardson RM and Rose SJ, *Thin Solid films*, 1988; **159**: 469.

27. Schultz H, Lehmann H, Rein M and Hanack M, *Struct. Bonding (Berlin),* 1991; **74**: 41.

28. Rosenthal I, *Photochem. Photobiol.,* 1991; **53**: 859.

29. Spikes JD, *Photochem. Photobiol. B: Biol.,* 1990; **6**: 259.

30. Bonnett R. In *Chemical Aspects of Photodynamic Therapy*, Gordon and Breach Science Publishers: Amsterdam, 2000.

31. Spikes JD, *Photochem. Photobiol.,* 1986; **43**: 691.

32. Bown SG, Tralau CJ, Colendge-Smith PD, Akdemir D and Wieman TJ, *Br. J. Cancer,* 1987; **54**: 43.

33. Brown SB and Truscott TG, *Chem. Br.* 1993: 955.

34. Isago H, (http://www.nims.gp.jp/molfunc/English/English.html).

35. Braun A and Tcherniac J, *Bre. Deut. Chem. Ges.* 1907; **40**: 2709.

36. Byrne GT, Linstead RP and Lowe AR, *J.Chem. Soc.,* 1934; 1017.

37. Linstead RP and Lowe AR, *J. Chem. Soc.,* 1934; 1022.

38. Dent CE, Linstead RP and Lowe AR, *J. Chem. Soc.,* 1934; 1033.

39. Elvidge JA and Linstead RP, *J. Chem. Soc.,* 1955; 3536.

40. Robertson JM, *J. Chem. Soc.,* 1935; 615.

41. Robertson JM, *J. Chem. Soc.,* 1936; 1195.

42. Robertson JM and Woodward I, *J. Chem. Soc.,* 1937; 219.

43. Mack J and Stillman MJ, *J. Am. Chem. Soc.,* 1994; **116**: 1292.

44. Kobayashi T, Ashida T, Uyeda N, Surro E and Kakuda M, *Bull. Chem. Soc. Jpn.,* 1971; **44**: 2095.

45. Walzer K and Hietschold M, *Surface Science*, 2001; **471**: 1.

46. Day PN, Wang Z and Pachter R, *J. Mol. Struc. (THEO-Chem)*, 1998; **455**: 33.

47. Stillman MJ and Nyokong T. In *Phthalocyanines: Properties and Applications.* Vol. 1, Leznoff CC and Lever ABP (Eds). VCH: New York, 1989; pp 139-247.

48. Fischer MS, Templeton DH, Zalkin A and Calvin M, *J. Am. Chem. Soc.,* 1975; **97**: 2676.

49. Gouterman M. In *The Porphyrins,* Vol. 3, Part A. Physical Chemistry, Dolphin D (Ed). Academic Press: New York, 1978; pp. 1-165.

50. McHugh AJ, Gouterman M and Weiss C, *Theoret. Chim. Acta,* 1987; **24**: 246.

51. Schaffer AM, Gouterman M and Davidson ER, *Theoret. Chim. Acta,* 1973; **30**: 9.

52. Lee LK, Sabelli NH and LeBreton PR, *J. Phys. Chem.,* 1982; **86**: 3926.

53. Nyokong T, Gasyna Z and Stillman MJ *Inorg. Chem.,* 1987; **26**: 548.

54. Nyokong T, Gasyna, Z and Stillman MJ, *Inorg. Chem.,* 1987; **26**: 1087.

55. Ough E.A, Nyokong T, Creber KA and Stillman MJ, *Inorg. Chem.,* 1988; **27**: 2724.

56. Ough EA, Gasyna Z and Stillman MJ, *Inorg. Chem.,* 1991; **30**: 2301.

57. Ough EA and Stillman MJ, *Inorg. Chem.,* 1994; **33**: 573.

58. Huang TH, Reickhoff KE and Voight EM, *J. Chem. Phys.,* 1982; **77**: 3424.

59. Huang,TH, Reickhoff KE and Voight EM, *J. Chem. Phys.,* 1981; **85**: 3322.

60. Stillman MJ. In *Phthalocyanines. Principles and Properties:* Lever ABP and Leznoff CC (Eds). VCH Publications: New York, 1993 pp 227-296.

61. Barrett FH, Frye DA and Linstead RP, *J.Chem. Soc.,* 1938; 1157.

62. Brach PJ, Grammatica SJ, Ossana OA and Weinberger L, *J. Heterocyclic Chem.,* 1970; **7** : 1403.

63. Barrett PA, Dent CE and Linstead RP, *J. Chem. Soc.,* 1936; 1719.

64. Linstead RP, *J. Chem. Soc.,* 1934; 1016.

65. Lever ABP, *Adv. Inorg. Chem. Radiochem.,* 1965; **7**: 27.

66. Moser FH and Thomas AL. In *Phthalocyanine Compounds,* Reinhold: New York; Chapman and Hall: London, 1963.

67. Kasuga K and Tsutsui M, *Coord. Chem. Rev.,* 1980; **32**: 67.

68. Moser FH and Thomas AL In *The Phthalocyanines,* Vols. 1 & 2, CRC: Boca Raton, 1983.

69. Tomoda H, Saito S and Shiaishi S, *Chem. Lett.,* 1983; 313.

70. Villemin D, Hammadi M, Hachemi M and Bar N, *Molecules* 2001; **6**: 831.

71. Shaabani A, *J. Chem. Res.,* 1998; **10**: 672.

72. Foley S, Jones Gurnos, Luizzi R, McGarvey DJ, Perry M and Truscott TG, *J. Chem. Soc., Perkin Trans., 2,* 1997; 1725.

73. Torre G and Torres AT, *J. Prophyrins Phthalocyanines,* 1997; **1**: 221.

74. Wöhrle D, Eskes M, Shigehara K and Yamada A, Synthesis, 1993; 194.

75. Ozoemena K and Nyokong T, *J. Chem. Soc., Dalton Trans.,* 2002; 1806.

76. Maree S, Phillips D and Nyokong T, *Prophyrins Phthalocyanines,* 2002; **6**: 17.

77. Maree S and Nyokong T, *Prophyrins Phthalocyanines,* 2001; **5**: 782.

78. Weber JH and Busch DH, *Inorg. Chem.,* 1965; **4**: 469.

79. Ambroz M, Beeby A, MacRobert AJ, Simpson MSC, Svensen RK and Phillips D, *J. Photochem. Photobiol. B: Biol.,* 1991; **9**: 87.

80. Dhami S and Phillips D, *J. Photochem. Photobiol. A: Chem.*, 1996; **100**: 77.

81. Choi MT, Li PP and Ng DK, *Tetrahedron,* 2000; **56**: 3881.

82. Ferencz A, Neher D, Schulze M, Wegner G, Viaene L and Achryver FC, *Chem. Phys. Lett.,* 1995; **245**: 23.

83. Yang Y, Ward JR and Seiders R, *Inorg. Chem.,* 1985; **24**: 1765.

84. Zhang X and Xu H, *J. Chem, Soc, Faraday Trans.,* 1993; **89**: 3347.

85. Nevin WA, Liu W, Greenberg S, Hempstead MR, Maruccio SM, Melnik MM, Leznoff CC and Lever ABP, *Inorg. Chem.,* 1987; **26**: 291.

86. Lever ABP, Hemstead MR, Leznoff CC, Liu W, Melnik M, Nevin WA and Seymour P, *Pure Appl. Chem.,* 1986; **58**: 1467.

87. Nensala N and Nyokong T, *Polyhedron,* 1998; **17**: 3467.

88. Nensala N and Nyokong T, *Polyhedron,* 1996; **15**: 867.

89. Sielcken OTE, van Tilborg MM, Rocks MFM, Hendricks R, Drenth W and Nolte RJM, *J. Am. Chem. Soc.,* 1987; **109**: 4261.

90. Szymczyk I and Abramczyk H, *Pure Appl. Chem.,* 2004; **76**: 183.

91. Wöhrle D. In *Phthalocyanines: Properties and Applications,* Leznoff CC and Lever ABP (Eds). VCH: New York, 1989; p 55.

92. Abramczyk H Szymczyk I, Waliszewska G and Lebioda A, *J. Phys. Chem.* 2004; **108**: 264.

93. Martin PC, Gouterman M, Pepich V, Renzoni GE and Schindele DC, *Inorg. Chem.,* 1991; **30**: 3305.

94. Van Lier JE and Spikes JD. In *Photosensitizinig compounds: their chemistry, biology and clinical use*, Bock GS and Harnett S (Eds). John Wiley and Sons: Chichester, 1989; pp 17-32.

95. Sastre A, Gouloumis A, Va´zquez P, Torres T, Doan V, Schwartz BJ, Wudl F, Echegoyen L and Rivera J, *Org. Lett.,* 1999; **1**: 1807.

96. George RE, Snow AW, Shirk JS and Barger WR, *J. Porphyrins Phthalocyanines,* 1998; **2**: 1.

97. Lever ABP, Milaeva ER and Speier G. In *Phthalocyanines: Properties and Applications,* Vol.3, Leznoff CC and Lever ABP (Eds). VCH: New York, 1989; p 55.

98. Lever ABP, Hempstead MR, Leznoff CC, Liu W, Melnik M, Nevin WA and Seymour P, *Pure Appl. Chem.,* 1986; **58**: 1467.

99. Gasyna Z and Stillman MJ, *Inorg. Chem.,* 1990; **29**: 5101.

100. Nyokong T, Gasyna Z and Stillman MJ, *ACS Symp. Ser.* 1986; **321**: 309.

101. Gasyna, Z, Browett, W.R and Stillman, M.J, *ACS Symp. Ser.* 1986; **321**: 298

102. Gasyna Z, Browett WR and Stillman MJ, *Inorg. Chem.,* 1984; **23**: 382.

103. Gasyna Z, Browett WR and Stillman MJ, *Inorg. Chem.,* 1985; **24**: 2440.

104. Clark DW and Yandle JR, *Inorg. Chem.,* 1972; **11**: 1738.

105. Felton RH and Linschitz H, *J. Am. Chem. Soc.,* 1966; **88**: 1113.

106. Dodd JW and Hush NS, *J. Chem. Soc.,* 1964; 4607.

107. Borisenkova SA, Denisova EP, Batanova EA, Girenko EG, Kaliya OL, Lukyanets EA and Vorozhtsov GN, *J. Porphyrins Phthalocyanines,* 2000; **4**: 684.

108. Pennesi G, Ercolani C, Ascenzi P, Brunori M and Monacelli F *J. Chem. Soc. Dalton Trans.* 1985; 1107.

109. Nyokong, T and Guthrie-Stratchan, Inorg. Chim. Acta 1993, **208**, 239.

110. Pennesi, G, Ercolani, C, Rossi, G, Ascenzi, P, P, Brunori, M and Monacelli, F J. Chem. Soc. Dalton Trans. 1985, 1113.

111. Jones GJ and Twigg MV, *Inorg. Chem.,* 1969; **8**: 2120.

112. Gaspard S, Verdaguer M and Viovy R *J. Chem. Res.,* 1979; 3072.

113. Borokov NY and Akopov AS, *Zh. Fiz. Khim.,* 1986; **60**: 750.

114. Gaspard S, Verdaguer M and Viovy R, *J. Chim. Phys. Phys.-Chim. Biol.,* 1972; **69**: 1740.

115. Stuzhin PA, Khelevina OG and Berezin BD. In *Phthalocyanines: Principles and Applications,* Vol. 4, Leznoff CC and Lever ABP (Eds). VCH Publishers: New York, 1996; p 19.

116. Bernstein PA and Lever ABP, *Inorg. Chim. Acta,* 1992; **543**: 198.

117. Akopov AS and Borokov NY, *Zh. Obsch. Khim.,* 1996; **56**: 931.

118. Akopov AS and Borokov NY, *Koord. Khim.,* 1988; **14**: 731.

119. Freyer W and Minh LQ, *J. Porphyrins Phthalocyanines,* 1997; **1**: 287.

120. Graczyk A and Bialkowska E, *Tetrahedron,* 1978; **34**: 3505.

121. Beeby A, FitzGerald S and Stanley CF, *Photochem. Photobiol.,* 2001; **74**: 566.

122. Iodko SS, Kaliya OL, Kondratenko NV, Lukyanets EA, Popov VI and Yagupol'skii LM, *Zh. Obsch. Khim.,* 1983; **53**: 901.

123. Beeby A, FitzGerald S and Stanley CF, *J. Chem. Soc., Perkin Trans 2,* 2001; 1978.

124. Solovev KN, Mashenko VA and Kachura TF, *Opt. Spektrosk.,* 1969; **27**: 24.

125. Weitman H, Schatz S, Gottlieb HE, Kobayashi N and Ehrenberg, *Photochem. Photobiol.,* 2001; **73**: 473.

126. Lang K, Wagnerova DM, Engst P and Kubat P, *J. Chem. Soc., Faraday Trans.,* 1992; **88**: 677.

127. Calvert JG and Pitts JN. In *photochemistry,* John Wiley & Sons, Inc.: New York, p 255.

128. McConnell H, *J. Chem. Phys.,* 1952; **20**: 700.

129. Nagakura S and Baba H., *J. Am. Chem. Soc.,* 1952; **74**: 5693.

130. Brooker LGS, Keyes GH, Sprague RH, VanDyke RH, VanLare E, VanZandt G, White FL, Cressman HWJ and Dent SG, *J. Am. Chem. Soc.,* 1951; **73**: 5332.

131. Ungnade HE, *J. Am. Chem. Soc.,* 1953; **75**: 432.

132. Bayliss NS and McRae EG, *J. Chem. Phys.,* 1954; **58**: 1002.

133. Law W-F, Liu RCW, Jiang J and Ng DKP, *Inorg. Chim. Acta,* 1997; **256**: 147.

134. Harazono T and Takagishi I, *Bull. Chem. Soc. Jpn.,* 1993; **66**: 1016.

135. Bayliss NS, *J. Chem. Phys.,* 1950; **18**: 292.

136. Lakowicz JR. In *Principles of fluorescence spectroscopy,* Kluwer Academic/ Plenum Publishers: New York, 1999; pp 184-210.

137. Boguta A, Wrobel D, Hoffmann TJ and Mazurkiewicz P, *Cryst. Res. Technol.,* 2003; **38**: 267.

138. Darwent JR, Douglas P, Harriman A, Porter G and Richoux M-C, *Cood. Chem. Rev.,* 1982; **44**: 83.

139. Maree MD, Nyokong T, Suhling K and Phillips D, *J. Porphyrins Phthalocyanines,* 2002; **6**: 373.

140. Maree MD, Kuznetsova N and Nyokong T, *J. Photochem. Photobiol. A; Chem.,* 2001; **140**: 117.

141. Gilat SL and Ebbesen TW, *J. Phys. Chem.,* 1993; **97**: 3551.

142. Bishop SM, Beeby A, Meunier H. Parker AW, Foley MSC and Phillips D, *J. Chem. Soc., Faraday Trans.,* 1996; **92**: 2689.

143. McCubbin I and Phillips D, *J. Photochem.,* 1986; **34**: 187.

144. Grofcsik A, Baranyai P, Bitter I, Csokai V, Kubinyi M, Szegletes K, Tatai J and Vidoczy T, *J. Mol. Struc.,* 2004; **704**: 11.

145. Howe I and Zhang JZ, *J. Phys. Chem. A.,* 1997; **101**: 3207.

146. Tokumaru K, *J. Porphyrins Phthalocyanines,* 2001; **5**: 77.

147. Tokumaru K and Kaneko Y. In *Phthalocyanines,* Shirai H and Kobayashi N (Eds). IPC: Tokyo, 1997; 224.

148. Tokumaru K. In *Phthalocyanines,* Shirai H and Kobayashi N (Eds). IPC: Tokyo, 1997; 170.

149. Prasad QR and Ferraudi G, *Inorg. Chem.,* 1982; **21**: 2967.

150. Muralidharan S and Ferraudi G, *J. Phys. Chem.,* 1983; **87**: 4877.

151. Ferraudi G and Muralidharan S, *Inorg. Chem.,* 1983; **22**: 1369.

152. Kaneko Y, Nishimura Y, Arai T, Sakuragi H, Tokumaru K, Umeda M, Yamamura S and Matsunaga D, *J. Photopolym. Sci. Technol.* 1994; **7**: 151.

153. Nishimura Y, Kaneko Y, Arai T, Sakuragi H, Tokumaru K, Kiten M, Yamamura S and Matsunaga D, *Chem. Lett.* 1990; 1935.

154. Kaneko Y, Arai T, Sakuragi H, Tokumaru K and Pac C, *J. Photochem. Photobiol. A; Chem.,* 1996; **97**: 155.

155. Kaneko Y, Nishimura Y, Takane N, Arai T, Sakuragi H, Kobayashi N, Matsunaga D, Pac C and Tokumaru K, *J. Photochem. Photobiol. A; Chem.,* 1997; **106**: 177.

156. Rückmann I, Zeug A, Herter R and Röder B, *Photochem. Photobiol.,* 1997; **66**: 576.

157. Delaire J, Giannotti C and Zakraweski J, *J. Photochem. Photobiol. A: Chem.,* 1998; **112**: 205.

158. Harriman A and Richoux M, J. *Chem. Soc., Faraday Trans 2,* 1980; **76**: 1618

159. Darwent JR, McCubbin I and Phillips D, *J Chem. Soc., Faraday Trans 2,* 1982; **78**: 347.

160. Yeow EK and Braslavsky SE, *Phys. Chem. Chem. Phys.,* 2002; **4**: 239.

161. Laia CAT, Costa SMB, Phillips D and Parker AW, *Photochem. Photobiol. Sci.,* 2003; **2**: 555.

162. Meyer GJ. In *Progress in Inorganic Chemistry,* Vol. 44*,"Molecular Level Artificial Photosynthetic material"* Jossey-Bass: New York, 1996.

163. Wagner RW and Lindsey JS, *J. Am. Chem. Soc.*, 1994; **116**: 9759.

164. Li J and Lindsey JS, *J. Org. Chem.,* 1999; **64**: 9101.

165. Li J, Diers JR, Seth J, Yang SI, Bocian DF, Holten D and Lindsey JS, *J. Org. Chem.,* 1999; **64**: 9090.

166. Yang SI, Li J, Cho HS, Kin D, Bocian DF, Holten D and Lindsey JS, *J. Mater. Chem.,* 2000; **10**: 283.

167. Tran-Thi TH, Desforge C and Thiec C, *J. Phys. Chem.*, 1989; **93**: 1226.

168. Phillips D, *Science Progress,* 1993; **77**: 295.

169. Wagner SJ, Skripchenko A, Robinette D, Foley JW and Cincotta L, *Photochem. Photobiol.,* 1998; **67**: 343.

170. Hudson JB, Imperial V, Haugland RP and Diwu Z, *Photochem. Photobiol.,* 1997; **65**: 352.

171. Grether-Beck S, Olaizola-Horn S, Schmitt H, Grewe M, Jahnke A, Johnson JP, Briviba K, Sies H. and Krutmann, J, *Proc. Natl. Acad. Sc. USA,* 1996; **93**: 14586.

172. Black HS and Mathews-Roth MM, *Photochem. Photobiol.* 1991; **53**: 707.

173. Angeletti G and Bjorsethi A. In *Organic Micropollutants in Aquatic Environment,* Kluwer Academic Publishers: Dordrecht, 1991.

174. Ozoemena K, Kuznetsova N and Nyokong T, *J. Mol. Cat. A: Chem.,* 2001; **176**: 29.

175. Schlenck GO and Dunlap DE, *Angew. Chem.,* 1956; **68**: 248.

176. Aubry J, Pierlot C, Rigaudy J and Schmidt R, *Acc. Chem. Res.,* 2003; **23**: 668.

177. MacDonald IJ and Dougherty TJ, *J. Porphyrins Phthalocyanines,* 2001; **5**: 105.

178. Gilbert A and Baggott J. In *Photo-oxidation reactions, Essentials of Molecular Photochemistry,* CRC Press: Boca Raton, 1991; pp 501-525.

179. Krinski NI. In *Singlet Oxygen,* Vol. 40, Wasserman HH (Ed). Academic press: New York, 1979; pp 597 – 641.

180. Schnurpfeil G, Sobbi AK, Spiller W, Kliesch H and Wöhrle D, J. *Porphyrins Phthalocyanines*, 1997; **1**: 159.

181. Sobbi AK, Wöhrle D, Schlettwein D, *J. Chem. Soc., Perkin Trans. 2,* 1993; 481,

182. Hamai S and Koshiyama T, *J. Photochem. Photobiol. A: Chem.,* 1999; **127**: 135.

183. Wang XP, Pan JH, Li WH and Zhang Y, *Talanta*, 2001; **54**: 805.

184. Wang XP, Pan JH and Shuang SM, *Spectrochim. Acta*, 2001; **57**: 2755.

185. Carofiglio T, Fomasier R, Lucchini V, Rosso C and Tonellato U, *Tetrahedron Lett.*, 1996; **37**: 8019.

186. Manka JS and Lawrence DS, *Tetrahedron Lett.*, 1989; **30**: 7341.

187. Venema F, Rowan AE and Nolte RJM, *J. Am. Chem. Soc.*, 1996; **118**: 257.

188. Hamai S and Satou H, *Spectrochim. Acta*, 2001; **57**: 1745.

189. Mosinger J, Deumié M, Lang K, Kubát P and Wagnerová DM, *J. Photochem. Photobiol. A: Chem.*, 2000; **130**: 13.

190. Nunes SMT, Sguilla FS and Tedesco AC, *Braz. J. Med. Bio. Res.*, 2004; **37**: 273.

191. Soncin M, Polo L, Reddi E, Jori G, Kenney ME, Cheng G and Rodgers MAJ, *Cancer Lett.*, 1995; **89**: 101.

192. Storm G and Crommelin DJA, *Pharma Sci Tech. Today,* 1998; **1**: 19.

193. Rodriguez ME, Awruch J and Dicelio L, *J. Porphyrins Phthalocyaines,* 2002; **6**: 122.

194. Carter DC and Ho JX, *Adv. Protein Chem.,* 1994; **45**: 153.

195. Figge J, Rossing TH and Fencl V, *J. Lab. Clin. Med.* 1991; **117**: 453.

196. Bordbar AK, Eslami A and Tangestaninejad S, *J. Porphyrins Phthalocyanines,* 2002; **6**: 225.

197. Bordbar AK, Tangestaninejad S and Eslami A, *J. Biochem., Mol. Biol. Biophys.* 2001; **5**: 143.

198. Tominaga TT, Yushmanov VE, Borissevitch IE, Imasato H and Tabak M, *Inorg. Biochem.,* 1997; **65**: 235.

199. Borissevitch IE, Tominaga TT, Imasoto H and Tabak M, *J. Lumin,* 1996; **69**: 65.

200. Silva D, Cortez CM and Louro SR., *Braz. J. Med. Bio. Res.,* 2004; **37**: 963.

201. Tabak GM, *Spectrochimica Acta* 2000; **56**: 2255,

202. Guo M, Zou JW, Yi PG, Shang ZC, Hu GX and Yu QS, *Analytical Sciences,* 2004; **20**: 465.

203. Ulrich KH, *J. Pharmacol. Rev.,* 1981; **33**: 17.

204. Mostafa S, El-Sadek M and Alla EA, *J. Pharm. Biomed. Anal.,* 2002; **27**: 133.

205. Aveline, BM, Hasan T and Redmond RW, *J. Photochem. Photobiol. B: Biol.,* 1995; **30**: 161.

206. Sil S, Kar M and Chakraborti AS, *J. Photochem. Photobiol. B: Biol.,* 1997; **41**: 67.

207. Rery-Forgues S and Lavabre D, *J. Chem. Ed.,* 1999; **76**: 1260.

208. Deman JN and Cosby GA, *J. Phys. Chem.,* 1971; **75**: 991.

209. Kubat P and Mosinger J, *J. Photochem. Photobiol. A: Chem.* 1996; **96**: 93.

210. Brannon JH and Magde D, *J. Am. Chem. Soc., 1980;* **102**: 62.

211. Li H and Guarr TF, *J. Chem. Soc. Chem. Commun.,* 1989; 833.

212. Rose J. In *Advanced Physico-chemical Experiments*, , 1st edition, Sir Isaac Pitman & Sons Ltd: London 1964; p 257.

213. Castanho MARB and Prieto MJE, *Biochemica et Biophysica Acta,* 1998; **1373**: 1.

214. Castanho MARB and Prieto M, *Eur. J. Biochem.,* 1992; **207**: 125.

215. Lakowikz JR. In *Principles of fluorescence spectroscopy,* Kluwer Academic/ Plenum Publishers: New York, 1999; chapt. 8.

216. Achar BN, Fohlen GM, Parker JA and Keshavaya J, *Polyhedron,* 1987; **6**: 1463.

217. Dirk CW, Inabe T, Schoch KF and Marks TJ, *J. Am. Chem. Soc.,* 1983; **105**: 1539.

218. Joyner RD and Kenney ME, *J. Am. Chem. Soc.,* 1960; **82**: 5790.

219. Davison JB and Wayne KJ, *Macromolecules,* 1978; **11**: 186.

220. Vogler A and Kunkley H, *Inorg. Chim. Acta,* 1980; **44**: L209.

221. Crossley MJ, King LG and Pyke SM, *Tetrahedron*, 1987; **43**: 4569.

222. Loftsson T and Masson M, *Int. J. Pharm,* 2001; **225**: 15.

223. Montalban A, Meunier H, Ostler R Barrett A, Hoffman B and Rumbles G, *J. Phys. Chem.,* 1999; **103**: 4352.

224. Murov SL, Carmichael I and Hug GL. In *Handbook of photochemistry,* 2nd edition, M. Decker: New York, 1993; p 40.

225. Seotsanyana-Mokhosi I, Kuznetsova N and Nyokong T, *J. Photochem. Photobiol. A: Chem.,* 2001; **140**: 215.

226. Spiller W, Kliesch H, Wöhrle D, GHackbarth S, Roder B and Schnurpfeil G, *J. Porphyrins Phthalocyanines,* 1998; **2**: 145.

227. Kuznetsova N, Makarova E, Dashkevich S, Gretsova N, Negrimovsky V, Kaliya O and Luk'yanets E, *Zh. Obshch. Khim.,* 2000; **70**: 140.

228. Luk'yanets E, *J. Porphyrins Phthalocyanines,* 1999; **3**: 424.

229. Wilkinson F, Helman WP and Ross AB, *J. Phys. Chem. Ref. Data,* 1993; **22**: 113.

230. Kasuga K, Matsuura N, Inoue K, Handa M, Sugimori T, Isa K and Nakata M, *Chem. Lett.,* 2002; 352.

231. Fernández DA, Awruch J and Dicelio LE, *J. Photochem. Photobiol. B: Biol.,* 1997; **41**: 227.

232. Ribeiro MG and Azzellini GC, J. Braz. Chem. Soc., 2003; 14: 914.

233. Gruen LC and Blagrove RJ, *Aust. J. Chem.* 1973; **26**: 319.

234. Dini D, Barthel M and Hanack M, *Eur. J. Org. Chem., (MICROREVIEW),* 2001; 3759.

235. Maclean AL, Foran GJ, Kennedy BJ, Turner P and Hambley TW, *Aust. J. Chem.,* 1996; **49**: 1273.

236. Kobayashi N, Fukuda T, Ueno K and Ogino H, *J. Am. Chem. Soc.,* 2001; **123**: 10740.

237. Nyokong T, *Polyhedron,* 1995; **14**: 2325.

238. Kobayashi N and Konami H. In *Phthalocyanines: Properties and Applications,* Vol. 4. Leznoff CC and Lever ABP (Eds.), VCH: New York, 1999; Chapt. 9.

239. *Handbook of Chemistry and Physics,* 64th Ed., Weast RC (Ed.), CRS Press, Inc.: Florida, 1984.

240. Kaneko Y, Nishimura Y, Arai T, Sakuragi H, Tokumaru K and Daisaku M, *J. Photochem. Photobiol., A:Chem.,* 1995; **89**: 37.

241. Mandal D, Pal SK, Sukul D and Bhattacharyya K, *J. Phys. Chem. A,* 1999; **103**: 8156.

242. Verkman AS, *Biochemistry* 1987; **26**: 4050.

243. Guldi DM, Gouloumis A, Vazquez P. and Torres T, *Chem. Commun.*, 2002; 2056.

244. Ohgushi T, Li ZC, Li FM, Komatsu T, Takeoka S and Tsuchida E, *J. Porphyrins Phthalocyanines*, 1999; **3:** 53.

245. Grczynsk I, Wiczk W, Johnson ML, Cheung HC, Wang CK and Lakowicz JR, *Biophys. J.,* 1988; **54:** 577.

246. Forster TD, *Faraday Soc.*, 1959; **27**: 7.

247. Turro J. In *Modern Molecular Photochemistry,* The Benjamin/Cummings Publishing Co., Inc.: New York, 1978, Chapt. 6.

248. McIlroy S, Cramer C and Falvey D, *Organic Letters,* 2000; **2**: 2451.

249. Jockusch S, Landis M, Freiermuth B and Turro N, *Macromolecules,* 2001; **34**: 1619.

250. Vincett S, Voight EM and Rieckhoff KE, *J. Chem. Phys.,* 1971; **55**: 4131.

251. Walzer K and Hietschold M, *Surface Science*, 2001; **471**: 1.

252. Shannon RD. Acta Cryst. 1976; A32: 751-767.

253. Shannon RD and Prewitt CT. Acta Cryst. 1969; **B25**: 925.

254. Shannon RD and Prewitt CT. Acta Cryst. 1970; **B26**: 105.

255. Huheey JE, Keiter EA. and Keiter RL. In Inorganic Chemistry: Principles of Structure and Reactivity, 4th edition, HarperCollins: New York, 1993.

256. Morishige K, Tomoyasu S, and Iwano G, *Langmuir,* 1997; **13**: 5184-5188.

257. Yasukawa T, Uchida I and Matsue T, *Biophys. J.,* 1999; **76**: 1129.

258. Catalán J, Díaz C, López V, Pérez P, de Paz JLG and Rodríguez JG, *Liebigs Ann.*, 1996; 1785.

259. Schmidt R, *J. Am. Chem. Soc.,* 1989; **111**: 6983.

260. Nilsson R and Kearns DR, *J. Phys. Chem.* 1974; **78**: 1681.

261. Young RH and Brewer DR. In *Singlet oxygen, reactions with organic compounds and polymers*, Ranby B and Rabek FF (Eds.), John Wiley & Sons: New York, N.Y., 1976, pp 36-47.

262. Aveline B, Delgado O and Brault D, *J. Chem. Soc., Faraday Trans.* 1992; **88**: 1971.

263. Stuzhin PA, *J. Porphyrins Phthalocyanines,* 1999; **3**: 500.

264. Stuzhin PA, Khelevina OG, Angeoni S and Berezin BD. In *Phthalocyanines: Properties and Applications,* Vol. 4 Leznoff CC and Lever ABP (Eds.), VCH: New York, 1996.

265. Weinkauf JR, Cooper SW, Schweiger A and Wamser CC, *J. Phys. Chem, A.,* 2003; **107**: 3486.

266. Vinogradskii G and Sidorov AN, *Teor. Ekssp. Khim.* 1982; **18**: 118.

267. Nicolau M, Rojo G, Torres T and Agulló-López F, *J. Porphyrins Phthalocyanines* 1999; **3**: 703.

268. Hanack M, Schneider T, Barthe M, Shirk JS, Flom RS and Pong RSG, *Coord. Chem. Rev.* 2001; **219-221**: 235.

269. Filyasova AI, Kudelina IA and Feofanov AV, *J. Mol. Struc.,* 2001; **565-566**: 173.

270. Ming G, Zou JW, Yi PG, Shang ZC, Hu GX and Yu QS, *Anal. Sci.,* 2004; **20**: 465.

271. Levi V and Flecha FLG, *Biochem. Mol. Biol. Educ.,* 2003; **31**: 333.

272. Davies MJ, *Photochem. Photobiol. Sci.,* 2004; **3**: 17.